Académie universitaire Wallonie-Europe
Université de Liège - Faculté des Sciences Appliquées
Collège de doctorat en Électricité, Électronique et Informatique

Multiscale Finite Element Modeling of Nonlinear Quasistatic Electromagnetic Problems

Innocent NIYONZIMA
Ingénieur civil physicien (sciences spatiales)

Doctoral Dissertation presented
in fulfillement of the requirements for the degree of
Docteur en sciences de l'ingénieur

July 2014

Abstract

The effective use of composite materials in the technology industry requires the development of accurate models. Typical such materials in electrotechnical applications are lamination stacks and soft magnetic composites, used in the so-called *magnetoquasistatic* (low frequency) regime.

Current homogenization models (e.g. the classical homogenization method, mean field homogenization, ...) fail to handle all the difficulties raised by the modeling of these materials, particularly taking into account the complexity of their microstructure and their nonlinear/hysteretic behaviour. In this thesis we develop a multiscale computational method which allows to effectively solve multiscale magnetoquasistatic problems.

The technique is inspired by the HMM (heterogeneous multiscale method), which involves the resolution of two types of problems: a macroscale problem that captures slow variations of the overall solution, and many mesoscale problems that allow to determine the constitutive laws at the macroscale and to construct accurate local fields. Macroscale and mesoscale weak, $\boldsymbol{b}$-conform and $\boldsymbol{h}$-conform formulations, are derived starting from the two-scale convergence and the periodic unfolding methods. We also use the asymptotic homogenization method for deriving the homogenized linear material laws and, in the end, we derive scale transitions for bridging the scales.

Numerical tests carried out in the two-dimensional case allow to validate the models. In the case of $\boldsymbol{b}$-conform formulations, it is shown that the macroscale solution approximates well the average of the reference solution and that the resolution of the mesoscale problems allows to reconstruct accurate local fields and to compute accurate Joule losses and this, for materials with (non)linear and hysteretic behavior. Similar findings were obtained for the $\boldsymbol{h}$-conform formulations.

In both cases, the deterioration of the accuracy for mesoscale problems located near the boundary of the computational domain could be treated by defining suitable mesoscale problems near such boundaries. The extension of the model to three-dimensional problems, to multiphysical problems and the inclusion of the mesoscale domains with a stochastic distribution of phases are also some of the possible prospects for improving this work.

Résumé

L'utilisation efficace des matériaux composites dans l'industrie nécessite le développement de modèles précis pour en caractériser le comportement. Un exemple de tels matériaux dans les applications électrotechniques inclut les empilements de tôles et les composites magnétiques doux, utilisés dans le régime *magnétoquasistatique* (basse fréquence).

Les modèles d'homogénéisation actuels (par exemple la méthode d'homogénéisation classique, l'homogénéisation à champ moyen, ...) ne parviennent pas à solutionner toutes les difficultés soulevées par la modélisation de ces matériaux composites, en particulier la prise en compte de la complexité de la microstructure et du comportement nonlinéaire/hystérétique de ces matériaux. Dans cette thèse, nous développons une méthode d'homogénéisation computationnelle qui permet de résoudre efficacement les problèmes multi-échelles de la magnétoquasistatique.

La technique, inspirée par la méthode HMM (heterogeneous multiscale method), fait intervenir la résolution de deux types de problèmes : un problème macroscopique qui capte les variations lentes de la solution globale, et de nombreux problèmes mésoscopiques qui permettent de déterminer les lois de comportement à l'échelle macroscopique et qui permettent de reconstruire les champs locaux précis. Les formulations faibles macro et méso de type $\boldsymbol{b}$-conformes et $\boldsymbol{h}$-conformes ont été dérivées à partir de la théorie de la convergence à deux échelles et de la méthode d'éclatement périodique. Nous utilisons également l'homogénéisation asymptotique pour dériver les lois de matériaux linéaires homogénéisées et dérivons à la même occasion les transitions d'échelle qui permettent de coupler les deux échelles.

Les tests numériques effectués pour le cas bidimensionnel permettent de valider les modèles développés. Dans le cas des formulations $\boldsymbol{b}$-conformes, on constate que la solution macroscopique approxime au mieux la moyenne de la solution de référence et que la résolution de problèmes méso permet de reconstruire les champs locaux précis et de calculer de manière précise les pertes par effet Joule et ce pour les matériaux avec une loi constitutive (non)linéaire/hystérétique. Des résultats similaires ont été obtenus pour les formulations $\boldsymbol{h}$-conformes.

Pour les deux formulations, la détérioration de la précision pour les problèmes méso situés près de la frontière du domaine computationnel pourrait être traitée par la définition des problèmes méso appropriés près de ces frontières. L'extension des modèles aux problèmes tri-dimensionnels, aux problèmes multiphysiques et la prise en compte de domaines méso avec une distribution stochastique de phases sont également quelques-unes des perspectives possibles pour améliorer ce travail.

Acknowledgment

First of all, I wish to thank Professor C. Geuzaine for his guidance throughout my thesis and for giving me an opportunity to do research under excellent conditions and with great freedom at the University of Liège's Department of Electrical Engineering. His dynamism, his advice and and his expertise in the world of electromagnetic modeling have been invaluable to me. I would also like to thank the Belgian Industry and Agriculture Research Training Fund (FRIA) for funding my research for four years, and the Trowbridge Award Committee's prize which helped fuel my thesis work.

I also thank: Dr. O. Bottauscio (Istituto Nazionale di Ricerca Metrologica, Italy), Dr. L. Daniel (Université Paris Sud, LGEP, France), Dr. G. Meunier (CNRS, G2Elab, France), Professor R. Sabariego (Katholieke Universiteit Leuven), Professor P. Dular (University of Liège), and Professor L. Noels (University of Liège) for accepting to be members of my thesis committee and for their comments which helped improve the quality of this work.

I want to thank my past and present colleagues in the applied and computational electromagnetics group: Alexandre V., Alexandre H., Axel, David, Frédéric, Kevin, JDD, Maxime G., Maxime S., Véronique, Vuong, and Yannick. Special thanks go to Ruth for having guided my first steps in the world of research, for her willingness to assist me, and for her encouragements during my thesis work. To Patrick whose expertise allowed me to increase my understanding of magnetodynamics $\boldsymbol{b}$-conform and $\boldsymbol{h}$-conform formulations. To Nicolas and Amaury for enabling me to understand object-oriented programming. To Ibrahim for our discussions on functional analysis and the distribution theory.

I would like to thank Christophe, Bambe, Alice, Kevin and Ibrahim for their carefully proofreading of this manuscript.

Many thanks to Arnaud for his long-lasting friendship, and to Caroline and Francois for all the much needed (and much appreciated) relaxing times spent together during our lunch breaks. I would like to thank my other friends who shared my daily life: Chrysostome, Theodore, Faustin, Lucien, Muzaliwa, Emmanuel and their families. To Amadou, Harona, Dodji, Ilaria, Paulin, Jacqueline and Vestine. To my godchildren Daniel, Noémie, Léon and Leroy whose presence in my life brought joy and comfort all throughout this period of study.

Finally, I would like to thank my family which supported me during the realization of my thesis: Cathérine, Innocent and his family, aunt Emmerence and her family, Ange, Alice, Albert, and all my family in Africa. To Jean de Dieu, his wife

Aimée and their family, Peter and his wife Zeburiya and their family.

Iki gitabo ngituye abavandimwe n'ababyeyi batuvuyemo imburagihe: ba nyogokuru Rahel na Martha, ba sogokuru Bangeranyinduga na Rukebesha rwa Gasimba, bene mama Maurice n'Alphonsine ariko cyane cyane ababyeyi bampaye ubuzima Mujawamariya na Libonande. Mwatuvuyemo imburagihe, ndabakunda kandi mbatekerezaho buri gihe.

Liège, September 2014 Innocent Niyonzima

Contents

List of Symbols

Alphanumeric symbols

Y	: Unit cell $]-\frac{Y_1}{2},\frac{Y_1}{2}[\times]-\frac{Y_2}{2},\frac{Y_2}{2}[\times]-\frac{Y_3}{2},\frac{Y_3}{2}[$ of $\mathbb{R}^3$
$\lvert Y\rvert$	: Measure of the set Y
$\boldsymbol{x}=(x_1,x_2,x_3)$	: Point of $\mathbb{R}^3$
$\boldsymbol{y}=(y_1,y_2,y_3)$	: Point of Y
t	: Time instant
T	: Final computational time
$U\subset\subset\Omega$	: U is compactly contained in Ω, i.e. $\bar{U}$ is compact and $\bar{U}\subset\Omega$
$\hat{\boldsymbol{u}}$	: The hat is used for the mean value $\hat{\boldsymbol{u}}(\boldsymbol{x},t):=\frac{1}{\lvert Y\rvert}\int_{\mathcal{Y}}\boldsymbol{u}(\boldsymbol{x},\boldsymbol{y},t)\mathrm{d}y$
$\widetilde{\boldsymbol{u}}$	: $\widetilde{\boldsymbol{u}}(\boldsymbol{x},\boldsymbol{y},t):=\boldsymbol{u}(\boldsymbol{x},\boldsymbol{y},t)-\hat{\boldsymbol{u}}(\boldsymbol{x},t)$
$\mathcal{V}$	: Any linear space
$\mathcal{V}'$	: The dual space of $\mathcal{V}$
$L^p(\Omega)$	: Space of scalar v defined in Ω such that $\lvert\lvert v\rvert\rvert_{L^p(\Omega)}=\Big(\int_\Omega\lvert v(\boldsymbol{x})\rvert^p\mathrm{d}x\Big)^{1/p}<\infty$
$\boldsymbol{L}^p(\Omega)$	: Space of all vector fields $\boldsymbol{v}$ defined in Ω such that resp. $\lvert\lvert\boldsymbol{v}\rvert\rvert_{\boldsymbol{L}^p(\Omega)}=\Big(\int_\Omega\lvert\boldsymbol{v}(\boldsymbol{x})\rvert^p\mathrm{d}x\Big)^{1/p}<\infty$
$L^\infty(\Omega)$	: Spaces of all functions $v:\Omega\to\mathbb{R}$ such that $\lvert\lvert v\rvert\rvert_{L^\infty(\Omega)}=\text{ess supp}_{\boldsymbol{x}\in\Omega}\lvert v(\boldsymbol{x})\rvert<\infty$
$H^p(\Omega)$, $\boldsymbol{H}^p(\Omega)$	: p^{th} order Sobolev spaces of scalar and vector fields over Ω
$\boldsymbol{H}(\mathbf{curl};\Omega)$	: Stream function space $\{\boldsymbol{v}\in\boldsymbol{L}^2(\Omega):\mathbf{curl}\,\boldsymbol{v}\in\boldsymbol{L}^2(\Omega)\}$
$\boldsymbol{H}(\mathrm{div};\Omega)$	: Flux space $\{\boldsymbol{v}\in\boldsymbol{L}^2(\Omega):\mathrm{div}\,\boldsymbol{v}\in L^2(\Omega)\}$
$\boldsymbol{H}(\mathbf{curl}\ \mathbf{0};\Omega)$	: Stream function space $\{\boldsymbol{v}\in\boldsymbol{L}^2(\Omega):\mathbf{curl}\,\boldsymbol{v}\in\boldsymbol{L}^2(\Omega):\mathbf{curl}\,\boldsymbol{v}=\mathbf{0}\}$
$\boldsymbol{H}(\mathrm{div}\ \mathbf{0};\Omega)$	: Flux space $\{\boldsymbol{v}\in\boldsymbol{L}^2(\Omega):\mathrm{div}\,\boldsymbol{v}\in\boldsymbol{L}^2(\Omega):\mathrm{div}\,\boldsymbol{v}=0\}$
$F(\Omega)$	: Any space of real-valued functions defined on Ω
$F_{loc}(\mathbb{R}^n)$	: All real-valued functions defined on $\mathbb{R}^n$ such that their restriction to any open bounded subset Ω of $\mathbb{R}^n$ belongs to $F(\Omega)$
$F_{loc}(\Omega)$	: All real-valued functions v defined on Ω such that $v\in F(\Omega)$ for each open $U\subset\subset\Omega$
$F_\#(Y)$	: All functions in $F_{loc}(\mathbb{R}^n)$ which are the periodical repetition of some function in $F(Y)$
$F(\mathcal{Y})$	: All functions defined on $\bar{Y}$ such that they belong to $F_\#(\bar{Y})$
$F_*(\mathcal{Y})$	: Space of all functions of $v\in F(\mathcal{Y})$ such that their mean value is zero i.e.:$\int_Y v(\boldsymbol{y})\mathrm{d}y=0$

$L^p(0,T;\mathcal{V})$	:	All measurable maps $v :]0,T[\to \mathcal{V}$ such that $\|\|v\|\|_{L^p(0,T;\mathcal{V})} = \Big(\int_0^T \|\|v(.,t)\|\|_{\mathcal{V}}^p \mathrm{d}t\Big)^{1/p} < \infty$
$L^\infty(0,T;\mathcal{V})$	:	All measurable maps $v :]0,T[\to \mathcal{V}$ such that $\|\|v\|\|_{L^\infty(0,T;\mathcal{V})} = \text{ ess sup }_{t\in]0,T[} \|\|v(.,t)\|\|_{\mathcal{V}} < \infty$
$H^m(0,T;L^2(\Omega))$	:	All functions $v \in L^2(\Omega_T)$ such that $\partial_t v \in L^2(\Omega_T)$, ..., $\partial_t^m v \in L^2(\Omega_T)$
$L^p(\Omega;\mathcal{V})$	:	Space of all scalar functions $v : \Omega \to \mathcal{V}$ such that $\|\|v\|\|_{L^p(\Omega;\mathcal{V})} = \Big(\int_\Omega \|\|v(\boldsymbol{x},.)\|\|_{\mathcal{V}}^p \mathrm{d}x\Big)^{1/p} < \infty$
$\boldsymbol{L}^p(\Omega;\mathcal{V})$	:	Space of all vector functions $\boldsymbol{v} : \Omega \to \mathcal{V}$ such that $\|\|\boldsymbol{v}\|\|_{\boldsymbol{L}^p(\Omega;\mathcal{V})} = \Big(\int_\Omega \|\|\boldsymbol{v}(\boldsymbol{x},.)\|\|_{\mathcal{V}}^p \mathrm{d}x\Big)^{1/p} < \infty$
$\boldsymbol{h}$	:	Magnetic field (A/m)
$\boldsymbol{b}$	:	Magnetic flux density (T)
$\boldsymbol{e}$	:	Electric field (V/m)
$\boldsymbol{d}$	:	Electric flux density (C/m^2)
$\boldsymbol{j}$	:	Current density (A/m^2)
q	:	Electric charge density (C/m^3)
$\boldsymbol{m}$	:	Magnetization (A/m)
$\boldsymbol{p}$	:	Electric polarization (C/m^2)
$\boldsymbol{a}$	:	Magnetic vector potential (Wb/m)
v	:	Electric scalar potential (V)

Greek symbols

Ω	:	Bounded open set of $\mathbb{E}^3$
Ω_T	:	The open bounded set defined by $\Omega_T := \Omega \times]0,T[$
Γ	:	Boundary of Ω ($= \partial\Omega$)
ϕ	:	Magnetic scalar potential (A)
σ	:	Electric conductivity (S/m)
μ	:	Magnetic permeability (H/m)
μ_0	:	Magnetic permeability of vacuum ($= 4\pi\, 10^{-7}$ H/m)
μ_r	:	Relative magnetic permeability ($= \mu/\mu_0$)
ϵ	:	Electric permittivity (F/m)
ϵ_0	:	Electric permittivity of vacuum ($\simeq 8.854187817\, 10^{-17}$ F/m)
ϵ_r	:	Relative electric permittivity ($= \epsilon/\epsilon_0$)
χ_m	:	Magnetic susceptibility
χ_e	:	Electric susceptibility (F/m)

Abbreviations

FEM	:	Finite element method
HMM	:	Heterogeneous multiscale method

MsFEM	:	Multiscale Finite element method
SMC	:	Soft magnetic composites

Operators

∂	:	Boundary operator
$^{\mathrm{C}}$	:	Complement
$\bar{\ }$	:	Closure
∂_x, ∂_y, ∂_z	:	Space derivatives
∂_t	:	Time derivative
grad	:	Gradient
curl	:	Curl
div	:	Divergence
supp	:	Support
$\times$	:	Vector product
$\cdot$	:	Scalar product

List of Figures

List of Tables

Chapter 1

Introduction

1.1 Motivation

The use of numerical methods for solving electromagnetic problems is nowadays widespread. Indeed, analytical solutions to Maxwell's equations (which govern the electromagnetic fields) are not always guaranteed to exist due to nonlinearities of the constitutive laws or the complexity of the involved geometries. One of the numerical methods frequently used in low frequency and near-field high frequency problems is the finite element (FE) method for its easiness to handle problems involving both nonlinearities and complex geometries. To this end, a mesh of the structure is generated and Maxwell's equations are verified on average on elements of the mesh, which is ensured by integrating these equations on each element of the mesh. If the problem is well-posed, the finer the mesh, the more accurate the numerical solution.

Some problems involve multiscale materials. In the medium and high frequency domains, this is the case for *soft ferrites* (Figure 1.2 (c) and (d)) used in radio frequency transformers, e.g. in telecommunication technology and in power electronics [35], *polymer nanocomposites* used for making electromagnetic wave absorbers and shields [23, 104, 132, 179, 191, 192] and *metamaterials* used for making cloaking devices and high resolution lenses [113, 156, 159, 182, 207]. Low frequency applications often involve *laminations* whose lamellar structure helps reducing eddy current losses in electric devices such as transformers, coils, motors, etc. (Figure 1.1) and *soft magnetic composites* used in high speed machines and whose isotropic properties allow for the manufacturing of three-dimensional paths electric machines (Figure 1.2 (a) and (b)). For problems involving such materials, the application of classical numerical methods such as the FE method becomes prohibitive in terms of the computational time and memory storage whence the use of multiscale and homogenization methods.

The first homogenization approach used to analytically characterize homogenized properties of composites materials was based on mixing rules [122, 181]. Using this method, it is possible to determine equivalent properties with little information on the microstructure (e.g., only the percentage of the different constitutive phases). More elaborate theoretical methods such as the asymptotic expansion method [20],

stator
rotor
transformer
coil

Figure 1.1: Laminated magnetic materials [177, 178].

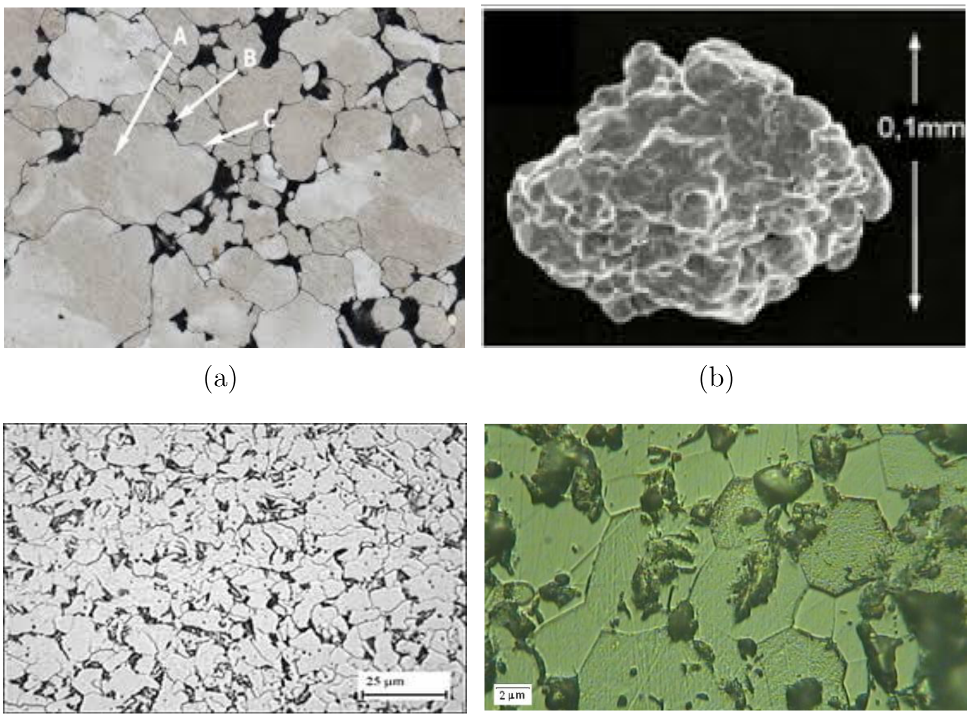

(a) (b)

(c) (d)

Figure 1.2: Soft magnetic composites ((a) and (b)) and soft ferrites ((c) and (d)) [35, 123, 193].

the G-convergence [139, 188, 190], the two-scale convergence [143, 196, 201] and the periodic unfolding methods [45, 47] allow to construct the homogenized problem and determine the associated constitutive laws. The convergence of the fields and of some functionals can also be shown using these methods. Equations resulting from these methods can be used to develop multiscale methods. A non-exhaustive list of these multiscale methods include the mean-field homogenization method [39,49,206], the multiscale finite element methods - MsFEM [37,76,77,100,101], the variational multiscale method - VMS [41,102,103,109,153] and the heterogeneous multiscale methods - HMM [68,73,152]. In most of these methods, an elementary-cell problem is solved and the solution is used for computing the homogenized constitutive laws (electric and magnetic).

In this thesis we are interested in multiscale magnetoquasistatic problems. These problems arise from Maxwell's equations by neglecting displacements currents with respect to eddy currents. The assumption is valid when the wavelength of the exciting source term is much greater compared to the size of the structure. When solving magnetoquasistatic problems, one is interested in electric and magnetic phenomena. In our developments we will consider linear electric constitutive laws and linear, nonlinear or hysteretic magnetic constitutive laws.

The resolution of multiscale magnetoquasistatic problems can become quite cumbersome: as mentioned above the use of classical numerical methods is very expensive in terms of computational time and storage memory as a very fine mesh is needed for capturing the small fluctuations of the solution. The main idea of homogenization and multiscale methods is to replace the multiscale heterogeneous computational domain by a homogeneous domain with equivalent properties. Such methods have been developed in electromagnetism mainly for materials with linear [27,28,95,124] and nonlinear [18,96] magnetic material laws and to the best of our knowledge, none is able to accurately predict the electromagnetic behavior in the presence of materials with hysteresis.

In this thesis we develop a multiscale method that can handle magnetoquasistatic problems involving multiscale materials, which can exhibit linear, nonlinear and hysteretic behavior. The method is inspired by the HMM method [1–4,6,7,43,67–69, 71–73,75] and based on the scale separation assumption $\varepsilon \ll 1$ where $\varepsilon = l/L$ is the ratio between the smallest scale l and the scale of the material or the characteristic length of external loadings L.

The fine-scale problem is replaced by a macroscale problem defined on a coarse mesh covering the entire domain and many mesoscale problems that are defined on small, finely meshed areas around some points of interest of the macroscale mesh (e.g. numerical quadrature points). The transfer of information between these problems is done during the *upscaling* and the *downscaling* stages (see Figure 1.3).

During the downscaling, proper boundary conditions for the mesoscale problems are imposed stemming from the consistency of the electromagnetic fields at both scales. Source terms for the mesoscale problems are also derived from the macroscale solution. In return, the missing macroscale constitutive laws at the macroscale are computed using the mesoscale fields in the upscaling stage.

We use the two-scale convergence and the period unfolding methods to derive the governing equations (at the macroscale and the mesoscale levels) as well as

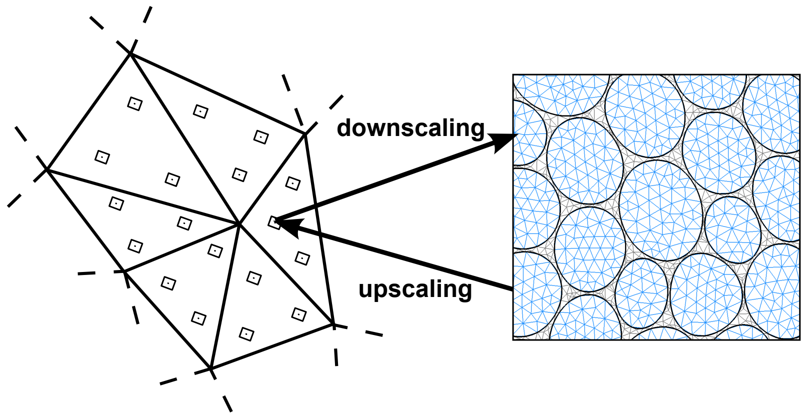

Figure 1.3: Scale transitions between macroscale (left) and mesoscale (right) finite element problems. Downscaling (macro to meso): obtaining proper boundary conditions and the source terms for the mesoscale problem from the macroscale solution at a numerical quadrature point in the macro finite element mesh. Upscaling (meso to macro): effective quantities for the macroscale problem calculated from the mesoscale solution [148].

for deriving nonlinear homogenized magnetic laws. We also use the asymptotic homogenization method for upscaling the linear conductive law.

The approach allows not only to upscale accurate homogenized constitutive laws but also provides a good framework for recovering accurate local fields and for upscaling more accurate global quantities (eddy current losses, magnetic energy, etc.).

1.2 Scope and goals of the work

This work contributes to the development and the testing of multiscale formulations for low frequency electromagnetic problems involving composite materials with an assumed periodic microstructure. To achieve this, a three-step approach has been adopted:

1. *The derivation of the differential forms of the governing equations at the macroscale and the mesoscale. The defined mesoscale problem can then be used for defining the elementary-cell problem.*
   The derivation is done using the asymptotic homogenization method for the $\text{div} - \mathbf{grad}$, linear problems and the two-scale convergence and the periodic unfolding methods for the $\text{div} - \mathbf{grad}/\mathbf{curl} - \mathbf{curl}$, nonlinear problems governed by maximal monotone operators. Note that the derived theory is not guaranteed to hold for problems involving materials with hysteresis.

2. *The design of multiscale formulations involving formulations for the macroscale problem, the mesoscale problem and the coupling between these*

problems (*scale transitions*).
Starting from the partial differential equations obtained from the homogenization theory, we derive weak forms for the macroscale and the mesoscale problems both for $\boldsymbol{h}$- and $\boldsymbol{b}$-conform formulations. The exchange of information between both problems through *scale transitions* is also detailed: source fields for the mesoscale problems are downscaled from the macroscale solution. Proper boundary conditions that respect the consistency of electromagnetic fields are also defined for the mesoscale problem. Likewise, the missing constitutive laws at the macroscale level are upscaled from mesoscale solutions. Hysteresis is numerically accounted for in the time-stepping procedure.

3. *Testing the formulations.*
The $\boldsymbol{h}$- and $\boldsymbol{b}$-conform formulations are tested on a laminated core and soft magnetic composites. The tests are done for materials governed by linear, nonlinear and hysteretic constitutive laws.

1.3 Outline

The thesis is divided into four chapters:

In chapter 2 we introduce Maxwell's equations and the constitutive laws. We then derive the magnetoquasistatic problem.

In chapter 3 we derive the homogenized problem for the magnetoquasistatic problem by applying homogenization theory. After a short review of the existing homogenization methods we choose the asymptotic homogenization for the $\text{div} - \textbf{grad}$, linear problem. This theory is based on an expansion of the fields and differential operators in terms of the macroscale and mesoscale coordinate systems. We also choose the two-scale convergence and the periodic unfolding methods for the nonlinear problems. The limiting macroscale and mesoscale problems are derived using the two-convergence theory.

Chapter 4 deals with the multiscale formulations for the magnetoquasistatic problem. Starting from the equations obtained from the homogenization methods we develop $\boldsymbol{h}$- and $\boldsymbol{b}$-conform formulations for the macroscale and the mesoscale problems. Scale transitions are also investigated thoroughly. Finally, an example of implementation for a $\boldsymbol{b}$-conform formulation is given.

Chapter 5 concerns the application of the theory to two-dimensional problems. Two types of materials (a laminated magnetic core and soft magnetic composites) are used for validating the formulations.

We end up with conclusions and perspectives in chapter 6.

1.4 Original contributions

The main original contributions of this work are:

– A comparative study of homogenization and convergence methods for the derivation of the homogenized problem for the magnetoquasistatic problem (chapter 3)

- Multiscale formulations and computations for a nonlinear div − **grad** type problem for application in magnetostatics (see [148], section 4.4.5 and chapter 5).

- Multiscale $\boldsymbol{b}$ - conform formulations and computations for magnetodynamic problems involving a nonlinear magnetic constitutive law. Derivation of the macroscale weak formulations, of a cell problem used for upscaling the constitutive law and of the scale transitions for bridging the scales. Definition of a mesoscale problem with eddy currents that allows to recover accurate local quantities (see [147, 149, 151, 152], section 4.3 and chapter 5). Applications of the developed multiscale method to a problem involving hysteresis.

- Application of the multiscale formulations for the computation of global quantities such as the eddy currents losses and the magnetic energy (see [150] and chapter 5).

- Multiscale $\boldsymbol{h}$-conform formulations and computations for magnetodynamic problems involving a nonlinear magnetic mapping. Derivation of the macroscale weak formulations, of a cell problem used for upscaling the constitutive law and of the scale transitions for bridging the scales. Definition of a mesoscale problem with eddy currents that allows to recover accurate local quantities (see section 4.4 and chapter 5).

A significant part of the thesis was devoted to the implementation of the proposed formulations. For this purpose we have developed a *c++/python* code named *hmm* in Gmsh [91, 92]. All the building block classes of the code (definition of the domain, constitutive laws, functions spaces, ...) have been built using only the mesh generated by Gmsh as input. The code has been used for the resolution of the macroscale problem and it uses GetDP [61, 62] for solving mesoscale problems.

This work has led to the publication of the following journal papers:

1. I. Niyonzima, R. V. Sabariego, P. Dular and C. Geuzaine, *Finite element computational homogenization of nonlinear multiscale materials in magnetostatics*, IEEE Transactions on Magnetics 48 (2012), no. 2, pp. 587-590.

2. I. Niyonzima, R. V. Sabariego, P. Dular, F. Henrotte, and C. Geuzaine, *Computational homogenization for laminated ferromagnetic cores in magnetodynamics*, IEEE Transactions on Magnetics 49 (2013), no. 5, pp. 2049-2052.

3. I. Niyonzima, R. V. Sabariego, P. Dular, and C. Geuzaine, *Nonlinear computational homogenization method for the evaluation of eddy currents in soft magnetic composites*, IEEE Transactions on Magnetics 50 (2014), no. 2.

and the following conference proceeding papers:

1. I. Niyonzima, R. V. Sabariego, P. Dular and C. Geuzaine, *Finite Element Computational Homogenization of Nonlinear Multiscale Materials in Magnetostatics*, Proceedings of the 18^{th} Conference on the Computation of Electromagnetic Fields (COMPUMAG2011) (Sydney, Australia), July 2011.

2. I. Niyonzima, R. V. Sabariego, P. Dular and C. Geuzaine, *Finite element computational homogenization for heterogeneous materials in magnetodynamics*, Proceedings of the Fifth International Conference on Advanced COmputational Methods in ENgineering (ACOMEN 2011) (Liège, Belgium), November 2011.

3. I. Niyonzima, R. V. Sabariego, P. Dular, F. Henrotte, and C. Geuzaine, *Multiscale quasistatic homogenization for laminated ferromagnetic cores*, Proceedings of the 7^{th} European Conference on Numerical Methods in Electromagnetism (NUMELEC 2012) (Marseille, France), July 2012.

4. I. Niyonzima, R. V. Sabariego, P. Dular, F. Henrotte, and C. Geuzaine, *Computational homogenization for laminated ferromagnetic cores in magnetodynamics*, Proceedings of the 15^{th} Biennial IEEE Conference on Electromagnetic Field Computation (CEFC2012) (Oita, Japan), November 2012.

5. I. Niyonzima, R. V. Sabariego, P. Dular and C. Geuzaine, *A computational homogenization method for the evaluation of eddy current in nonlinear soft magnetic composites*, Proceeding of the 9^{th} International Symposium on Electric and Magnetic Fields, EMF 2013 (Bruges, Belgium), April 2013.

6. I. Niyonzima, R. V. Sabariego, P. Dular and C. Geuzaine, *Nonlinear computational homogenization method for the evaluation of eddy currents in soft magnetic composites*, Proceedings of the 19^{th} Conference on the Computation of Electromagnetic Fields (COMPUMAG2013) (Budapest, Hungary), July 2013.

Chapter 2

Electromagnetic models

2.1 Introduction

In this chapter, we derive weak formulations for the magnetoquasistatic problem, amenable to finite element discretization. The chapter is organized as follows: in section 2.2 we introduce the differential and integral forms of Maxwell's equations. From these equations we derive interface conditions that express the continuity of electromagnetic fields across the interface between two media and appropriate boundary conditions of the problem. In section 2.3 we define the constitutive laws. In section 2.4 we define a general magnetoquasistatic problem and use it in section 2.5 for defining a proper functional setting for magnetodynamic and magnetostatic problems.

2.2 Maxwell's equations

In the range of validity of the classical electromagnetic theory, electromagnetic phenomena are governed by the following Maxwell's equations [98, 186]:

$$\mathbf{curl}\,\boldsymbol{h} - \partial_t \boldsymbol{d} = \boldsymbol{j}, \tag{2.1}$$

$$\mathbf{curl}\,\boldsymbol{e} + \partial_t \boldsymbol{b} = \mathbf{0}, \tag{2.2}$$

$$\operatorname{div} \boldsymbol{d} = \rho, \tag{2.3}$$

$$\operatorname{div} \boldsymbol{b} = 0. \tag{2.4}$$

Equations (2.1)-(2.4) are Ampère's, Faraday's, Gauss electric and magnetic equations, respectively. The four fields $\boldsymbol{h}, \boldsymbol{e}, \boldsymbol{b}$ and $\boldsymbol{d}$ that appear in these equations are the magnetic field (A/m), the electric field (V/m), the magnetic flux density (T) and the electric flux density (C/m^2), respectively. The electric charge ρ (C/m^3) and the electric current density $\boldsymbol{j}(A/m^2)$ are source terms of the problem. Equations (2.1)–(2.4) are solved in a bounded subdomain Ω of the Euclidean space $\mathbb{R}^3$ using a cartesian coordinate system $\boldsymbol{x} = (x, y, z)$.

Applying the div operator to (2.1) and using (2.3) we get the equation of con-

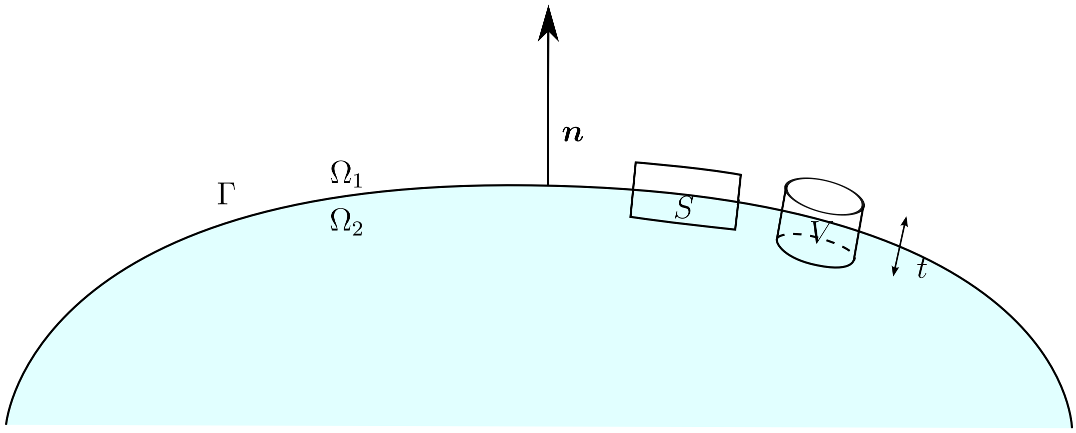

Figure 2.1: Interface condition between two media Ω_1 and Ω_2.

servation of the charge:

$$\partial_t \rho + \operatorname{div} \boldsymbol{j} = 0, \tag{2.5}$$

which governs the time evolution of the charge ρ as a function of the electric current density $\boldsymbol{j}$.

At the interface of two different materials, electromagnetic fields can become discontinuous and therefore non-differentiable. Figure 2.1 depicts two such materials Ω_1 and Ω_2 that share the same interface Γ. The fields in Ω_1 and Ω_2 are indexed 1 and 2, respectively and $\boldsymbol{n}$ denotes the normal to Γ directed from Ω_2 towards Ω_1. The surface densities ρ_s and $\boldsymbol{j}_s$ can be concentrated at the interface Γ (e.g. in the case of a perfect conductor). For any surface $S \in \mathbb{R}^3$ with boundary ∂S, the integration of (2.1) and (2.2) together with the application of Stokes theorem leads to the following equations:

$$\oint_{\partial S} \boldsymbol{h} \cdot \mathrm{d}\boldsymbol{l} = \int_S (\partial_t \boldsymbol{d} + \boldsymbol{j}) \cdot \mathrm{d}\boldsymbol{s}, \tag{2.6}$$

$$\oint_{\partial S} \boldsymbol{e} \cdot \mathrm{d}\boldsymbol{l} = -\int_S \partial_t \boldsymbol{b} \cdot \mathrm{d}\boldsymbol{s}. \tag{2.7}$$

Likewise, for any volume $V \in \mathbb{R}^3$ with boundary ∂V, the integration of (2.3) and (2.4) together with the application of Gauss theorem leads to the following equations:

$$\oint_{\partial V} \boldsymbol{b} \cdot \mathrm{d}\boldsymbol{s} = 0, \tag{2.8}$$

$$\oint_{\partial V} \boldsymbol{d} \cdot \mathrm{d}\boldsymbol{s} = \int_V \rho \, \mathrm{d}V. \tag{2.9}$$

For a particular choice of the volume V and the surface S (e.g. the volume and the surface on Figure 2.1 with vanishing thickness t), the integral equations (2.6)-(2.9) yield the interface conditions [116]:

$$\boldsymbol{n} \times (\boldsymbol{h}_1 - \boldsymbol{h}_2)|_{\partial S} = \boldsymbol{j}_s, \tag{2.10}$$

$$\boldsymbol{n} \times (\boldsymbol{e}_1 - \boldsymbol{e}_2)|_{\partial S} = \boldsymbol{0}, \tag{2.11}$$

$$\boldsymbol{n} \cdot (\boldsymbol{b}_1 - \boldsymbol{b}_2)|_{\partial V} = 0, \tag{2.12}$$
$$\boldsymbol{n} \cdot (\boldsymbol{d}_1 - \boldsymbol{d}_2)|_{\partial V} = \rho_s, \tag{2.13}$$

relating tangential components of $\boldsymbol{h}$ or $\boldsymbol{e}$ and normal components of $\boldsymbol{b}$ or $\boldsymbol{d}$ across the interface Γ. They express the discontinuity of the tangential component of $\boldsymbol{h}$ and the normal component of $\boldsymbol{d}$ and the continuity of the tangential component of $\boldsymbol{e}$ and the normal component of $\boldsymbol{b}$. The tangential component of $\boldsymbol{h}$ and the normal component of $\boldsymbol{d}$ across the interface Σ become continuous when there are no sources ρ_s and $\boldsymbol{j}_s$.

Using equation (2.10), we can deduce boundary conditions for a (theoretically) perfect magnetic material Ω_{pm} ($\boldsymbol{h} = \boldsymbol{0}$ in Ω_{pm}). Likewise, we can use (2.13) in order to get the boundary condition for a (theoretically) perfect electric material Ω_{pe} ($\boldsymbol{e} = \boldsymbol{0}$ in Ω_{pe}). At the interfaces with these materials, (2.10) and (2.11) become $\boldsymbol{n} \times \boldsymbol{h} = \boldsymbol{0}$ and $\boldsymbol{n} \times \boldsymbol{e} = \boldsymbol{0}$, respectively. These conditions can also be used for representing the vanishing behaviour of fields at infinity or for imposing symmetry conditions (see section 2.5).

2.3 Constitutive laws

Maxwell's system of equations (2.1)–(2.4) is undetermined and additional relationships need to be defined in order to close the problem. These relationships are the constitutive laws that relate two of the fields $\boldsymbol{h}, \boldsymbol{e}, \boldsymbol{b}, \boldsymbol{d}$ and $\boldsymbol{j}$ to the others, thus allowing to account for the influence of the materials on the distribution of electromagnetic fields.

In the vacuum the constitutive laws read:

$$\boldsymbol{d} = \epsilon_0 \boldsymbol{e}, \tag{2.14}$$
$$\boldsymbol{b} = \mu_0 \boldsymbol{h}, \tag{2.15}$$

where the constant $\mu_0 = 4\pi 10^{-7}$ H/m is the vacuum permeability and $\epsilon_0 = 1/(\mu_0 c_0^2)$ F/m is the vacuum permittivity. The constant c_0 denotes the speed of light in the vacuum.

In media that interact with the electromagnetic fields, the following general mesoscale/macroscale constitutive laws can be written [57, 88, 105, 107]:

$$\boldsymbol{j} = \boldsymbol{\mathcal{J}}(\boldsymbol{e}, \boldsymbol{b}). \tag{2.16}$$
$$\boldsymbol{d} = \boldsymbol{\mathcal{D}}(\boldsymbol{e}, \boldsymbol{b}), \tag{2.17}$$
$$\boldsymbol{h} = \boldsymbol{\mathcal{H}}(\boldsymbol{e}, \boldsymbol{b}), \tag{2.18}$$

In practice, relations (2.16)–(2.18) can be obtained either using a phenomenological approach or directly derived from mesoscale models obtained using models of physics at small scales (quantum mechanics, molecular dynamics, statistical physics, etc.) In this thesis we consider multiscale materials for which (2.16)–(2.18) are valid for each constituting phases and leave aside the mesoscale models. Relations (2.16)–(2.18)

Table 2.1: Electric conductivity σ of some materials [87, 142].

Materials	σ (S/m)	Materials	σ (S/m)
Silver	$6.17\ 10^{7}$	Fresh water	10^{-3}
Copper	$5.8\ 10^{7}$	Distilled water	10^{-5}
Gold	$4.1\ 10^{7}$	Dry soil	10^{-11}
Aluminum	$3.54\ 10^{7}$	Transformer	10^{-12}
Brass	$1.57\ 10^{7}$	Glass	$2\ 10^{-4}$
Bronze	10^{7}	Porcelain	$2\ 10^{-13}$
Iron	10^{6}	Rubber	10^{-15}
Sea water	4	Fused quartz	10^{-17}

can be nonlinear and possibly depend on the history of the material (hysteresis). A special case of these material laws are linear materials with memory effect (e.g. bi-anisotropic materials) for which the constitutive laws can be written as a convolution product. In this case, the use of Fourier analysis allows to conclude the frequency-dependency of material laws. In most applications the following constitutive laws hold:

$$\boldsymbol{j} = \boldsymbol{\mathcal{J}}(\boldsymbol{e}) = \sigma \boldsymbol{e} + \boldsymbol{j}_s. \tag{2.19}$$
$$\boldsymbol{d} = \boldsymbol{\mathcal{D}}(\boldsymbol{e}) = \epsilon_0 \boldsymbol{e} + \boldsymbol{\mathcal{P}}(\boldsymbol{e}), \tag{2.20}$$
$$\boldsymbol{b} = \boldsymbol{\mathcal{H}}(\boldsymbol{h}) = \mu_0(\boldsymbol{h} + \boldsymbol{\mathcal{M}}(\boldsymbol{h})), \tag{2.21}$$

The electric polarization vector $\boldsymbol{\mathcal{P}}(\boldsymbol{e}) = \boldsymbol{d} - \epsilon_0 \boldsymbol{e}$ and the magnetization $\boldsymbol{\mathcal{M}}(\boldsymbol{h}) = \mu_0^{-1}\boldsymbol{b} - \boldsymbol{h}$ are introduced to account for the deviation of the electric displacement current and the magnetic induction of a given material with respect to the vacuum. The source current density $\boldsymbol{j}_s$ is introduced to model current densities imposed by generators and considered independent of the local electromagnetic field.

2.3.1 Ohm's law

Ohm's law (2.19) relates the electric current density $\boldsymbol{j}$ and the electric field $\boldsymbol{e}$. It is valid in conductors where $\boldsymbol{j}$ is proportional to $\boldsymbol{e}$. The coefficient of proportionality is the electric conductivity σ (S/m), which is positive in conducting regions and zero in non-conducting regions. Table 2.1 contains the values of the electric conductivity of some materials. Relation (2.19) is valid for non-moving materials. If moving domains are present, the constitutive law becomes:

$$\boldsymbol{j} = \sigma(\boldsymbol{e} + \boldsymbol{v} \times \boldsymbol{b}) + \boldsymbol{j}_s, \tag{2.22}$$

where $\boldsymbol{v}$ is the velocity of the moving domain. Relation (2.22) can also be used for modelling the Hall effect. Equation (2.19) remains valid in most of the materials used in engineering applications. The electric conductivity can be a tensor $[\sigma]$. This is the case for instance if we consider the macroscopic properties of a laminated

Table 2.2: Relative permittivity ϵ_r of some materials [142].

Materials	ϵ_r	Materials	ϵ_r
Air	1.0	Polyethylene	2.3
Bakelite	5.0	Plystryrene	2.6
Glass	$4-10$	Porcelain	5.7
Mica	6.0	Rubber	$2.3-4.0$
Oil	2.3	Soil	$3-4$
Paper	$2-4$	Teflon	2.1
Paraffin max	2.2	Water	8.0
Methanol	32.6	Sea water	7.2

structure. The electric conductivity $[\sigma]$ then becomes:

$$[\sigma] = \begin{pmatrix} \sigma_{11} & \sigma_{12} & \sigma_{13} \\ \sigma_{21} & \sigma_{22} & \sigma_{23} \\ \sigma_{31} & \sigma_{32} & \sigma_{33} \end{pmatrix}. \tag{2.23}$$

For two-dimensional problems, we will assume anisotropic electric conductivity where the components $\sigma_{13}, \sigma_{23}, \sigma_{31}$ and σ_{32} are zero.

2.3.2 Dielectric constitutive laws

Equation (2.20) relates the electric flux density $\boldsymbol{d}$ to the electric field $\boldsymbol{e}$. Compared with (2.14), an additional term that accounts for the interaction of the field with the electrons of the medium is accounted for by adding the electric polarization $\boldsymbol{\mathcal{P}}(\boldsymbol{e})$. This term establishes a relation between the electric polarization vector $\boldsymbol{\mathcal{P}}$ and the electric field $\boldsymbol{e}$ as if the charges were elastically bound to the atoms of the medium with a restoring force $\boldsymbol{\mathcal{P}}(\boldsymbol{e})$. Materials with $\boldsymbol{\mathcal{P}}$ are called *dielectrics*. For linear *dielectric* materials, the electric polarization vector is a linear function of the electric field $\boldsymbol{\mathcal{P}}(\boldsymbol{e}) = \epsilon_0 \chi_e \boldsymbol{e} + \boldsymbol{p}_e$ and therefore

$$\boldsymbol{d} = \epsilon_0(1+\chi_e)\boldsymbol{e} + \boldsymbol{p}_e = \epsilon_0\epsilon_r \boldsymbol{e} + \boldsymbol{p}_e = \epsilon \boldsymbol{e} + \boldsymbol{p}_e. \tag{2.24}$$

In this relation, $\boldsymbol{p}_e$ is the permanent polarisation present in materials exhibiting permanent polarization such as the electrets, χ_e is the electric susceptibility (which is always positive), ϵ_r is the relative permittivity and ϵ is the electric permittivity. For a reversible medium, the electric permittivity can be represented by a symmetric, anisotropic tensor:

$$[\epsilon] = \begin{pmatrix} \epsilon_{11} & \epsilon_{12} & \epsilon_{13} \\ \epsilon_{21} & \epsilon_{22} & \epsilon_{23} \\ \epsilon_{31} & \epsilon_{32} & \epsilon_{33} \end{pmatrix}. \tag{2.25}$$

The symmetry can be derived using a thermodynamical approach.

Table 2.2 contains values of relative permittivity for some dielectric materials. Dielectric materials gather the *paraelectric* materials and the *ferroelectric* materials, which are characterized by nonlinear reversible and irreversible $\boldsymbol{d}$–$\boldsymbol{e}$ curves, respectively.

Table 2.3: Relative permeability μ_r of some materials [107, 142].

Ferromagnetic	μ_r	Diamagnetic	μ_r	Paramagnetic	μ_r
Nickel	250	Bismuth	0.99983	Aluminum	1.000021
Cobalt	600	Gold	0.99996	Magnesium	1.000012
Iron	4,000	Silver	0.99998	Palladium	1.00082
μ-metal	100,000	Copper	0.99999	Titanium	1.00018

2.3.3 Magnetic constitutive laws

Equation (2.21) relates the magnetic flux density $\boldsymbol{b}$ and the magnetic field $\boldsymbol{h}$. In this equation, an additional term called the *magnetization* vector $\boldsymbol{\mathcal{M}}(\boldsymbol{h})$ is added as compared to the case of vacuum and it gives the reaction of the medium when submitted to an external applied magnetic field.

For linear magnetic materials, the magnetization vector becomes $\boldsymbol{\mathcal{M}}(\boldsymbol{h}) = \chi_m \boldsymbol{h}$ and therefore the magnetic constitutive law becomes:

$$\boldsymbol{b} = \mu_0(1+\chi_m)\boldsymbol{h} + \mu_0\boldsymbol{h}_m = \mu_0\mu_r\boldsymbol{h} + \mu_0\boldsymbol{h}_m = \mu\boldsymbol{h} + \mu_0\boldsymbol{h}_m, \tag{2.26}$$

where χ_m is the magnetic susceptibility, μ_r is the relative permeability and $\boldsymbol{h}_m$ is the permanent magnetic field used for modelling permanent magnets [115]. Unlike the dielectric case, the magnetic susceptibility can be positive and negative. Materials with negative magnetic susceptibility are called *diamagnetic* and their magnetization vector points in the opposite direction to that of $\boldsymbol{h}$. *Paramagnetic* materials have positive values of magnetic susceptibility. Both diamagnetic and paramagnetic materials have small values of susceptibility (see Table 2.3). In many electromagnetic applications (electric transfomers, electric machines, electromagnetic shielding, etc.), materials with high values of the magnetic permeability are desired as they allow to effectively concentrate the magnetic flux density. These are *ferromagnetic* materials. Ferromagnetic materials exhibit nonlinear and possibly hysteretic behaviour (see Figures 2.2 and 2.3) and possibly a hysteretic behaviour (see Figure 2.3). The hysteresis curve in Figure 2.3 shows the evolution of the magnetic flux density $\boldsymbol{b}$ as a function of the magnetic field $\boldsymbol{h}$. An equivalent curve relating the magnetization vector $\boldsymbol{\mathcal{M}}$ as a function of the magnetic field $\boldsymbol{h}$ can be easily deduced. The portion of the curve in (b) exhibits the evolution of the $\boldsymbol{bh}$ curve for the first magnetization curve. When the magnetic field is increased until a maximum value, the saturation value of the magnetization is reached. When $\boldsymbol{h}$ decreases, the $\boldsymbol{bh}$ curve does not follow the same path as the first magnetization curve. Therefore when $\boldsymbol{h}$ is set back to zero there exists a non-zero magnetic flux density called *remanent induction* $\boldsymbol{b}_r$ and it is necessary to apply the *coercive magnetic field* $\boldsymbol{h}_c$ in order to cancel the magnetization. The magnetic work required for increasing $\boldsymbol{b}$ by the amount d$\boldsymbol{b}$ is derived from Poynting theorem [105, 116] and given by:

$$\mathrm{d}W_m = \boldsymbol{h}\cdot\mathrm{d}\boldsymbol{b} = \mu_0\boldsymbol{h}\cdot\mathrm{d}\boldsymbol{h} + \mu_0\boldsymbol{h}\cdot\mathrm{d}\boldsymbol{\mathcal{M}}, \tag{2.27}$$

and comprises two contributions: the energy required for increasing the energy in vacuum $\mu_0\boldsymbol{h}\cdot\mathrm{d}\boldsymbol{h}$ and the energy for magnetizing the material $\mu_0\boldsymbol{h}\cdot\mathrm{d}\boldsymbol{\mathcal{M}}$. The latter

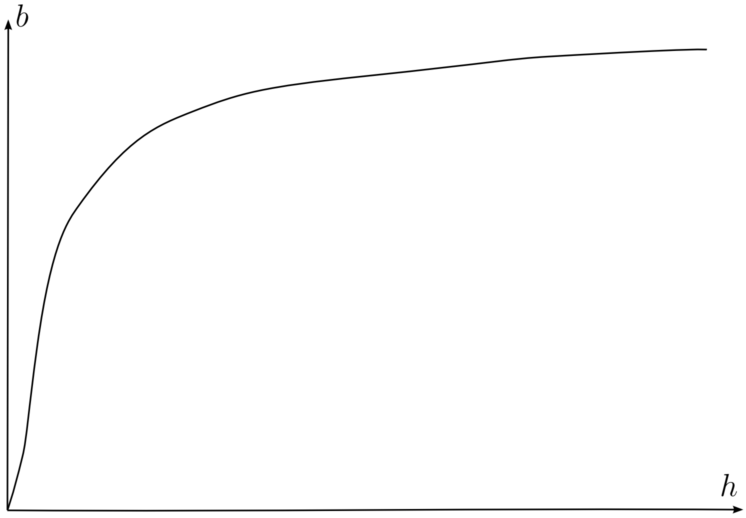

Figure 2.2: The bh curve for a nonlinear reversible magnetic material.

contribution is associated with hysteretic losses. Indeed, the density of the magnetic energy required for increasing the magnetic field from $\mathbf{0}$ to $\boldsymbol{h}$ is given by:

$$W_{m1} = \int_{\mathbf{0}}^{\boldsymbol{h}} \mathrm{d}W_m = \int_{\mathbf{0}}^{\boldsymbol{b}} \boldsymbol{h} \cdot \mathrm{d}\boldsymbol{b}. \tag{2.28}$$

The density of energy required to get the magnetic field from $\boldsymbol{h}$ to $\mathbf{0}$ is:

$$W_{m2} = \int_{\boldsymbol{h}}^{\mathbf{0}} \mathrm{d}W_m = \int_{\boldsymbol{b}}^{\boldsymbol{b}_r} \boldsymbol{h} \cdot \mathrm{d}\boldsymbol{b}, \tag{2.29}$$

and the sum of both integrals is the density of energy dissipated by hysteresis (see Figure 2.4).

$$W_{m1} + W_{m2} = \int_{\mathbf{0}}^{\boldsymbol{b}_r} \boldsymbol{h} \cdot \mathrm{d}\boldsymbol{b}. \tag{2.30}$$

The total energy dissipated over one cycle Q is given by:

$$Q = \int_{\Omega} \oint_{cycle} \boldsymbol{h} \cdot \mathrm{d}\boldsymbol{b} = \mu_0 \int_{\Omega} \oint_{cycle} \boldsymbol{h} \cdot \mathrm{d}\boldsymbol{\mathcal{M}} \tag{2.31}$$

where Ω is the computational domain.

Ferromagnetic materials can be classified in two categories depending on the value of their coercive magnetic field (Figure 2.5). *Hard* magnetic materials have large coercive magnetic fields (typically $\boldsymbol{h}_c > 10^3 A/m$). A great amount of energy

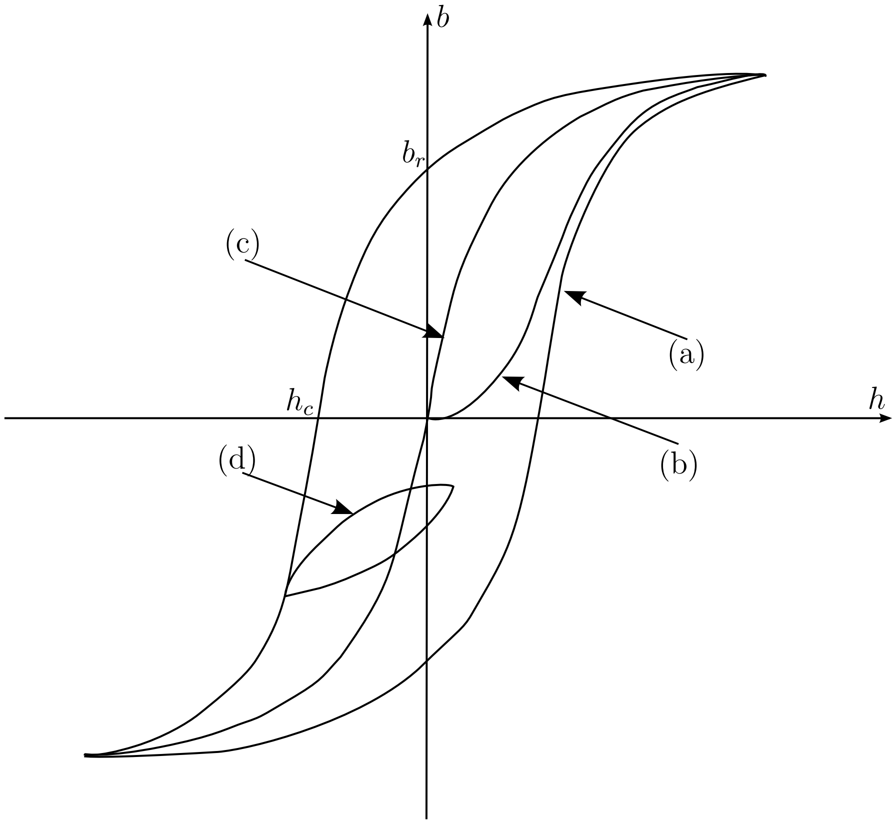

Figure 2.3: The bh curve for a nonlinear irreversible magnetic material. (a) Major hysteresis loop, (b) first magnetization curve, (c) anhysteretic curve and (d) minor hysteresis loop.

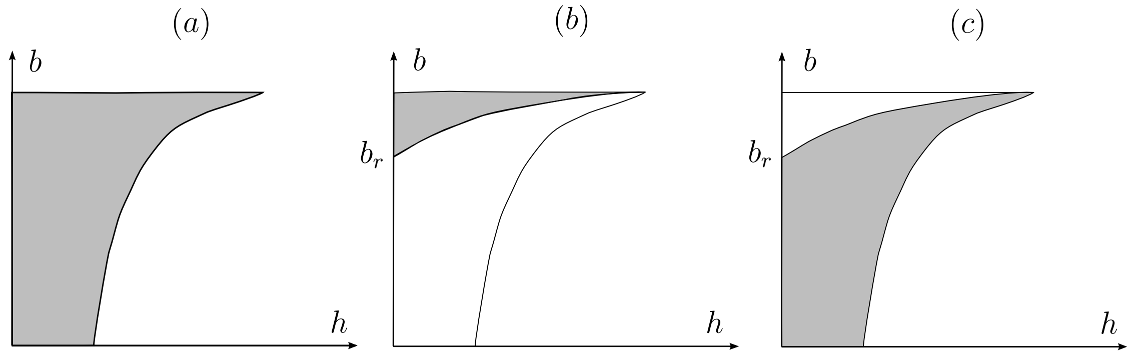

Figure 2.4: (a) Energy required to change the magnetic field from $\mathbf{0}$ to $\boldsymbol{h}$. (b) Energy required to get back the magnetic field from $\boldsymbol{h}$ to $\mathbf{0}$. (c) Hysteresis losses.

is required to demagnetize them. Therefore they are used for making permanent magnets. *Soft* magnetic materials have small coercive magnetic fields and are often used in electromagnetic devices for reducing magnetic losses.

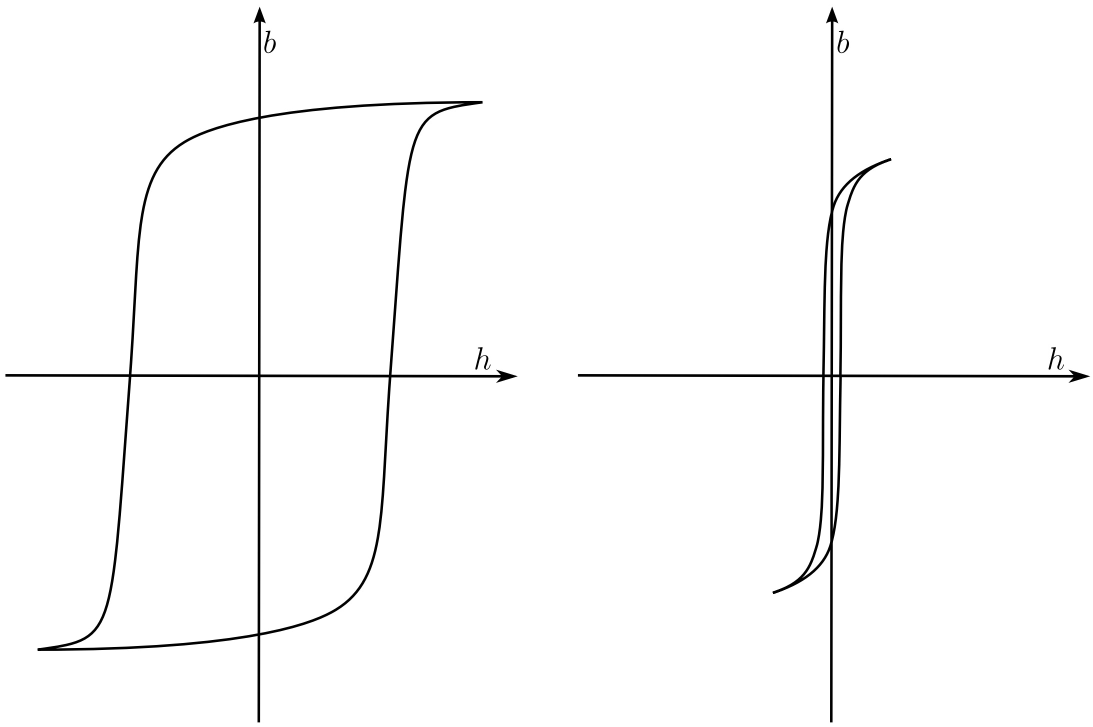

Figure 2.5: The bh hysteretic curves of ferromagnetic materials (hard magnetic material on the left and soft magnetic material on the right.)

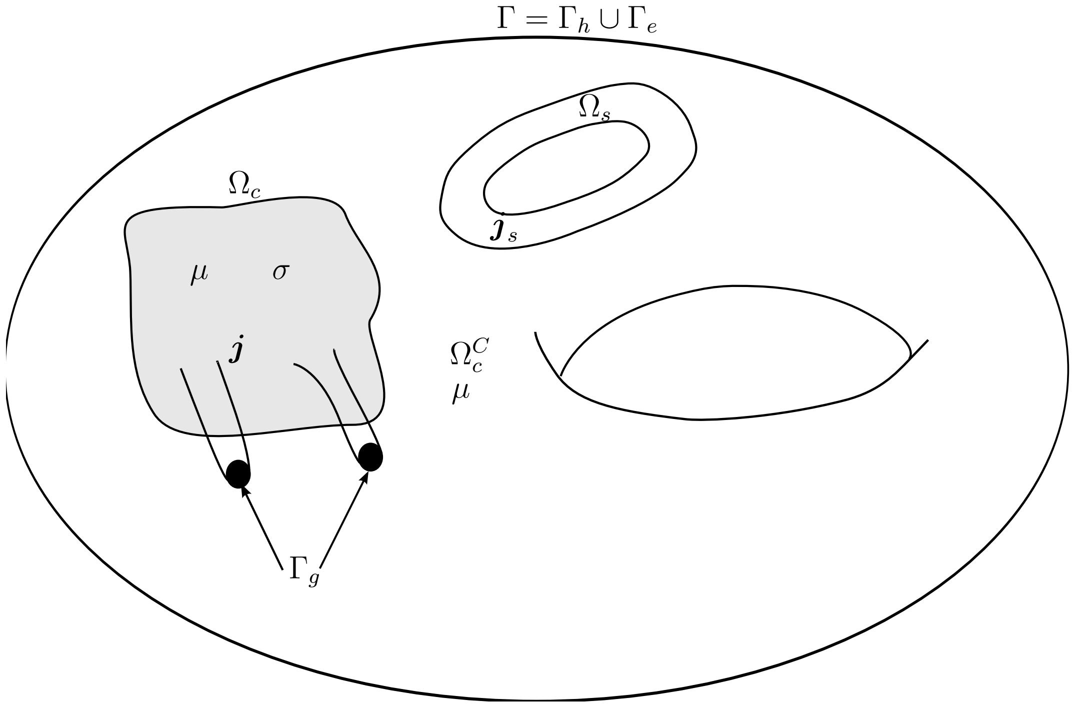

Figure 2.6: Bounded domain Ω and its subregions.

Often the constitutive law for soft magnetic materials is approximated by the anhysteretic curve. Each point of this curve is obtained by applying a combination of a DC field with and a AC field with a decreasing amplitude. The stationary solution then converges to one point of the anhysteretic curve (see Figure 2.3).

2.4 Description of the problem

We want to solve (2.1)–(2.4) together with (2.16)–(2.18) in a bounded domain Ω. This domain can be split into two non-overlapping regions: the conducting region Ω_c (with $\sigma > 0$) and the non-conducting region $\Omega_c^C = \Omega \setminus \Omega_c$ (with $\sigma = 0$). The non-conducting region is assumed to contain inductors Ω_s where the current density $\boldsymbol{j}_s$ is imposed. This assumption is equivalent to consider a perfect stranded inductor without skin or proximity effects. The modeling of each of these inductors is done by computing a source magnetic field $\boldsymbol{h}_s$ satisfying the following problems [65, 105]:

$$\begin{cases} \mathbf{curl}\, \boldsymbol{h}_s = \boldsymbol{j}_s & \text{in } \Omega_s \\ \mathbf{curl}\, \boldsymbol{h}_s = \mathbf{0} & \text{in } \Omega \setminus \Omega_s. \end{cases} \tag{2.32}$$

A gauge condition should be imposed to ensure the uniqueness of the field $\boldsymbol{h}_s$. One possible choice is the Coulomb gauge $\operatorname{div} \boldsymbol{h}_s = 0$. It is automatically ensured by choosing the source term from the Biot-Savart law [65, 105]:

$$\boldsymbol{h}_s(\boldsymbol{x}) = \frac{1}{4\pi} \int_{\mathbb{R}^3} \frac{\boldsymbol{j}_s(\boldsymbol{y}) \times (\boldsymbol{x} - \boldsymbol{y})}{|\boldsymbol{x} - \boldsymbol{y}|^3} \mathrm{d}\boldsymbol{y}. \tag{2.33}$$

The boundary of the domain Ω is denoted Γ. It is the union of two other regions Γ_e and Γ_h such that

$$\Gamma = \Gamma_e \cup \Gamma_h, \ \Gamma_e \cap \Gamma_h = \emptyset. \tag{2.34}$$

The region Γ_e is the part of the boundary where the tangential trace of $\boldsymbol{e}$ (resp. the normal trace of $\boldsymbol{b}$) is imposed and Γ_h is the part of the boundary where the tangential trace of $\boldsymbol{h}$ (resp. the normal trace of $\boldsymbol{d}$ or $\boldsymbol{j}$) is imposed. The boundary $\Gamma_g \in \Gamma_h$ is the part of the boundary of Ω_c which is crossed by an electric current.

2.5 The magnetoquasistatic approximation

In this thesis we focus on the magnetoquasistatic problem:

$$\mathbf{curl}\, \boldsymbol{h} = \boldsymbol{j}, \tag{2.35}$$
$$\mathbf{curl}\, \boldsymbol{e} = -\partial_t \boldsymbol{b}, \tag{2.36}$$
$$\operatorname{div} \boldsymbol{b} = 0, \tag{2.37}$$
$$\boldsymbol{b}(\boldsymbol{x}, t) = \boldsymbol{\mathcal{B}}(\boldsymbol{h}(\boldsymbol{x}, t), \boldsymbol{x}), \tag{2.38}$$
$$\boldsymbol{j}(\boldsymbol{x}, t) = \boldsymbol{\mathcal{J}}(\boldsymbol{e}(\boldsymbol{x}, t), \boldsymbol{x}). \tag{2.39}$$

This problem is derived from Maxwell's equations by neglecting the displacement currents $\partial_t \boldsymbol{d}$ with respect to the conduction currents $\boldsymbol{j}$. The system of equations must be completed by an initial condition on the magnetic flux density $\boldsymbol{b}(\boldsymbol{x}, t = 0) = \boldsymbol{b}^0(\boldsymbol{x})$. We also assume that the source current density $\boldsymbol{j}_s$ is divergence-free.

For the analytical and theoretical study of problem (2.35)–(2.39) in chapter 3 we will assume that the nonlinear mapping $\boldsymbol{\mathcal{B}} : \mathbb{R}^3 \times \Omega \to \mathbb{R}^3$ is maximal monotone. Therefore it has an inverse $\boldsymbol{\mathcal{B}}^{-1} := \boldsymbol{\mathcal{H}} : \mathbb{R}^3 \times \Omega \to \mathbb{R}^3$ and it can be derived from a convex, lower semi-continuous functional φ [10, 30, 55, 83, 85, 173, 174] (the derivation of the magnetic material law is done in Appendix A). Note that the time-dependence in the mapping $\boldsymbol{\mathcal{B}}$ occurs only through the magnetic field $\boldsymbol{h}(\boldsymbol{x}, t)$ (resp. the magnetic indution $\boldsymbol{b}(\boldsymbol{x}, t)$ for the mapping $\boldsymbol{\mathcal{H}}$), which excludes magnetic materials with memory effect and thus hysteresis.

The computational homogenization approach that we will propose in chapter 4 will allow us to include hysteretic effects numerically, through the use of classical hysteresis models (e.g. Preisach, Jiles-Atherton). In all cases we will still assume that the mapping $\boldsymbol{\mathcal{J}} : \mathbb{R}^3 \times \Omega \to \mathbb{R}^3$ is maximal monotone and has an inverse $\boldsymbol{\mathcal{E}} : \mathbb{R}^3 \times \Omega \to \mathbb{R}^3$. In practice, this assumption holds as the materials we consider in this thesis are electrically linear with the constitutive laws $\boldsymbol{j} = \sigma \boldsymbol{e}$ and $\boldsymbol{e} = \sigma^{-1} \boldsymbol{j}$.

In the next sections, we develop the weak formulations of the magnetoquasistatic problem (2.35)–(2.39). More details on these formulations can be found in [59, 90, 176].

2.5.1 Maxwell's house

In order to write (2.35)–(2.39) in weak form, let us introduce the domains of the differential operators $\mathbf{grad}, \mathbf{curl}$ and div with appropriate boundary conditions on

$$
\begin{tikzcd}
H_h^1(\Omega) \arrow[r, leftrightarrow] \arrow[d, "\mathbf{grad}_h"'] & L^2(\Omega) \\
\boldsymbol{H}_h(\mathbf{curl};\Omega) \arrow[r, leftrightarrow] \arrow[d, "\mathbf{curl}_h"'] & \boldsymbol{H}_e(\mathrm{div};\Omega) \arrow[u, "\mathrm{div}_e"'] \\
\boldsymbol{H}_h(\mathrm{div};\Omega) \arrow[r, leftrightarrow] \arrow[d, "\mathrm{div}_h"'] & \boldsymbol{H}_e(\mathbf{curl};\Omega) \arrow[u, "\mathbf{curl}_e"'] \\
L^2(\Omega) \arrow[r, leftrightarrow] & H_e^1(\Omega) \arrow[u, "\mathbf{grad}_e"']
\end{tikzcd}
$$

Figure 2.7: Tonti diagram for Maxwell's equations [24, 25].

Γ_h and Γ_e, respectively, as follows:

$$H_h^1(\Omega) = \{u \in L^2(\Omega) : \mathbf{grad}\, u \in \boldsymbol{L}^2(\Omega), u|_{\Gamma_h} = u_h\}, \tag{2.40}$$
$$\boldsymbol{H}_h(\mathbf{curl};\Omega) = \{\boldsymbol{u} \in \boldsymbol{L}^2(\Omega) : \mathbf{curl}\,\boldsymbol{u} \in \boldsymbol{L}^2(\Omega), \boldsymbol{n} \times \boldsymbol{u}|_{\Gamma_h} = \boldsymbol{u}_h\}, \tag{2.41}$$
$$\boldsymbol{H}_h(\mathrm{div};\Omega) = \{\boldsymbol{u} \in \boldsymbol{L}^2(\Omega) : \mathrm{div}\,\boldsymbol{u} \in L^2(\Omega), \boldsymbol{n} \cdot \boldsymbol{u}|_{\Gamma_h} = u_h\}, \tag{2.42}$$

$$H_e^1(\Omega) = \{u \in L^2(\Omega) : \mathbf{grad}\, u \in \boldsymbol{L}^2(\Omega), u|_{\Gamma_e} = u_e\}, \tag{2.43}$$
$$\boldsymbol{H}_e(\mathbf{curl};\Omega) = \{\boldsymbol{u} \in \boldsymbol{L}^2(\Omega) : \mathbf{curl}\,\boldsymbol{u} \in \boldsymbol{L}^2(\Omega), \boldsymbol{n} \times \boldsymbol{u}|_{\Gamma_e} = \boldsymbol{u}_e\}, \tag{2.44}$$
$$\boldsymbol{H}_e(\mathrm{div};\Omega) = \{\boldsymbol{u} \in \boldsymbol{L}^2(\Omega) : \mathrm{div}\,\boldsymbol{u} \in L^2(\Omega), \boldsymbol{n} \cdot \boldsymbol{u}|_{\Gamma_e} = u_e\}. \tag{2.45}$$

The spaces $H_h^{10}(\Omega)$, $\boldsymbol{H}_h^0(\mathbf{curl};\Omega)$, $\boldsymbol{H}_h^0(\mathrm{div};\Omega)$, $H_e^{10}(\Omega)$, $\boldsymbol{H}_e^0(\mathbf{curl};\Omega)$ and $\boldsymbol{H}_e^0(\mathrm{div};\Omega)$ denote the same spaces as the corresponding spaces in (2.40)–(2.45) with traces equal to zero.

These function spaces can be represented on the Tonti diagram of Figure 2.7, where they form two sequences denoted by the vertical arrows. Constitutive laws will link these sequences (horizontal arrows), as will be explained in the next sections.

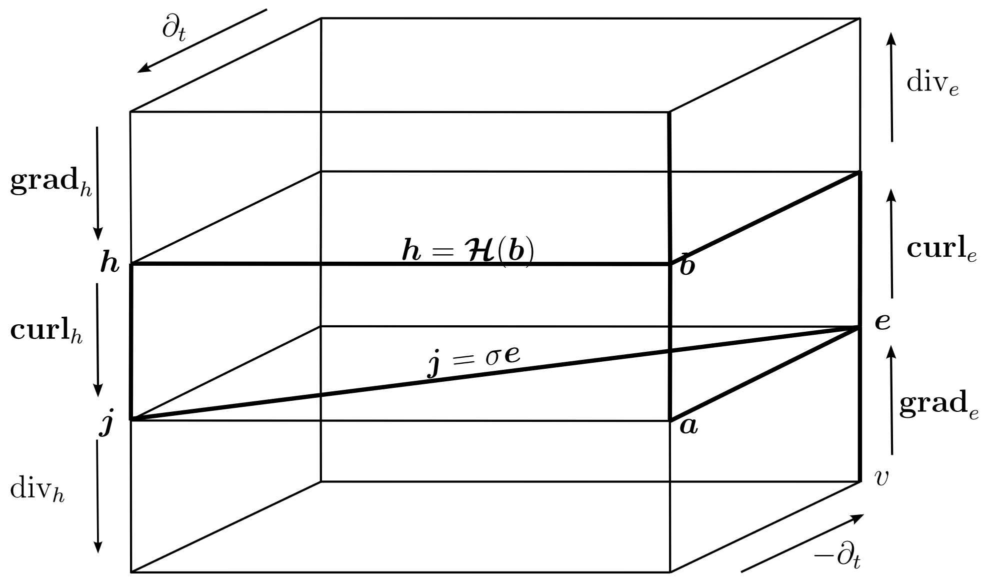

Figure 2.8: Tonti diagram for the magnetic flux density conforming magnetodynamic formulation.

2.5.2 Magnetic flux density conforming formulations: dynamic case

We want to solve (2.35)–(2.39) using the so-called magnetic flux density conforming formulation [64, 169–171]. Thus, we want to satisfy the right branch of the Tonti diagram (2.8) together with the constitutive laws (2.38)-(2.39) in a strong sense. The electric field $\boldsymbol{e}$ and magnetic flux density $\boldsymbol{b}$ can be derived from (2.37) and (2.36):

$$\boldsymbol{b} = \mathbf{curl}\,\boldsymbol{a} \quad \text{and} \quad \boldsymbol{e} = -\partial_t \boldsymbol{a} - \mathbf{grad}\, v, \tag{2.46}$$

where $\boldsymbol{a}$ is the magnetic vector potential and v is the electric scalar potential. We therefore derive the following weak form of Ampère's equation (2.35) [26, 29]: find $\boldsymbol{a} \in \boldsymbol{H}_e(\mathbf{curl}, \Omega)$ such that

$$(\boldsymbol{h}, \mathbf{curl}\,\boldsymbol{a}')_\Omega + \langle \boldsymbol{n} \times \boldsymbol{h}, \boldsymbol{a}' \rangle_{\Gamma_h} = (\boldsymbol{j}, \boldsymbol{a}')_\Omega, \tag{2.47}$$

where $\boldsymbol{a}^{'}$ is a field of test functions independent of time. Using $\boldsymbol{h} = \boldsymbol{\mathcal{H}}(\boldsymbol{b})$ and (2.19) and introducing (2.46) in (2.47); one gets the weak form [26, 29]: find $\boldsymbol{a} \in \boldsymbol{H}_e(\mathbf{curl}, \Omega)$ and $v \in H^1_e(\Omega)$ such that

$$(\boldsymbol{\mathcal{H}}(\mathbf{curl}\,\boldsymbol{a}), \mathbf{curl}\,\boldsymbol{a}')_\Omega + (\sigma\, \partial_t \boldsymbol{a}, \boldsymbol{a}')_{\Omega_c} + (\sigma\, \mathbf{grad}\, v, \boldsymbol{a}')_{\Omega_c} \\ + \langle \boldsymbol{n} \times \boldsymbol{h}, \boldsymbol{a}' \rangle_{\Gamma_h} = (\boldsymbol{j}_s, \boldsymbol{a}')_{\Omega_s}, \tag{2.48}$$

for all $\boldsymbol{a}' \in \boldsymbol{H}^0_e(\mathbf{curl}; \Omega)$. The vector potential $\boldsymbol{a}$ is uniquely defined in the conducting region Ω_c and a gauge condition must be defined in the non-conducting region Ω_c^C. The boundary term in (2.48) contains the tangential component of the magnetic field which is subject to natural boundary condition on Γ_h. It can take several forms [59, 176]: homogenenous Neumann boundary condition, fields associated with the global quantities, trace defining an integral operator used to define an exterior problem, etc. In this thesis we only consider the case of homogeneous Neumann condition. In practice, such Neumann condition can be used for imposing the symmetry condition on a plane crossed by a zero electric current or for imposing homogeneous boundary conditions on a perfect magnetic material, i.e., a material with $\mu \sim \infty$ (section 2.2).

The electric scalar potential v is only defined in the conducting regions Ω_c. Using the test functions $\boldsymbol{a}' = \mathbf{grad}\, v'$ in (2.48) we get the following equation:

$$(\sigma\, \partial_t \boldsymbol{a}, \mathbf{grad}\, v')_{\Omega_c} + (\sigma\, \mathbf{grad}\, v, \mathbf{grad}\, v')_{\Omega_c} \\ = \langle \boldsymbol{n} \times \boldsymbol{h}, \mathbf{grad}\, v' \rangle_{\Gamma_h} = \langle \boldsymbol{n} \cdot \boldsymbol{j}, v' \rangle_{\Gamma_g} \quad \forall v' \in H_e^{10}(\Omega), \quad (2.49)$$

which is also the weak form of $\operatorname{div} \boldsymbol{j} = 0$. The boundary Γ_g in (2.49) has been defined in section 2.4 as the part of Γ_h which is crossed by an electric current.

The two-dimensional case with all currents perpendicular to the two-dimensional section is obtained by assuming the source current density $\boldsymbol{j}_s = j_s(x, y)\mathbf{1}_z$ where $\mathbf{1}_z$ is the unit vector aligned along the z axis. If the electric conductivity tensor σ is such that $\sigma_{13} = 0 = \sigma_{23}$, then z-components of the magnetic field $\boldsymbol{h}$ and of the magnetic flux density $\boldsymbol{b}$ vanish and it is possible to derive the magnetic flux density $\boldsymbol{b}$ from a scalar potential $a_z(\boldsymbol{x}, \boldsymbol{y})$ with $\boldsymbol{a} = a_z \mathbf{1}_z$. In this case the **curl** operator can be expressed in terms of the **grad** operator as $\mathbf{curl} := \mathbf{1}_z \times \mathbf{grad}$ and the magnetic flux density reads $\boldsymbol{b} = \mathbf{curl}\, \boldsymbol{a} = \mathbf{1}_z \times \mathbf{grad}\, a_z$. The weak form of (2.48) and (2.49) becomes: find $a_z \in H_e^1(\Omega)$ and u_r that is constant in each connected conducting region such that

$$(\boldsymbol{\mathcal{H}}(\mathbf{1}_z \times \mathbf{grad}\, a_z), \mathbf{1}_z \times \mathbf{grad}\, a_z^{'})_{\Omega} + (\sigma\, \partial_t a_z, a_z^{'})_{\Omega_c} \\ + (\sigma\, u_r, a_z^{'})_{\Omega_c} + \langle \boldsymbol{n} \times \boldsymbol{h}, a_z^{'} \mathbf{1}_z \rangle_{\Gamma_h} = (j_s, a_z^{'})_{\Omega_s}, \quad (2.50)$$

and

$$(\sigma\, \partial_t a_z, u_r^{'})_{\Omega_c} + (\sigma\, u_r, u_r^{'})_{\Omega_c} = 0 \quad (2.51)$$

for all $a_z^{'} \in H_e^{10}(\Omega)$ and $u_r^{'}$ that is constant for each connected conducting region. The field u_r represents a voltage per unit length.

2.5.3 Magnetic flux density conforming formulations: static case

The magnetostatic case can be derived as a particular case of the magnetodynamic problem where eddy currents are neglected. The following three-dimensional weak form is derived from (2.48): find $\boldsymbol{a} \in \boldsymbol{H}_e(\mathbf{curl}, \Omega)$ such that

$$(\boldsymbol{\mathcal{H}}(\mathbf{curl}\, \boldsymbol{a}), \mathbf{curl}\, \boldsymbol{a}')_{\Omega} + \langle \boldsymbol{n} \times \boldsymbol{h}, \boldsymbol{a}' \rangle_{\Gamma_h} = (\boldsymbol{j}_s, \boldsymbol{a}')_{\Omega_s}, \quad (2.52)$$

for all $\boldsymbol{a}' \in \boldsymbol{H}_e^0(\mathbf{curl}, \Omega)$.

Likewise, the following two-dimensional weak form is derived from (2.50): find $a_z \in H_e^1(\Omega)$ such that

$$(\boldsymbol{\mathcal{H}}(\mathbf{1}_z \times \mathbf{grad}\, a_z), \mathbf{1}_z \times \mathbf{grad}\, a_z^{'})_{\Omega} + \langle \boldsymbol{n} \times \boldsymbol{h}, a_z^{'} \mathbf{1}_z \rangle_{\Gamma_h} = (j_s, a_z^{'})_{\Omega_s}, \quad (2.53)$$

for all $a_z^{'} \in H_e^{10}(\Omega)$.

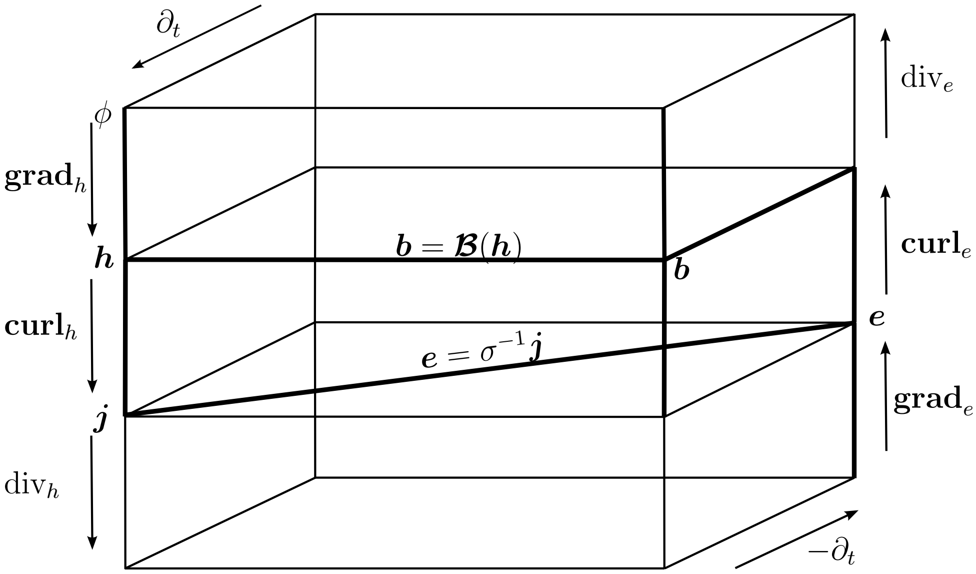

Figure 2.9: Tonti diagram for the magnetic field conforming magnetodynamic formulation.

2.5.4 Magnetic field conforming formulations: dynamic case

In this section we derive magnetic field conforming formulations for (2.35)-(2.39). We want to satisfy the left branch of Tonti diagram (see Figure 2.9) together with the constitutive laws (2.38)-(2.39) in a strong sense. We therefore derive the following weak form for Faraday's equation [32, 33, 63]: find $\boldsymbol{h} \in \boldsymbol{H}_h(\mathbf{curl}, \Omega)$ such that

$$(\partial_t \boldsymbol{b}, \boldsymbol{h}^{'})_\Omega + (\boldsymbol{e}, \mathbf{curl}\, \boldsymbol{h}^{'})_\Omega + \langle \boldsymbol{n} \times \boldsymbol{e}, \boldsymbol{h}' \rangle_{\Gamma_e} = 0 \quad \forall \boldsymbol{h}^{'} \in \boldsymbol{H}_h^0(\mathbf{curl}, \Omega). \tag{2.54}$$

Using Ampère's equation, the magnetic constitutive law (2.21) $\boldsymbol{b} = \boldsymbol{\mathcal{B}}(\boldsymbol{h})$ and Ohm's law in the conducting region $\boldsymbol{e} = \sigma^{-1}\boldsymbol{j} = \sigma^{-1}\mathbf{curl}\, h$, equation (2.54) becomes [32, 33, 63]:

$$(\partial_t \boldsymbol{\mathcal{B}}(\boldsymbol{h}), \boldsymbol{h}^{'})_\Omega + (\sigma^{-1}\mathbf{curl}\, \boldsymbol{h}, \mathbf{curl}\, \boldsymbol{h}^{'})_{\Omega_c} + (\boldsymbol{e}, \mathbf{curl}\, \boldsymbol{h}^{'})_{\Omega_c^C} + \\ \langle \boldsymbol{n} \times \boldsymbol{e}, \boldsymbol{h}' \rangle_{\Gamma_e} = 0 \quad \forall \boldsymbol{h}^{'} \in \boldsymbol{H}_h^0(\mathbf{curl}, \Omega). \tag{2.55}$$

The magnetic field $\boldsymbol{h}$ in Ω_c^C can be decomposed into two components $\boldsymbol{h} = \boldsymbol{h}_s + \boldsymbol{h}_r$ where $\boldsymbol{h}_s$ is the source term that can be computed using (2.32) and $\boldsymbol{h}_r$ is the reaction field. In the non-conducting domain the total field $\boldsymbol{h}$ is governed by:

$$\begin{cases} \mathbf{curl}\, \boldsymbol{h} = \boldsymbol{j}_s & \text{in } \Omega_s \\ \mathbf{curl}\, \boldsymbol{h} = \mathbf{0} & \text{in } \Omega_c^C \setminus \Omega_s. \end{cases} \tag{2.56}$$

Combining (2.32) and (2.57) we can deduce the governing equation for the reaction field $\boldsymbol{h}_r$:

$$\mathbf{curl}\, \boldsymbol{h}_r = \mathbf{0} \qquad \text{in } \Omega_c^C. \tag{2.57}$$

This means that the reaction term $\boldsymbol{h}_r$ can be derived from a magnetic scalar potential ϕ in Ω_c^C. In addition in Ω_c^C, the test functions $\boldsymbol{h}^{'}$ must be chosen in the subspace of

$\boldsymbol{H}_h^0(\mathbf{curl}, \Omega_c^C)$ such that $\mathbf{curl}\, \boldsymbol{h}_r^{'} = \mathbf{0}$ in Ω_c^C. Using Ohm's law in $\Omega_c : \boldsymbol{e} = \sigma^{-1}\boldsymbol{j}$ the weak form (2.55) becomes:

$$(\partial_t \boldsymbol{\mathcal{B}}(\boldsymbol{h}), \boldsymbol{h}^{'})_\Omega + (\sigma^{-1}\mathbf{curl}\, \boldsymbol{h}, \mathbf{curl}\, \boldsymbol{h}^{'})_{\Omega_c} + (\sigma^{-1}\boldsymbol{j}_s, \mathbf{curl}\, \boldsymbol{h}^{'})_{\Omega_s} + \\ \langle \boldsymbol{n} \times \boldsymbol{e}, \boldsymbol{h}' \rangle_{\Gamma_e} = 0 \quad \forall \boldsymbol{h}^{'} \in \boldsymbol{H}_h^0(\mathbf{curl}, \Omega). \tag{2.58}$$

Note that the electric field $\boldsymbol{e}$ is not defined in the non-conducting region Ω_c^C using this equation.

The boundary term contains the tangential component of the electric field which is subject to natural boundary conditions on Γ_e. In this thesis we consider the case of homogeneous Neumann conditions. In practice, this case can be used for imposing the symmetry condition on a plane crossed by a null flux density ($\boldsymbol{n} \times \boldsymbol{e}|_{\Gamma_e} = \mathbf{0} \implies \boldsymbol{n} \cdot \operatorname{div} \boldsymbol{b}|_{\Gamma_e} = 0$). It can also be used to impose homogeneous boundary condition on a perfect conducting material, i.e., a material for which $\sigma \sim \infty$ (section 2.2).

2.5.5 Magnetic field conforming formulations: static case

The magnetostatic problem is derived from the magnetoquasistatic problem by neglecting the time derivatives and the eddy currents. Electric and magnetic problems can then be decoupled and problem (2.35)-(2.39) becomes:

$$\mathbf{curl}\, \boldsymbol{h} = \boldsymbol{j}_s, \tag{2.59}$$

$$\operatorname{div} \boldsymbol{b} = \mathbf{0}, \tag{2.60}$$

$$\boldsymbol{b}(\boldsymbol{x}) = \boldsymbol{\mathcal{B}}(\boldsymbol{h}(\boldsymbol{x}), \boldsymbol{x}). \tag{2.61}$$

We want to satisfy Ampère's equation and the constitutive law in a strong sense. Using results of section (2.5.4) we get $\boldsymbol{h} = \boldsymbol{h}_s + \boldsymbol{h}_r$ where the reaction magnetic field satisfies $\boldsymbol{h}_r = \mathbf{0}$ in Ω_c^C. It can be derived from a scalar potential ϕ as:

$$\boldsymbol{h}_r = -\mathbf{grad}\, \phi. \tag{2.62}$$

In the case the domain Ω_c^C is not simply connected, the derivation is valid after defining cuts that make it simply connected [59, 176]. The weak form of Gauss equation then reads: find $\phi \in H_h^1(\Omega)$ such that

$$(\boldsymbol{\mathcal{B}}(\boldsymbol{h}_s - \mathbf{grad}\, \phi), \mathbf{grad}\, \phi')_\Omega + \langle \boldsymbol{n} \cdot \boldsymbol{b}, \phi' \rangle_{\Gamma_h} = 0, \tag{2.63}$$

for all test functions $\phi' \in H_h^{10}(\Omega)$.

Chapter 3

Homogenization theory

3.1 Introduction

In this chapter, we apply the classical homogenization theory to derive homogenized problems for Maxwell's equations. The theory is introduced progressively to solve more and more complex problems (i.e. problems involving complex geometries and nonlinear constitutive laws). We present results of simple effective medium theory (Maxwell–Garnett and Bruggeman models) and then develop the asymptotic homogenization method for the div $-$ **grad** and **curl** $-$ **curl** problems. We also summarize results for the two-scale convergence and the periodic unfolding methods.

Results from the asymptotic homogenization method will be used in chapter 4 for computing the homogenized material law for linear materials and those from the two-scale convergence and the periodic unfolding methods will be used for the homogenization of Maxwell's equations as well as the computation of the homogenized material law for nonlinear materials.

The chapter is organized as follows: section 3.2 provides the state of art of homogenization methods and convergence theories. Particular attention is paid to three methods: the effective medium theory in section 3.3, the asymptotic homogenization method in section 3.4 and the two-scale convergence and the periodic unfolding methods in section 3.5.

3.2 Generalities

Homogenization theory is a mathematical formalism used for solving problems with structures on multiple scales. These problems may arise when modeling physical phenomena in mechanics, chemistry, electromagnetism, fluid dynamics, etc. The modeling process leads to defining an equation of the form:

$$\mathcal{A}^{\varepsilon} u^{\varepsilon} = f, \tag{3.1}$$

where $\mathcal{A}^{\varepsilon} : \mathcal{V} \to \mathcal{V}'$ is an operator (linear or not) acting on the unknown fields u^{ε} that vary on a very small spatial scale "ε", from the function space $\mathcal{V}$ into its dual

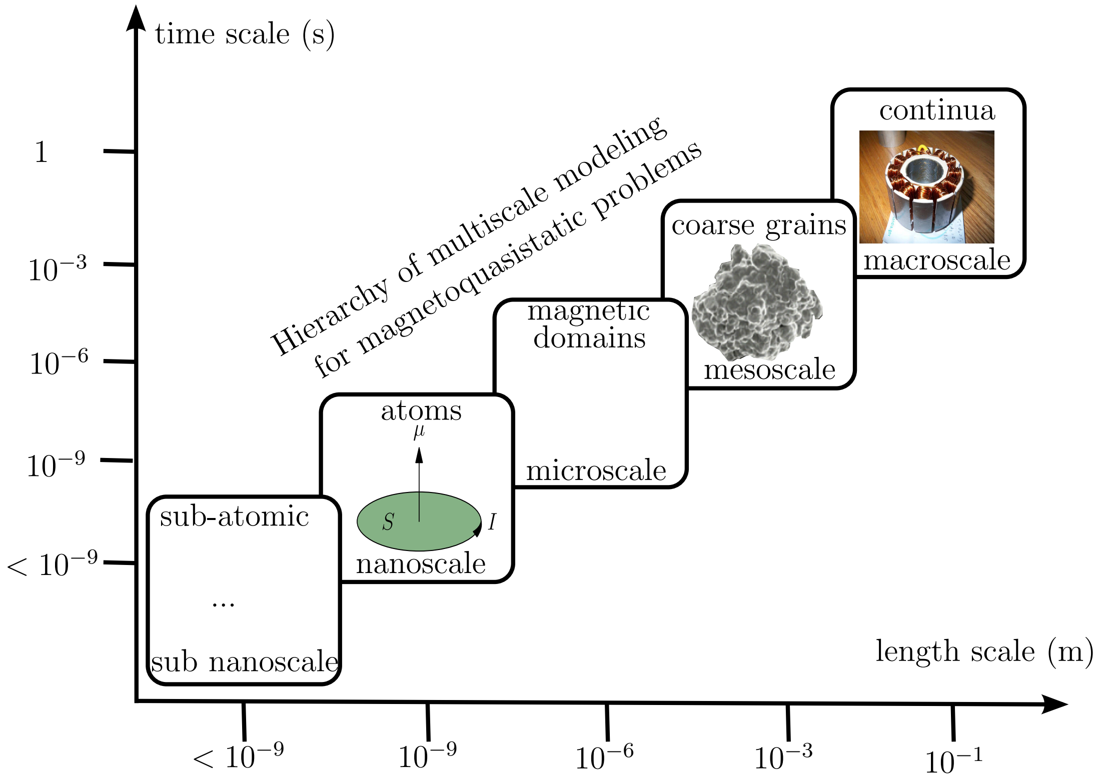

Figure 3.1: The homogenization theory may involve different scales with different physical models (image inspired by [42, 111]).

$\mathcal{V}'$.

Problem (3.1) may involve differential equations (ordinary or partial) and the operator $\mathcal{A}^\varepsilon$ may possibly contain information about the initial and/or boundary conditions necessary for ensuring the well-posedness of the problem. The multiscale aspect is referred to by means of the superscript "ε". Scales involved can range from the nanoscale to the macroscale (Figure 3.1). Numerically solving the multiscale problem (3.1) at the finest scale is usually extremely expensive in terms of computational time and memory storage. Homogenization theory aims at replacing this original problem by the following homogenized macroscopic problem:

$$\mathcal{A}_M u_M = f, \tag{3.2}$$

where the dependency with ε has been eliminated and that can be "cheaply" solved. In (3.2), the operator $\mathcal{A}_M$ is the homogenized operator of $\mathcal{A}^\varepsilon$ and u_M captures the slow component of u^ε. Adapted convergence theories have been developed for proving the convergence of fields across scales, including fields that result from the application of differential operators (e.g. **grad**, **curl** and div) and integral functionals (e.g. global quantities).

In this thesis we focus on problems governed by partial differential equations which involve the mesoscale and the macroscale. We are especially interested by the magnetoquasistatic multiscale problem:

$$\mathbf{curl}\,\boldsymbol{h}^\varepsilon = \boldsymbol{j}^\varepsilon, \tag{3.3}$$

$$\mathbf{curl}\,\boldsymbol{e}^\varepsilon = -\partial_t \boldsymbol{b}^\varepsilon, \tag{3.4}$$

$$\operatorname{div} \boldsymbol{b}^\varepsilon = \mathbf{0}, \tag{3.5}$$

$$\boldsymbol{b}^\varepsilon(\boldsymbol{x},t) = \boldsymbol{\mathcal{B}}(\boldsymbol{h}^\varepsilon(\boldsymbol{x},t), \boldsymbol{x}, \frac{\boldsymbol{x}}{\varepsilon}), \tag{3.6}$$

$$\boldsymbol{j}^\varepsilon(\boldsymbol{x},t) = \boldsymbol{\mathcal{J}}(\boldsymbol{e}^\varepsilon(\boldsymbol{x},t), \boldsymbol{x}, \frac{\boldsymbol{x}}{\varepsilon}), \tag{3.7}$$

that results from the magnetoquasistatic problem of section 2.5, where $\frac{\boldsymbol{x}}{\varepsilon}$ is introduced to denote possibly rapid fluctuations in the constitutive laws. Examples of application of this problem involve the computation of fields in multiscale materials such as laminated structures, soft magnetic composites and soft ferrites (see Figure 1.2).

In the next paragraphs we briefly describe the Γ-convergence, the G-convergence and the H-convergence methods. In the rest of the chapter we give more details about the effective medium theory (section 3.3), the asymptotic expansion method (section 3.4), the two-scale convergence and the periodic unfolding method (section 3.5).

Γ-convergence concerns the convergence of sequences of minimization problems. The sequence is indexed by "ε" due to the change of the geometry or of the material law. Γ-convergence can only be derived for problems that can be written as minimization problems of some energy functional $\Phi^\varepsilon(v)$. Under coercivity and compactness assumptions on the functional and some additional assumptions on the structure of the space $\mathcal{V}$ of the solution u^ε, it can be shown that:

$$\arg\min_{v\in\mathcal{V}} \Phi^\varepsilon(v) = u^\varepsilon \underset{\varepsilon\to 0}{\to} u_M = \arg\min_{v\in\mathcal{V}} \Phi_M(v), \tag{3.8}$$

where the notation $\arg\min_{v\in\mathcal{V}} \Phi^\varepsilon(v)$ is used to denote the set of all u^ε in $\mathcal{V}$ for which the functional $\Phi^\varepsilon(v)$ attains its smallest value and where $\Phi_M(v)$ is the homogenized energy functional that may eventually include the homogenized material law obtained by solving a cell problem. Γ-convergence is well defined for convex functionals. In this case, the average minimal energy obtained solving the cell problem on periodicity cells $k\mathcal{Y}$ (with $k = 1, 2, ...$) is the same [121]. For non-convex functionals, Muller [136] has shown that there exists a number k (a priori unknown) of periodicity cells $k\mathcal{Y}$ that minimizes the energy functional. In this case the homogenization depends on the size of the cell even for periodic structures.

G-convergence and H-convergence have been introduced by Spagnolo [183] and Murat [139], respectively. The letters G stands for Green (as in Green kernel) and H stands for homogenization. G-convergence concerns the convergence of operators for symmetric problems for which there exist Green kernels and H-convergence extends G-convergence to non-symmetric problems. Back to problem (3.1), we have a sequence of operators $\mathcal{A}^\varepsilon$ that, when applied to the sequence $u^\varepsilon \in \mathcal{V}$ gives $f \in \mathcal{V}'$.

If the space $\mathcal{V}$ has an appropriate structure the sequence u^ε converges to u_M. G-convergence and H-convergence theories allow to determine conditions under which the operator $\mathcal{A}^\varepsilon$ converges to the operator $\mathcal{A}_M$ such that $\mathcal{A}_M u_M = f$ for all f in $\mathcal{V}'$.

References [58, 185] contain a brief history of homogenization and convergence methods. More details can also be found in [51, 56] for the Γ-convergence and in [139,140,154,157,183,184,188–190] for the G-convergence and the H-convergence. In the next sections, we present the effective medium theory, the asymptotic expansion method, the two-scale convergence and the periodic unfolding method as results from these methods will be used in the remainder of the thesis. We use the following criteria for comparing these methods:

1. the possibility to deal with problem (3.3)–(3.7) involving **curl** operators;
2. the possibility to derive a homogenized problem that can be easily solved;
3. the possibility to handle nonlinearities. For magnetic materials, three constitutive laws are used to illustrate the complexity of deriving a homogenized problem: a linear material law, a nonlinear reversible material law and a nonlinear irrevesible law;
4. the possibility to deal with materials with complex microstructures. Figure 1.2 shows some of the structures of magnetic materials that can be involved in various electromagnetic applications. The applications for these materials range from low to medium frequencies;
5. the possibility to recover local fields in critical points of interest. An example of such critical points occur in transfomers where one may want to verify if the value is smaller than some breakdown value of the electric field;
6. the possibility to compute global quantities such as the eddy current or the magnetic losses.

Another desirable property is the possibility to account for the realistic random distribution of heterogeneities in multiscale materials. For our theoretical developments we consider the case of periodic media i.e. those media made of a repetitive periodic cell. This assumption is realistic for periodic structures (e.g.: laminated structures) and for points located away from the domain boundary. In the computational homogenization developed in chapter 4, we extend its use to non-periodic media (soft magnetic composites, soft ferrites, etc.) by choosing an equivalent periodic periodicity cell $\mathcal{Y}$. Note however that for the non-periodic media with a deterministic or a probabilistic distribution of heterogeneities, stochastic approaches have been developed for the asymptotic expansion method [20], the Γ-convergence method [52], the G-convergence and the H-convergence [157] and the two-scale convergence [44, 106, 144].

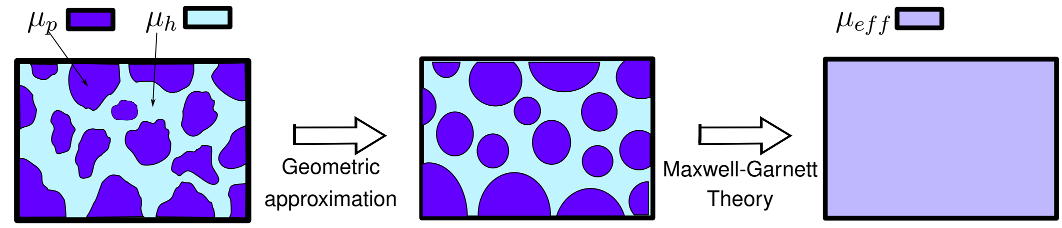

Figure 3.2: Diagram explaining the derivation of the effective medium using the Maxwell-Garnett theory.

3.3 Effective medium theory

The theory of effective medium can be used for computing the homogenized properties of a composite with only a limited quantity of information on the microstructure. A medium with a microstructure comprises a matrix with magnetic permeability μ_h and (complex-shaped) inclusions with magnetic permeability μ_p. These inclusions are replaced by simple shapes (e.g.: spheres, ellipsoids, cylinders, ...) for which the problem of inclusion in a matrix has an exact solution. The considered geometries of inclusions can allow to account for the anisotropy of the material laws. For instance, the anisotropy of the distribution of phases leads to anisotropy of material laws. Several variants of the theory can be found in the litterature. These theories include the Maxwell–Garnett model [122], the Clausius-Mossotti model [48,134], the Rayleigh model [168], the Bruggeman model [131], the coherent potential approximation model [112], etc. Herein we give details about the Maxwell-Garnett and the Bruggeman models.

3.3.1 Maxwell-Garnet model

The Maxwell-Garnett model is well suited for the case of materials with a small volume ratio of inclusion f. The principle of the method is described on the figure 3.2. Two phases are considered: the matrix and the inclusions with respective permeabilities μ_h and μ_p. The effective magnetic permeability relates the homogenized magnetic flux density $\boldsymbol{b}_M$ to the homogenized magnetic field $\boldsymbol{h}_M$ by the formula:

$$\boldsymbol{b}_M = \mu_{eff}\boldsymbol{h}_M. \tag{3.9}$$

The macroscale fields $\boldsymbol{h}_M$ and $\boldsymbol{b}_M$ are given by:

$$\boldsymbol{h}_M = f\boldsymbol{h}_p + (1-f)\boldsymbol{h}_h, \qquad \boldsymbol{b}_M = f\mu_p\boldsymbol{h}_p + (1-f)\mu_h\boldsymbol{h}_h, \tag{3.10}$$

where $\boldsymbol{h}_p, \boldsymbol{h}_h$ are values of the magnetic field in the inclusion and in the matrix, respectively and f is the volume ratio. The solution of the problem for spherical inclusion relates the fields $\boldsymbol{h}_h$ and $\boldsymbol{h}_p$ as [181]:

$$\boldsymbol{h}_p = \frac{3\mu_h}{\mu_p + 2\mu_p}\boldsymbol{h}_h, \tag{3.11}$$

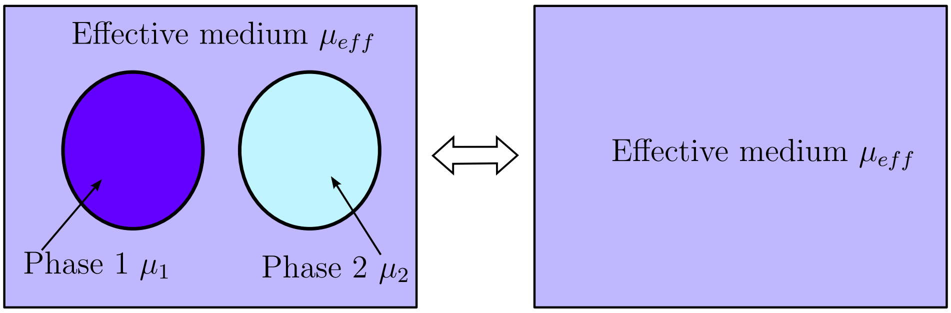

$$\boldsymbol{b} = \mu_{eff}\boldsymbol{h} + \mu_1\boldsymbol{\mathcal{M}}_1 + \mu_2\boldsymbol{\mathcal{M}}_2 \quad = \quad \boldsymbol{b} = \mu_{eff}\boldsymbol{h}$$

Figure 3.3: Diagram explaining the derivation of the effective medium using Bruggeman's approach.

and therefore the following effective magnetic permeability is derived:

$$\mu_{eff} = \mu_h + 3\mu_h \frac{\mu_p - \mu_h}{\mu_p - 2\mu_h - f(\mu_p - \mu_h)}. \tag{3.12}$$

3.3.2 Bruggeman model

In the Bruggeman model, the two phases can play the same role and therefore they can be used either as the inclusion or the matrix. The model is therefore valid even at high values of volume ratio. The model then consists in replacing the external medium to each inclusion by an equivalent effective medium computed in an auto-coherent way (Figure 3.3). The idea of Bruggeman is to assume the existence of this effective medium such that the magnetic induction resulting from the magnetization of the 2 spheres cancels i.e. $\mu_1\boldsymbol{\mathcal{M}}_1 + \mu_2\boldsymbol{\mathcal{M}}_2 = \boldsymbol{0}$. This allows to derive the formula [181]:

$$(1-f)\frac{\mu_1 - \mu_{eff}}{\mu_1 + 2\mu_{eff}} + f\frac{\mu_2 - \mu_{eff}}{\mu_2 + 2\mu_{eff}}. \tag{3.13}$$

3.3.3 Advantages and limitations of the effective medium theory

The main advantage of the effective medium theory presented in this section is its ability to easily to derive the effective properties. However, the approach is only adapted for linear problems with a small contrast of material properties between different phases. [49]

As presented above, the method does not account for the distribution of heterogeneities in the microstructure. This means that two microstructures with the same volume ratio of inclusion but with different distribution of phases will yield the same effective quantities.

Mean field homogenization [50, 117–119] uses semi-analytical results from the effective medium [21, 99, 133] at the mesoscale level for computing homogenized constitutive laws used for numerically solving the macroscale problem. This technique initially used for linear problems has evolved over the last decade and extended to nonlinear problems. To our best knowledge, it has not yet been used in electromagnetism for problems with high nonlinearity/hysteresis. Using this method, it is possible to get more accurate effective quantities by providing additional information of the distribution of phases [50]. Extension to high frequency problems with consideration of eddy currents at the level of inclusions has been proposed [163, 165, 166]. The accuracy of the mesoscale solution obtained using this method may sometimes be bad. [164] [165]

3.4 Asymptotic expansion method

The asymptotic homogenization method is a constructive method that can be used for homogenizing linear problems. The idea of the method is to split the physical coordinate system $\boldsymbol{x}$ into a coarse-scale and a fine-scale coordinate system $(\boldsymbol{x}, \boldsymbol{y})$ where $\boldsymbol{y} = \dfrac{\boldsymbol{x}}{\varepsilon}$ is used for capturing the rapid fluctuations of the solution and then expand the operator $\mathcal{A}^\varepsilon$ and the unknown field u^ε in terms of the powers of a small parameter ε. We treat $\boldsymbol{x}$ and $\boldsymbol{y}$ as independent variables.

In order to construct the homogenized problem of (3.1) the following expansion for the solution is assumed:

$$u^\varepsilon(\boldsymbol{x}) = u_0(\boldsymbol{x}, \boldsymbol{y}) + \varepsilon u_1(\boldsymbol{x}, \boldsymbol{y}) + \varepsilon^2 u_2(\boldsymbol{x}, \boldsymbol{y}) + \ldots = \sum_{i=0}^{\infty} \varepsilon^i u_i(\boldsymbol{x}, \boldsymbol{y}), \tag{3.14}$$

with $u_i(\boldsymbol{x}, \boldsymbol{y})$ that are periodic in the variable $\boldsymbol{y}$ (they are said to be Y-periodic with the basic cell denoted by Y). We also use the differentiation rule:

$$\frac{\partial}{\partial \boldsymbol{x}} u_i(\boldsymbol{x}, \boldsymbol{y}) := \frac{\partial}{\partial \boldsymbol{x}} u_i(\boldsymbol{x}, \boldsymbol{y}) + \varepsilon^{-1} \frac{\partial}{\partial \boldsymbol{y}} u_i(\boldsymbol{x}, \boldsymbol{y}), \tag{3.15}$$

for all the derivatives appearing in $\mathcal{A}^\varepsilon$. The **grad**, **curl** and div operators are transformed accordingly:

$$\mathbf{grad} \quad \rightarrow \mathbf{grad}_x + \varepsilon^{-1} \mathbf{grad}_y, \tag{3.16}$$

$$\mathbf{curl} \quad \rightarrow \mathbf{curl}_x + \varepsilon^{-1} \mathbf{curl}_y, \tag{3.17}$$

$$\mathrm{div} \quad \rightarrow \mathrm{div}_x + \varepsilon^{-1} \mathrm{div}_y. \tag{3.18}$$

Applying (3.15) to (3.14), it is then possible to gather terms with the same powers of ε and derive the homogenized macroscale equation and a cell problem that can be used to calculate the homogenized operator $\mathcal{A}_0$.

3.4.1 Elliptic equations

In order to illustrate the asymptotic homogenization method, we consider the following div-**grad** and **curl**-**curl** problems with homogeneous boundary conditions:

$$\begin{cases} -\mathrm{div}\,(a^\varepsilon \mathbf{grad}\, u^\varepsilon) + a_0^\varepsilon u^\varepsilon = f & \text{in } \Omega \\ u^\varepsilon = 0 & \text{on } \Gamma. \end{cases} \tag{3.19}$$

$$\begin{cases} \mathbf{curl}\,(a^\varepsilon \mathbf{curl}\, \boldsymbol{u}^\varepsilon) + a_1^\varepsilon \boldsymbol{u}^\varepsilon = \boldsymbol{f} & \text{in } \Omega \\ \boldsymbol{n} \times \boldsymbol{u}^\varepsilon = 0 & \text{on } \Gamma. \end{cases} \tag{3.20}$$

The extension to problems with non-homogeneous boundary conditions is straightforward [20].

The quantities $a^\varepsilon, a_0^\varepsilon$ and a_1^ε are assumed to be $\mathcal{Y}$-periodic, depend only on the coordinate $\boldsymbol{y}$ (i.e. of the form $K^\varepsilon = K(\frac{\boldsymbol{x}}{\varepsilon})$) and bounded on the periodicity cell $\mathcal{Y}$. It is also assumed that there exist c, c_0 and $\alpha_0 \in \mathbb{R}^+$ such that

$$c|\boldsymbol{\xi}|^2 \leq \boldsymbol{\xi}^T a(\boldsymbol{y})\boldsymbol{\xi} \quad , \quad c_0|\boldsymbol{\xi}|^2 \leq \boldsymbol{\xi}^T a_1(\boldsymbol{y})\boldsymbol{\xi} \quad \text{and} \quad \alpha_0 \leq a_0(\boldsymbol{y}), \tag{3.21}$$

for all $\boldsymbol{\xi}$ in $\mathbb{R}^3$. The case of non-uniformly oscillating coefficients $K(\boldsymbol{x}, \frac{\boldsymbol{x}}{\varepsilon})$ and the case of reiterated homogenization $K^\varepsilon = K(\boldsymbol{x}, \frac{\boldsymbol{x}}{\varepsilon}, \frac{\boldsymbol{x}}{\varepsilon^2}, ..., \frac{\boldsymbol{x}}{\varepsilon^n})$ can be treated using a similar approach [20, 154]. Source terms f and $\boldsymbol{f}$ are also assumed to be regular enough (e.g. $f \in H^{-1}(\Omega)$ and $\boldsymbol{f} \in \boldsymbol{L}^2(\Omega)$) and the boundary Γ is smooth enough (e.g. Lipschitz continuous). Conditions (3.21) allow to define a coercive, bounded bilinear form that guarantees the existence and the uniqueness of the solution by the Lax-Milgram theorem [40, 85].

3.4.1.1 The div-grad problem

Applying (3.16)–(3.18) to the div $-$ **grad** operator in (3.19), we get the operator:

$$\mathcal{A} = \varepsilon^{-2}\mathcal{A}_0 + \varepsilon^{-1}\mathcal{A}_1 + \mathcal{A}_2, \tag{3.22}$$

where:

$$\mathcal{A}_0 = -\mathrm{div}_y \Big(a(\boldsymbol{y})\mathbf{grad}_y\Big), \tag{3.23}$$

$$\mathcal{A}_1 = -\mathrm{div}_y \Big(a(\boldsymbol{y})\mathbf{grad}_x\Big) - \mathrm{div}_x \Big(a(\boldsymbol{y})\mathbf{grad}_y\Big), \tag{3.24}$$

$$\mathcal{A}_2 = -\mathrm{div}_x \Big(a(\boldsymbol{y})\mathbf{grad}_x\Big) + a_0(\boldsymbol{y}). \tag{3.25}$$

Applying this operator to the expression (3.14), we get the following system of equations after identifying terms with the same power of ε:

$$\mathcal{O}(\varepsilon^{-2}) : \mathcal{A}_0 u_0(\boldsymbol{x}, \boldsymbol{y}) = 0, \tag{3.26}$$

$$\mathcal{O}(\varepsilon^{-1}) : \mathcal{A}_0 u_1(\boldsymbol{x}, \boldsymbol{y}) + \mathcal{A}_1 u_0(\boldsymbol{x}, \boldsymbol{y}) = 0, \tag{3.27}$$

$$\mathcal{O}(\varepsilon^{0}) : \mathcal{A}_0 u_2(\boldsymbol{x}, \boldsymbol{y}) + \mathcal{A}_1 u_1(\boldsymbol{x}, \boldsymbol{y}) + \mathcal{A}_2 u_0(\boldsymbol{x}, \boldsymbol{y}) = f, \tag{3.28}$$

$$\mathcal{O}(\varepsilon^i) : \mathcal{A}_0 u_{i+2}(\boldsymbol{x},\boldsymbol{y}) + \mathcal{A}_1 u_{i+1}(\boldsymbol{x},\boldsymbol{y}) + \mathcal{A}_2 u_i(\boldsymbol{x},\boldsymbol{y}) = 0 \ \ ; i = 1, 2, ... \tag{3.29}$$

For having a unique, $\mathcal{Y}$-periodic solution (up to an additive constant) in any equation of the form $\mathcal{A}_0 u_i(\boldsymbol{x},\boldsymbol{y}) = g$, the following condition must be fulfilled:

$$\int_Y g \,\mathrm{d}y = \int_Y \mathcal{A}_0 u_i(\boldsymbol{x},\boldsymbol{y}) \,\mathrm{d}y = \int_{\partial Y} \boldsymbol{n} \cdot \Big(a(\boldsymbol{y}) \mathbf{grad}_y \, u_i(\boldsymbol{x},\boldsymbol{y}) \Big) \mathrm{d}y = 0 \tag{3.30}$$

for all $\boldsymbol{x} \in \Omega$. This condition results from the Gauss theorem and the ε-periodicity of $u_i(\boldsymbol{x},\boldsymbol{y})$ and $a(\boldsymbol{y})$. Now, let us examine equations corresponding to different powers of ε.

Order $\mathcal{O}(\varepsilon^{-2})$: applying (3.30) to (3.26), we deduce that $u_0(\boldsymbol{x},\boldsymbol{y})$ must be independent from the $\boldsymbol{y}$ coordinate i.e.:

$$u_0(\boldsymbol{x},\boldsymbol{y}) = u_0(\boldsymbol{x}). \tag{3.31}$$

Order $\mathcal{O}(\varepsilon^{-1})$: plugging (3.31) into (3.27) we get:

$$\mathcal{A}_0 u_1 \mathrm{d}y = -\mathrm{div}_y \, a(\boldsymbol{y}) \mathbf{grad}_x \, u_0(\boldsymbol{x}). \tag{3.32}$$

Notice that the right hand side of (3.32) can be separated in terms depending only on $\boldsymbol{x}$ and $\boldsymbol{y}$. Thanks to the linearity of the operator $\mathcal{A}_0$ the method of separation of variables can be used to solve (3.32). The resolution consists in solving the following cell problem [20]: find $\chi^i \in \boldsymbol{H}^1(\mathcal{Y})$ such that

$$\mathcal{A}_0 \chi^i(\boldsymbol{y}) = -\mathrm{div}_y \, a(\boldsymbol{y}) \boldsymbol{e}_i. \tag{3.33}$$

Problem (3.33) is the so-called cell problem and the field $\chi^i(\boldsymbol{y})$ is used to compute the homogenized quantity a^h. It is obtained by applying a unit source term in the direction $\boldsymbol{e}_i$ with $\boldsymbol{e}_1 = (1,0,0), \boldsymbol{e}_2 = (0,1,0)$ and $\boldsymbol{e}_3 = (0,0,1)$. The first order term $u_1(\boldsymbol{x},\boldsymbol{y})$ is deduced:

$$u_1(\boldsymbol{x},\boldsymbol{y}) = \boldsymbol{\chi}(\boldsymbol{y}) \cdot \mathbf{grad}_x \, u_0(\boldsymbol{x}) + \widetilde{u}_1(\boldsymbol{x}), \tag{3.34}$$

with $\boldsymbol{\chi}(\boldsymbol{y}) = (\chi^1(\boldsymbol{y}), \chi^2(\boldsymbol{y}), \chi^3(\boldsymbol{y}))$.

Order $\mathcal{O}(\varepsilon^{0})$: To get macroscale equations, we apply (3.30) to (3.28):

$$\int_Y \mathcal{A}_0 u_2(\boldsymbol{x},\boldsymbol{y}) \mathrm{d}y = \int_Y \Big(f - \mathcal{A}_1 u_1(\boldsymbol{x},\boldsymbol{y}) - \mathcal{A}_2 u_0(\boldsymbol{x},\boldsymbol{y}) \Big) \mathrm{d}y = 0. \tag{3.35}$$

Replacing $u_1(\boldsymbol{x},\boldsymbol{y})$ by (3.34) in (3.35) we get the following macroscale equation:

$$-\,\mathrm{div}_x \Big(a^h \mathbf{grad}_x \, u_0(\boldsymbol{x}) \Big) + a_0^h u_0(\boldsymbol{x}) = f, \tag{3.36}$$

where a^h and a_0^h are the so-called homogenized quantities given by [20]:

$$a^h = \frac{1}{|Y|} \int_Y a(\boldsymbol{y})(\bar{\bar{\mathbf{1}}} - \mathbf{grad}_y \, \boldsymbol{\chi}(\boldsymbol{y})) \mathrm{d}y, \tag{3.37}$$

$$a_0^h = \frac{1}{|Y|}\int_Y a_0(\boldsymbol{y})\mathrm{d}y, \tag{3.38}$$

where $\bar{\bar{\mathbf{1}}}$ is the identity matrix. In (3.37)–(3.38), $|Y|$ denotes the size of the periodic cell Y. Equations in $\mathcal{O}(\varepsilon^i), i = 1, 2, ...$ can be solved to get the higher order corrector terms. More details on these developments can be found in [20].

3.4.1.2 The curl-curl problem

Applying (3.16)–(3.18) to the **curl-curl** problem (3.20) leads to expressions similar to (3.23)–(3.25) but with different operators:

$$\mathcal{A}_0 = -\mathbf{curl}_y\Big(a(\boldsymbol{y})\mathbf{curl}_y\Big), \tag{3.39}$$

$$\mathcal{A}_1 = -\mathbf{curl}_y\Big(a(\boldsymbol{y})\mathbf{curl}_x\Big) - \mathbf{curl}_x\Big(a(\boldsymbol{y})\mathbf{curl}_y\Big), \tag{3.40}$$

$$\mathcal{A}_2 = -\mathbf{curl}_x\Big(a(\boldsymbol{y})\mathbf{curl}_x\Big) + a_1(\boldsymbol{y}), \tag{3.41}$$

It is again possible to examine the equations corresponding to different powers of ε. From the **curl** − **curl** equation equivalent to (3.26) and (3.27), it can be shown that:

$$\mathbf{curl}_y\, \boldsymbol{u}_0(\boldsymbol{x}, \boldsymbol{y}) = \mathbf{0}, \qquad \mathrm{div}_y\, \boldsymbol{u}_0(\boldsymbol{x}, \boldsymbol{y}) = 0, \tag{3.42}$$

meaning that $\boldsymbol{u}_0(\boldsymbol{x}, \boldsymbol{y})$ is independent from $\boldsymbol{y}$. Equation (3.27) in the **curl-curl** context becomes:

$$\mathcal{A}_0\boldsymbol{u}_1(\boldsymbol{x}, \boldsymbol{y}) = -\mathbf{curl}_y\, a(\boldsymbol{y})\mathbf{curl}_x\, \boldsymbol{u}_0(\boldsymbol{x})). \tag{3.43}$$

Two options that lead to dual definitions of the homogenized quantities are then available [20]:

1. The first one consists in defining a div-**grad** cell problem: find $\chi^i \in \boldsymbol{H}^1(\mathcal{Y})$ such that
$$\mathrm{div}_y\Big(a^{-1}(\boldsymbol{y})(\mathbf{grad}_y\, \chi_i(\boldsymbol{y}) - \boldsymbol{e}_i)\Big) = 0, \tag{3.44}$$
and then solve the macroscale equation:
$$\mathbf{curl}_x\Big(((a^{-1})^h)^{-1}\mathbf{curl}_x\, \boldsymbol{u}_0(\boldsymbol{x})\Big) + a_1^h\boldsymbol{u}_0(\boldsymbol{x}) = \boldsymbol{f}, \tag{3.45}$$
where the homogenized tensors $(a^{-1})^h$ and a_1^h are obtained by replacing $a(\boldsymbol{y})$ by $a^{-1}(\boldsymbol{y})$ and $a_0(\boldsymbol{y})$ by $a_1(\boldsymbol{y})$ in (3.37)–(3.38).

2. The second consists in defining a **curl-curl** cell problem: find $\boldsymbol{\chi}^i \in \boldsymbol{H}(\mathrm{div}\, 0, \mathcal{Y})$ such that
$$\mathbf{curl}_y\Big(a(\boldsymbol{y})(\mathbf{curl}_y\, \boldsymbol{\chi}_i(\boldsymbol{y}) - \boldsymbol{e}_i)\Big) = 0, \tag{3.46}$$
and then solve the macroscale equation:
$$\mathbf{curl}_x\Big(a^h\mathbf{curl}_x\, \boldsymbol{u}_0(\boldsymbol{x})\Big) + a_1^h\boldsymbol{u}_0(\boldsymbol{x}) = \boldsymbol{f}, \tag{3.47}$$

where the homogenized a^h and a_1^h are given by:

$$a^h = \frac{1}{|Y|}\int_Y a(\boldsymbol{y})(\bar{\bar{\mathbf{1}}} - \mathbf{curl}_y\,\boldsymbol{\chi}(\boldsymbol{y}))\mathrm{d}y, \tag{3.48}$$

$$a_1^h = \frac{1}{|Y|}\Big(\int_Y a_1(\boldsymbol{y})\mathrm{d}y\Big), \tag{3.49}$$

with

$$\boldsymbol{\chi}(\boldsymbol{y}) = (\boldsymbol{\chi}^1(\boldsymbol{y}), \boldsymbol{\chi}^2(\boldsymbol{y}), \boldsymbol{\chi}^3(\boldsymbol{y})). \tag{3.50}$$

Further details on these developments can be found in [20]. In this thesis, we consider a linear electric constitutive law $\boldsymbol{j} = \sigma\boldsymbol{e}$ and therefore the results of mesoscale problems (3.37) and (3.48) can be used to calculate the electrical homogenized conductivity and resistivity.

3.4.2 Parabolic equations

The analysis for the parabolic case is quite similar to the analysis for elliptic equations developed in section 3.4.1. In this case, we assume the div-**grad** problem:

$$\partial_t u^\varepsilon - \mathrm{div}\,(a^\varepsilon \mathbf{grad}\, u^\varepsilon) = f \text{ in } \Omega_T, \tag{3.51}$$

and the **curl-curl** equation:

$$\partial_t \boldsymbol{u}^\varepsilon + \mathbf{curl}\,(a^\varepsilon \mathbf{curl}\, \boldsymbol{u}^\varepsilon) = \boldsymbol{f} \text{ in } \Omega_T, \tag{3.52}$$

where $\Omega_T = \Omega\times]0,T[$.

In order to have a well-posed problem, equations (3.51) and (3.52) must be completed with appropriate initial conditions in Ω for $t = 0$ and appropriate boundary conditions on Γ_T.

For the sake of simplicity, let us consider the case of coefficients a^ε that are independent of time. In addition, assume that conditions (3.21) are respected. In this case, the div-**grad** homogenized equation becomes:

$$\partial_t u_0 - \mathrm{div}_x \left(a^h \mathbf{grad}_x\, u_0\right) = f, \tag{3.53}$$

with a^h given by (3.37). The **curl-curl** homogenized equation reads:

$$\partial_t \boldsymbol{u}_0 + \mathbf{curl}_x \left(a^h \mathbf{curl}_x\, \boldsymbol{u}_0\right) = \boldsymbol{f}, \tag{3.54}$$

with a^h given by (3.48).

The case of (multiscale) time-dependent coefficients and reiterated homogenization $a^\varepsilon(t,\boldsymbol{x}) = a(t, \frac{t}{\varepsilon^k}, \frac{t}{\varepsilon^{2k}}, ...\boldsymbol{x}, \frac{\boldsymbol{x}}{\varepsilon}, \frac{\boldsymbol{x}}{\varepsilon^2}...)$ leads to the same equations as (3.53) and (3.54) [20, 204]. However depending on the values of k, the cell problem may be time-dependent.

3.4.3 Advantages and limitations of the asymptotic expansion method

The asymptotic homogenization method developed in this section can be used to construct the homogenized problem: equations (3.36) , (3.45) and (3.47) have been derived for the elliptic case while equations (3.53) and (3.54) have been derived for the parabolic case. The method has been derived for materials with linear constitutive laws and with periodic microstructures. Local fields can also be recovered by solving the cell problem for the first (and higher) order term.

The div $-$ **grad** problem (3.19) can be used for modeling the elastic behaviour of a linear material, for studying the heat conduction in a linear material, etc. The Helmholtz equation in acoustics also falls into this category with pressure as the quantity of interest. In electromagnetism, problem (3.19) can be used for linear electrostatic, electrokinetic or magnetostatic problems formulated using scalar potentials. In this case, the unknown field u^ε represents scalar potentials (either electric or magnetic) and the tensor a^ε represents the electric permittivity ϵ, electric conductivity σ or magnetic permeability μ. The **curl** $-$ **curl** problem (3.20) can be used for modeling the behaviour of electromagnetic fields in the presence of linear electrostatic, electrokinetic, magnetostatic and magnetodynamic (frequency-domain) problems in the case vector potential formulations are used. The unknown vector field $\boldsymbol{u}^\varepsilon$ represent vector potentials or the physical fields (electric or magnetic) and the tensor a^ε represents the electric permittivity, the electric conductivity or the magnetic permeability or their inverse.

The asymptotic expansion method has some limitations:

1. using the method, it is not possible to get convergence results for the field u^ε, for fields involving differential operators and for functional integrals and one must resort to convergence theories (Γ-convergence, G-convergence, H-convergence or two-scale convergence) in order to get these results;

2. for linear problems, the method always yields good results for the div $-$ **grad** problem as the solution obtained belongs to the space $H^1(\Omega)$ (or one of its closed subspace). This space has an interesting property, the so-called *compactness of the injection* $H^1(\Omega)$ in $L^2(\Omega)$ [40, 54, 85] that guarantees the possibility to extract a strong convergent sequence in $L^2(\Omega)$ from any bounded sequence in $H^1(\Omega)$ resulting in the zero order term of (3.14) being independent from the fine-scale variable $\boldsymbol{y}$. This result cannot be generalized for problems involving **curl** operators; strong convergence of bounded sequences of $\boldsymbol{H}(\mathbf{curl};\Omega)$ (resp. $\boldsymbol{H}(\mathrm{div};\Omega)$) in $\boldsymbol{L}^2(\Omega)$ cannot be guaranteed [201] meaning that the zero order term of (3.14) may depend on the fine-scale variable $\boldsymbol{y}$ for fields belonging to $\boldsymbol{H}(\mathbf{curl};\Omega)$ (resp. $\boldsymbol{H}(\mathrm{div};\Omega)$);

3. the method is not adapted for nonlinear problems and convergence theories become indispensable in this case. The homogenization of the nonlinear div $-$ **grad** problem has been investigated using the classical theory of convergence [20, 204]. The approach was based on the compactness results that can be

obtained for the div $-$ **grad** but cannot be generalized for nonlinear **curl** $-$ **curl** problems.

For illustrating the limitations of the asymptotic expansion method for linear problems in electromagnetism, we define the following direct linear magnetostatic problem:

$$\mathbf{curl}\,\boldsymbol{h}^{\varepsilon} = \boldsymbol{j}_s, \tag{3.55}$$

$$\operatorname{div}\left(\mu^{\varepsilon}\boldsymbol{h}^{\varepsilon}\right) = 0, \tag{3.56}$$

and the dual magnetostatic problem:

$$\mathbf{curl}\left(\nu^{\varepsilon}\boldsymbol{b}^{\varepsilon}\right) = \boldsymbol{j}_s, \tag{3.57}$$

$$\operatorname{div}\boldsymbol{b}^{\varepsilon} = 0, \tag{3.58}$$

where $\nu^{\varepsilon} = 1/\mu^{\varepsilon}$ and $\boldsymbol{h}^{\varepsilon}$ and $\boldsymbol{b}^{\varepsilon}$ are the magnetic field and the magnetic induction, respectively. The asymptotic homogenization method fails in this case. Indeed, from problem (3.55)–(3.56) one gets the following $\mathcal{O}(\varepsilon^{-1})$ equations:

$$\mathbf{curl}_y\,\boldsymbol{h}_0(\boldsymbol{x},\boldsymbol{y}) = \mathbf{0}, \tag{3.59}$$

$$\operatorname{div}_y\Big(\mu(\boldsymbol{y})\boldsymbol{h}_0(\boldsymbol{x},\boldsymbol{y})\Big) = 0, \tag{3.60}$$

The following expression for $\boldsymbol{h}_0(\boldsymbol{x},\boldsymbol{y})$ can be deduced from (3.59):

$$\boldsymbol{h}_0(\boldsymbol{x},\boldsymbol{y}) = -\mathbf{grad}_y\,\varphi_0(\boldsymbol{x},\boldsymbol{y}) + \boldsymbol{h}_K(\boldsymbol{x}). \tag{3.61}$$

Notice that $\boldsymbol{h}_K$ is independent from the variable $\boldsymbol{y}$. Substituting (3.61) into (3.60) leads to:

$$\operatorname{div}_y\Big(\mu(\boldsymbol{y})(\mathbf{grad}_y\,\varphi_0(\boldsymbol{x},\boldsymbol{y}))\Big) = \operatorname{div}_y\mu(\boldsymbol{y})\boldsymbol{h}_K(\boldsymbol{x}). \tag{3.62}$$

The method of separation of variables can be used for solving (3.62). The solution:

$$\boldsymbol{h}_0(\boldsymbol{x},\boldsymbol{y}) = \Big(\bar{\bar{\mathbf{1}}} - \mathbf{grad}_y\,\boldsymbol{\chi}(\boldsymbol{y})\Big)\boldsymbol{h}_K(\boldsymbol{x}), \tag{3.63}$$

is obtained, where $\boldsymbol{\chi}$ is defined from (3.33). This means that $\boldsymbol{h}_0$ depends on the variable $\boldsymbol{y}$ and that it is not possible to define the cell problem as (3.33). This could also be deduced from results of the div $-$ **grad** problem obtained solving (3.55)–(3.56) using the following scalar potential formulation: find $\phi^{\varepsilon} \in \mathcal{V}$ such that

$$\operatorname{div}\mu^{\varepsilon}\mathbf{grad}\,\phi^{\varepsilon}(\boldsymbol{x}) = \mathcal{F}(\boldsymbol{j}_s), \tag{3.64}$$

where $\mathcal{F}(\boldsymbol{j}_s)$ is the new source term and $H_0^1(\Omega) \subset \mathcal{V} \subset H^1(\Omega)$. The scalar potential ϕ^{ε} defined in (3.64) is different from the potential φ_0 defined in (3.61). While the first order term of the expansion ϕ_0 is independent from $\boldsymbol{y}$ (see equation (3.31)), the same cannot be said for the magnetic field $\boldsymbol{h}_0(\boldsymbol{x},\boldsymbol{y}) = -\mathbf{grad}_x\,\phi_0(\boldsymbol{x}) - \mathbf{grad}_y\,\phi_1(\boldsymbol{x},\boldsymbol{y})$.

Convergence theory can be used to explain mathematically these two results. Indeed, using the weak compactness theorem (see Theorem 1 in the Appendix B and the references [40, 85]), it is possible to extract a converging subsequence from $\phi^\varepsilon \in H_0^1(\Omega)$ that weakly converges in $H_0^1(\Omega)$. The weak convergence in $H_0^1(\Omega)$ implies strong convergence in $L^2(\Omega)$ as a result of the Rellich-Kondrachov theorem [40, 85]. The strong convergence in $L^2(\Omega)$ is expressed as:

$$\lim_{\varepsilon \to 0} \left|\left| \phi^\varepsilon - \phi_0 \right|\right|_{L^2(\Omega)} = \lim_{\varepsilon \to 0} \left(\int_\Omega |\phi^\varepsilon(\boldsymbol{x}) - \phi_0(\boldsymbol{x}, \boldsymbol{y})|^2 \mathrm{d}\boldsymbol{x} \right)^{\frac{1}{2}} = 0 \tag{3.65}$$

for all $\boldsymbol{y} \in Y$. This is only possible if the limit ϕ_0 does not depend on the variable $\boldsymbol{y} \in Y$ as the integral is carried out independent of the variable $\boldsymbol{y}$. Strong convergence cannot be generalized for sequences in any Banach space $\mathcal{V}$ solution to the problem (3.1). For instance, the weak convergence of the sequences $\boldsymbol{h}^\varepsilon \in \boldsymbol{H}(\mathbf{curl}; \Omega)$ in (3.55)–(3.56) (resp. $\boldsymbol{b}^\varepsilon \in \boldsymbol{H}(\mathrm{div}; \Omega)$ in (3.57)–(3.58)) does not entail strong convergence in $\boldsymbol{L}^2(\Omega)$ as $\boldsymbol{H}(\mathbf{curl}; \Omega)$ (resp. $\boldsymbol{H}(\mathrm{div}; \Omega)$) is not compactly embedded in $\boldsymbol{L}^2(\Omega)$. Thus, the limits (first order terms) $\boldsymbol{h}_0$ and $\boldsymbol{b}_0$ may depend on the fine-scale variable $\boldsymbol{y}$ and therefore it is not always possible to get a slowly varying homogenized problem for the $\mathbf{curl} - \mathbf{curl}$ problem using the asymptotic expansion method as developed in section 3.4. Similar conclusions can be made for the dual problem (3.57)–(3.58). We obtain the following $\mathcal{O}(\varepsilon^{-1})$ equations:

$$\mathbf{curl}_y \Big(\nu(\boldsymbol{y}) \boldsymbol{b}_0(\boldsymbol{x}, \boldsymbol{y}) \Big) = 0, \tag{3.66}$$

$$\mathrm{div}_y\, \boldsymbol{b}_0(\boldsymbol{x}, \boldsymbol{y}) = 0, \tag{3.67}$$

and the solution:

$$\boldsymbol{b}_0(\boldsymbol{x}, \boldsymbol{y}) = \mathbf{curl}_y\, \boldsymbol{a}_0(\boldsymbol{x}, \boldsymbol{y}) + \boldsymbol{b}_K(\boldsymbol{x}) = \Big(\bar{\bar{\mathbf{1}}} - \mathbf{curl}_y\, \boldsymbol{\chi}(\boldsymbol{y}) \Big) \boldsymbol{b}_K(\boldsymbol{x}), \tag{3.68}$$

with $\boldsymbol{\chi}$ defined as in (3.50) and $\boldsymbol{b}_K$ is a function independent from the variable $\boldsymbol{y}$. Here again, $\boldsymbol{b}_0$ depends on the variable $\boldsymbol{y}$ and it is not possible to define a cell problem as in equation (3.33).

In order to circumvert the limitations of the asymptotic expansion method we use the two-scale convergence theory and the periodic unfolding method. More details on this theories are given in the next section.

3.5 Two-scale convergence and the periodic unfolding method

In this section, we use the two-scale convergence and the periodic unfolding methods to overcome the limitations of the asymptotic expansion method. These methods are based on the convergence of the field u^ε and the derived fields involving the differential operators $\mathbf{grad}, \mathbf{curl}$ and div.

The two-scale convergence was introduced by Nguetseng [143] and further developed by Allaire [11]. It allows to capture the fine-scale oscillations of the limit of u^ε that can be lost when passing to the classical weak limit u_0 in (3.14). The

idea of two-scale convergence is to use test functions $\psi(\cdot, \frac{\cdot}{\varepsilon})$ that are periodic in the second argument and that allow to sample rapid fluctuations that can occur at the fine-scale $\boldsymbol{y}$.
The concept of two-scale convergence (Appendix C.1) may seem completely disconnected from the classical concept of convergence (Appendix B) as it involves two quantities, $u^\varepsilon \in L^p(\Omega)$ and $u_0 \in L^p(\Omega \times \mathcal{Y})$ that belong to different function spaces. However, the periodic unfolding method introduced by Cioranescu [45] allows to link these two notions. Indeed, the use of the periodic unfolding method makes it possible to express the two-scale convergence of a sequence $u^\varepsilon \in L^p(\Omega)$ as the one-scale convergence in $L^p(\mathbb{R}^3 \times \mathcal{Y})$ of the sequence $\mathcal{T}^\varepsilon u^\varepsilon$ obtained by applying the periodic unfolding operator $\mathcal{T}^\varepsilon$ to the original sequence u^ε (see Appendix C for the definition of $\mathcal{Y}$ and of the periodic unfolding operator $\mathcal{T}^\varepsilon$).

See [11, 120, 141, 143] for more details about the two-scale convergence and [31, 45, 46, 130, 197] for details about the periodic unfolding method. References [155] contains applications for Maxwell's equations and Appendix C also contains a brief introduction of these two concepts.

Using the two-scale version of the weak compactness theorem, from any sequence of $u^\varepsilon \in L^2(\Omega)$ it is possible to extract a subsequence that two-scale weakly converges to $u_0 \in L^2(\Omega \times Y)$.The following properties link results of the classical convergence and the two-scale convergence [11, 141, 197, 205]:

1. Whenever the limit u_0 is independent of $\boldsymbol{y}$, strong one-scale convergence is equivalent to the strong two-scale convergence:

$$u^\varepsilon \to u_0 \text{ in } L^2(\Omega) \quad \Leftrightarrow \quad u^\varepsilon \underset{2}{\to} u_0 \text{ in } L^2(\mathbb{R}^3 \times \mathcal{Y}). \tag{3.69}$$

   This result is always true for the fields of $H^1(\Omega)$ thanks to the compact injection of $H^1(\Omega)$ in $L^2(\Omega)$.

2. Strong two-scale convergence implies weak two-scale convergence.

3. A sequence u^ε that weakly two-scale converges to u_0 also converges (in the classical sense) to the mean value $u_M = \hat{u}_0$:

$$u^\varepsilon \underset{2}{\rightharpoonup} u_0 \text{ in } L^2(\mathbb{R}^3 \times \mathcal{Y}) \quad \Longrightarrow$$
$$u^\varepsilon \rightharpoonup u_M = \hat{u}_0 = \int_Y u_0(., \boldsymbol{y})\mathrm{d}y \text{ in } L^2(\mathbb{R}^3). \tag{3.70}$$

4. The two-scale limit u_0 has the following two-scale orthogonal decomposition:

$$u_0 = u_M + u_c \qquad \text{with} \qquad \int_Y u_c(\cdot, \boldsymbol{y})\mathrm{d}y = 0, \tag{3.71}$$

with u_c the correction term that accounts for rapid fluctuations of the two-scale limit u_0. Expression (3.71) expresses a decomposition of u_0. This decomposition is orthogonal in $L^2(\mathbb{R}^3 \times \mathcal{Y}) or \boldsymbol{L}^2(\mathbb{R}^3 \times \mathcal{Y})$ [195].

Results (3.69)-(3.71) lead to the following conclusion between the classical and the two-scale convergence: **strong classical convergence $\Longrightarrow$ strong two-scale convergence $\Longrightarrow$ weak two-scale convergence $\Longrightarrow$ weak classical convergence**.

As an illustration example, we consider bounded fields $\phi^\varepsilon \in H^1(\Omega), \boldsymbol{h}^\varepsilon \in \boldsymbol{H}(\mathbf{curl};\Omega)$ and $\boldsymbol{b}^\varepsilon \in \boldsymbol{H}(\mathrm{div};\Omega)$. From the definition of these function spaces, the sequence ϕ^ε is bounded in $L^2(\Omega)$ and the sequences $\boldsymbol{h}^\varepsilon$ and $\boldsymbol{b}^\varepsilon$ are bounded in $\boldsymbol{L}^2(\Omega)$. The function spaces $L^2(\Omega)$ and $\boldsymbol{L}^2(\Omega)$ are appropriate for the two-scale convergence and convergence results derived in Appendix C.3 can be used. Therefore there exist $\phi_0 \in H^1(\Omega)$, $\boldsymbol{h}_0 \in \boldsymbol{L}^2(\mathbb{R}^3; \boldsymbol{H}(\mathbf{curl}\ \mathbf{0}; \mathcal{Y}))$ and $\boldsymbol{b}_0 \in \boldsymbol{L}^2(\mathbb{R}^3; \boldsymbol{H}(\mathrm{div}\ \mathbf{0}; \mathcal{Y})))$ [11,143,198] such that

$$\phi^\varepsilon \to \phi_0, \tag{3.72}$$

$$\boldsymbol{h}^\varepsilon \underset{2}{\rightharpoonup} \boldsymbol{h}_0 = \boldsymbol{h}_M - \mathbf{grad}\, \phi_c, \tag{3.73}$$

$$\boldsymbol{b}^\varepsilon \underset{2}{\rightharpoonup} \boldsymbol{b}_0 = \boldsymbol{b}_M + \mathbf{curl}\, \boldsymbol{a}_c, \tag{3.74}$$

in $\boldsymbol{L}^2(\mathbb{R}^3 \times \mathcal{Y}))$. In addition, the following classical convergence results:

$$\boldsymbol{h}^\varepsilon \rightharpoonup \boldsymbol{h}_M = \hat{\boldsymbol{h}}_0, \tag{3.75}$$

$$\boldsymbol{b}^\varepsilon \rightharpoonup \boldsymbol{b}_M = \hat{\boldsymbol{b}}_0. \tag{3.76}$$

are obtained.

The convergence $\boldsymbol{h}^\varepsilon \underset{2}{\rightharpoonup} \boldsymbol{h}_0$ in $\boldsymbol{L}^2(\mathbb{R}^3 \times \mathcal{Y}))$ is the two-scale convergence as defined in Appendix C and the convergence $\boldsymbol{h}^\varepsilon \rightharpoonup \boldsymbol{h}_M$ in $\boldsymbol{L}^2(\mathbb{R}^3)$ is the weak convergence as defined in Appendix B.

Results (3.72)–(3.76) are obtained using the properties of the two-scale convergence (3.69)–(3.71) with the correction terms expressed as $\boldsymbol{h}_c(\boldsymbol{x},\boldsymbol{y}) = -\mathbf{grad}_y\, \phi_c(\boldsymbol{x},\boldsymbol{y})$ and $\boldsymbol{b}_c(\boldsymbol{x},\boldsymbol{y}) = \mathbf{curl}_y\, \boldsymbol{a}_c(\boldsymbol{x},\boldsymbol{y})$ [157, 201, 208].

We are also interested in the convergence of the derived field that involves the differential operator div, **curl** and **grad**. If $\{\phi^\varepsilon\}$ is a bounded sequence in the $H^1(\Omega)$ (resp. $\{\boldsymbol{h}^\varepsilon\}$ is a bounded sequence in $\boldsymbol{H}(\mathbf{curl};\Omega)$ and $\{\boldsymbol{b}^\varepsilon\}$ is a bounded sequence in $\boldsymbol{H}(\mathrm{div};\Omega)$), then $\{\mathbf{grad}\, \phi^\varepsilon\}$ is a bounded sequence of $\boldsymbol{L}^2(\Omega)$, ($resp.$ $\{\mathbf{curl}\, \boldsymbol{h}^\varepsilon\}$ is a bounded sequence of $\boldsymbol{L}^2(\Omega)$ and $\{\mathrm{div}\, \boldsymbol{b}^\varepsilon\}$ is a bounded sequence of $L^2(\Omega)$. Using results in Appendix C.3, it can be shown that for any $\phi_M \in H^1(\mathbb{R}^3)$, $\boldsymbol{h}_M \in \boldsymbol{H}(\mathbf{curl};\mathbb{R}^n)$, $\boldsymbol{b}_M \in \boldsymbol{H}(\mathrm{div};\mathbb{R}^n)$, , $\phi_1 \in L^2(\mathbb{R}^3; H^1_*(\mathcal{Y}))$, $\boldsymbol{h}_1 \in \boldsymbol{L}^2(\mathbb{R}^n; \boldsymbol{H}(\mathbf{curl};\mathcal{Y}))$ and $\boldsymbol{b}_1 \in \boldsymbol{L}^2(\mathbb{R}^n; \boldsymbol{H}(\mathrm{div};\mathcal{Y}))$, there exist sequences $\{\phi^\varepsilon\}$ of $H^1(\mathbb{R}^n)$, $\{\boldsymbol{h}^\varepsilon\}$ of $\boldsymbol{H}(\mathbf{curl};\mathbb{R}^n)$ and $\{\boldsymbol{b}^\varepsilon\}$ of $\boldsymbol{H}(\mathrm{div};\mathbb{R}^n)$ [11, 143, 198, 202] such that

$$\mathbf{grad}\, \phi^\varepsilon \underset{2}{\rightharpoonup} \mathbf{grad}_x\, \phi_M + \mathbf{grad}_y\, \phi_1, \tag{3.77}$$

$$\mathbf{curl}\, \boldsymbol{h}^\varepsilon \underset{2}{\rightharpoonup} \mathbf{curl}_x\, \boldsymbol{h}_M + \mathbf{curl}_y\, \boldsymbol{h}_1, \tag{3.78}$$

$$\mathrm{div}\, \boldsymbol{b}^\varepsilon \underset{2}{\rightharpoonup} \mathrm{div}_x\, \boldsymbol{b}_M + \mathrm{div}_y\, \boldsymbol{b}_1, \tag{3.79}$$

where the fields ϕ_1, $\boldsymbol{h}_1$ and $\boldsymbol{b}_1$ correspond to the first order terms of the expansion (3.14). An additional condition (gauge condition) must be imposed for these first order terms to be uniquely defined and one possibility is to choose $\mathrm{div}_y\, \boldsymbol{h}_1(\boldsymbol{x},\boldsymbol{y}) = \mathbf{0}$ and $\mathbf{curl}_y\, \boldsymbol{b}_1(\boldsymbol{x},\boldsymbol{y}) = 0$ [31, 198]. The first order terms should not be confused with the correction terms (e.g. $\boldsymbol{h}_1 \neq \boldsymbol{h}_c = -\mathbf{grad}_y\, \phi_c$ and $\boldsymbol{b}_1 \neq \boldsymbol{b}_c = \mathbf{curl}_y\, \boldsymbol{a}_c$).

The results developed above still hold for $p \neq 2$. In section 3.6 we deal with spaces with $p = \infty$. In that case, the two-scale star convergence and a new notation are used. For instance, if the time-domain field $\boldsymbol{h}^\varepsilon \in L^\infty(0,T;\boldsymbol{H}(\mathbf{curl};\Omega))$ then there exists $\boldsymbol{h}_0 \in \boldsymbol{L}^2(\mathbb{R}^3_T;\boldsymbol{H}(\mathbf{curl}\ \mathbf{0};\mathcal{Y}))$ such that

$$\boldsymbol{h}^\varepsilon \underset{2}{\overset{*}{\rightharpoonup}} \boldsymbol{h}_0 = \boldsymbol{h}_M - \mathbf{grad}\, \phi_c, \tag{3.80}$$

and

$$\boldsymbol{h}^\varepsilon \overset{*}{\rightharpoonup} \boldsymbol{h}_M = \hat{\boldsymbol{h}}_0. \tag{3.81}$$

In (3.80)-(3.81) we use the weak star convergence as the field belong to the space L^∞. Note however that the sequence converges in L^2. More details about the convergence of differential operators can be found in Appendix C.3.

3.6 Homogenization of the magnetoquasistatic Maxwell problem

In this section, we focus on the homogenization of magnetoquasistatic problem described in section 3.1. Our first goal is to derive the convergence of the fields and of their derivatives. Then we derive the homogenized model for the quasistatic problem and convergence results for the quadratic quantities. We focus on the quasistatic problems formulated using electromagnetic fields: formulations in terms of electromagnetic potentials on non-trivial domains would require to use the theory of cohomology and definition of gauges for guaranteeing the uniqueness of the solution []. Results used in this section are based on the work of Augusto Visintin about the homogenization of nonlinear magnetodynamic problems governed by maximal monotone operators [196, 201]. Additional results can be found in [199] for the two-scale convergence of integral functionals, in [11, 141, 198] for the two-scale convergence of differential operators and in [137, 138, 189, 190, 200] for the div $-$ **curl** lemma.

3.6.1 Homogenization of electromagnetic fields

We look for the weak solution of problems (3.3)–(3.7). All the derivatives should be understood in the sense of distribution. If the mappings $\boldsymbol{\mathcal{B}}$ and $\boldsymbol{\mathcal{J}}$ are maximal monotone, $\mathcal{Y}$-periodic, coercive and bounded [196, 201], then the electromagnetic fields are bounded and they belong to appropriate function spaces for the two-scale convergence (see expressions (A.27)–(A.30) of section A.4 in Appendix A and in the references [196,201]). Then it makes sense to talk about the so-called weak star two-scale convergence of the fields $\boldsymbol{h}^\varepsilon, \boldsymbol{b}^\varepsilon, \boldsymbol{e}^\varepsilon$ and the two-scale convergence of the field $\boldsymbol{j}^\varepsilon$. There exist $\boldsymbol{h}_0, \boldsymbol{e}_0 \in \boldsymbol{L}^2(\mathbb{R}^3_T;\boldsymbol{H}(\mathbf{curl}\ \mathbf{0};\mathcal{Y}))$ and $\boldsymbol{b}_0, \boldsymbol{j}_0 \in \boldsymbol{L}^2(\mathbb{R}^3_T;\boldsymbol{H}(\mathrm{div}\ \mathbf{0};\mathcal{Y})))$

such that

$$\boldsymbol{e}^\varepsilon \xrightharpoonup[2]{*} \boldsymbol{e}_0 = \boldsymbol{e}_M - \mathbf{grad}\, v_c \qquad \text{in } \mathcal{V}, \tag{3.82}$$
$$\boldsymbol{h}^\varepsilon \xrightharpoonup[2]{*} \boldsymbol{h}_0 = \boldsymbol{h}_M - \mathbf{grad}\, \phi_c \qquad \text{in } L^\infty(0,T;\boldsymbol{L}^2(\mathbb{R}^3 \times \mathcal{Y})), \tag{3.83}$$
$$\boldsymbol{b}^\varepsilon \xrightharpoonup[2]{*} \boldsymbol{b}_0 = \boldsymbol{b}_M + \mathbf{curl}\, \boldsymbol{a}_c \qquad \text{in } L^\infty(0,T;\boldsymbol{L}^2(\mathbb{R}^3 \times \mathcal{Y})), \tag{3.84}$$
$$\boldsymbol{j}^\varepsilon \xrightharpoonup[2]{} \boldsymbol{j}_0 = \boldsymbol{j}_M + \mathbf{curl}\, \boldsymbol{t}_c \qquad \text{in } \boldsymbol{L}^2(\mathbb{R}^3_T \times \mathcal{Y}), \tag{3.85}$$

with $\mathcal{V} = \boldsymbol{L}^2(\Omega_T \times \mathcal{Y}) \cap L^\infty(0,T;\boldsymbol{L}^2((\mathbb{R}^3 \setminus \Omega) \times \mathcal{Y}))$ and

$$\boldsymbol{e}^\varepsilon \overset{*}{\rightharpoonup} \boldsymbol{e}_M \qquad \text{in } \mathcal{W}, \tag{3.86}$$
$$\boldsymbol{h}^\varepsilon \overset{*}{\rightharpoonup} \boldsymbol{h}_M \qquad \text{in } L^\infty(0,T;\boldsymbol{L}^2(\mathbb{R}^3)), \tag{3.87}$$
$$\boldsymbol{b}^\varepsilon \overset{*}{\rightharpoonup} \boldsymbol{b}_M \qquad \text{in } L^\infty(0,T;\boldsymbol{L}^2(\mathbb{R}^3)), \tag{3.88}$$
$$\boldsymbol{j}^\varepsilon \rightharpoonup \boldsymbol{j}_M \qquad \text{in } \boldsymbol{L}^2(\mathbb{R}^3_T), \tag{3.89}$$

with $\mathcal{W} = \boldsymbol{L}^2(\Omega_T) \cap L^\infty(0,T;\boldsymbol{L}^2((\mathbb{R}^3 \setminus \Omega)))$.
Results in (3.82)–(3.85) have been obtained using properties of the two-scale convergence (3.70)-(3.71). The derived fields also belong to the suitable function spaces and Using results in Appendix C.3, it can be shown that for any $\phi_M \in H^1(\mathbb{R}^3)$, $\boldsymbol{h}_M \in \boldsymbol{H}(\mathbf{curl};\mathbb{R}^n)$, $\boldsymbol{b}_M \in \boldsymbol{H}(\mathrm{div};\mathbb{R}^n)$, $\phi_1 \in L^2(\mathbb{R}^3;H^1_*(\mathcal{Y}))$, $\boldsymbol{h}_1 \in \boldsymbol{L}^2(\mathbb{R}^n;\boldsymbol{H}(\mathbf{curl};\mathcal{Y}))$ and $\boldsymbol{b}_1 \in \boldsymbol{L}^2(\mathbb{R}^n;\boldsymbol{H}(\mathrm{div};\mathcal{Y}))$, there exist sequences $\{\phi^\varepsilon\}$ of $H^1(\mathbb{R}^n)$, $\{\boldsymbol{h}^\varepsilon\}$ of $\boldsymbol{H}(\mathbf{curl};\mathbb{R}^n)$ and $\{\boldsymbol{b}^\varepsilon\}$ of $\boldsymbol{H}(\mathrm{div};\mathbb{R}^n)$ such that

$$\mathbf{curl}\, \boldsymbol{h}^\varepsilon \xrightharpoonup[2]{} \mathbf{curl}_x\, \boldsymbol{h}_M + \mathbf{curl}_y\, \boldsymbol{h}_1, \tag{3.90}$$
$$\mathbf{curl}\, \boldsymbol{e}^\varepsilon \xrightharpoonup[2]{} \mathbf{curl}_x\, \boldsymbol{e}_M + \mathbf{curl}_y\, \boldsymbol{e}_1, \tag{3.91}$$
$$\mathrm{div}\, \boldsymbol{b}^\varepsilon \xrightharpoonup[2]{} \mathrm{div}_x\, \boldsymbol{b}_M + \mathrm{div}_y\, \boldsymbol{b}_1. \tag{3.92}$$

Replacing (3.82)–(3.85) and (3.90)–(3.92) in (3.3)–(3.7) we get the following two-scale problem: find $\boldsymbol{h}_0, \boldsymbol{e}_0 \in \boldsymbol{L}^2(\mathbb{R}^3_T;\boldsymbol{H}(\mathbf{curl};0;\mathcal{Y}))$ and $\boldsymbol{b}_0, \boldsymbol{j}_0, \boldsymbol{h}_1$ and $\boldsymbol{e}_1 \in \boldsymbol{L}^2(\mathbb{R}^3_T;\boldsymbol{H}(\mathrm{div};0;\mathcal{Y}))$ such that

$$\mathbf{curl}_x\, \boldsymbol{h}_M + \mathbf{curl}_y\, \boldsymbol{h}_1 = \boldsymbol{j}_0, \tag{3.93}$$
$$\mathbf{curl}_x\, \boldsymbol{e}_M + \mathbf{curl}_y\, \boldsymbol{e}_1 = -\partial_t \boldsymbol{b}_0, \tag{3.94}$$
$$\boldsymbol{b}_0(\boldsymbol{x},\boldsymbol{y},t) = \boldsymbol{\mathcal{B}}\Big(\boldsymbol{h}_0(\boldsymbol{x},\boldsymbol{y},t),\boldsymbol{x},\boldsymbol{y}\Big), \tag{3.95}$$
$$\boldsymbol{j}_0(\boldsymbol{x},\boldsymbol{y},t) = \boldsymbol{\mathcal{J}}\Big(\boldsymbol{e}_0(\boldsymbol{x},\boldsymbol{y},t),\boldsymbol{x},\boldsymbol{y}\Big), \tag{3.96}$$

where $\boldsymbol{h}_M = \hat{\boldsymbol{h}}_0$ and $\boldsymbol{e}_M = \hat{\boldsymbol{e}}_0$. Using test functions independent from the variable $\boldsymbol{y}$, it has been shown [196, 201] that this problem can be averaged to the following one-scale problem without loss of information: find $\boldsymbol{h}_M, \boldsymbol{e}_M, \boldsymbol{b}_M$ and $\boldsymbol{j}_M \in \boldsymbol{L}^2(\mathbb{R}^3_T)$ such that

$$\mathbf{curl}_x\, \boldsymbol{h}_M = \boldsymbol{j}_M, \tag{3.97}$$

$$\mathbf{curl}_x\, \boldsymbol{e}_M = -\partial_t \boldsymbol{b}_M, \tag{3.98}$$

$$\boldsymbol{b}_M(\boldsymbol{x},t) = \boldsymbol{\mathcal{B}}_M\Big(\boldsymbol{h}_M(\boldsymbol{x},t),\boldsymbol{x}\Big), \tag{3.99}$$

$$\boldsymbol{j}_M(\boldsymbol{x},t) = \boldsymbol{\mathcal{J}}_M\Big(\boldsymbol{e}_M(\boldsymbol{x},t),\boldsymbol{x}\Big), \tag{3.100}$$

All the derivatives should be understood in the distribution sense. The macroscale fields $\boldsymbol{h}_M, \boldsymbol{e}_M, \boldsymbol{b}_M$ and $\boldsymbol{j}_M$ are given by $\boldsymbol{h}_M = \hat{\boldsymbol{h}}_0, \boldsymbol{e}_M = \hat{\boldsymbol{e}}_0, \boldsymbol{b}_M = \hat{\boldsymbol{b}}_0$ and $\boldsymbol{b}_M = \hat{\boldsymbol{b}}_0$. The mappings $\boldsymbol{\mathcal{B}}_M$ and $\boldsymbol{\mathcal{J}}_M$ are also maximal monotone, coercive and bounded and they are obtained by solving the following mesoscale problems [201]:

1. For the mapping $\boldsymbol{\mathcal{B}}_M$: find $\phi_c \in H^1_*(\mathcal{Y})$ such that

$$\mathrm{div}_y\, \boldsymbol{b}_0 = 0, \tag{3.101}$$

$$\boldsymbol{b}_0(\boldsymbol{x},\boldsymbol{y},t) = \boldsymbol{\mathcal{B}}\Big(\boldsymbol{h}_M(\boldsymbol{x},t) - \mathbf{grad}\,\phi_c(\boldsymbol{x},\boldsymbol{y},t),\boldsymbol{x},\boldsymbol{y}\Big), \tag{3.102}$$

   and then derive

$$\boldsymbol{\mathcal{B}}_M\Big(\boldsymbol{h}_M(\boldsymbol{x},t),\boldsymbol{x}\Big) = \int_{\mathcal{Y}} \boldsymbol{\mathcal{B}}\Big(\boldsymbol{h}_M(\boldsymbol{x},t) - \mathbf{grad}\,\phi_c(\boldsymbol{x},\boldsymbol{y},t),\boldsymbol{x},\boldsymbol{y}\Big)\mathrm{d}\boldsymbol{y}. \tag{3.103}$$

2. For the mapping $\boldsymbol{\mathcal{J}}_M$: find $v_c \in H^1_*(\mathcal{Y})$ such that

$$\mathrm{div}_y\, \boldsymbol{j}_0 = 0, \tag{3.104}$$

$$\boldsymbol{j}_0(\boldsymbol{x},\boldsymbol{y},t) = \boldsymbol{\mathcal{J}}\Big(\boldsymbol{e}_M(\boldsymbol{x},t) - \mathbf{grad}\,v_c(\boldsymbol{x},\boldsymbol{y},t),\boldsymbol{x},\boldsymbol{y}\Big), \tag{3.105}$$

   and then derive

$$\boldsymbol{\mathcal{J}}_M\Big(\boldsymbol{e}_M(\boldsymbol{x},t),\boldsymbol{x}\Big) = \int_{\mathcal{Y}} \boldsymbol{\mathcal{J}}\Big(\boldsymbol{e}_M(\boldsymbol{x},t) - \mathbf{grad}\,v_c(\boldsymbol{x},\boldsymbol{y},t),\boldsymbol{x},\boldsymbol{y}\Big)\mathrm{d}\boldsymbol{y}. \tag{3.106}$$

The variables $\boldsymbol{x}$ and t are considered as parameters in the mesoscale problems (3.101)–(3.102) and (3.104)–(3.105). If the mapping $\boldsymbol{\mathcal{J}}$ is linear, problem (3.104)–(3.105) is equivalent to the cell problem obtained in section 3.4.1.1 using the asymptotic method [203].
Problems (3.101)–(3.102) and (3.104)–(3.105) represent the magnetostatic and electrokinetic problems solved using scalar potential formulations, respectively. It is possible to use the dual approach and define the following mesoscale dual problems:

1. For the mapping $\boldsymbol{\mathcal{B}}_M^{-1} = \boldsymbol{\mathcal{H}}_M$: find $\boldsymbol{a}_c \in \boldsymbol{H}_*(\mathbf{curl};\mathcal{Y})$ such that

$$\mathbf{curl}_y\, \boldsymbol{h}_0 = 0, \tag{3.107}$$

$$\boldsymbol{h}_0(\boldsymbol{x},\boldsymbol{y},t) = \boldsymbol{\mathcal{H}}\Big(\boldsymbol{b}_M(\boldsymbol{x},t) + \mathbf{curl}\,\boldsymbol{a}_c(\boldsymbol{x},\boldsymbol{y},t),\boldsymbol{x},\boldsymbol{y}\Big), \tag{3.108}$$

   and then derive

$$\boldsymbol{\mathcal{H}}_M\Big(\boldsymbol{b}_M(\boldsymbol{x},t),\boldsymbol{x}\Big) = \int_{\mathcal{Y}} \boldsymbol{\mathcal{H}}\Big(\boldsymbol{b}_M(\boldsymbol{x},t) + \mathbf{curl}\,\boldsymbol{a}_c(\boldsymbol{x},\boldsymbol{y},t),\boldsymbol{x},\boldsymbol{y}\Big)\mathrm{d}\boldsymbol{y}. \tag{3.109}$$

2. For the mapping $\boldsymbol{\mathcal{J}}_M^{-1} = \boldsymbol{\mathcal{E}}_M$: find $\boldsymbol{t}_c \in \boldsymbol{H}_*(\mathbf{curl}; \mathcal{Y})$ such that

$$\mathbf{curl}_y\, \boldsymbol{e}_0 = 0, \tag{3.110}$$

$$\boldsymbol{e}_0(\boldsymbol{x},\boldsymbol{y},t) = \boldsymbol{\mathcal{E}}\Big(\boldsymbol{j}_M(\boldsymbol{x},t) + \mathbf{curl}\,\boldsymbol{t}_c(\boldsymbol{x},\boldsymbol{y},t), \boldsymbol{x}, \boldsymbol{y}\Big), \tag{3.111}$$

and then derive

$$\boldsymbol{\mathcal{E}}_M\Big(\boldsymbol{j}_M(\boldsymbol{x},t), \boldsymbol{x}\Big) = \int_{\mathcal{Y}} \boldsymbol{\mathcal{E}}\Big(\boldsymbol{j}_M(\boldsymbol{x},t) + \mathbf{curl}\,\boldsymbol{t}_c(\boldsymbol{x},\boldsymbol{y},t), \boldsymbol{x}, \boldsymbol{y}\Big)\mathrm{d}\boldsymbol{y}. \tag{3.112}$$

Problems (3.107)–(3.108) and (3.110)–(3.111) represent the magnetostatic and electrokinetic problems solved using vector potential formulations, respectively. If the mapping $\boldsymbol{\mathcal{J}}$ is linear, problem (3.110)–(3.111) is equivalent to the cell problem obtained in section 3.4.1.2 using the asymptotic expansion approach.

3.6.2 Homogenization of some quadratic quantities

In addition to the two-scale convergence of electromagnetic fields we want to know which quadratic quantities converge. Indeed, for any domain Ω (bounded or not), it is known [105, 116] that the divergence of the Poynting vector $\boldsymbol{S} = \boldsymbol{e} \times \boldsymbol{h}$ is equal to the rate of electromagnetic energy plus the energy dissipated by Joule effect:

$$P = -\int_\Omega \operatorname{div} \boldsymbol{S}\,\mathrm{d}x = -\int_\Omega \operatorname{div}(\boldsymbol{e}\times\boldsymbol{h})\,\mathrm{d}x = -\int_\Gamma \boldsymbol{n}\cdot(\boldsymbol{e}\times\boldsymbol{h})\,\mathrm{d}x = \int_\Omega (\boldsymbol{h}\cdot\partial_t\boldsymbol{b})\,\mathrm{d}x + \int_\Omega (\boldsymbol{e}\cdot\partial_t\boldsymbol{d})\,\mathrm{d}x + \int_\Omega (\boldsymbol{j}\cdot\boldsymbol{e})\,\mathrm{d}x. \tag{3.113}$$

The last three terms of (3.113) represent the rate of change of the magnetic energy, the rate change of the electric energy and the eddy current losses, respectively.

The convergence of such quadratic quantities is not straightforward. Indeed even if $\boldsymbol{u}^\varepsilon$ and $\boldsymbol{w}^\varepsilon$ are weakly converging sequences of $\boldsymbol{L}^2(\Omega)$:

$$\boldsymbol{u}^\varepsilon \rightharpoonup \boldsymbol{u} \quad \text{in } \boldsymbol{L}^2(\Omega), \tag{3.114}$$

$$\boldsymbol{w}^\varepsilon \rightharpoonup \boldsymbol{w} \quad \text{in } \boldsymbol{L}^2(\Omega), \tag{3.115}$$

their product $\boldsymbol{w}^\varepsilon\cdot\boldsymbol{u}^\varepsilon$ is not guaranteed to converge. In order to have the convergence of the product, a stronger compactness assumption must be made (e.g. $\boldsymbol{u}^\varepsilon$ or $\boldsymbol{w}^\varepsilon$ strongly converge in $\boldsymbol{L}^2(\Omega)$) [40, 54, 85]. This assumption is too strong in most cases and it cannot be easily guaranteed for Maxwell's equations. The div $-$ **curl** lemma allows to obtain the convergence of the sequence of type $\boldsymbol{w}^\varepsilon\cdot\boldsymbol{u}^\varepsilon$ using less restrictive assumptions (regularity conditions on derivatives of $\boldsymbol{u}^\varepsilon$ and $\boldsymbol{w}^\varepsilon$).

Using the two-scale div $-$ **curl** lemma (see Appendix C.4) for time-dependent problems we get the following convergence results for the magnetic energy:

$$\int_{\mathbb{R}^3_T} \Big(\boldsymbol{b}^\varepsilon(\boldsymbol{x},t)\cdot\boldsymbol{h}^\varepsilon(\boldsymbol{x},t)\Big)\theta(\boldsymbol{x},t)\,\mathrm{d}x\,\mathrm{d}t \to \int_{\mathbb{R}^3_T} \Big(\boldsymbol{b}_M(\boldsymbol{x},t)\cdot\boldsymbol{h}_M(\boldsymbol{x},t)\Big)\theta(\boldsymbol{x},t)\,\mathrm{d}x\,\mathrm{d}t$$

$$= \int_{\mathbb{R}^3_T \times \mathcal{Y}} \Big(\boldsymbol{b}_0(\boldsymbol{x}, \boldsymbol{y}, t) \cdot \boldsymbol{h}_0(\boldsymbol{x}, \boldsymbol{y}, t) \Big) \theta(\boldsymbol{x}, t) \, \mathrm{d}x \, \mathrm{d}y \, \mathrm{d}t \quad . \tag{3.116}$$

This result is valid for all test functions $\theta \in \mathcal{C}_c(\mathbb{R}^3_T)$. These functions are independent from the variable $\boldsymbol{y}$ and therefore the convergence is not valid pointwise but on average. Equation (3.116) expresses the consistency of magnetic energy between the macroscale and the mesoscale. Note that the eddy current losses are not guaranteed to converge.

3.6.3 Advantages and limitations of the method of two-scale convergence for the magnetoquasistatic problem

Compared to the asymptotic expansion method, the two-scale convergence method provides the possibility to deal with problems involving **curl** operators. Indeed, the first order term of the expansion of the fields in this case may depend on the rapidly fluctuating variable $\boldsymbol{y}$ which makes it impossible to build a homogenized problem using the asymptotic expansion method. Materials with nonlinear reversible laws and periodic microstructures can be handled. Note however that for nonlinear problems the mesoscale problems (3.101)–(3.102) and (3.107)–(3.108) should be solved for different values of the macroscale source fields in order to derive the homogenized mappings $\boldsymbol{\mathcal{B}}_M$ or $\boldsymbol{\mathcal{H}}_M$. The method also offers the possibility to recover the local fields by solving the mesoscale problem (3.93)–(3.96) and a way of computing the magnetic energy of the system.

Problems (3.101)–(3.102) and (3.107)–(3.108) are not adapted for materials with hysteresis as the constitutive laws of these materials may depend on the history. For instance, the $\boldsymbol{b} - \boldsymbol{h}$ curve may depend on the profile of the exciting source and this is not accounted for in the mesoscale problem. Note finally that these mesoscale problems do not allow to account for the influence of eddy currents on the nonlinear/hysteretic behaviour. In order to overcome these shortcomings we develop a computational homogenization method in the next chapter.

Chapter 4

Computational multiscale methods

4.1 Introduction

In section 3.6 we have derived the homogenized problem for the magnetoquasistatic problem. This problem involves the resolution of mesoscale problems used for computing the homogenized constitutive laws: equations (3.37) and (3.48) for the homogenization of the linear electric laws (e.g. Ohm's law) and (3.101)–(3.102) and (3.107)–(3.108) for the homogenization of the nonlinear magnetic laws, respectively.

The resolution of these problems on complex microstructures may require the use of numerical methods. In this thesis, we focus on FE based methods. Indeed, FEM is well adapted for solving problems involving complex geometries. When using the FE method the first step consists in converting the original partial differential equation into an equivalent weak formulation which is then discretized using finite dimensional polynomial functional spaces on simple-shaped elements obtained after meshing the domain. This leads to the following discrete problem:

$$f(\overline{\boldsymbol{u}}) = 0, \tag{4.1}$$

where $\overline{\boldsymbol{u}}$ is the vector of discrete unknowns also known as degrees of freedom (dof). For a linear problem, (4.1) can be written as $A\overline{\boldsymbol{u}} = \boldsymbol{b}$ and $\overline{\boldsymbol{u}}$ is obtained by solving the linear algebraic system. For nonlinear problems, the discrete form (4.1) can be solved using techniques such as the fixed point method, the Newton–Raphson method, the secant method, etc. In this thesis we use the Newton–Raphson method. Although a quadratic convergence can be obtained using this method, this convergence is not always guaranteed especially for problems with hysteresis. The method can also be computationally inefficient since the derivative has to be calculated at each time step.

The resolution of one mesoscale problem suffices for deriving the homogenized constitutive law for the linear electric laws. For the nonlinear constitutive laws, two approaches can be used.

The first consists in pre-computing the nonlinear magnetic law $\boldsymbol{\mathcal{B}}_M$ or $\boldsymbol{\mathcal{H}}_M$ prior to any FE computations and then use the computed law in the FE resolution using equations (3.103) and (3.109). This approach is adapted for nonlinear problems e.g. involving maximal monotone operators but it is not adapted for problems with magnetic hysteresis.

The second approach, which is developed in this chapter, is inspired by the heterogeneous multiscale method – HMM and the definition of a different mesoscale problem that accounts for eddy currents at the mesoscale level. This problem is defined from the two-scale equations of the magnetoquasistatic problem (3.93)–(3.96).

The chapter is organized as follows: in section 4.2 we review multiscale methods and focus on the HMM method. In section 4.3, we develop the computational homogenization method for the magnetodynamic problems using the $\boldsymbol{a} - v$ formulation. We then derive the magnetic flux density conforming multiscale formulations for the magnetostatic problem. The methodology is further applied to the $\boldsymbol{h} - \phi$ formulation in section 4.4 for both the dynamic and the static cases.

4.2 Multiscale methods

Classical multiscale methods such as the multigrid methods [38], the domain decomposition method [167], the wavelet-based methods [53] and the adapted refinement method [9] allow to reduce the computational cost as compared to classical numerical methods such as the FE method. However in these methods, the fine-scale problem is still solved on the entire domain.

Modern multiscale methods most often use special features of the problem (e.g. scale separation, periodicity, ergodicity, etc.) to derive a multiscale problem that is computationally cheaper to solve. Several modern multiscale methods have been developed over the last few years. They include among others the equation-free computations methods [110, 172, 180], the upscaling methods [66], the mortar multiscale methods [14, 160, 161], the variational multiscale methods–VMS [41, 102, 103, 109, 153], the generalized finite element method–GFEM [16, 17], the fast Fourier transform–FFT-based homogenization [127, 128, 135], the multiscale finite element methods–MsFEM [76, 100, 101], the heterogeneous multiscale methods–HMM [68, 73], etc. They can be classified in two categories [76]:

1. the *fine-to-coarse* methods for which the macroscale equations are not formulated explicitly and representative fine-scale information is carried out throughout the simulations;

2. the *coarse-to-fine* methods that assume a form of macroscale equations and the macroscale parameters are computed based on the calculations in the representative cells.

In the following paragraphs we give details for two of these methods: the MsFEM for the fine-to-coarse approach and the HMM for the coarse-to-fine approach. However a comparison of all multiscale methods can help distinguish advantages and disadvantages of different approaches.

4.2.1 Multiscale finite element method (MsFEM)

This method has been introduced by Hou and Wu [100] inspired by the generalized finite element method by Babuska [16, 17]. The MsFEM method has later been extended by other authors such as Efendiev, Ginting, etc. [76–82]. The basic principle of the method is the use at the macroscale level of multiscale basis functions that contain information about the heterogeneities of the microstructure. These basis functions are computed solving fine-scale problems on the elements of the macroscale mesh and are then used for computing the discrete system of algebraic equations and/or for the post processing at the macroscale level.

To illustrate this, we use the approach in [100, 101] and consider the div − **grad** elliptic equation (3.19) where we neglect the term $a_0^\varepsilon u^\varepsilon(\boldsymbol{x})$. In chapter 3, we have shown that the solution $u^\varepsilon(\boldsymbol{x})$ has the expansion (3.14) and therefore it can be approximated by:

$$u^\varepsilon(\boldsymbol{x}) \simeq u_{app}(\boldsymbol{x},\boldsymbol{y}) = u_0(\boldsymbol{x}) + \varepsilon u_1(\boldsymbol{x},\boldsymbol{y}) = u_0(\boldsymbol{x}) + \varepsilon \boldsymbol{\chi}(\boldsymbol{y}) \cdot \mathbf{grad}\, u_0(\boldsymbol{x}). \tag{4.2}$$

The macroscale component $u_0(\boldsymbol{x})$ satisfies the same boundary conditions as $u^\varepsilon(\boldsymbol{x})$ on Γ, therefore $u_{app} = \varepsilon u_1$ is periodic. It is then possible to define a boundary corrector $\theta_1(\boldsymbol{x},\boldsymbol{y})$ such that [76]

$$z(\boldsymbol{x},\boldsymbol{y}) = u_{app}(\boldsymbol{x},\boldsymbol{y}) - \varepsilon\theta_1(\boldsymbol{x},\boldsymbol{y}) = u_0(\boldsymbol{x}) + \varepsilon(u_1(\boldsymbol{x},\boldsymbol{y}) - \theta_1(\boldsymbol{x},\boldsymbol{y})) \tag{4.3}$$

converges strongly to zero even near the boundary. This first order boundary corrector θ_1 is governed by the following partial differential equation:

$$-\mathrm{div}\,(a(\boldsymbol{y})\mathbf{grad}\,\theta_1(\boldsymbol{x},\boldsymbol{y})) = 0 \qquad \text{in } \Omega, \tag{4.4}$$

$$\theta_1(\boldsymbol{x},\boldsymbol{y}) = u_1(\boldsymbol{x},\boldsymbol{y}) \qquad \text{on } \Gamma. \tag{4.5}$$

For this div − **grad** equation, the idea of MsFEM [100, 101] is to use an expansion similar to (4.3) for the test functions, i.e.:

$$\phi^{i\varepsilon} = \phi_0^i + \varepsilon(\phi_1^i - \theta^i) + ... \tag{4.6}$$

where the basis functions ϕ_0^i, ϕ_1^i and θ_1^i can be computed on every macroscale element K of the macroscale mesh. The functions ϕ_0^i and ϕ_1^i are governed by the following equations:

$$\mathrm{div}\,(a\,\mathbf{grad}\,\phi_0^i) = 0 \qquad \text{in } K, \tag{4.7}$$

$$\phi_0^i = \mu^i \qquad \text{on } \partial K, \tag{4.8}$$

$$\phi_1^i = -\boldsymbol{\chi} \cdot \mathbf{grad}_x\, \phi_0^i \qquad \text{in } K, \tag{4.9}$$

where $\boldsymbol{\chi}$ is obtained solving the cell problem (3.33). The solution can be used to compute the correction term θ_1^i, which is governed by:

$$\mathrm{div}\,(a\,\mathbf{grad}\,\theta_1^i) = 0 \qquad \text{in } K, \tag{4.10}$$

$$\theta_0^i = \phi_1^i \qquad\qquad \text{on } \partial K. \tag{4.11}$$

The superscript "i" in (4.7)–(4.11) denotes the node number of a given macro-element and $\mu_i = \phi_0^i|_{\partial K}$ is the boundary condition. Details on the computation of this boundary condition can be found in [100]. From (4.7)–(4.11), it can be seen that the functions ϕ_0^i form an appropriate basis for approximating the unknown $u_0(\boldsymbol{x})$. In addition, the first order term $u_1(\boldsymbol{x}, \boldsymbol{y})$ can also be approximated using the multiscale test functions ϕ_1^i. Finally, the functions θ_1^i can be used for getting the boundary corrector.

From the implementation point of view, the method exhibits some technical difficulties. Indeed, the method is not readily usable in the existing codes as new functional spaces need to be defined for the basis functions ϕ_0^i, ϕ_1^i and θ_1^i at the macroscale level. For the linear case analyzed above, the complexity of the problem may also depend on the macroscale mesh. Indeed, if all the elements of the macroscale mesh are identical then the solution of one single problem on a macroscale element suffices to construct the multiscale basis functions. Otherwise, these functions must be computed for each macroscale element.

The MsFEM method has already been used in [36, 37] for solving a multiscale linear electromagnetic problem. To the best of our knowledge, this approach has never been applied to nonlinear/hysteretic magnetoquasistatic problems.

4.2.2 Heterogeneous multiscale methods (HMM)

Hereafter, we develop a coarse-to-fine method inspired by the HMM method, first introduced by Weinan E and Enqguist [67–73, 75]. Among other major contributors to the method are Abdulle Assyr, Vanden-Eijnden, etc. [1–4, 6, 7, 74, 194, 194]. Note that the FE^2 method [89, 114] popular in the computational mechanics community predates the introduction of the HMM method and is based on the same overall philosophy, albeit in a more restrictive setting.

Other methods that use the HMM approach are the non-local quasi-continuum method – QCM [187], the macro atomistic ab-initio dynamics – MAAD [8], the gap-tooth scheme [110], etc. The models used at different scales in these methods can range from quantum mechanics, molecular dynamics, all the way up to the continuum physics. A quite complete but non-exhaustive list of these methods can be found in [12, 15].

The principle of the method is schematically shown in Figure (4.1). A fine-scale model p governs the evolution of the unknown u under the constraints c. Solving this model on the entire domain (e.g. $\Omega \times]0, T[$) is computationally prohibitive. The problem is thus replaced by the macroscale model $P(U, C) = 0$ where U and C are the new unknowns and constraints, respectively. This macroscale model has to be chosen properly for ensuring accurate solutions.

The missing information of the macroscale model (e.g. the constitutive laws) is computed by solving the fine-scale model $p(u, c) = 0$ on smaller domains called representative volume elements – RVE. The scale separation assumption must hold. Other assumptions such as periodicity or ergodicity also allow to reduce the compu-

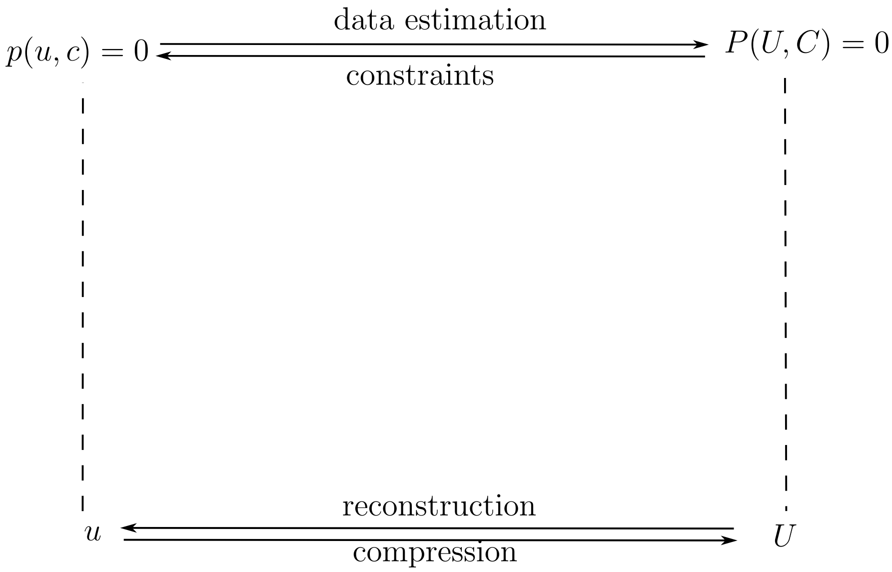

Figure 4.1: Schematic of the HMM framework (image inspired by [5]).

tational cost. The mesoscale problems need to be constrained so as to be consistent with the macroscale information at the local level.

As an application example, we consider the div − **grad** problem (3.19) treated in the previous section. Using results of chapter 3, we can derive the following governing partial differential equation for the macroscale problem:

$$\mathrm{div}_x \left(a^h \,\mathbf{grad}_x\, u_0(\boldsymbol{x}) \right) = f, \tag{4.12}$$

where the homogenized quantity a^h is given by (3.37). The solution $u_0(\boldsymbol{x})$ belongs to the space $H^1(\Omega)$ and therefore it can be discretized using classical conformal finite element. This approach can be readily used in existing codes and it is not necessary to define new function spaces as the MsFEM method. In the case of a material with a linear law and periodic microstructure, only one mesoscale problem must be solved in order to get the homogenized quantity a^h independent of the macroscale mesh.

In the case of the magnetoquasistatic problem (3.3)–(3.7), the macroscale problem has been derived in (3.97)–(3.100). The missing magnetic constitutive law (3.99) can be computed solving the mesoscale problem (3.93)–(3.96).

If the magnetic law is a maximal monotone mapping, the homogenized magnetic law $\boldsymbol{h}_M = \boldsymbol{\mathcal{H}}_M(\boldsymbol{b}_M)$ or $\boldsymbol{b}_M = \boldsymbol{\mathcal{B}}_M(\boldsymbol{h}_M)$ can be pre-computed by solving problems (3.107)–(3.108) and (3.101)–(3.102), respectively. Let us consider the case $\boldsymbol{h}_M = \boldsymbol{\mathcal{H}}_M(\boldsymbol{b}_M)$. The points of the material law $\boldsymbol{\mathcal{H}}_M$ can then be computed for different values of the macroscale magnetic flux density $\boldsymbol{b}_M$ by solving the following static mesoscale problem (3.107)–(3.108): find $\boldsymbol{a}_c \in \boldsymbol{H}_*(\mathbf{curl};\mathcal{Y})$ such that

$$\mathbf{curl}_y\, \boldsymbol{h}_0 = \mathbf{0}, \tag{4.13}$$

$$\boldsymbol{h}_0(\boldsymbol{x},\boldsymbol{y}) = \boldsymbol{\mathcal{H}}\Big(\boldsymbol{b}_M(\boldsymbol{x}) + \mathbf{curl}\, \boldsymbol{a}_c(\boldsymbol{x},\boldsymbol{y}), \boldsymbol{x}, \boldsymbol{y}\Big), \tag{4.14}$$

and then derive:

$$\boldsymbol{\mathcal{H}}_M\Big(\boldsymbol{b}_M(\boldsymbol{x}), \boldsymbol{x}\Big) = \frac{1}{|\mathcal{Y}|}\int_{\mathcal{Y}} \boldsymbol{\mathcal{H}}\Big(\boldsymbol{b}_M(\boldsymbol{x}) + \mathbf{curl}\, \boldsymbol{a}_c(\boldsymbol{x},\boldsymbol{y}), \boldsymbol{x}, \boldsymbol{y}\Big)\mathrm{d}\boldsymbol{y}. \tag{4.15}$$

As a result of the definition of the function space for $\boldsymbol{a}_c(\boldsymbol{x},\boldsymbol{y})$, periodic boundary conditions and a zero-average value must be imposed for the tangential component of $\boldsymbol{a}_c(\boldsymbol{x},\boldsymbol{y})$. The macroscale source $\boldsymbol{b}_M$ can be obtained by discretizing the continuous variable $\boldsymbol{b}_M \in \mathbb{R}^3$ on a subdomain of $\mathbb{R}^3$ valid for the application at hand. For instance, one can consider values of $\boldsymbol{b}_M$ from the matrix of vectors $\overline{\overline{\boldsymbol{\mathcal{B}}}}_M$ where elements of $\overline{\overline{\boldsymbol{\mathcal{B}}}}_M$ are given by:

$$\left(\overline{\overline{\boldsymbol{\mathcal{B}}}}_M\right)_{i\,j\,k} = (-b_M + i\,\Delta b_M, -b_M + k\,\Delta b_M, -b_M + j\,\Delta b_M). \tag{4.16}$$

The indices $i, j, k = 0, 1, ..., N$ with N the number of samples in each direction and the discretization step $\Delta b_M = 2\,b_M/N$. It is then possible to solve (4.13) in order to derive the discrete mapping $\boldsymbol{\mathcal{H}}_M$. Interpolation can then be used for getting the value of the $\boldsymbol{h}_M = \boldsymbol{\mathcal{H}}_M(\boldsymbol{b}_M)$ in any point of the application range. This approach was used in [34] for computing the homogenized nonlinear magnetic law.

In this thesis we use a different approach and compute the nonlinear magnetic law using the HMM approach. This allows us to upscale on-the-fly a homogenized material law from mesoscale problems that account for eddy currents at the mesoscale level. These mesoscale problems also allow to recover exact electromagnetic fields at the mesoscale level. The approach also becomes quasi-unavoidable when dealing with problems with hysteresis and for which the pre-computation of the homogenized magnetic laws described above is not adapted as it does not account for the history of the material.

In sections 4.3 and 4.4 we use equations (3.93)-(3.96) to define mesoscale problems and equations (3.97)-(3.100) to define macroscale problems

We consider electromagnetic fields indexed by m as the restriction - on the mesoscale domain Ω_m - of their equivalent indexed 0 in equations (3.93)-(3.100) (e.g. the field $\boldsymbol{b}_0(\boldsymbol{x},\boldsymbol{y},t)$) is replaced by $\boldsymbol{b}_m(\boldsymbol{x},\boldsymbol{y},t)$). We also consider the spatial coordinate $\boldsymbol{x}$ and the time instance t as parameters in mesoscale problems.

We denote $\boldsymbol{\mathcal{V}}(\mathcal{Y})$ the space $\boldsymbol{\mathcal{V}}(\Omega_m)$ defined with periodic boundary conditions (e.g. $H^1(\mathcal{Y})$ is the space of all functions $u \in H^1(\Omega_m)$ such that u is periodic and $\boldsymbol{H}(\mathbf{curl};\mathcal{Y})$ is the space of all functions $\boldsymbol{v} \in \boldsymbol{H}(\mathbf{curl};\Omega_m)$ such that $\boldsymbol{v}$ has periodic tangential component).

4.3 Magnetic flux density conforming multiscale formulations: dynamic case

4.3.1 The macroscale problem

The macroscale magnetoquasistatic problem has been derived using the two-scale convergence theory:

$$\mathbf{curl}_x \boldsymbol{h}_M = \boldsymbol{j}_M, \tag{4.17}$$
$$\mathbf{curl}_x \boldsymbol{e}_M = -\partial_t \boldsymbol{b}_M, \tag{4.18}$$
$$\operatorname{div}_x \boldsymbol{b}_M = 0, \tag{4.19}$$
$$\boldsymbol{h}_M(\boldsymbol{x},t) = \boldsymbol{\mathcal{H}}_M(\boldsymbol{b}_M(\boldsymbol{x},t),\boldsymbol{x}), \tag{4.20}$$
$$\boldsymbol{j}_M(\boldsymbol{x},t) = \boldsymbol{\mathcal{J}}_M(\boldsymbol{e}_M(\boldsymbol{x},t),\boldsymbol{x}). \tag{4.21}$$

The unknown homogenized fields $\boldsymbol{h}_M, \boldsymbol{b}_M, \boldsymbol{e}_M$ and $\boldsymbol{j}_M$ exhibit slow fluctuations; they can therefore be solved on a coarse mesh. The macroscale fields satisfy the same boundary conditions as the multiscale fields in (3.3)–(3.7). Appropriate initial conditions must also be provided for (4.17)–(4.21) to be well-posed. Note however that the constitutive laws (4.20)–(4.21) are missing at the macroscale level.

In the case of a linear electric law, equation (4.21) becomes $\boldsymbol{j}_M(\boldsymbol{x},t) = \boldsymbol{\mathcal{J}}_M(\boldsymbol{e}_M(\boldsymbol{x},t),\boldsymbol{x}) = \sigma_M(\boldsymbol{x})\boldsymbol{e}_M(\boldsymbol{x},t)$ and only one computation suffices for extracting the homogenized conductivity σ_M (see details in section 3.4.1 and [20]).

In the case of maximal monotone mappings $\boldsymbol{\mathcal{H}}$ (resp $\boldsymbol{\mathcal{B}}$) (see Appendix A.4), the nonlinear magnetic law $\boldsymbol{\mathcal{H}}_M(\boldsymbol{b}_M)$ can be pre-computed solving the mesoscale problem (4.13). In section 4.3.2 we derive another mesoscale problem which accounts for the effects of the eddy currents at the mesoscale level. Combined with the HMM approach, this mesoscale problem allows to compute on-the-fly the constitutive homogenized magnetic law accounting for the eddy currents. It can also be used for getting accurate local mesoscale fields and for upscaling more accurate global quantities such as the eddy currents losses.

Using results of section 2.5.2 we get the following three-dimensional macroscale weak formulation of (4.17)-(4.21): find $\boldsymbol{a}_M \in \boldsymbol{H}_e(\mathbf{curl},\Omega)$ and $v_M \in H^1_e(\Omega_c)$ such that

$$\Big(\boldsymbol{\mathcal{H}}_M(\mathbf{curl}_x\, \boldsymbol{a}_M), \mathbf{curl}_x\, \boldsymbol{a}'_M\Big)_\Omega + \Big(\sigma_M \partial_t \boldsymbol{a}_M, \boldsymbol{a}'_M\Big)_{\Omega_c} + \Big(\sigma_M \mathbf{grad}_x\, v_M, \boldsymbol{a}'_M\Big)_{\Omega_c} + \Big\langle \boldsymbol{n}\times\boldsymbol{h}_M, \boldsymbol{a}'_M\Big\rangle_{\Gamma_h} = \Big(\boldsymbol{j}_s, \boldsymbol{a}'_M\Big)_{\Omega_s}, \tag{4.22}$$

$$\Big(\sigma_M \partial_t \boldsymbol{a}_M, \mathbf{grad}_x v'_M\Big)_{\Omega_c} + \Big(\sigma_M \mathbf{grad}_x v_M, \mathbf{grad}_x v'_M\Big)_{\Omega_c} = \langle \boldsymbol{n}\cdot\boldsymbol{j}_M, v'_M\rangle_{\Gamma_g}, \tag{4.23}$$

hold for all test functions $\boldsymbol{a}'_M \in \boldsymbol{H}^0_e(\mathbf{curl},\Omega)$ and $v'_M \in H^{10}_e(\Omega_c)$. The vector $\boldsymbol{j}_M$ represents the eddy currents crossing the boundary Γ_g of Ω_c and $\boldsymbol{j}_s$ represents the source current density which is imposed in the inductors Ω_s. The macroscale domain Ω (resp. Ω_c) can be divided into the multiscale domain Ω^h (resp. Ω^h_c) where the homogenization is done and a non-multiscale domain Ω^{nh} (resp. Ω_c^{nh}) where clasiccal weak formulations can be used..

For the two-dimensional case, the weak formulation reduces to: find $a_{zM} \in H_e^1(\Omega)$ and u_M piecewise constant on Ω_c such that

$$\begin{aligned}\Big(\boldsymbol{\mathcal{H}}_M(\mathbf{1}_z \times \mathbf{grad}_x\, a_{zM}), \mathbf{1}_z \times \mathbf{grad}_x\, a_{zM}^{'}\Big)_{\Omega} + \Big(\sigma_M \partial_t a_{zM}, a_{zM}^{'}\Big)_{\Omega_c} \\ + \Big(\sigma_M u_M, a_{zM}^{'}\Big)_{\Omega_c} + \langle \boldsymbol{n} \times \boldsymbol{h}_M, a_{zM}^{'} \mathbf{1}_z \rangle_{\Gamma_h} = \Big(j_s, a_{zM}^{'}\Big)_{\Omega_s}\end{aligned} \tag{4.24}$$

$$\Big(\sigma_M \partial_t a_{zM}, u_M^{'}\Big)_{\Omega_c} - \Big(\sigma_M u_M, u_M^{'}\Big)_{\Omega_c} = 0, \tag{4.25}$$

hold for all test functions $a_{zM}^{'} \in H_e^{10}(\Omega)$ and $u_M^{'}$ constant piecewise on Ω_c.

The homogenized magnetic law $\boldsymbol{\mathcal{H}}_M$ missing in equations (4.22) and (4.24) is computed using the mesoscale problem defined in the following section.

4.3.2 The mesoscale problem

In order to define a mesoscale problem which includes eddy currents and which - unlike problem (4.13)-(4.15) - can be used for recovering accurate local electromagnetic fields, we start with the following modified two-scale version of the problem (3.93)–(3.96):

$$\mathbf{curl}\, \boldsymbol{h}_m^{\varepsilon} = \boldsymbol{j}_m, \tag{4.26}$$

$$\mathbf{curl}_{\,x} \boldsymbol{e}_M + \mathbf{curl}_{\,y} \boldsymbol{e}_1 = -\partial_t \boldsymbol{b}_m, \tag{4.27}$$

$$\mathrm{div}_{\,x} \boldsymbol{b}_M + \mathrm{div}_y\, \boldsymbol{b}_1 = 0, \tag{4.28}$$

$$\boldsymbol{h}_m(\boldsymbol{x}, \boldsymbol{y}, t) = \boldsymbol{\mathcal{H}}(\boldsymbol{b}_m(\boldsymbol{x}, \boldsymbol{y}, t), \boldsymbol{x}, \boldsymbol{y}), \tag{4.29}$$

$$\boldsymbol{j}_m(\boldsymbol{x}, \boldsymbol{y}, t) = \boldsymbol{\mathcal{J}}(\boldsymbol{e}_m(\boldsymbol{x}, \boldsymbol{y}, t), \boldsymbol{x}, \boldsymbol{y}), \tag{4.30}$$

in which we keep Ampère's equation (4.26). In this equation, $\boldsymbol{h}_m^{\varepsilon}$ is the restriction of the multiscale magnetic field $\boldsymbol{h}^{\varepsilon}$ to the representative volume element Ω_m, hereafter called "mesoscale domain". We can thus use both nonlinear reversible and irreversible (hysteretic) material laws.

Problems (4.26)–(4.30) contain macroscale fields considered constant at the mesoscale level. We want to derive a mesoscale problem that can be written in terms of mesoscale coordinates $\boldsymbol{y}$.

The two-scale convergence theory allows us to express the **curl** of the electric field at the mesoscale in terms of the **curl** of the electric field at the macroscale and the **curl** of the mesoscale correction term such that

$$\mathbf{curl}_y\, \boldsymbol{e}_m = \mathbf{curl}_x\, \boldsymbol{e}_M + \mathbf{curl}_y\, \boldsymbol{e}_1. \tag{4.31}$$

Using the Faraday law at the macroscale together with the vector identity $\mathbf{curl}_y\,(\partial_t b_M \times \boldsymbol{y}) = (n-1)\partial_t b_M$ ($n = 2, 3$ for 2D and 3D problems, respectively) we can write:

$$\mathbf{curl}_y\, \boldsymbol{e}_m = \mathbf{curl}_y \left(\boldsymbol{e}_1 + \boldsymbol{e}_M + \kappa(\mathbf{curl}_y\, \boldsymbol{e}_M \times \boldsymbol{y}) \right) = \mathbf{curl}_y \left(\boldsymbol{e}_1 + \boldsymbol{e}_M - \kappa(\partial_t \boldsymbol{b}_M \times \boldsymbol{y}) \right) \tag{4.32}$$

with $\kappa = (n-1)^{-1}$, since $\mathbf{curl}_y\, \boldsymbol{e}_M \equiv 0$. Similar developments have been proposed in [124] and [84] for the electric and the magnetic fields in linear cases. Inserting the orthogonal decomposition $\boldsymbol{b}_m = \boldsymbol{b}_M + \mathbf{curl}_y\, \boldsymbol{a}_c$ derived from (3.84) in (4.27) we get the following equation:

$$\mathbf{curl}_x \boldsymbol{e}_M + \mathbf{curl}_y \boldsymbol{e}_1 = -\partial_t(\boldsymbol{b}_M + \mathbf{curl}_y\, \boldsymbol{a}_c). \tag{4.33}$$

We can use (4.18) to express the first order term of the electric field $\boldsymbol{e}_1$ in terms of the correction term $\boldsymbol{a}_c$ as:

$$\boldsymbol{e}_1 = -\partial_t \boldsymbol{a}_c - \mathbf{grad}_y\, v_c. \tag{4.34}$$

At the mesoscale level, the first order term $\boldsymbol{e}_1$ can be chosen in $\boldsymbol{H}(\mathbf{curl};\mathcal{Y})$ for every $t \in]0,T[$ (see (3.91) and C.3 in Appendix C.3). This means that the tangential component of $\boldsymbol{e}_1$ on $\mathcal{Y}$ is periodic. In section 4.3.3 we will show that $\boldsymbol{a}_c$ is tangentially periodic and and we will choose v_c which is periodic on the mesoscale domain Ω_m. Using these developments, we can derive the following mesoscale three-dimensional weak formulation: find $\boldsymbol{a}_c \in \boldsymbol{H}(\mathbf{curl};\mathcal{Y})$ and $v_c \in H^1(\mathcal{Y})$ such that

$$\left(\boldsymbol{\mathcal{H}}(\mathbf{curl}_y \boldsymbol{a}_c + \boldsymbol{b}_M), \mathbf{curl}_y \boldsymbol{a}_c^{'} \right)_{\Omega_m} + \left(\sigma \partial_t \boldsymbol{a}_c, \boldsymbol{a}_c^{'} \right)_{\Omega_{mc}} + \left(\sigma \mathbf{grad}_y v_c, \boldsymbol{a}_c^{'} \right)_{\Omega_{mc}} = \left(\sigma(\boldsymbol{e}_M - \kappa \partial_t \boldsymbol{b}_M \times \boldsymbol{y}), \boldsymbol{a}_c^{'} \right)_{\Omega_{mc}} \tag{4.35}$$

$$\left(\sigma \partial_t \boldsymbol{a}_c, \mathbf{grad}_y v_c^{'} \right)_{\Omega_{mc}} + \left(\sigma \mathbf{grad}_y v_c, \mathbf{grad}_y v_c^{'} \right)_{\Omega_{mc}} = \left(\sigma(\boldsymbol{e}_M - \kappa \partial_t \boldsymbol{b}_M \times \boldsymbol{y}), \mathbf{grad}_y v_c^{'} \right)_{\Omega_{mc}} + \left\langle \boldsymbol{n} \cdot \boldsymbol{j}_M, v_c^{'} \right\rangle_{\Gamma_{gm}} \tag{4.36}$$

hold for all test functions $\boldsymbol{a}_c^{'} \in \boldsymbol{H}(\mathbf{curl};\mathcal{Y})$ and $v_c^{'} \in H^1(\mathcal{Y})$ and for every $t \in]0,T[$. Domains Ω_{mc} and Γ_{gm} are the conducting part of the mesoscale domain and the boundary of Ω_{mc}, respectively. The electric current density $\boldsymbol{j}_M = \sigma_M \boldsymbol{e}_M$ is obtained from the macroscale solution.

For the two-dimensional case, the mesoscale weak formulation becomes: find $a_{zc} \in H^1(\mathcal{Y})$ and u_c piecewise constant on Ω_{mc} such that

$$\left(\boldsymbol{\mathcal{H}}(\mathbf{1}_z \times \mathbf{grad}_y\, a_{zc} + \boldsymbol{b}_M), \mathbf{1}_z \times \mathbf{grad}_y\, a_{zc}^{'} \right)_{\Omega_m} + \left(\sigma \partial_t a_{zc}, a_{zc}^{'} \right)_{\Omega_{mc}} + \left(\sigma u_c, a_{zc}^{'} \right)_{\Omega_{mc}} = \left(\sigma(\boldsymbol{e}_M - \kappa \partial_t \boldsymbol{b}_M \times \boldsymbol{y}), \mathbf{1}_z a_{zc}^{'} \right)_{\Omega_{mc}} \tag{4.37}$$

$$\left(\sigma \partial_t a_{zc}, u_c^{'} \right)_{\Omega_{mc}} + \left(\sigma u_c, u_c^{'} \right)_{\Omega_{mc}} = \left(\sigma(\boldsymbol{e}_M - \kappa \partial_t \boldsymbol{b}_M \times \boldsymbol{y}), \mathbf{1}_z u_c^{'} \right)_{\Omega_{mc}} = \left(\sigma \boldsymbol{e}_M, \mathbf{1}_z u_c^{'} \right)_{\Omega_{mc}} \tag{4.38}$$

hold for all test functions $a_{zc}^{'} \in H^1(\mathcal{Y})$ and $u_c^{'}$ piecewise constant on Ω_{mc} and for all $t \in]0,T[$.

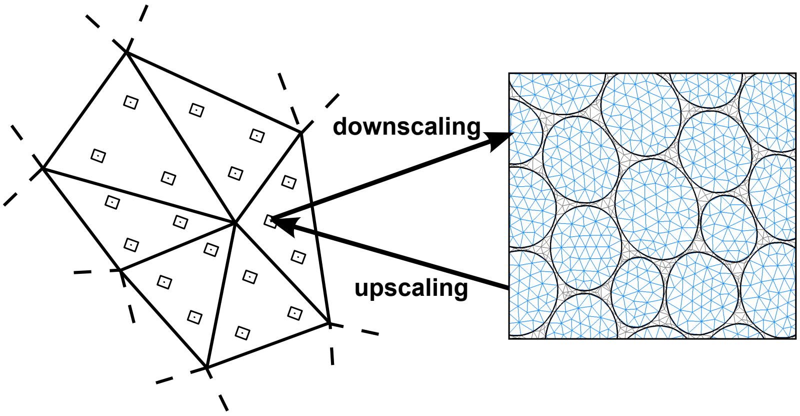

Figure 4.2: Scale transitions between macroscale (left) and mesoscale (right) problems. Downscaling (macro to meso): obtaining proper boundary conditions and the source terms for the mesoscale problem from the macroscale solution. Upscaling (meso to macro): effective quantities for the macroscale problem calculated from the mesoscale solution [148].

4.3.3 Scale transitions

The macroscale and the mesoscale problems in sections 4.3.1 and 4.3.2 are not yet well-defined: the macroscale magnetic law $\boldsymbol{\mathcal{H}}_M(\boldsymbol{b}_M)$ is not defined at the macroscale level and the mesoscale problem needs source terms $\boldsymbol{b}_M, \boldsymbol{e}_M$ and $\boldsymbol{j}_M$ and proper boundary conditions to be well-posed. These two problems need to exchange information through scale transitions to fill in the missing information at both levels. This information is exchanged through the *downscaling* and the *upscaling* stages (see Figure 4.2).

During the *downscaling*, the macroscale fields are imposed as source terms for the mesoscale problem. Boundary conditions for the mesoscale problem are also determined so as to respect the two-scale convergence of the physical fields: the convergence of the magnetic flux density $\boldsymbol{b}$ leads to the following condition on the tangential component of the correction term of the magnetic vector potential $\boldsymbol{a}_c$:

$$\frac{1}{|\Omega_m|}\int_{\Omega_m} \boldsymbol{b}_m(\boldsymbol{x},\boldsymbol{y},t)\,\mathrm{d}y = \boldsymbol{b}_M(\boldsymbol{x},t) \quad \Longrightarrow$$
$$\int_{\Omega_m} \mathbf{curl}\,\boldsymbol{a}_c(\boldsymbol{x},\boldsymbol{y},t)\,\mathrm{d}y = \oint_{\Gamma_m} \boldsymbol{n}\times\boldsymbol{a}_c(\boldsymbol{x},\boldsymbol{y},t)\,\mathrm{d}y = \mathbf{0}. \quad (4.39)$$

This condition is fulfilled if $\boldsymbol{a}_c$ belongs to the space $\boldsymbol{H}(\mathbf{curl};\mathcal{Y})$, i.e. if $\boldsymbol{a}_c$ is periodic on the cell. This implies that $\mathbf{grad}_y\, v_c = \boldsymbol{e}_1 - \partial_t \boldsymbol{a}_c$ also belongs to $\boldsymbol{H}(\mathbf{curl};\mathcal{Y})$. This is automatically ensured by the *curl theorem*:

$$\int_{\Gamma_m} \boldsymbol{n}\times\mathbf{grad}_y\, v_c \mathrm{d}y = \int_{\Omega_m} \mathbf{curl}_y\,\mathbf{grad}_y\, v_c \mathrm{d}y. \quad (4.40)$$

We also choose v_c to be periodic.

The convergence of the electric current density also leads to the following relation:

$$\frac{1}{|\Omega_m|}\int_{\Omega_{mc}} \boldsymbol{j}_m(\boldsymbol{x},\boldsymbol{y},t)\,\mathrm{d}y = \boldsymbol{j}_M(\boldsymbol{x},t) \implies \frac{1}{|\Omega_m|}\int_{\Omega_{mc}} \boldsymbol{j}_c(\boldsymbol{x},\boldsymbol{y},t)\,\mathrm{d}y$$
$$= -\int_{\Omega_{mc}} \sigma\Big(\partial_t \boldsymbol{a}_c(\boldsymbol{x},\boldsymbol{y},t) + \mathbf{grad}\, v_c(\boldsymbol{x},\boldsymbol{y},t)\Big)\,\mathrm{d}y = \mathbf{0}. \quad (4.41)$$

Equation (4.41) holds for every $t \in]0,T[$.

The *upscaling* consists in computing the missing constitutive laws σ_M, $\boldsymbol{\mathcal{H}}_M(\boldsymbol{b}_M)$ together with $\partial\boldsymbol{\mathcal{H}}_M/\partial\boldsymbol{b}_M$ at the macroscale using the mesoscale fields. Due to the linearity of the electric law, the asymptotic expansion theory (see section 3.4.1.1) can be applied. Therefore, we compute once and for all the homogenized electric conductivity by solving a cell problem. A similar approach was also adopted in [34]. The electric conductivity is then upscaled by means of:

$$(\sigma_M)_{ij} = \frac{1}{|\Omega_m|}\int_{\Omega_m}\Big(\sigma_{ij}(\boldsymbol{y}) - \sigma_{ik}(\boldsymbol{y})\frac{\partial\chi_j(\boldsymbol{y})}{\partial y_k}\Big)\mathrm{d}y, \quad (4.42)$$

where the periodic functions χ_j are solutions of the cell problem:
find $\chi_j(\boldsymbol{y}) \in H^1(\mathcal{Y})$ such that

$$\int_{\Omega_m} (\mathbf{grad}_y\psi')^T\sigma\Big(\mathbf{grad}_y\chi_j - \boldsymbol{e}_j\Big)\;\mathrm{d}y = 0 \quad (4.43)$$

holds for all $\psi'(\boldsymbol{y}) \in H^1(\mathcal{Y})$. The vector $\boldsymbol{e}_j$ is the unit vector in the j^{th} spatial direction.

The upscaling of the nonlinear magnetic law is performed by simple average as a consequence of the two-scale convergence of $\boldsymbol{h}$:

$$\frac{1}{|\Omega_m|}\int_{\mathcal{Y}} \boldsymbol{h}_m \mathrm{d}y = \boldsymbol{h}_M. \quad (4.44)$$

We use a finite difference difference approach [129] in order to obtain the tangent matrix $\partial\boldsymbol{\mathcal{H}}_M/\partial\boldsymbol{b}_M$ for the Newton-Raphson scheme. First we solve the problem (4.35)–(4.36) for the three-dimensional problems (resp. (4.48)–(4.38) for the two-dimensional problems) in order to find the solution to the macroscale field $\boldsymbol{b}_M$. Then we solve three problems similar to (4.35)–(4.36) (resp. (4.48)–(4.38) for the two-dimensional problems where we have added a time- and space-independent magnetic induction perturbation term $\delta\boldsymbol{b}_i$ in the direction i to the macroscale source terms. The total magnetic induction $\boldsymbol{b}_m$ for these problems becomes:

$$\boldsymbol{b}_m = \boldsymbol{b}_M + \mathbf{curl}_y\,\boldsymbol{a}_c + \delta\boldsymbol{b}_i = \mathbf{curl}_y\,\boldsymbol{a}_c + \kappa(\boldsymbol{b}_M \times \boldsymbol{y}) + \kappa(\delta\boldsymbol{b}_i \times \boldsymbol{y}), \quad (4.45)$$

which can be derived from the total magnetic vector potential:

$$\boldsymbol{a}_m = \boldsymbol{a}_c - \mathbf{grad}_y\, v_c + \kappa(\boldsymbol{b}_M \times \boldsymbol{y}) + \kappa(\delta\boldsymbol{b}_i \times \boldsymbol{y}). \quad (4.46)$$

These developments allow to change the three dimensional equation (4.35) into

$$\Big(\boldsymbol{\mathcal{H}}(\mathbf{curl}_y\boldsymbol{a}_c+\boldsymbol{b}_M+\delta\boldsymbol{b}_i),\mathbf{curl}_y\boldsymbol{a}_c^{'}\Big)_{\Omega_m}+\Big(\sigma\partial_t\boldsymbol{a}_c,\boldsymbol{a}_c^{'}\Big)_{\Omega_{mc}}+\\ \Big(\sigma\mathbf{grad}_y v_c,\boldsymbol{a}_c^{'}\Big)_{\Omega_{mc}}=\Big(\sigma(\boldsymbol{e}_M-\kappa\partial_t\boldsymbol{b}_M\times\boldsymbol{y}),\boldsymbol{a}_c^{'}\Big)_{\Omega_{mc}}. \quad (4.47)$$

Notice that the time derivative of the constant term in equation (4.46) disappears. We also change the two dimensional equation (4.48) into

$$\Big(\boldsymbol{\mathcal{H}}(\mathbf{1}_z\times\mathbf{grad}_y\, a_{zc}+\boldsymbol{b}_M+\delta\boldsymbol{b}_i),\mathbf{1}_z\times\mathbf{grad}_y\, a_{zc}^{'}\Big)_{\Omega_m}+\Big(\sigma\partial_t a_{zc},a_{zc}^{'}\Big)_{\Omega_{mc}}+\\ \Big(\sigma u_c,a_{zc}^{'}\Big)_{\Omega_{mc}}=\Big(\sigma(\boldsymbol{e}_M-\kappa\partial_t\boldsymbol{b}_M\times\boldsymbol{y}),\mathbf{1}_z a_{zc}^{'}\Big)_{\Omega_{mc}}. \quad (4.48)$$

Equations (4.36) and (4.38) remain unchanged. This leads to the solution $\boldsymbol{h}_M+\delta_{\boldsymbol{b}_i}\boldsymbol{h}_M$ where $\delta_{\boldsymbol{b}_i}\boldsymbol{h}_M$ is the perturbation of the magnetic field in direction i. We can therefore deduce the tangent matrix as:

$$\Big(\frac{\partial\boldsymbol{\mathcal{H}}_M}{\partial\boldsymbol{b}_M}\Big)_{ij}\approx\frac{(\delta_{\boldsymbol{b}_i}\boldsymbol{h}_M)_j}{\delta\boldsymbol{b}_i}. \quad (4.49)$$

4.3.4 Finite element implementation

The macroscale and the mesoscale problems are solved in a staggered way with the FE method. Both problems are nonlinear and solved with the Newton–Raphson scheme. In this subsection we give implementation details of the computational multiscale method for a mesoscale problem with a hysteretic magnetic constitutive law. The numerical schemes of the macroscale and the mesoscale problems remain almost the same. We will point out the differences if they exist.

The first step for the numerical solution is to spatially discretize the fields. We use mixed elements and get the following expressions:

$$\boldsymbol{a}(\boldsymbol{x},t)=\sum_{i\in\mathcal{N}_e}a_i(t)\boldsymbol{S}_e^i(\boldsymbol{x}), \quad (4.50)$$

$$v(\boldsymbol{x})=\sum_{k\in\mathcal{N}_n}v_k S_n^k(\boldsymbol{x}) \quad (4.51)$$

$$\boldsymbol{b}(\boldsymbol{x},t)=\sum_{i\in\mathcal{N}_e}a_i(t)\mathbf{curl}\,\boldsymbol{S}_e^i(\boldsymbol{x}), \quad (4.52)$$

$$\partial_t\boldsymbol{a}(\boldsymbol{x},t)=\sum_{i\in\mathcal{N}_e}\frac{\mathrm{d}a_i(t)}{\mathrm{d}t}\boldsymbol{S}_e^i(\boldsymbol{x}), \quad (4.53)$$

$$\mathbf{grad}\,v(\boldsymbol{x})=\sum_{k\in\mathcal{N}_n}v_k\mathbf{grad}\,S_n^k(\boldsymbol{x}). \quad (4.54)$$

The fields $\boldsymbol{a}$ and v are used to represent both the macroscale fields $\boldsymbol{a}_M$ and v_M and the mesoscale fields $\boldsymbol{a}_m$ and v_m. The basis functions $\boldsymbol{S}_e^i(\boldsymbol{x})$ and $S_n^k(\boldsymbol{x})$ are chosen as the standard edge and nodal Whitney forms, spanning discrete subspaces of $\boldsymbol{H}(\mathbf{curl};\Omega)$ and $H^1(\Omega)$, respectively [90]. The degree of freedom $a_i(t)$ and v_k

are the unknowns of the FE problem and $\mathcal{N}_e$ and $\mathcal{N}_n$ the total numbers of the unknowns of the fields $\boldsymbol{a}_M$ and v_M, respectively. With formulae (4.50)–(4.54) we get the following discretized equations:

$$\overline{\overline{\boldsymbol{C}}}\frac{\mathrm{d}\overline{\boldsymbol{A}}}{\mathrm{d}t} + \overline{\overline{\boldsymbol{D}}}\overline{\boldsymbol{V}} + \boldsymbol{f}(\overline{\boldsymbol{A}}) = \boldsymbol{g}, \tag{4.55}$$

where $\overline{\boldsymbol{A}}$ and $\overline{\boldsymbol{V}}$ are vectors of the unknowns $a_i(t)$ and v_k, respectively.

Equation (4.55) has two contributions:

$$\overline{\overline{\boldsymbol{C}}}^{\prime}\frac{\mathrm{d}\overline{\boldsymbol{A}}}{\mathrm{d}t} + \overline{\overline{\boldsymbol{D}}}^{\prime}\overline{\boldsymbol{V}} + \boldsymbol{f}(\overline{\boldsymbol{A}}) = \boldsymbol{g}, \tag{4.56}$$

$$\overline{\overline{\boldsymbol{C}}}^{\prime\prime}\frac{\mathrm{d}\overline{\boldsymbol{A}}}{\mathrm{d}t} + \overline{\overline{\boldsymbol{D}}}^{\prime\prime}\overline{\boldsymbol{V}} = \boldsymbol{h}. \tag{4.57}$$

These equations are valid for the macroscale and mesoscale problems. For the macroscale problem, equation (4.56) can be derived from (4.22) or (4.35) and equation (4.57) can be derived from (4.23) or (4.36). The elements of matrices in (4.56)–(4.57) are given by the expressions:

$$c^{\prime}_{i\,j} = \sum_{\Omega_e\in\Omega_c}\sum_{i,j\in\mathcal{N}_e}\Big(\sigma_M(\boldsymbol{x})\boldsymbol{S}^i_e(\boldsymbol{x}), \boldsymbol{S}^j_e(\boldsymbol{x})\Big)_{\Omega_e}, \tag{4.58}$$

$$c^{\prime\prime}_{i\,j} = \sum_{\Omega_e\in\Omega_c}\sum_{i\in\mathcal{N}_e,j\in\mathcal{N}_n}\Big(\sigma_M(\boldsymbol{x})\boldsymbol{S}^i_e(\boldsymbol{x}), \mathbf{grad}\,\boldsymbol{S}^j_n(\boldsymbol{x})\Big)_{\Omega_e}, \tag{4.59}$$

$$d^{\prime}_{i\,j} = \sum_{\Omega_e\in\Omega_c}\sum_{i\in\mathcal{N}_n,j\in\mathcal{N}_e}\Big(\sigma_M(\boldsymbol{x})\mathbf{grad}\,S^i_n(\boldsymbol{x}), \boldsymbol{S}^j_e(\boldsymbol{x})\Big)_{\Omega_e}, \tag{4.60}$$

$$d^{\prime\prime}_{i\,j} = \sum_{\Omega_e\in\Omega_c}\sum_{i,j\in\mathcal{N}_n}\Big(\sigma_M(\boldsymbol{x})\mathbf{grad}\,S^i_n(\boldsymbol{x}), \mathbf{grad}\,S^j_n(\boldsymbol{x})\Big)_{\Omega_e}, \tag{4.61}$$

$$f_j = \sum_{\Omega_e\in\Omega}\sum_{j\in\mathcal{N}_e}\Big(\boldsymbol{\mathcal{H}}_M\Big(\sum_{i\in\mathcal{N}_e}a_i(t)\mathbf{curl}\,\boldsymbol{S}^i_e(\boldsymbol{x}), \boldsymbol{x}\Big), \mathbf{curl}\,\boldsymbol{S}^j_e(\boldsymbol{x})\Big)_{\Omega_e}, \tag{4.62}$$

$$g_j = \sum_{\Omega_e\in\Omega_s}\sum_{j\in\mathcal{N}_e}\Big(\boldsymbol{j}_s(\boldsymbol{x}), \mathbf{curl}\,\boldsymbol{S}^j_e(\boldsymbol{x})\Big)_{\Omega_e}, \tag{4.63}$$

where the summation is carried out on elements Ω_e of domains Ω or Ω_c and $h_j = 0$. In (4.58)–(4.63), the integrals over domains Ω, Ω_s and Ω_c are split into elementary integrals (the first sum $\sum_{\Omega_e\in\Omega_i}$) in which only neighbouring basis functions contribute (the second sum).

For the mesoscale problem, the elements of matrices in (4.56)–(4.57) are given by:

$$c^{\prime}_{i\,j} = \sum_{\Omega_e\in\Omega_{mc}}\sum_{i,j\in\mathcal{N}_e}\Big(\sigma(\boldsymbol{y})\boldsymbol{S}^i_e(\boldsymbol{y}), \boldsymbol{S}^j_e(\boldsymbol{y})\Big)_{\Omega_e}, \tag{4.64}$$

$$c^{\prime\prime}_{i\,j} = \sum_{\Omega_e\in\Omega_{mc}}\sum_{i\in\mathcal{N}_e,j\in\mathcal{N}_n}\Big(\sigma(\boldsymbol{y})\boldsymbol{S}^i_e(\boldsymbol{y}), \mathbf{grad}\,\boldsymbol{S}^j_n(\boldsymbol{y})\Big)_{\Omega_e}, \tag{4.65}$$

$$d'_{i\,j} = \sum_{\Omega_e \in \Omega_{mc}} \sum_{i \in \mathcal{N}_n, j \in \mathcal{N}_e} \Big(\sigma(\boldsymbol{y})\mathbf{grad}\, S_n^i(\boldsymbol{y}), \boldsymbol{S}_e^j(\boldsymbol{y})\Big)_{\Omega_e}, \tag{4.66}$$

$$d''_{i\,j} = \sum_{\Omega_e \in \Omega_{mc}} \sum_{i,j \in \mathcal{N}_n} \Big(\sigma(\boldsymbol{y})\mathbf{grad}\, S_n^i(\boldsymbol{y}), \mathbf{grad}\, S_n^j(\boldsymbol{y})\Big)_{\Omega_e}, \tag{4.67}$$

$$f_j = \sum_{\Omega_e \in \Omega} \sum_{j \in \mathcal{N}_e} \Big(\boldsymbol{\mathcal{H}}\Big(\boldsymbol{b}_M + \sum_{i \in \mathcal{N}_e} a_i(t)\mathbf{curl}\, \boldsymbol{S}_e^i(\boldsymbol{y}), \boldsymbol{y}\Big), \mathbf{curl}\, \boldsymbol{S}_e^j(\boldsymbol{y})\Big)_{\Omega_e}, \tag{4.68}$$

$$g_j = \sum_{\Omega_e \in \Omega_{mc}} \sum_{j \in \mathcal{N}_e} \Big(\sigma(\boldsymbol{e}_M - \kappa\partial_t \boldsymbol{b}_M \times \boldsymbol{y}), \boldsymbol{S}_e^j(\boldsymbol{x})\Big)_{\Omega_e}, \tag{4.69}$$

$$h_j = \sum_{\Omega_e \in \Gamma_{mg}} \sum_{j \in \mathcal{N}_n} \Big(\boldsymbol{n} \cdot \boldsymbol{j}_M, S_n^j(\boldsymbol{x})\Big)_{\Omega_e}. \tag{4.70}$$

In (4.64)–(4.70), the integrals over domains Ω_m, Ω_{mc} are split into elemental integrals.

We use the Euler-implicit time-discretization scheme for the time derivative in (4.55). This leads to the following nonlinear full-discrete equation:

$$\overline{\overline{\boldsymbol{C}}}\frac{\overline{\boldsymbol{A}}^{n+1} - \overline{\boldsymbol{A}}^{n}}{\Delta t} + \overline{\overline{\boldsymbol{D}}}\overline{\boldsymbol{V}} + \boldsymbol{f}(\overline{\boldsymbol{A}}^{n+1}) = \boldsymbol{g}. \tag{4.71}$$

which relates the vector unknowns $\overline{\boldsymbol{A}}^{n+1}$ at time $t_{n+1} = t_n + \Delta t$ with previous values $\overline{\boldsymbol{A}}^{n}$ computed at t_n. Problem (4.71) is nonlinear and needs to be solved using nonlinear techniques.

We use the Newton–Raphson method for solving both the mesoscale and the macroscale problems. To this end, we define the residual:

$$\boldsymbol{r}(\overline{\boldsymbol{A}}^{n+1}, \overline{\boldsymbol{V}}) = \overline{\overline{\boldsymbol{C}}}\frac{\overline{\boldsymbol{A}}^{n+1} - \overline{\boldsymbol{A}}^{n}}{\Delta t} + \overline{\overline{\boldsymbol{D}}}\overline{\boldsymbol{V}} + \boldsymbol{f}(\overline{\boldsymbol{A}}^{n+1}) - \boldsymbol{g}. \tag{4.72}$$

which is goes to zero with a prescribed tolerance. The residual for the nonlinear iteration $m+1$ can be expressed in terms of the residual at the previous timestep m plus a linear tangent contribution:

$$\begin{aligned}\boldsymbol{r}(\overline{\boldsymbol{A}}_{m+1}^{n+1}, \overline{\boldsymbol{V}}_{m+1}) = \boldsymbol{r}(\overline{\boldsymbol{A}}_{m}^{n+1}, \overline{\boldsymbol{V}}_{m}) &+ \frac{\partial \boldsymbol{r}}{\partial \overline{\boldsymbol{A}}^{n+1}}\Big|_{\overline{\boldsymbol{A}}_m^{n+1}, \overline{\boldsymbol{V}}_m}(\overline{\boldsymbol{A}}_{m+1}^{n+1} - \overline{\boldsymbol{A}}_{m}^{n+1}) \\ &+ \frac{\partial \boldsymbol{r}}{\partial \overline{\boldsymbol{V}}}\Big|_{\overline{\boldsymbol{A}}_m^{n+1}, \overline{\boldsymbol{V}}_m}(\overline{\boldsymbol{V}}_{m+1} - \overline{\boldsymbol{V}}_{m}) \simeq \boldsymbol{0}.\end{aligned} \tag{4.73}$$

which leads to the final system:

$$\overline{\overline{\boldsymbol{K}}}(\overline{\boldsymbol{A}}_{m+1}^{n+1} - \overline{\boldsymbol{A}}_{m}^{n+1}) + \overline{\overline{\boldsymbol{D}}}(\overline{\boldsymbol{V}}_{m+1} - \overline{\boldsymbol{V}}_{m}) = -\boldsymbol{r}(\overline{\boldsymbol{A}}_{m}^{n+1}, \overline{\boldsymbol{V}}_{m}). \tag{4.74}$$

The elements of the tangent matrix in (4.74) is given by:

$$k_{ij} = \frac{1}{\Delta t}c_{ij} + \frac{\partial f_j}{\partial a_i^{n+1}} = \frac{1}{\Delta t}c_{ij} + \sum_e \Big(\frac{\partial \boldsymbol{\mathcal{H}}}{\partial \boldsymbol{b}}\mathbf{curl}\, \boldsymbol{S}_e^i(\boldsymbol{x}), \mathbf{curl}\, \boldsymbol{S}_e^j(\boldsymbol{x})\Big)_{\Omega_e}. \tag{4.75}$$

and therefore one needs to know $\partial\boldsymbol{\mathcal{H}}/\partial\boldsymbol{b}$ in order to compute $\overline{\overline{K}}$.

For the macroscale problem, $\partial\boldsymbol{\mathcal{H}}_M/\partial\boldsymbol{b}_M$ is computed using finite differences as explained in section 4.3.3. For the mesoscale problem with hysteresis, we use a $\boldsymbol{b}$-driven vectorized Jiles-Atherton model [19, 94, 108, 162]. In [94], authors have obtained the tangent matrix $\partial\boldsymbol{\mathcal{H}}/\partial\boldsymbol{b}_m$ by inverting the formula:

$$\partial\boldsymbol{\mathcal{B}}/\partial\boldsymbol{h}_m = \mu_0(\overline{\overline{1}} + \partial\boldsymbol{\mathcal{M}}/\partial\boldsymbol{h}_m), \tag{4.76}$$

where $\overline{\overline{1}}$ is the unit matrix. In (4.76), the total magnetization $\boldsymbol{\mathcal{M}} = \boldsymbol{\mathcal{M}}_{irr} + \boldsymbol{\mathcal{M}}_r$ has two contributions: the irreversible part $\boldsymbol{\mathcal{M}}_{irr}$ associated with energy dissipated through the pinning sites during a domain wall displacement. It is governed by the following differential equation:

$$\frac{\mathrm{d}\boldsymbol{\mathcal{M}}_{irr}}{\mathrm{d}\boldsymbol{h}_e} = \frac{\boldsymbol{\mathcal{M}}_{an} - \boldsymbol{\mathcal{M}}_{irr}}{k\delta}, \tag{4.77}$$

where the anhysteretic magnetization:

$$\boldsymbol{\mathcal{M}}_{an} = \boldsymbol{\mathcal{M}}_{sat} \coth\left(\frac{|\boldsymbol{h}_e|}{a} - \frac{a}{|\boldsymbol{h}_e|}\right)\frac{\boldsymbol{h}_e}{|\boldsymbol{h}_e|}, \tag{4.78}$$

represents the ideal curve obtained in the absence of hysteretic losses (see section (2.3)). The magnetic field $\boldsymbol{h}_e = \boldsymbol{h} + \alpha\boldsymbol{\mathcal{M}}$ is the effective magnetic field experienced by the domains. The reversible part $\boldsymbol{\mathcal{M}}_r = \boldsymbol{\mathcal{M}} - c\boldsymbol{\mathcal{M}}_{irr}$ is due to the reversible bonding of the Bloch walls. The Jiles-Atherton model is thus characterized by 5 parameters: α, k, c, a and $\boldsymbol{\mathcal{M}}_{sat}$.

The pseudocode of the overall multiscale algorithm is presented in Figure 4.3.

4.3.5 The static case

The static problem can be seen as a simplified version of the dynamic problem obtained by neglecting the time derivatives and the eddy currents.

The macroscale weak formulation is derived from the $\boldsymbol{a}-v$ formulation described in section 4.3.1. The three-dimensional macroscale weak formulation reads: find $\boldsymbol{a}_M \in \boldsymbol{H}_e(\mathbf{curl}, \Omega)$ such that

$$\left(\boldsymbol{\mathcal{H}}_M(\mathbf{curl}_x\,\boldsymbol{a}_M), \mathbf{curl}_x\,\boldsymbol{a}'_M\right)_\Omega + \left\langle \boldsymbol{n} \times \boldsymbol{h}_M, \boldsymbol{a}'_M\right\rangle_{\Gamma_h} = \left(\boldsymbol{j}_s, \boldsymbol{a}'_M\right)_{\Omega_s} \tag{4.79}$$

holds for all test functions $\boldsymbol{a}'_M \in \boldsymbol{H}^0_e(\Omega)$.

The two-dimensional macroscale problem reads: find $a_{zM} \in H^1_e(\Omega)$ such that

$$\left(\boldsymbol{\mathcal{H}}_M(\mathbf{1}_z \times \mathbf{grad}_x\, a_{zM}), \mathbf{1}_z \times \mathbf{grad}_x\, a'_{zM}\right)_\Omega + \langle \boldsymbol{n} \times \boldsymbol{h}_M, a'_{zM}\mathbf{1}_z\rangle_{\Gamma_h} = \left(j_s, a'_{zM}\right)_{\Omega_s} \tag{4.80}$$

holds for all test functions $a'_{zM} \in H^{10}_e(\Omega)$.

Macro	**Meso**
• Read input (macro mesh, material laws, etc.).	Generate meso meshes
• Prescribe BCs.	
• Initialize $\boldsymbol{a}_M(t=0)$	
• **Begin time loop** while $t_n < t_f$ do:	
(a) **Begin nonlinear loop** while $(m < m_{max})$ and (res $>$ tol) do:	
◦ For each quadrature point: $\xrightarrow[\textbf{downscaling}]{\boldsymbol{e}_M,\, \boldsymbol{b}_M,\, \boldsymbol{j}_M}$	<u>**Cell problem analysis**</u>
	1. Prescribe the BCs
	2. Impose the macro sources
	3. Initialize $\boldsymbol{a}_m(t=t_n)$
	4. Solve the cell problem
◦ Assemble matrix and RHS: $\xleftarrow[\textbf{upscaling}]{\boldsymbol{h}_M,\, \partial\boldsymbol{\mathcal{H}}_M/\partial\boldsymbol{b}_M}$	5. Compute $\boldsymbol{h}_M$ and $\partial\boldsymbol{\mathcal{H}}_M/\partial\boldsymbol{b}_M$
◦ Solve	
◦ Check convergence 1. If not, $m \leftarrow m+1$. 2. Else, save. Leave the nonlinear loop and go to (b).	
End nonlinear loop.	
(b) $t_n \leftarrow t_n + \Delta t$.	
• **End time loop**.	

Figure 4.3: Pseudocode of the multiscale algorithm for the nonlinear multiscale magnetic flux density conforming formulations.

The three-dimensional mesoscale problem can be derived from (4.35): find $\boldsymbol{a}_c \in$

$\boldsymbol{H}(\mathbf{curl};\mathcal{Y})$ such that

$$\left(\boldsymbol{\mathcal{H}}(\mathbf{curl}_y \boldsymbol{a}_c + \boldsymbol{b}_M), \mathbf{curl}_y \boldsymbol{a}_c^{'}\right)_{\Omega_m} = 0, \tag{4.81}$$

holds for all test functions $\boldsymbol{a}_c^{'} \in \boldsymbol{H}(\mathbf{curl};\mathcal{Y})$ and the two-dimensional mesoscale formulation reads: find $a_{zc} \in H^1(\mathcal{Y})$ such that

$$\left(\boldsymbol{\mathcal{H}}(\mathbf{1}_z \times \mathbf{grad}_y\, a_{zc} + \boldsymbol{b}_M), \mathbf{1}_z \times \mathbf{grad}_y\, a_{zc}^{'}\right)_{\Omega_m} = 0 \tag{4.82}$$

holds for all test functions $a_{zc}^{'} \in H^1(\mathcal{Y})$.

4.4 Magnetic field conforming multiscale formulations: dynamic case

4.4.1 The macroscale problem

This problem is derived from the macroscale equations:

$$\mathbf{curl}\,_x \boldsymbol{h}_M = \boldsymbol{j}_M, \tag{4.83}$$

$$\mathbf{curl}\,_x \boldsymbol{e}_M = -\partial_t \boldsymbol{b}_M, \tag{4.84}$$

$$\operatorname{div}\,_x \boldsymbol{b}_M = 0, \tag{4.85}$$

$$\boldsymbol{b}_M(\boldsymbol{x},t) = \boldsymbol{\mathcal{B}}_M(\boldsymbol{h}_M(\boldsymbol{x},t),\boldsymbol{x}), \tag{4.86}$$

$$\boldsymbol{e}_M(\boldsymbol{x},t) = \boldsymbol{\mathcal{E}}_M(\boldsymbol{j}_M(\boldsymbol{x},t),\boldsymbol{x}). \tag{4.87}$$

In this case, Ampère's equation (4.83) together with the constitutive laws (4.86)–(4.87) are strongly satisfied. Therefore Faraday's equation must be satisfied in the weak sense. Using results of section 2.5.4, we get the following three-dimensional macroscale weak equation: find $\boldsymbol{h}_M \in \boldsymbol{H}_h(\mathbf{curl};\Omega)$ such that

$$\left(\partial_t \boldsymbol{\mathcal{B}}_M(\boldsymbol{h}_M), \boldsymbol{h}_M^{'}\right)_{\Omega} + \left(\sigma_M^{-1}\mathbf{curl}_x\, \boldsymbol{h}_M, \mathbf{curl}_x\, \boldsymbol{h}_M^{'}\right)_{\Omega_c} + \left(\sigma_M^{-1}\boldsymbol{j}_s, \mathbf{curl}_x\, \boldsymbol{h}_M^{'}\right)_{\Omega_s} + \left\langle \boldsymbol{n} \times \boldsymbol{e}_M, \boldsymbol{h}_M^{'}\right\rangle_{\Gamma_e} = 0, \tag{4.88}$$

holds for all $\boldsymbol{h}_M^{'} \in \boldsymbol{H}_h^0(\mathbf{curl};\Omega)$. In the case of magnetic laws without memory $\boldsymbol{\mathcal{B}}_M(\boldsymbol{h}_M(\boldsymbol{x},t),\boldsymbol{x})$, the time derivative of the magnetic induction can be expressed as:

$$\partial_t \boldsymbol{\mathcal{B}}_M = \frac{\partial \boldsymbol{\mathcal{B}}_M}{\partial \boldsymbol{h}_M}\partial_t \boldsymbol{h}_M. \tag{4.89}$$

Equation (4.88) becomes:

$$\left(\frac{\partial \boldsymbol{\mathcal{B}}_M}{\partial \boldsymbol{h}_M}\partial_t \boldsymbol{h}_M, \boldsymbol{h}_M^{'}\right)_{\Omega} + \left(\sigma_M^{-1}\mathbf{curl}_x\, \boldsymbol{h}_M, \mathbf{curl}_x\, \boldsymbol{h}_M^{'}\right)_{\Omega_c} +$$

$$\left(\sigma_M^{-1}\boldsymbol{j}_s, \mathbf{curl}_x\, \boldsymbol{h}_M^{'}\right)_{\Omega_s} + \left\langle \boldsymbol{n} \times \boldsymbol{e}_M, \boldsymbol{h}_M^{'} \right\rangle_{\Gamma_e} = 0. \quad (4.90)$$

In the non-conducting region Ω_c^C only the first term of (4.88) exists. The magnetic field can therefore be derived from a magnetic scalar potential ϕ_M governed by the following partial differential equation:

$$\operatorname{div} \boldsymbol{\mathcal{B}}_M(\boldsymbol{h}_s - \mathbf{grad}_x\, \phi_M) = 0. \quad (4.91)$$

The weak form in Ω_c^C then reads: find $\phi_M \in H^1(\Omega_c^C)$ such that

$$\left(\boldsymbol{\mathcal{B}}_M(\boldsymbol{h}_s - \mathbf{grad}_x\, \phi_M), \mathbf{grad}_x\, \phi_M^{'}\right)_{\Omega_c^C} + \left\langle \boldsymbol{n} \cdot \boldsymbol{b}_M, \phi_M^{'} \right\rangle_{\Gamma_h} = 0. \quad (4.92)$$

4.4.2 The mesoscale problem

In the case of $\boldsymbol{b}$-conform formulations, the spatial differential operator was applied to the term with the magnetic constitutive law (see equation (4.26)). This is not the case for $\boldsymbol{h}$-conform formulations; the term $\boldsymbol{b}_m$ for which we want to compute the homogenized constitutive law is involved with time derivative (equation (4.95)). Therefore we are going to define two types of problems for $\boldsymbol{h}$-conform formulations.

The first one used for computing the homogenized magnetic constitutive laws is derived from equations of the two-scale convergence theory (equations (3.101)–(3.102)). The three-dimensional weak formulation of this problem reads: find $\phi_c \in H^1(\mathcal{Y})$ such that

$$\left(\boldsymbol{\mathcal{B}}(\boldsymbol{h}_M - \mathbf{grad}_y\, \phi_c), \mathbf{grad}_y\, \phi_c^{'}\right)_{\Omega_m} = 0, \quad (4.93)$$

hold for all test functions $\phi_c^{'} \in H^1(\mathcal{Y}_c^C)$ and for every $t \in]0, T[$

The second will be used for defining a mesoscale problem that includes eddy currents. In order to define this problem, we use the same approach as the one used in section 4.3.2. We start with the modified two-scale version of the problem (3.93)–(3.96) :

$$\mathbf{curl}_x\, \boldsymbol{h}_M + \mathbf{curl}_y\, \boldsymbol{h}_1 = \boldsymbol{j}_m, \quad (4.94)$$
$$\mathbf{curl}\, \boldsymbol{e}_m^{\varepsilon} = -\partial_t \boldsymbol{b}_m, \quad (4.95)$$
$$\operatorname{div}_x \boldsymbol{b}_M + \operatorname{div}_y \boldsymbol{b}_1 = 0, \quad (4.96)$$
$$\boldsymbol{b}_m(\boldsymbol{x}, \boldsymbol{y}, t) = \boldsymbol{\mathcal{B}}(\boldsymbol{h}_m(\boldsymbol{x}, \boldsymbol{y}, t), \boldsymbol{x}, \boldsymbol{y}), \quad (4.97)$$
$$\boldsymbol{e}_m(\boldsymbol{x}, \boldsymbol{y}, t) = \boldsymbol{\mathcal{E}}(\boldsymbol{j}_m(\boldsymbol{x}, \boldsymbol{y}, t), \boldsymbol{x}, \boldsymbol{y}), \quad (4.98)$$

in which we keep Faraday's equation (4.95) intact. The electric field $\boldsymbol{e}_m^{\varepsilon}$ is the restriction of the multiscale electric field $\boldsymbol{e}^{\varepsilon}$ to the domain Ω_m. Using the two-scale convergence theory we can express the **curl** of the magnetic field at the mesoscale in terms of the **curl** of the magnetic field at the macroscale and the **curl** of the mesoscale correction term such that

$$\mathbf{curl}_y\, \boldsymbol{h}_m = \mathbf{curl}_x\, \boldsymbol{h}_M + \mathbf{curl}_y\, \boldsymbol{h}_1. \quad (4.99)$$

Using Ampère's law at the macroscale together with the vector identity $\mathbf{curl}_y\,(\boldsymbol{j}_M \times \boldsymbol{y}) = (n-1)\boldsymbol{j}_M$ ($n = 2,3$ for 2D and 3D problems, respectively) we can write:

$$\begin{aligned}\mathbf{curl}_y\,\boldsymbol{h}_m = \mathbf{curl}_y &\Big(\boldsymbol{h}_1 + \boldsymbol{h}_M + \kappa(\mathbf{curl}_x\,\boldsymbol{h}_M \times \boldsymbol{y})\Big)\\ &= \mathbf{curl}_y\Big(\boldsymbol{h}_1 + \boldsymbol{h}_M - \kappa(\boldsymbol{j}_M \times \boldsymbol{y})\Big)\end{aligned} \tag{4.100}$$

with $\kappa = (n-1)^{-1}$, since $\mathbf{curl}_y\,\boldsymbol{h}_M \equiv 0$. This provides a natural development of $\boldsymbol{h}_m$ in terms of a local, rapidly fluctuating component and a large scale component.

Inserting the orthogonal decomposition $\boldsymbol{j}_m = \boldsymbol{j}_M + \mathbf{curl}_y\,\boldsymbol{t}_c$ derived from (3.85) in (4.94) we get the following equation:

$$\mathbf{curl}\,_x\boldsymbol{h}_M + \mathbf{curl}\,_y\boldsymbol{h}_1 = \boldsymbol{j}_M + \mathbf{curl}_y\,\boldsymbol{t}_c. \tag{4.101}$$

We can use (4.100) to express the first order term of the electric field $\boldsymbol{h}_1$ in terms of the correction term $\boldsymbol{t}_c$ as:

$$\boldsymbol{h}_1 = \boldsymbol{t}_c - \mathbf{grad}_y\,\omega_c, \tag{4.102}$$

possibly leading to the $\boldsymbol{h}$ formulation [33, 63, 64] or the $\boldsymbol{t}-\omega$ formulation [125, 126]. In the remainder of this section, we adopt the $\boldsymbol{h}$ formulation.

The electric current density is not defined in the non-conducting regions. For such regions, Ampère's equation reads;

$$\mathbf{curl}_y\,(\boldsymbol{h}_1 + \boldsymbol{h}_M + \kappa(\mathbf{curl}_x\,\boldsymbol{h}_M \times \boldsymbol{y})) = \boldsymbol{0}, \tag{4.103}$$

so that:

$$\boldsymbol{h}_1 + \boldsymbol{h}_M + \kappa(\mathbf{curl}_x\,\boldsymbol{h}_M \times \boldsymbol{y}) = -\mathbf{grad}_y\,\overline{\phi}_c. \tag{4.104}$$

Instead of using the total scalar potential $\overline{\phi}_c$, we rather define a reduced potential ϕ_c such that

$$-\,\mathbf{grad}_y\,\overline{\phi}_c = \boldsymbol{h}_M - \mathbf{grad}_y\,\phi_c. \tag{4.105}$$

The mesoscale magnetic field $\boldsymbol{h}_m$ can therefore be developed as:

$$\begin{cases} \boldsymbol{h}_m = \boldsymbol{h}_M + \kappa(\boldsymbol{j}_M \times \boldsymbol{y}) + \boldsymbol{h}_1 & \text{in } \Omega_{mc},\\ \boldsymbol{h}_m = \boldsymbol{h}_M - \mathbf{grad}_y\,\phi_c & \text{in } \Omega_{mc}^C,\end{cases} \tag{4.106}$$

where the fields $\boldsymbol{h}_M$ and $\boldsymbol{j}_M$ are source terms from the macroscale problem.

Using these developments together with the expression (4.89) of the time derivative we get the following equations for the conducting and the non-conducting regions:

$$\begin{aligned}&\mathbf{curl}_y\Big(\sigma^{-1}(\boldsymbol{y})\Big(\mathbf{curl}_y\,\boldsymbol{h}_1 + \boldsymbol{j}_M\Big)\Big) +\\ &\qquad\frac{\partial \boldsymbol{\mathcal{B}}}{\partial \boldsymbol{h}_m}\Big(\partial_t\boldsymbol{h}_1 + \partial_t\boldsymbol{h}_M + \kappa(\partial_t\boldsymbol{j}_M \times \boldsymbol{y})\Big) = 0 \quad \text{in} \quad \Omega_{mc},\end{aligned} \tag{4.107}$$

$$\operatorname{div}_y \boldsymbol{\mathcal{B}}(\boldsymbol{h}_M - \mathbf{grad}\, \phi_c) = 0 \quad \text{in} \quad \Omega_{mc}^C, \tag{4.108}$$

with $\boldsymbol{h}_m = \boldsymbol{h}_1 + \boldsymbol{h}_M + \kappa(\boldsymbol{j}_M \times \boldsymbol{y})$. The mesoscale three-dimensional weak formulation then reads: find $\boldsymbol{h}_1 \in \boldsymbol{H}(\mathbf{curl}; \mathcal{Y}_c)$ and $\phi_c \in H^1(\mathcal{Y}_c^C)$ such that

$$\Big(\sigma_m^{-1}(\mathbf{curl}_y\, \boldsymbol{h}_1 + \boldsymbol{j}_M), \mathbf{curl}_y\, \boldsymbol{h}_1^{'}\Big)_{\Omega_{mc}} + \Big(\frac{\partial \boldsymbol{\mathcal{B}}}{\partial \boldsymbol{h}_m}\Big(\partial_t \boldsymbol{h}_1 + \partial_t \boldsymbol{h}_M + \kappa(\partial_t \boldsymbol{j}_M \times \boldsymbol{y})\Big), \boldsymbol{h}_1^{'}\Big)_{\Omega_{mc}} = 0, \tag{4.109}$$

$$\Big(\boldsymbol{\mathcal{B}}(\boldsymbol{h}_M - \mathbf{grad}_y\, \phi_c), \mathbf{grad}_y\, \phi_c^{'}\Big)_{\Omega_{mc}^C} = 0, \tag{4.110}$$

hold for all test functions $\boldsymbol{h}_1^{'} \in \boldsymbol{H}(\mathbf{curl}; \mathcal{Y}_c)$ and $\phi_c^{'} \in H^1(\mathcal{Y}_c^C)$ and for every $t \in]0, T[$. The domain Ω_{mc} is the conducting part of the mesoscale domain Ω_m.

For the two-dimensional case, the mesoscale weak formulation becomes: find $h_{1z} \in H^1(\mathcal{Y}_c)$ and $\phi_c \in H^1(\mathcal{Y}_c^C)$ such that

$$\Big(\sigma_m^{-1}(\mathbf{1}_z \times \mathbf{grad}_y\, h_{1z} + \boldsymbol{j}_M), \mathbf{1}_z \times \mathbf{grad}_y\, h_{1z}^{'}\Big)_{\Omega_{mc}} + \Big(\frac{\partial \boldsymbol{\mathcal{B}}}{\partial \boldsymbol{h}_m}\Big(\mathbf{1}_z \times \mathbf{grad}_y\, (\partial_t h_{1z}) + \partial_t \boldsymbol{h}_M + \kappa(\partial_t \boldsymbol{j}_M \times \boldsymbol{y})\Big), \mathbf{1}_z h_{1z}^{'}\Big)_{\Omega_{mc}} = 0, \tag{4.111}$$

$$\Big(\boldsymbol{\mathcal{B}}(\boldsymbol{h}_M - \mathbf{grad}_y\, \phi_c), \mathbf{grad}_y\, \phi_c^{'}\Big)_{\Omega_{mc}^C} = 0, \tag{4.112}$$

hold for all test functions $h_{1z}^{'} \in H^1(\mathcal{Y}_c)$ and $\phi_c^{'} \in H^1(\mathcal{Y}_c^C)$ and for every $t \in]0, T[$. The mesoscale magnetic field $\boldsymbol{h}_m$ is given by $\boldsymbol{h}_m = \mathbf{1}_z \times \mathbf{grad}_y\, h_{1z} + \boldsymbol{h}_M + \kappa(\boldsymbol{j}_M \times \boldsymbol{y})$.

4.4.3 The scale transitions

The macroscale and the mesoscale problems need to exchange information through the scale transitions like in the case of the $\boldsymbol{a} - v$ formulation.

During the *downscaling*, the macroscale fields $\boldsymbol{h}_M$ and $\boldsymbol{j}_M$ are imposed as source terms for the mesoscale problem. Boundary conditions for the mesoscale problem are determined so as to respect the two-scale convergence of the fields. The convergence of the correction term of the electric current density $\boldsymbol{j}_c$ leads to the following condition for the tangential component of $\boldsymbol{h}_1$:

$$\frac{1}{|\Omega_{mc}|} \int_{\Omega_{mc}} \boldsymbol{j}_m \mathrm{d}\boldsymbol{y} = \boldsymbol{j}_M \implies \int_{\Omega_{mc}} \mathbf{curl}_y\, \boldsymbol{h}_1 \mathrm{d}\boldsymbol{y} = \oint_{\Gamma_{mc}} \boldsymbol{n} \times \boldsymbol{h}_1\, \mathrm{d}y = \mathbf{0}. \tag{4.113}$$

This condition is fulfilled if $\boldsymbol{h}_1$ belongs to the space $\boldsymbol{H}(\mathbf{curl}; \mathcal{Y})$, i.e. if $\boldsymbol{h}_1$ is periodic on the cell. This condition is fulfilled thanks to the two-scale convergence result in Appendix C.3.

The *upscaling* consists in computing the missing constitutive laws σ_M^{-1}, $\boldsymbol{b}_M$ together with $\partial \boldsymbol{\mathcal{B}}_M / \partial \boldsymbol{h}_M$ at the macroscale using the mesoscale fields. Due to the linearity of the electric law, the asymptotic expansion theory can be applied (see section 3.4.1.1). Therefore, we compute once for all the homogenized electric resistivity by solving a cell problem. The electric resistivity is then upscaled by means of:

$$\sigma_M^{-1} = \frac{1}{|\Omega_m|} \int_{\Omega_m} \Big((\sigma_m)^{-1} (\bar{\bar{1}} - \mathbf{curl}_y \, \bar{\bar{\theta}}(\boldsymbol{y})) \Big) \mathrm{d}y, \tag{4.114}$$

where the periodic functions $\bar{\bar{\theta}} = (\boldsymbol{\theta}_1, \boldsymbol{\theta}_2, \boldsymbol{\theta}_3)^T$ are solutions of the cell problem: find $\boldsymbol{\theta}_i \in \boldsymbol{H}(\mathbf{curl}; \mathcal{Y})$ such that

$$\int_{\Omega_m} (\mathbf{curl}_y \, \boldsymbol{\theta}^{'})^T (\sigma_m)^{-1} \Big(\mathbf{curl}_y \, \boldsymbol{\theta}_i - \boldsymbol{e}_i \Big) \; \mathrm{d}y = 0 \tag{4.115}$$

holds for all $\boldsymbol{\theta}^{'} \in \boldsymbol{H}(\mathbf{curl}; \mathcal{Y})$. Another approach consists in computing the homogenized electric conductivity σ_M using the approach described in the section 4.3.3 and then invert it.

The *upscaling* of the nonlinear magnetic law is performed by simple averaging as a consequence of the two-scale convergence of the magnetic flux density $\boldsymbol{b}$:

$$\frac{1}{|\Omega_{mc}|} \int_{\Omega_{mc}} \boldsymbol{\mathcal{B}}(\boldsymbol{h}_1 + \boldsymbol{h}_M + \kappa(\boldsymbol{j}_M \times \boldsymbol{y})) \mathrm{d}y + \frac{1}{|\Omega_{mc}^C|} \int_{\Omega_{mc}^C} \boldsymbol{\mathcal{B}}(\boldsymbol{h}_M - \mathbf{grad}_y \, \phi_c) \mathrm{d}y = \boldsymbol{\mathcal{B}}_M. \tag{4.116}$$

The tangent matrix $\partial \boldsymbol{\mathcal{B}}_M / \partial \boldsymbol{h}_M$ for the Newton–Raphson scheme is obtained using the finite differences method like the one used in section 4.3.3. Three mesoscale problems similar to (4.93) with constant (time and space independent) magnetic field perturbation terms $\delta \boldsymbol{h}_i$ are solved. The term $\delta \boldsymbol{h}_i$ is added to the macroscale source in the direction "i" and the total (perturbed) mesoscale magnetic field becomes: $\boldsymbol{h}_m = \boldsymbol{h}_M + \mathbf{grad}_y \, \phi_c + \delta \boldsymbol{h}_i$. The three-dimensional perturbed problem then reads: find $\phi_c \in H^1(\mathcal{Y})$ such that

$$\Big(\boldsymbol{\mathcal{B}}(\boldsymbol{h}_M - \mathbf{grad}_y \, \phi_c + \delta \boldsymbol{h}_i), \mathbf{grad}_y \, \phi_c^{'} \Big)_{\Omega_{mc}^C} = 0, \tag{4.117}$$

hold for all test functions $\phi_c^{'} \in H^1(\mathcal{Y})$ and for every $t \in]0, T[$ and the two-dimensional mesoscale weak formulation becomes: $\phi_c \in H^1(\mathcal{Y})$ such that

$$\Big(\boldsymbol{\mathcal{B}}(\boldsymbol{h}_M - \mathbf{grad}_y \, \phi_c + \delta \boldsymbol{h}_i), \mathbf{grad}_y \, \phi_c^{'} \Big)_{\Omega_{mc}^C} = 0, \tag{4.118}$$

hold for all test functions $\phi_c^{'} \in H^1(\mathcal{Y})$ and for almost every $t \in]0, T[$.

4.4.4 Finite element implementation

An approach similar to the one used in section 4.3.4 is hereby described for the $\boldsymbol{h}$-conform formulations. The macroscale and the mesoscale problems are solved in a staggered way using the FE method. Both problems are nonlinear and solved using the Newton–Raphson scheme. The numerical schemes of the macroscale and the mesoscale problems remain almost the same. We will point out the differences if they exist.

The first step for the numerical solution is to spatially discretize the fields. We use mixed elements and get the following expressions:

$$\boldsymbol{h}(\boldsymbol{x},t) = \sum_{i\in\mathcal{N}_e} h_i(t)\boldsymbol{S}_e^i(\boldsymbol{x}), \tag{4.119}$$

$$\phi(\boldsymbol{x}) = \sum_{k\in\mathcal{N}_n} \phi_k S_n^k(\boldsymbol{x}) \tag{4.120}$$

$$\boldsymbol{j}(\boldsymbol{x},t) = \sum_{i\in\mathcal{N}_e} h_i(t)\,\mathbf{curl}\,\boldsymbol{S}_e^i(\boldsymbol{x}), \tag{4.121}$$

$$\partial_t\boldsymbol{h}(\boldsymbol{x},t) = \sum_{i\in\mathcal{N}_e} \frac{\mathrm{d}h_i(t)}{\mathrm{d}t}\boldsymbol{S}_e^i(\boldsymbol{x}), \tag{4.122}$$

$$\mathbf{grad}\,\phi(\boldsymbol{x}) = \sum_{k\in\mathcal{N}_n} \phi_k\mathbf{grad}\,S_n^k(\boldsymbol{x}). \tag{4.123}$$

The fields $\boldsymbol{h}$ and ϕ are used to represent both the macroscale fields $\boldsymbol{h}_M$ and ϕ_M and the mesoscale fields $\boldsymbol{h}_m$ and ϕ_m. The basis functions $\boldsymbol{S}_e^i(\boldsymbol{x})$ and $S_n^k(\boldsymbol{x})$ are chosen as the standard edge and nodal Whitney forms, spanning discrete subspaces of $\boldsymbol{H}(\mathbf{curl};\Omega)$ and $H^1(\Omega)$, respectively [90]. The degree of freedom $h_i(t)$ and ϕ_k are the unknowns of the FE problem and $\mathcal{N}_e$ and $\mathcal{N}_n$ the total numbers of the unknowns of the fields $\boldsymbol{h}$ and ϕ, respectively. With formulae (4.119)–(4.123) we get the following discretized equations:

$$\overline{\overline{\boldsymbol{M}}}(\overline{\boldsymbol{H}})\frac{\mathrm{d}\overline{\boldsymbol{H}}}{\mathrm{d}t} + \overline{\overline{\boldsymbol{R}}}\overline{\boldsymbol{H}} + \boldsymbol{g}(\overline{\boldsymbol{\phi}}) = \boldsymbol{j}, \tag{4.124}$$

where $\overline{\boldsymbol{H}}$ and $\overline{\boldsymbol{\phi}}$ are vectors of the unknowns $h_i(t)$ and ϕ_k, respectively. These equations are valid for the macroscale and the mesoscale problems.

For the macroscale problem, the matrices in (4.124) are given by:

$$m_{i\,j} = \sum_{\Omega_e\in\Omega_c}\sum_{i,j\in\mathcal{N}_e}\left(\frac{\partial\boldsymbol{\mathcal{B}}_M}{\partial\boldsymbol{h}_M}\Big(\sum_{i\in\mathcal{N}_e} h_{M\,i}(t)\mathbf{curl}_x\,\boldsymbol{S}_e^i(\boldsymbol{x}),\boldsymbol{x}\Big)\boldsymbol{S}_e^i(\boldsymbol{x}),\boldsymbol{S}_e^j(\boldsymbol{x})\right)_{\Omega_e}, \tag{4.125}$$

$$r_{i\,j} = \sum_{\Omega_e\in\Omega_c}\sum_{i,j\in\mathcal{N}_e}\left(\sigma_M^{-1}(\boldsymbol{x})\mathbf{curl}_x\,S_e^i(\boldsymbol{x}),\mathbf{curl}_x\,S_e^j(\boldsymbol{x})\right)_{\Omega_e}, \tag{4.126}$$

$$g_j = \sum_{\Omega_e\in\Omega}\sum_{j\in\mathcal{N}_n}\left(\boldsymbol{\mathcal{B}}_M\Big(\boldsymbol{h}_s - \sum_{i\in\mathcal{N}_n}\phi_{M\,i}\mathbf{grad}_x\,\boldsymbol{S}_n^i(\boldsymbol{x}),\boldsymbol{x}\Big),\mathbf{grad}_x\,\boldsymbol{S}_n^j(\boldsymbol{x})\right)_{\Omega_e}, \tag{4.127}$$

$$j_j = \sum_{\Omega_e\in\Omega_s}\sum_{j\in\mathcal{N}_e}\left(\sigma_M^{-1}(\boldsymbol{x})\boldsymbol{j}_s(\boldsymbol{x}),\mathbf{curl}_x\,\boldsymbol{S}_e^j(\boldsymbol{x})\right)_{\Omega_e}, \tag{4.128}$$

where $h_{M\,i}$ and $\phi_{M\,i}$ are the degrees of freedom of the macroscale fields.

For the mesoscale problem, the matrices in (4.124) are given by:

$$m_{ij} = \sum_{\Omega_e\in\Omega_c}\sum_{i,j\in\mathcal{N}_e}\Big(\frac{\partial\boldsymbol{\mathcal{B}}}{\partial\boldsymbol{h}_m}(\boldsymbol{h}_M+\kappa(\boldsymbol{j}_M\times\boldsymbol{y})+\sum_{i\in\mathcal{N}_e}h_{ci}(t)\mathbf{curl}_y\,\boldsymbol{S}_e^i(\boldsymbol{y}),\boldsymbol{y})$$
$$\boldsymbol{S}_e^i(\boldsymbol{y}),\boldsymbol{S}_e^j(\boldsymbol{y})\Big)_{\Omega_e}, \quad (4.129)$$

$$r_{ij} = \sum_{\Omega_e\in\Omega_c}\sum_{i,j\in\mathcal{N}_e}\Big(\sigma^{-1}(\boldsymbol{y})\mathbf{curl}_y\,S_e^i(\boldsymbol{y}),\mathbf{curl}_y\,S_e^j(\boldsymbol{y})\Big)_{\Omega_e}, \quad (4.130)$$

$$g_j = \sum_{\Omega_e\in\Omega}\sum_{j\in\mathcal{N}_n}\Big(\boldsymbol{\mathcal{B}}\Big(\boldsymbol{h}_M-\sum_{i\in\mathcal{N}_n}\phi_{ci}\mathbf{grad}_y\,\boldsymbol{S}_n^i(\boldsymbol{y}),\boldsymbol{y}\Big),\mathbf{grad}_y\,\boldsymbol{S}_n^j(\boldsymbol{y})\Big)_{\Omega_e}, \quad (4.131)$$

$$j_j = \sum_{\Omega_e\in\Omega_s}\sum_{j\in\mathcal{N}_e}\Big(\sigma^{-1}(\boldsymbol{y})\boldsymbol{j}_s(\boldsymbol{y}),\mathbf{curl}_y\,\boldsymbol{S}_e^j(\boldsymbol{y})\Big)_{\Omega_e}, \quad (4.132)$$

where h_{ci} and ϕ_{ci} are the degrees of freedom of the mesoscale, correction fields.

We use the Euler-implicit time-discretization scheme for the time derivative in (4.55). This leads to the following nonlinear full-discrete equation:

$$\overline{\overline{\boldsymbol{M}}}(\overline{\boldsymbol{H}}^{n+1})\frac{\overline{\boldsymbol{H}}^{n+1}-\overline{\boldsymbol{H}}^{n}}{\Delta t}+\overline{\boldsymbol{R}\boldsymbol{H}}^{n+1}+\boldsymbol{g}(\overline{\boldsymbol{\phi}})=\boldsymbol{j}, \quad (4.133)$$

which relates the vector unknowns $\overline{\boldsymbol{H}}^{n+1}$ at time $t_{n+1}=t_n+\Delta t$ with previous values $\overline{\boldsymbol{H}}^{n}$ computed at t_n. Problem (4.133) is nonlinear and needs to be solved using nonlinear techniques.

We use the Newton – Raphson method for solving both the mesoscale and the macroscale problems. To this end, we define the residual:

$$\boldsymbol{r}(\overline{\boldsymbol{H}}^{n+1},\overline{\boldsymbol{\phi}})=\overline{\overline{\boldsymbol{M}}}(\overline{\boldsymbol{H}}^{n+1})\frac{\overline{\boldsymbol{H}}^{n+1}-\overline{\boldsymbol{H}}^{n}}{\Delta t}+\overline{\overline{\boldsymbol{R}}}\overline{\boldsymbol{H}}^{n+1}+\boldsymbol{g}(\overline{\boldsymbol{\phi}})-\boldsymbol{j}, \quad (4.134)$$

which must go to zero with a prescribed tolerance. The residual for the nonlinear iteration $m+1$ can be expressed in terms of the residual at the previous timestep m plus a linear tangent contribution:

$$\boldsymbol{r}(\overline{\boldsymbol{H}}_{m+1}^{n+1},\overline{\boldsymbol{\phi}}_{m+1})=\boldsymbol{r}(\overline{\boldsymbol{H}}_{m}^{n+1},\overline{\boldsymbol{\phi}}_{m})+\frac{\partial\boldsymbol{r}}{\partial\overline{\boldsymbol{H}}^{n+1}}\Big|_{\overline{\boldsymbol{H}}_m^{n+1},\overline{\boldsymbol{\phi}}_m}(\overline{\boldsymbol{H}}_{m+1}^{n+1}-\overline{\boldsymbol{H}}_{m}^{n+1})$$
$$+\frac{\partial\boldsymbol{r}}{\partial\overline{\boldsymbol{\phi}}}\Big|_{\overline{\boldsymbol{H}}_m^{n+1},\overline{\boldsymbol{\phi}}_m}(\overline{\boldsymbol{\phi}}_{m+1}-\overline{\boldsymbol{\phi}}_{m})\simeq\boldsymbol{0}, \quad (4.135)$$

which leads to the final system:

$$\overline{\overline{\boldsymbol{K}}}(\overline{\boldsymbol{H}}_{m+1}^{n+1}-\overline{\boldsymbol{H}}_{m}^{n+1})+\overline{\overline{\boldsymbol{L}}}(\overline{\boldsymbol{\phi}}_{m+1}-\overline{\boldsymbol{\phi}}_{m})=-\boldsymbol{r}(\overline{\boldsymbol{H}}_{m}^{n+1},\overline{\boldsymbol{\phi}}_{m}). \quad (4.136)$$

The elements of the tangent matrix in (4.136) are given by:

$$k_{ij}=\frac{1}{\Delta t}m_{ij}+r_{ij}, \quad (4.137)$$

$$l_{ij} = \frac{\partial g_j}{\partial \phi_{m\,i}} = \sum_{\Omega_e \in \Omega_c^C} \sum_{i,j \in \mathcal{N}_n} \Big(\boldsymbol{\mathcal{B}}(\boldsymbol{h}_{tot}) \,\mathbf{grad}\, \boldsymbol{S}_n^i(\boldsymbol{y}), \mathbf{grad}\, \boldsymbol{S}_n^j(\boldsymbol{y}) \Big)_{\Omega_e}, \tag{4.138}$$

and therefore one needs to know $\partial \boldsymbol{\mathcal{B}} / \partial \boldsymbol{h}$ in order to compute $\overline{\overline{K}}$.

The pseudocode of the overall multiscale algorithm for the $\boldsymbol{h}$-conform formulations is presented in Figure 4.4.

Macro	**Meso**
• Read input (macro mesh, material laws, etc.).	Generate meso meshes
• Prescribe BCs.	
• Initialize $\boldsymbol{h}_M(t=0)$	
• **Begin time loop** while $t_n < t_f$ do:	
(a) **Begin nonlinear loop** while $(m < m_{max})$ and (res > tol) do:	
◦ For each quadrature point: $\xrightarrow[\textbf{downscaling}]{\boldsymbol{h}_M, \boldsymbol{j}_M}$	**Cell problem analysis**
	1. Prescribe the BCs
	1. Initialize $\boldsymbol{h}_m(t=t_n)$
	2. Impose the macro sources
	3. Solve the cell problem
◦ Assemble matrix and RHS: $\xleftarrow[\textbf{upscaling}]{\boldsymbol{h}_M, \partial\boldsymbol{\mathcal{B}}_M/\partial\boldsymbol{h}_M}$	4. Compute $\boldsymbol{b}_M$ and $\partial\boldsymbol{\mathcal{B}}_M/\partial\boldsymbol{h}_M$
◦ Solve	
◦ Check convergence 1. If not, $m \leftarrow m+1$. 2. Else, save. Leave the nonlinear loop and go to (b).	
End nonlinear loop.	
(b) $t_n \leftarrow t_n + \Delta t$.	
• **End time loop**.	

Figure 4.4: Pseudocode of the multiscale algorithm for the nonlinear multiscale magnetic flux field conforming formulations.

4.4.5 The static case

The formulations for the static case are defined from the following magnetostatic multiscale problem:

$$\mathbf{curl}\, \boldsymbol{h}^{\varepsilon} = \boldsymbol{j}_s, \tag{4.139}$$

$$\operatorname{div} \boldsymbol{b}^{\varepsilon} = 0, \tag{4.140}$$

$$\boldsymbol{b}^{\varepsilon}(\boldsymbol{x}) = \boldsymbol{\mathcal{B}}\Big(\boldsymbol{h}^{\varepsilon}(\boldsymbol{x}), \boldsymbol{x}, \frac{\boldsymbol{x}}{\varepsilon}\Big), \tag{4.141}$$

obtained from equations (2.59)–(2.59) (see section 2.5.5). In this case, the magnetic field reads $\boldsymbol{h}^{\varepsilon} = \boldsymbol{h}_s - \mathbf{grad}\, \phi^{\varepsilon}$ and the weak form (4.140) reads: find $\phi^{\varepsilon} \in H_h^1(\Omega)$ such that

$$\Big(\boldsymbol{\mathcal{B}}(\boldsymbol{h}_s - \mathbf{grad}\, \phi^{\varepsilon}(\boldsymbol{x})), \mathbf{grad}\, \phi'^{\varepsilon}(\boldsymbol{x})\Big)_{\Omega} + \langle \boldsymbol{n} \cdot \boldsymbol{b}, \phi'^{\varepsilon} \rangle_{\Gamma_h} = 0, \tag{4.142}$$

holds for all $\phi'^{\varepsilon} \in H_h^{1\,0}(\Omega)$. The source term $\boldsymbol{h}_s$ can be computed using the approach described in section 2.4. This problem can be solved using the HMM approach.

The macroscale problem is governed by the following weak equation: find $\phi_M \in H_h^1(\Omega)$ such that

$$\Big(\boldsymbol{\mathcal{B}}_M(\boldsymbol{h}_s - \mathbf{grad}\, \phi_M), \mathbf{grad}\, \phi_M'\Big)_{\Omega_M} + \langle \boldsymbol{n} \cdot \boldsymbol{\mathcal{B}}_M(\boldsymbol{h}_s - \mathbf{grad}\, \phi_M), \phi_M' \rangle_{\Gamma_h} = 0, \tag{4.143}$$

holds for all $\phi_M' \in H_h^{1\,0}(\Omega)$.

The mesoscale problem is governed by the weak form: find $\phi_c \in H^1(\mathcal{Y})$ such that

$$\Big(\boldsymbol{\mathcal{B}}(\boldsymbol{h}_M - \mathbf{grad}\, \phi_c), \mathbf{grad}\, \phi_c'\Big)_{\Omega_m} = 0, \tag{4.144}$$

holds for all $\phi_c' \in H^1(\mathcal{Y})$. The macroscale field $\boldsymbol{h}_M$ in (4.144) is given by $\boldsymbol{h}_M = \boldsymbol{h}_s - \mathbf{grad}\, \phi_M$.

We can use the same approach like the one used for the dynamic problem in section 4.3. To this end we express the mesoscale magnetic scalar potential ϕ_m in terms of the macroscale magnetic scalar potential ϕ_M with slow variations and the correction term ϕ_c that accounts for the rapid variations

$$\phi_m(\boldsymbol{x}, \boldsymbol{y}) = \phi_M^{lin}(\boldsymbol{x}) + \phi_c(\boldsymbol{x}, \boldsymbol{y}) = \phi_M(\boldsymbol{x}) + \boldsymbol{y} \cdot \mathbf{grad}_x\, \phi_M(\boldsymbol{x}) + \phi_c(\boldsymbol{x}, \boldsymbol{y}). \tag{4.145}$$

Applying the gradient operator to both sides of (4.145) and integrating over the mesoscale computational domain gives:

$$\int_{\Omega_m} \mathbf{grad}_y\, \phi_m(\boldsymbol{x}, \boldsymbol{y})\, \mathrm{d}\boldsymbol{y} = \int_{\Omega_m} \mathbf{grad}_x\, \phi_M(\boldsymbol{x})\, \mathrm{d}\boldsymbol{y} + \int_{\Gamma_m} \boldsymbol{n} \phi_c(\boldsymbol{x}, \boldsymbol{y})\, \mathrm{d}\boldsymbol{y}, \tag{4.146}$$

where and Γ_m is the boundary of the microdomain Ω_m. Assuming that the average of the mesoscale magnetic field is equal to the mesoscale magnetic field (and therefore that the surface integral in (4.146) vanishes), we can write:

$$\frac{1}{|\Omega_m|} \int_{\Omega_m} \mathbf{grad}_y\, \phi_m(\boldsymbol{x}, \boldsymbol{y})\, \mathrm{d}y = \frac{1}{|\Omega_m|} \int_{\Omega_m} \mathbf{grad}_x\, \phi_M(\boldsymbol{x}) \mathrm{d}y \tag{4.147}$$

which implies that the magnetic field is consistent between the macroscale and the mesoscale. Furthermore, it infers periodic boundary conditions for the correction term $\phi_c(\boldsymbol{x}, \boldsymbol{y})$. Note that the surface integral in (4.146) vanishes.

The upscaling of the nonlinear magnetic law is performed by simple average as a consequence of the two-scale convergence of the magnetic flux density $\boldsymbol{b}$:

$$\frac{1}{|\Omega_m|} \int_{\Omega_m} \boldsymbol{b}_m \mathrm{d}y = \boldsymbol{b}_M. \tag{4.148}$$

This overall homogenization process can then be shown to be equivalent to a variational formulation with equal magnetic energies at the mesoscale and the macroscale levels:

$$\begin{aligned} \frac{1}{|\Omega_m|} \int_{\Omega_m} \boldsymbol{h}_m(\boldsymbol{x}, \boldsymbol{y}) \cdot \boldsymbol{\mathcal{B}}(\boldsymbol{h}_m(\boldsymbol{x}, \boldsymbol{y}), \boldsymbol{x}, \boldsymbol{y})\, \mathrm{d}y = \\ \boldsymbol{h}_M(\boldsymbol{x}) \cdot \boldsymbol{\mathcal{B}}_M(\boldsymbol{h}_M(\boldsymbol{x}), \boldsymbol{x}). \end{aligned} \tag{4.149}$$

The tangent matrix $\partial \boldsymbol{\mathcal{B}}_M / \partial \boldsymbol{h}_M$ for the Newton–Raphson scheme is obtained using the finite difference method described in section 4.3.3.

Chapter 5

Numerical tests

5.1 Introduction

In this chapter, we carry out numerical tests to validate the homogenization theory and the multiscale methods developed in chapter 3 and chapter 4. For simplicity, we restrict ourselves to two-dimensional problems that can be solved using standard conforming finite elements, and chose validation problems accordingly. We consider $\boldsymbol{b}$-conform and $\boldsymbol{h}$-conform formulations which allows for in-plane and out-of-plane configurations of eddy currents. Two types of applications are also considered: soft magnetic composites (SMC) and lamination stacks. The choice of these examples was motivated by the many applications in electrotechnics (electric transformers, electric motors, electric generators, etc.) due to their interesting electromagnetic properties resulting from their multiscale nature.

To start with, we consider in section 5.2 two SMC geometries for validating the $\boldsymbol{b}$- and $\boldsymbol{h}$-conform multiscale formulations. We focus on the convergence of the fields with respect to the meshes, the consistency between the fine-scale, the local mesoscale and the macroscale fields and the convergence of the global quantities (eddy currents losses, magnetic energy). We also test the limitations of the multiscale models by checking the influence of the different terms in the formulations, in particular the influence of eddy currents in the mesoscale problems. As a second validation example, we present in section 5.3 results obtained by applying the theory to a lamination stack.

5.2 Soft magnetic composites

The actual geometry of SMC is an aggregation of three-dimensional metallic grains surrounded by a dielectric binder (Figure 5.1 (a)). In this section we assume an idealized SMC toroidal structure with grains stretched in one direction and that rather looks like wires (Figure 5.1 (b)). The obtained geometry is similar to the geometry made of wound wires with each wire modeled by a cylinder (Figure 5.1 (c)).

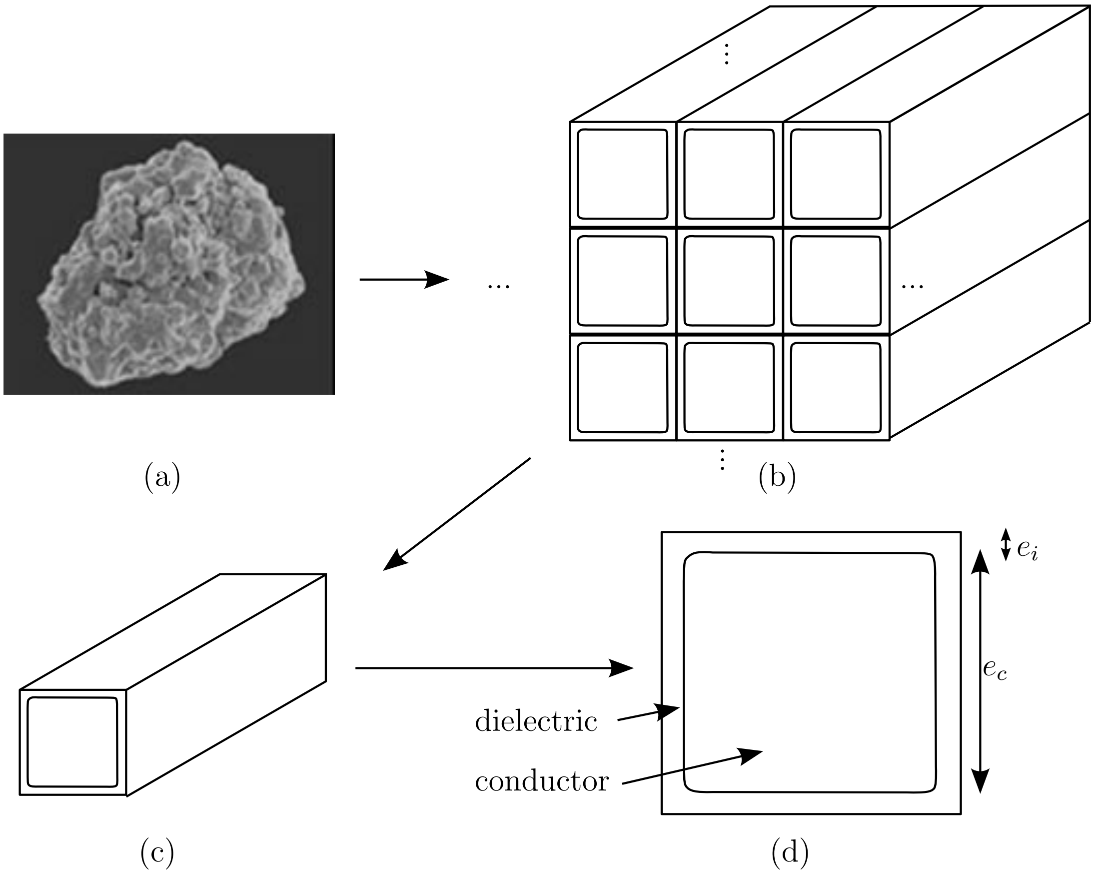

Figure 5.1: SMC two-dimensional geometry used for the multiscale formulations. (a): The real three-dimensional coarse-grained geometry. (b): Stretched SMC structures. (c): A single stretched SMC structure. (d): Basic two-dimensional elementary cell used for solving the cell problem ($e_c = 45\,\mu$m and $e_i = 2.5\,\mu$m).

With such an assumption, all the vertical cuts passing through the axis of the toroid are similar and therefore the problem can be reduced to a two-dimensional problem where the basic elementary cell looks like the one depicted in Figure 5.1 (d). This cell is made of two parts: a metallic part labeled *conductor* which is conducting and magnetic and a dielectric part labeled *dielectric* which is non-magnetic. We consider it non-conducting for the $\boldsymbol{b}$-conform formulations and slightly conducting for the $\boldsymbol{h}$-conform formulations. The latter case enables to consider problems with global eddy currents at the macroscale.

5.2.1 Description of the problem for the $\boldsymbol{b}$-conform formulations

The primal unknown field is the magnetic flux density $\boldsymbol{b}$ which can be derived from a vector potential $\boldsymbol{a}$ as: $\boldsymbol{b} = \mathbf{curl}\,\boldsymbol{a}$. We want the unknown $\boldsymbol{a}$ to have only the z-component, i.e., $\boldsymbol{a} = (0, 0, a_z)$ so that nodal elements can be used. This means that $\boldsymbol{b}$ will be constrained in the xy-plane. We want also the magnetic field $\boldsymbol{h}$ to

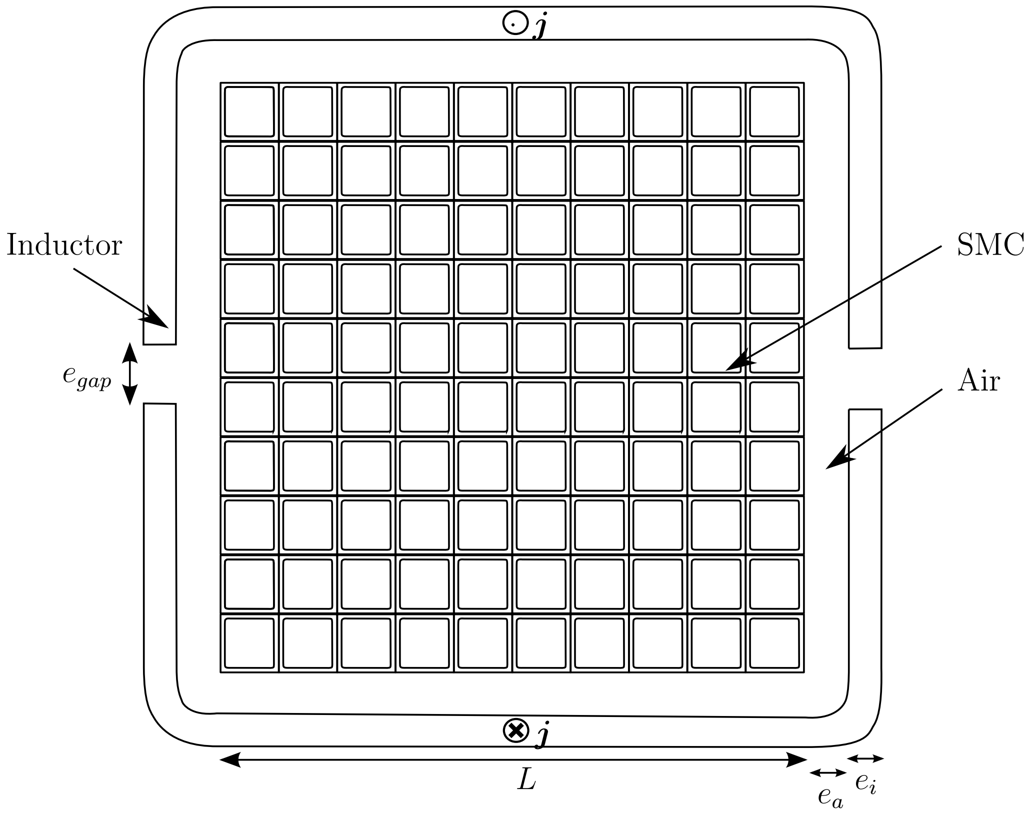

Figure 5.2: Soft magnetic composite two-dimensional geometry used for the $\boldsymbol{a}-v$ multiscale formulations. Two opposite source current are imposed in the top and bottom inductors. The lengths are given by $L = 1000\,\mu$m, $e_a = 150\sqrt{2}/2\,\mu$m, $e_i = 100\,\mu$m and $e_{gap} = 100\,\mu$m. Only 100 grains out of 400 are drawn on the image.

have only xy components (which is true for isotropic and orthotropic materials but not always true for arbitrary anisotropic materials).

Using Ampère's equation $\textbf{curl}\,\boldsymbol{h} = \boldsymbol{j}_s + \sigma\boldsymbol{e}$, the source current $\boldsymbol{j}_s$ must be imposed perpendicular to the xy-plane $\boldsymbol{j}_s = (0, 0, j_s)$ with $j_s = j_{s0}\,f(t)$ where j_{s0} is the constant amplitude and $f(t) = \sin(2\pi f t)$.

Depending on the operating frequencies (the maximum frequency that has been tested is $f = 50\,$kHz and corresponds to $\lambda = 6000\,$m), the resulting wavelengths are huge in comparison to the size of the structure (around $500\,\mu$m) and therefore the assumption of a magnetoquasistatic problem can be made.

We consider the elementary cell in Figure 5.1-(d). The dielectric is a perfect insulator governed by a linear magnetic law with $\mu_r = 1$. The conductor has an isotropic electric conductivity $\sigma = 5\,10^6\,$S/m and is governed by the following magnetic laws:

1. a nonlinear exponential law $\boldsymbol{\mathcal{H}}(\boldsymbol{b}) = \Big(\alpha + \beta\,\exp(\gamma||\boldsymbol{b}||^2)\Big)\,\boldsymbol{b}$ with $\alpha = 388, \beta = 0.3774$ and $\gamma = 2.97$ [57].

2. a Jiles - Atherton hysteresis model with parameters $\boldsymbol{\mathcal{M}}_s = 1,145,500\,$A/m, $a = 59\,$A/m, $k = 99\,$A/m, $c = 0.55$ and $\alpha = 1.3\,10^{-4}$ (see section 4.3.4 [19,94].)

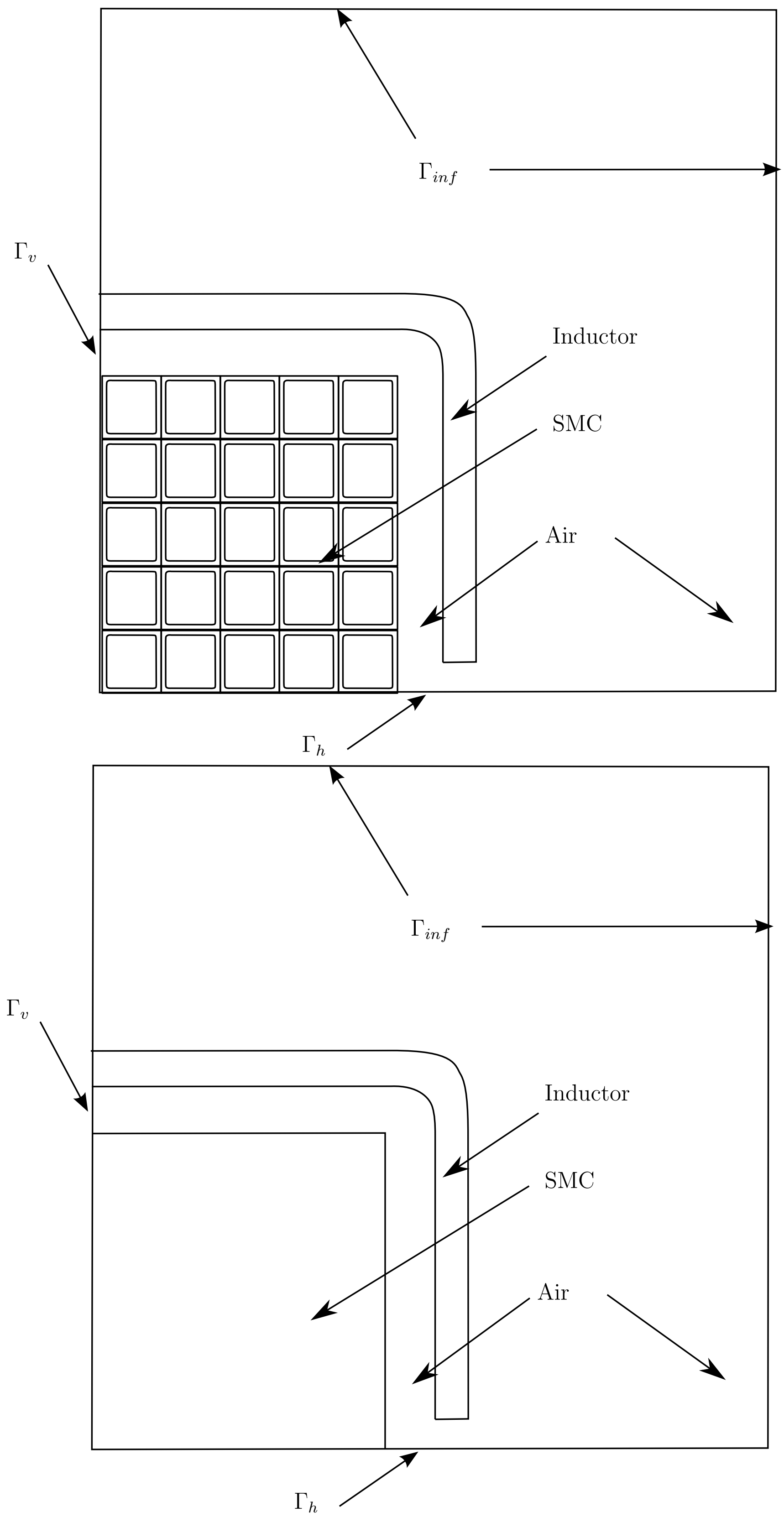

Figure 5.3: Geometry used for the $\boldsymbol{a} - v$ computations. Only a quarter of the geometry is used thanks to the symmetries. Top: Reference geometry. Only 25 grains out of 100 are drawn on the image. Bottom: Homogenized geometry.

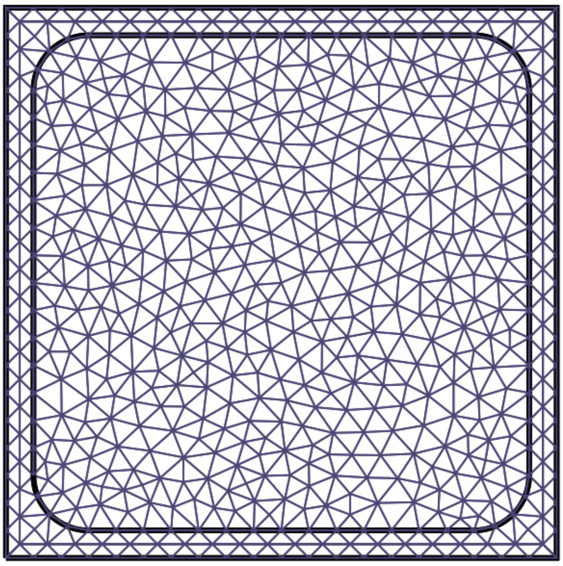

Figure 5.4: Typical mesh used for mesoscale computations.

Thanks to the symmetries of the geometry, of physical properties and boundary conditions, only a quarter of the geometry is used (top image of Figure 5.3 for the reference case and bottom image of Figure 5.3 for the computational case.)

The following boundary conditions are also imposed on the boundary in order for the problem to be well-posed:

$$\boldsymbol{n} \cdot \boldsymbol{b}|_{\Gamma inf} = 0 \longrightarrow \boldsymbol{n} \times \boldsymbol{a}|_{\Gamma inf} = \boldsymbol{0}, \tag{5.1}$$

$$\boldsymbol{n} \cdot \boldsymbol{b}|_{\Gamma_h} = 0, \tag{5.2}$$

$$\boldsymbol{n} \cdot \boldsymbol{j}|_{\Gamma_v} = 0 \longrightarrow \boldsymbol{n} \times \boldsymbol{h}|_{\Gamma_v} = \boldsymbol{0}. \tag{5.3}$$

Equations (5.1) and (5.2) express the impermeability of the boundary Γ_h to the magnetic flux density and the vanishing of the magnetic flux density $\boldsymbol{b}$ at infinity Γ_{inf}. The condition $\boldsymbol{n} \times \boldsymbol{a}|_{\Gamma inf} = \boldsymbol{0}$ in (5.1) is one possible way of imposing a zero flux density across Γ_{inf} and, in the two-dimensional setting, this amounts to imposing $a_z|_{\Gamma_{inf}} = 0$. Equation (5.3) expresses the zero net electric current crossing the boundary Γ_v.

5.2.2 Results for the *b*-conform formulations

In this section, we compare computational results for the ***b***-conform multiscale formulations to the reference results.The latter are obtained by solving a finite element problem on the entire, finely meshed multiscale domain (Figure 5.5 - top). A total

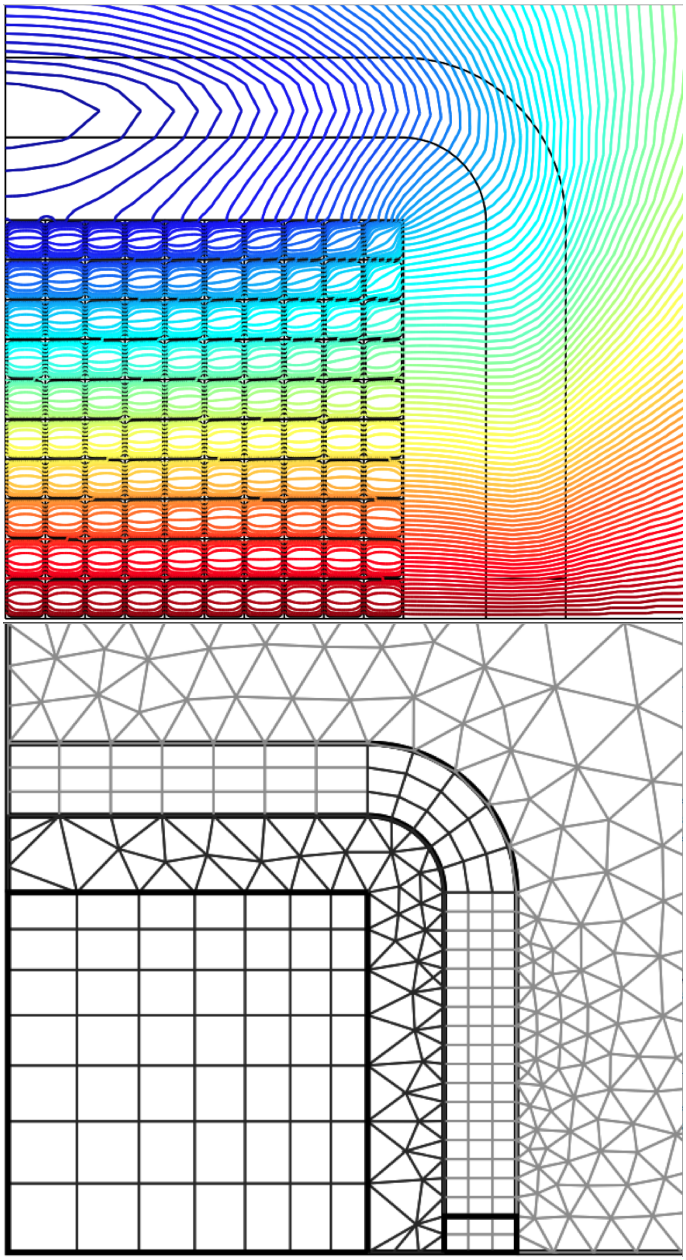

Figure 5.5: Top: geometry used for the validation of the ***b***-conform multiscale formulations taking advantage of symmetry. Flux lines are depicted as well. Bottom: typical mesh used for the macroscale problem.

of 110282 triangular elements are used for the fine-scale problem.

Computational results are carried out on a macroscale, coarse mesh (a typical

Table 5.1: SMC problem - $\boldsymbol{b}$-conform formulations. Comparison of the reference magnetic flux density and the computational (macroscale and mesoscale) magnetic flux density ($\|\boldsymbol{b}\|$, in T) in different points of the macroscale domain $\{\ t = 6 \times 10^{-6} s\}$
.

Position (μm)	Reference	Meso	Macro	err_{meso} (%)	$\text{err}_{\text{Macro}}$ (%)
$(25, 25, 0)$	0.0157652	0.0158937	0.0347775	0.82	120.60
$(25, 475, 0)$	0.0186482	0.0181317	0.0403767	2.77	116.52
$(175, 175, 0)$	0.0158077	0.0158738	0.0346577	0.42	119.25
$(475, 25, 0)$	0.0156693	0.0158615	0.0345838	1.23	120.70
$(475, 475, 0)$	0.0184396	0.0158563	0.0417285	14.01	126.30

mesh is depicted in Figure 5.5 - bottom) using triangular elements and mesoscale problems are solved around each numerical quadrature point of the macroscale mesh using a mesh that looks like the one in Figure 5.4.

Figure 5.6 depicts the different contributing terms involved in the resolution of the mesoscale problem. The projection term which varies linearly on the mesoscale domain is computed from the macroscale fields as $\boldsymbol{a}_{proj}(\boldsymbol{x}, \boldsymbol{y}, t) = \boldsymbol{a}_M(\boldsymbol{x}, t) + \kappa(\boldsymbol{y} \times \boldsymbol{b}_M(\boldsymbol{x}, t))$. This term is then used as a source for the computation of the correction term $\boldsymbol{a}_c(\boldsymbol{x}, \boldsymbol{y}, t)$ at the mesoscale level which allows to derive the total magnetic vector potential $\boldsymbol{a}_{tot}(\boldsymbol{x}, \boldsymbol{y}, t) = \boldsymbol{a}_c(\boldsymbol{x}, \boldsymbol{y}, t) + \boldsymbol{a}_M(\boldsymbol{x}, t) + \kappa(\boldsymbol{y} \times \boldsymbol{b}_M(\boldsymbol{x}, t))$.

The comparison of spatial cuts of the magnetic induction $\boldsymbol{b}$, of the eddy currents $\boldsymbol{j}$ and of the magnetic field $\boldsymbol{h}$ shows an excellent agreement between the reference solution and the local solution computed on the mesoscale cells centered around points of the computational domain and this for the nonlinear case (Figure 5.7) and the hysteresis case (Figures 5.8–5.9). Small discrepancies are however observed near the boundary of the domain (see Tables 5.1 and 5.2).

Table 5.1 displays the values $||\boldsymbol{b}||$ obtained from the reference solution (Reference), the macroscale solution (Macro) and the mesoscale solution (Meso) and the relative pointwise errors err_{meso} and $\text{err}_{\text{macro}}$ defined by:

$$\text{err}_{\text{meso}}(\boldsymbol{x}, t) = \frac{|\boldsymbol{b}_{\text{ref}}(\boldsymbol{x}, t) - \boldsymbol{b}_{\text{meso}}(\boldsymbol{x}, t)|}{|\boldsymbol{b}_{\text{ref}}(\boldsymbol{x}, t)|}, \tag{5.4}$$

and

$$\text{err}_{\text{Macro}}(\boldsymbol{x}, t) = \frac{|\boldsymbol{b}_{\text{ref}}(\boldsymbol{x}, t) - \boldsymbol{b}_{\text{macro}}(\boldsymbol{x}, t)|}{|\boldsymbol{b}_{\text{ref}}(\boldsymbol{x}, t)|}, \tag{5.5}$$

for $t = 6 \times 10^{-6} s$. From this table, it can be concluded that the mesoscale error which is small in the bulk (an error of about 1 %) becomes greater the closer to the boundary of the computational domain (up to 14 %). Indeed, the periodicity assumption is no longer respected in this case and therefore a cell located near the boundary is not immersed in a periodic environment.

The macroscale error is huge and almost independent of the location of the considered point.

Table 5.2: SMC problem - $\boldsymbol{b}$-conform formulations. Relative $L^2(0,T)$ errors between the reference magnetic flux density and the mesoscale magnetic flux density ($\mathrm{err}_{\mathrm{L}^2\,\mathrm{meso}}$) and between the reference magnetic flux density and the macroscale magnetic flux density ($\mathrm{err}_{\mathrm{L}^2\,\mathrm{Macro}}$) for different points of the computational domain.

Position (μm)	$\mathrm{err}_{\mathrm{L}^2\,\mathrm{meso}}$ (%)	$\mathrm{err}_{\mathrm{L}^2\,\mathrm{Macro}}$ (%)
$(25, 25, 0)$	3.27	11.49
$(25, 475, 0)$	4.93	15.13
$(175, 175, 0)$	3.01	11.88
$(475, 25, 0)$	3.04	12.27
$(475, 475, 0)$	15.46	22.91

Table 5.2 provides relative $L^2(0,T)$ errors between the reference magnetic induction $\boldsymbol{b}_{\mathrm{ref}}(\boldsymbol{x},t)$, the mesoscale magnetic induction $\boldsymbol{b}_{\mathrm{meso}}(\boldsymbol{x},t)$ and the macroscale magnetic induction $\boldsymbol{b}_{\mathrm{Macro}}(\boldsymbol{x},t)$. For a point $\boldsymbol{x}$ of the computational domain, these L^2 errors are given by the formula:

$$\mathrm{err}_{\mathrm{L}^2\,\mathrm{meso}}(\boldsymbol{x},t) = \frac{||\boldsymbol{b}_{\mathrm{ref}}(\boldsymbol{x},t) - \boldsymbol{b}_{\mathrm{meso}}(\boldsymbol{x},t)||_{L^2(0,T)}}{||\boldsymbol{b}_{\mathrm{ref}}(\boldsymbol{x},t)||_{L^2(0,T)}}, \tag{5.6}$$

and

$$\mathrm{err}_{\mathrm{L}^2\,\mathrm{Macro}}(\boldsymbol{x},t) = \frac{||\boldsymbol{b}_{\mathrm{ref}}(\boldsymbol{x},t) - \boldsymbol{b}_{\mathrm{Macro}}(\boldsymbol{x},t)||_{L^2(0,T)}}{||\boldsymbol{b}_{\mathrm{ref}}(\boldsymbol{x},t)||_{L^2(0,T)}}. \tag{5.7}$$

$$\tag{5.8}$$

Results of Table 5.2 lead to the same conclusions as the ones of Table 5.1, i.e., the errors increase as the point gets close to the boundary of the computational domain.

In Figure 5.10 we compare the $\boldsymbol{hb}$ reference (Reference) and computational (Computational) curves obtained from the local field computed in cells located in the bulk (top) and near the boundary (bottom). A good agreement is shown for points located in the bulk and minor differences can be observed for points located near the boundary as it has been noted from Tables 5.1 and 5.2.

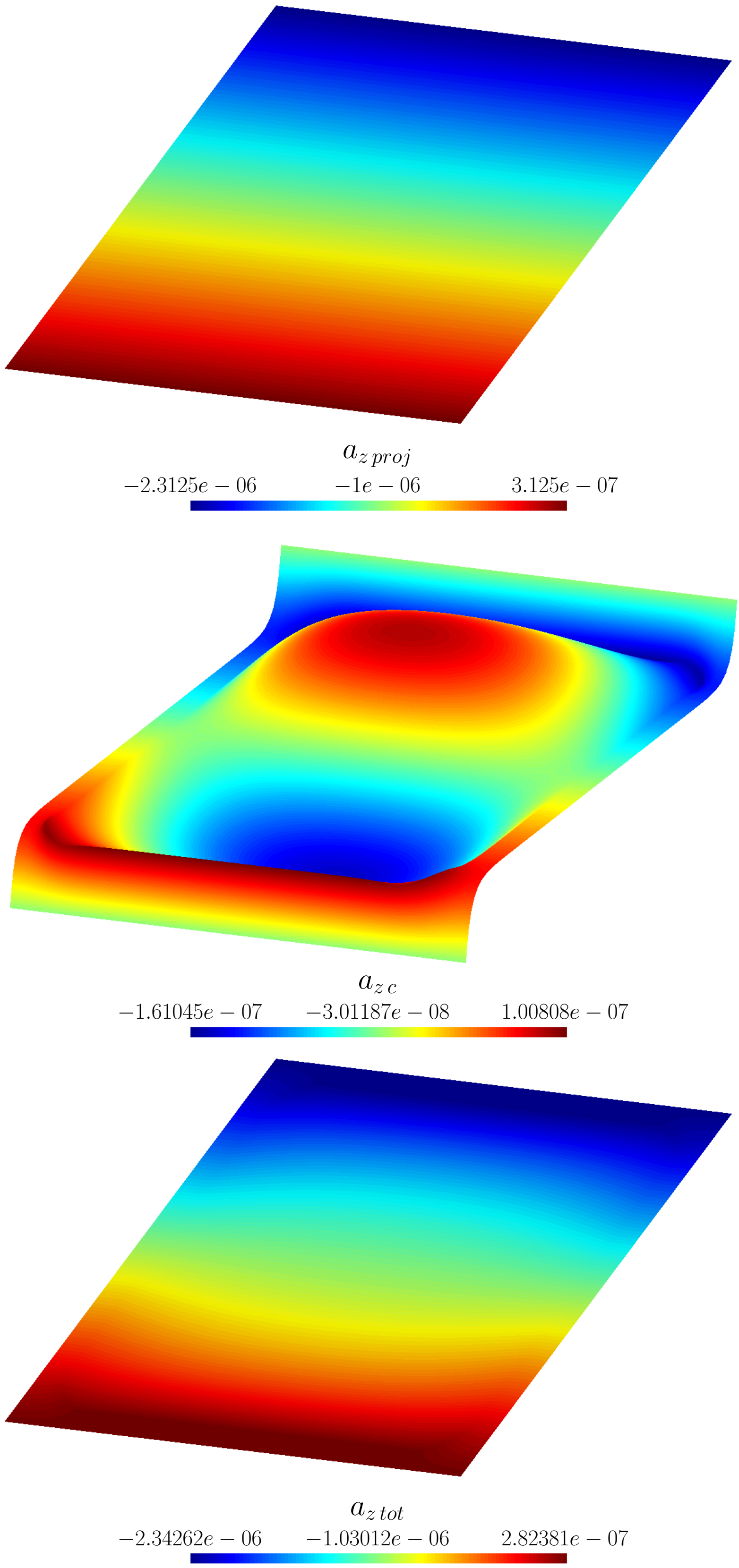

Figure 5.6: Terms contributing to the total mesoscale magnetic vector potential for a cell problem centered in $(325, 25, 0.0)\mu m$. Top: the z-component of the projection term $\boldsymbol{a}_{proj}(\boldsymbol{x}, \boldsymbol{y}, t) = \boldsymbol{a}_M(\boldsymbol{x}, t) + \kappa(\boldsymbol{y} \times \mathbf{b}_M(\boldsymbol{x}, t))$. Middle: the z-component of the correction term $\boldsymbol{a}_c(\boldsymbol{x}, \boldsymbol{y}, t)$. Bottom: the z-component of the total mesoscale vector potential $\boldsymbol{a}_{tot}(\boldsymbol{x}, \boldsymbol{y}, t)$ {nonlinear case with $j_{s0} = 35\,10^7\,\mathrm{A/m^2}$, $f = 25\,\mathrm{kHz}$}.

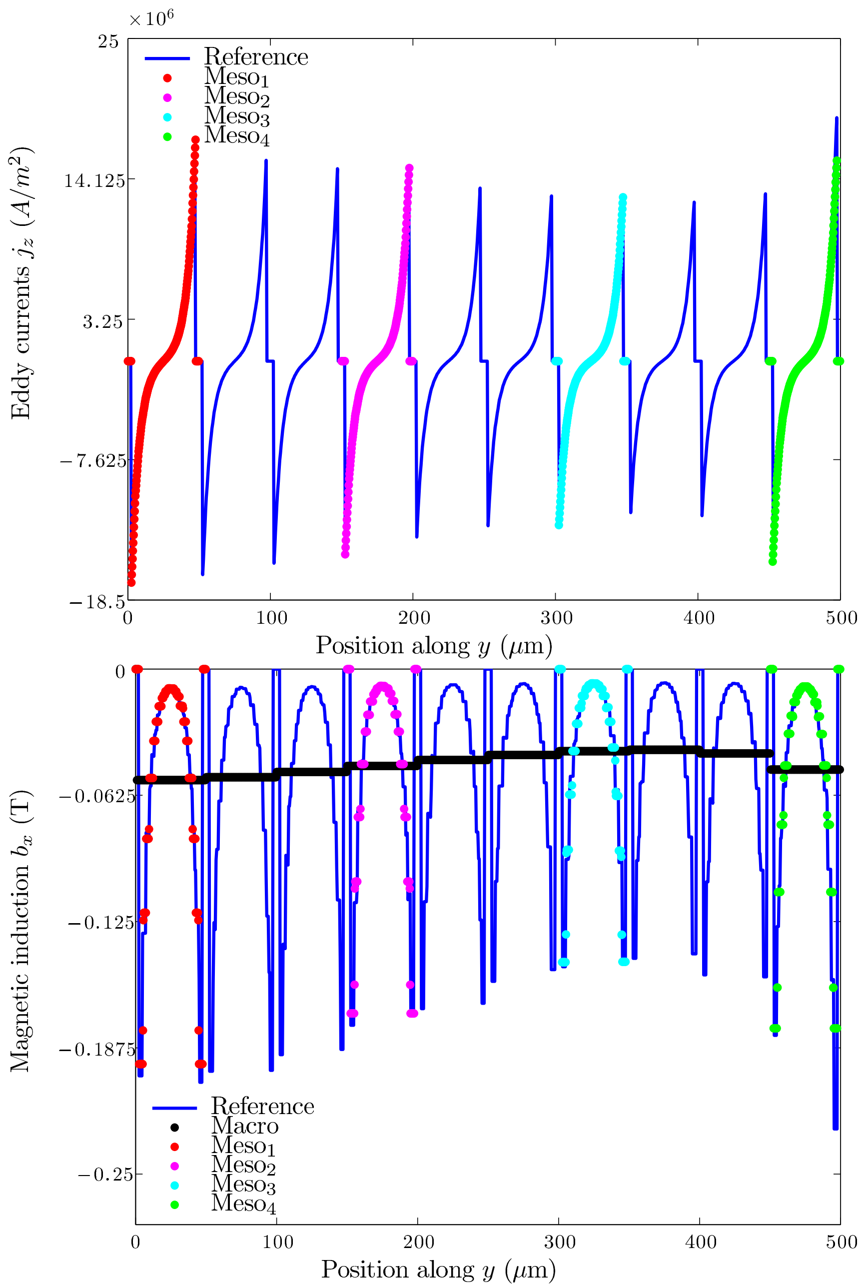

Figure 5.7: SMC problem, $\boldsymbol{b}$-conform formulations, nonlinear case. Spatial cuts of the z-component of the eddy currents $\boldsymbol{j}$ (top) and of the x-component of the magnetic induction $\boldsymbol{b}$ (bottom) along the line $\{x = 475, z = 0\}\,\mu$m. ($f = 50\,$kHz and $t = 6 \times 10^{-7}$s).

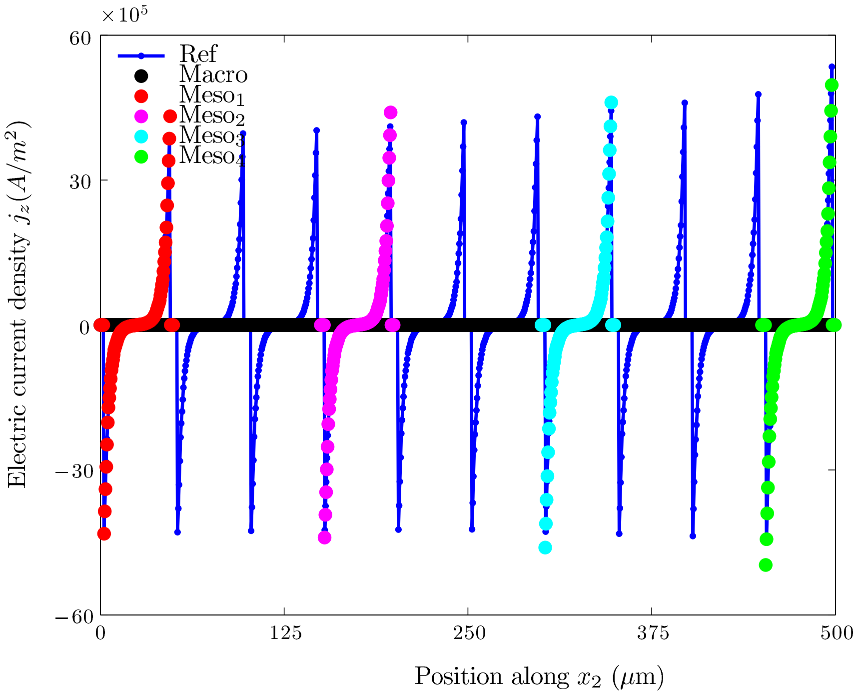

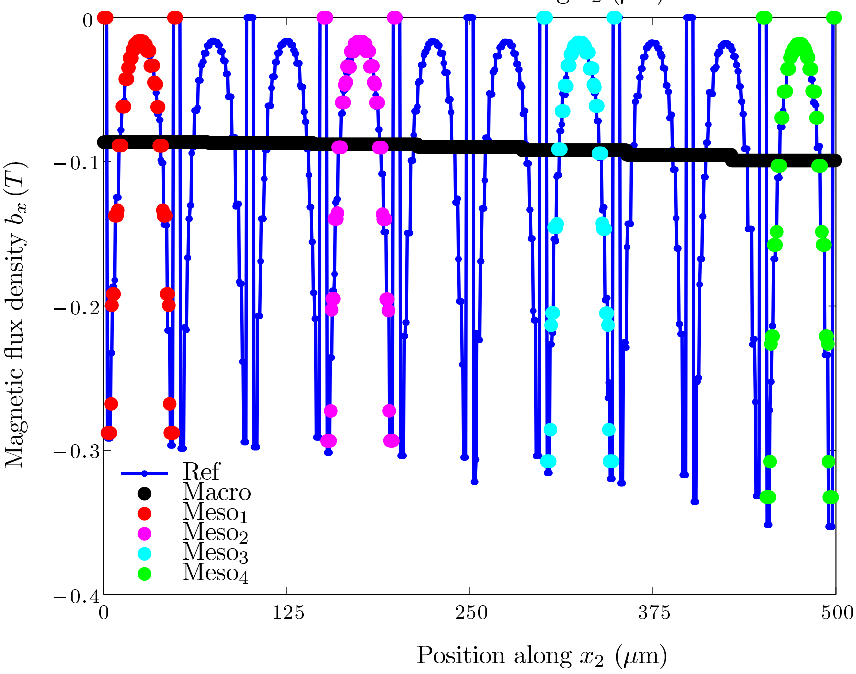

Figure 5.8: SMC problem, $\boldsymbol{b}$-conform formulations, hysteretic case. Spatial cuts of the z-component of the eddy currents $\boldsymbol{j}$ (top) and of the x-component of the magnetic induction $\boldsymbol{b}$ (bottom) along the line $\{x = 25, z = 0\}\,\mu$m. ($f = 10\,$kHz, $t = 5\,10^{-7}$s for the curve of eddy currents and $t = 25\,10^{-7}$s for the curve of the magnetic induction).

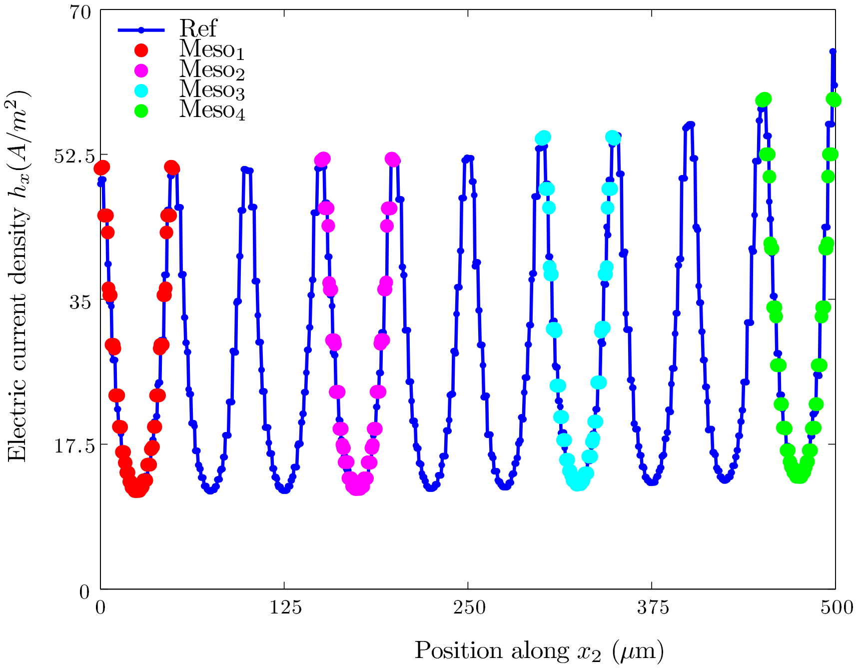

Figure 5.9: SMC problem, $\boldsymbol{b}$-conform formulations, hysteretic case. Spatial cuts of the x-component of the magnetic field $\boldsymbol{h}$ along the line $\{x = 25, z = 0\}\,\mu$m. ($f = 10\,$kHz and $t = 5\,10^{-5}$s).

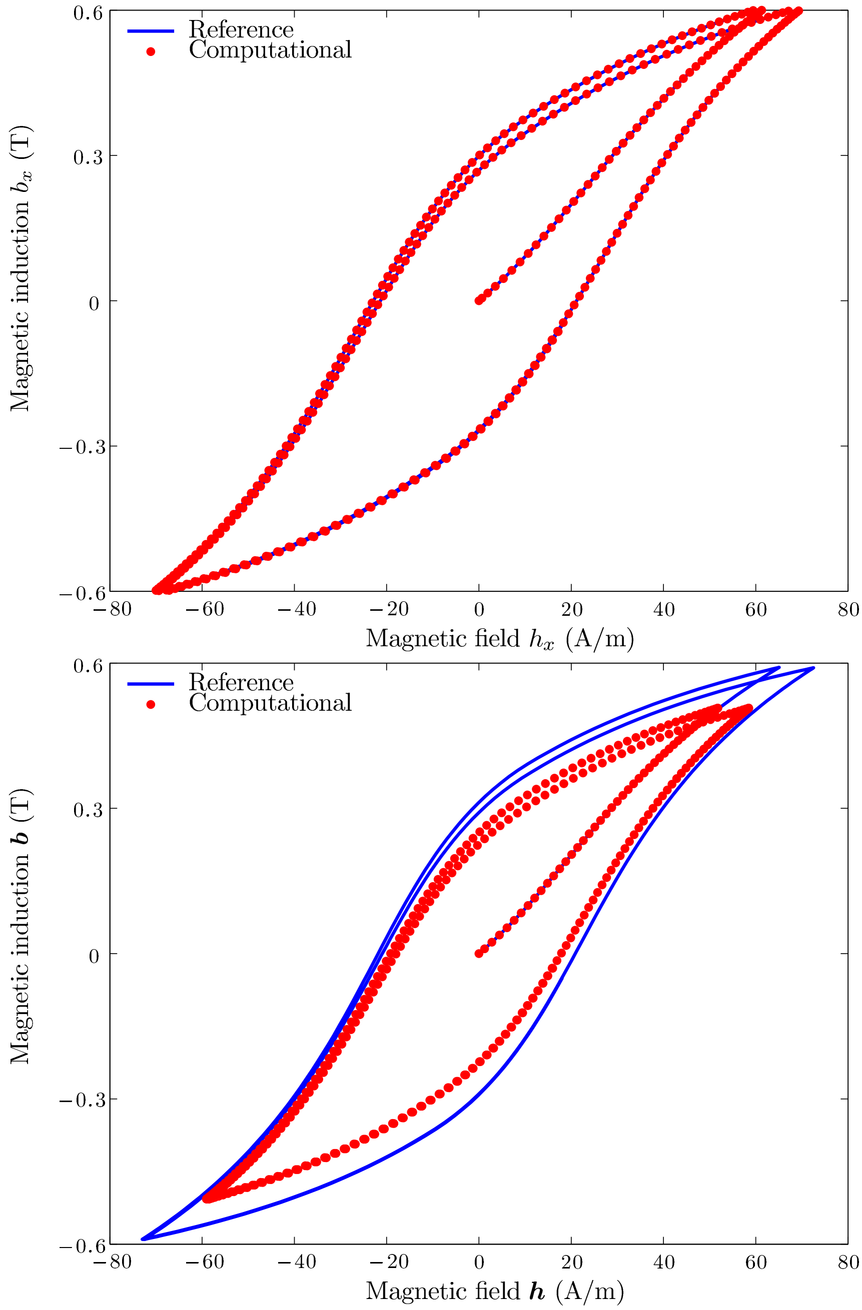

Figure 5.10: SMC problem, $\boldsymbol{b}$-conform formulations, hysteretci case. Reference (Reference) and computational (Computational) $\boldsymbol{hb}$ hysteresis curves for points located at $(175, 175, 0\ )\,\mu$m (top) and $(475, 475, 0)\,\mu$m (bottom) $\{f = 2500\,\text{Hz.}\}$

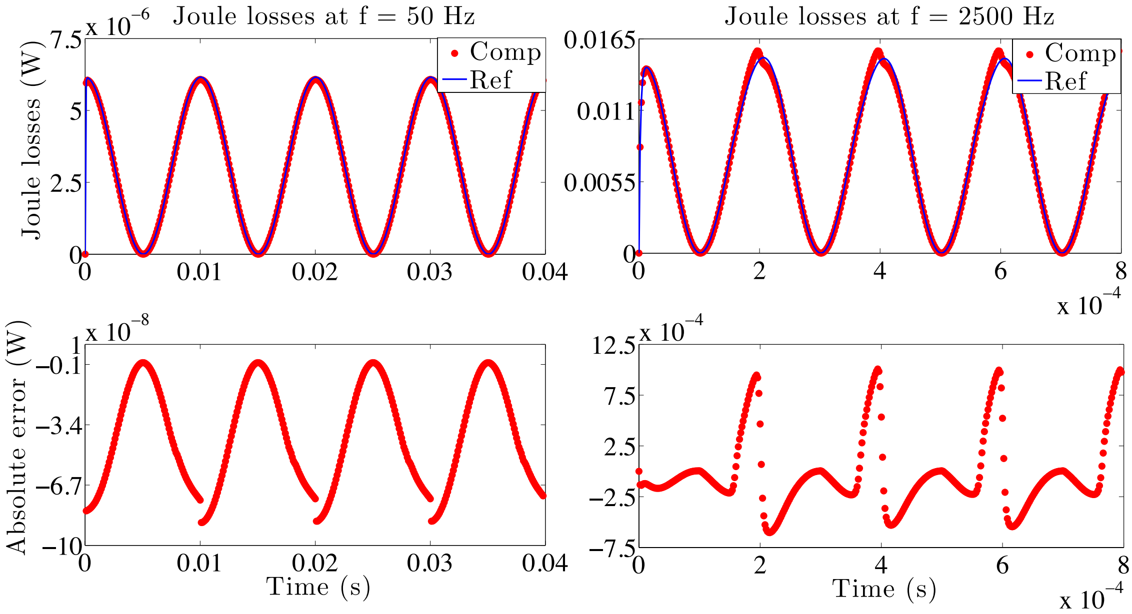

Figure 5.11: SMC problem, $\boldsymbol{b}$-conform formulations, hysteretitc case. Instantaneous Joule losses and absolute error between the reference (Ref) and the computational (Comp) solutions. Two frequencies are considered: $f = 50\,\mathrm{Hz}$ and $f = 2500\,\mathrm{Hz}$.

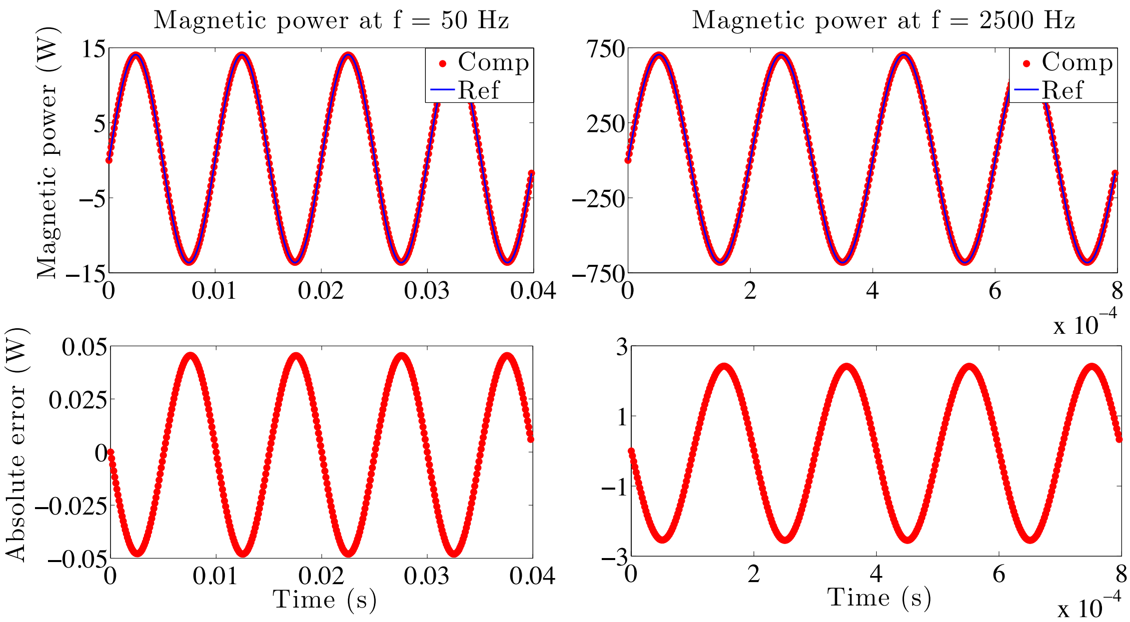

Figure 5.12: SMC problem, $\boldsymbol{b}$-conform formulations, hysteretitc case. Evolution of magnetic power and of the absolute error on magnetic power as a function of time. Two frequencies are considered: $f = 50\,\mathrm{Hz}$ and $f = 2500\,\mathrm{Hz}$.

Figures 5.11 and 5.12 depict evolution of global quantities (Joule losses and the magnetic power) for excitations at two different frequencies: 50 Hz and 2500 Hz (which correspond to the case with higher skin effect). A good agreement between Joules losses is observed for both frequencies: a maximum error of 1.41 % and 6.69 % are observed for $f = 50\,\text{Hz}$ and $f = 2500\,\text{Hz}$, respectively. A good agreement for magnetic energy is also shown in Figure 5.12.

Table 5.3 contains the relative $L^\infty(0,T)$ error of the Joule losses as a function of frequency. This $L^\infty(0,T)$ error is given by:

$$\text{err}_{L^\infty(0,T)} = \frac{||\Sigma_{\text{ref}}(t) - \Sigma_{\text{comp}}(t)||_{L^\infty(0,T)}}{||\Sigma_{\text{ref}}(t)||_{L^\infty(0,T)}}, \tag{5.9}$$

where $\Sigma_{ref}(t)$ is the curve of reference eddy current losses and $\Sigma_{\text{comp}}(t)$ is the curve of computational eddy current losses (the mesoscale eddy current losses $\Sigma_{\text{meso}}(t)$ and the macroscale eddy current losses $\Sigma_{\text{macro}}(t)$). As can be seen from Table 5.3,

Table 5.3: Soft magnetic composite problem - $\boldsymbol{b}$-conform formulations. Relative $L^\infty(0,T)$ norm error on the total Joule losses as a function of the frequency.

Frequency (Hz)	$\text{err}_{L^\infty(0,T)}$ (%)
50	1.41
100	1.46
250	1.61
500	2.12
1000	3.42
2500	6.69
5000	15.1
10000	20.4

the relative $L^\infty(0,T)$ error increases as a function of the frequency suggesting that greater errors are made in the case of enhanced skin effect.

The influence of different terms has also been tested. The top image of Figure 5.13 shows the evolution of the component $(\partial\boldsymbol{\mathcal{H}}_M/\partial\boldsymbol{b}_M)_{11}$ as a function of time. for both the case where the tangent matrix $\partial\boldsymbol{\mathcal{H}}_M/\partial\boldsymbol{b}_M$ and $\boldsymbol{h}_M$ are upscaled and used in the macrocale model and the case where only $\partial\boldsymbol{\mathcal{H}}_M/\partial\boldsymbol{b}_M$ is upscaled and then the homogenized magnetic field is computed as $(\boldsymbol{h}_M = \partial\boldsymbol{\mathcal{H}}_M/\partial\boldsymbol{b}_M)\boldsymbol{b}_M$. A perfect agreement is shown in both cases. The bottom image of 5.13 depicts the evolution of $(\partial\boldsymbol{\mathcal{H}}_M/\partial\boldsymbol{b}_M)_{11}$ as a function of time for the case the mesoscale problems include eddy currents (see problem (4.26)-(4.30)) and for the case the mesoscale problems are solved using equations from the homogenization theory (see problem (3.107)-(3.109)). From this figure, it can be concluded that the eddy currents have no great influence on the computation of the homogenized tangent matrix. However these currents are essential for recovering accurate local fields (see Figures (5.7)-(5.12)).

The influence of the mesoscale mesh is also investigated in Figure 5.15. In this case, the mesoscale mesh seems to have no great influence on the computation of eddy current losses even if a high skin is considered at the mesoscale level.

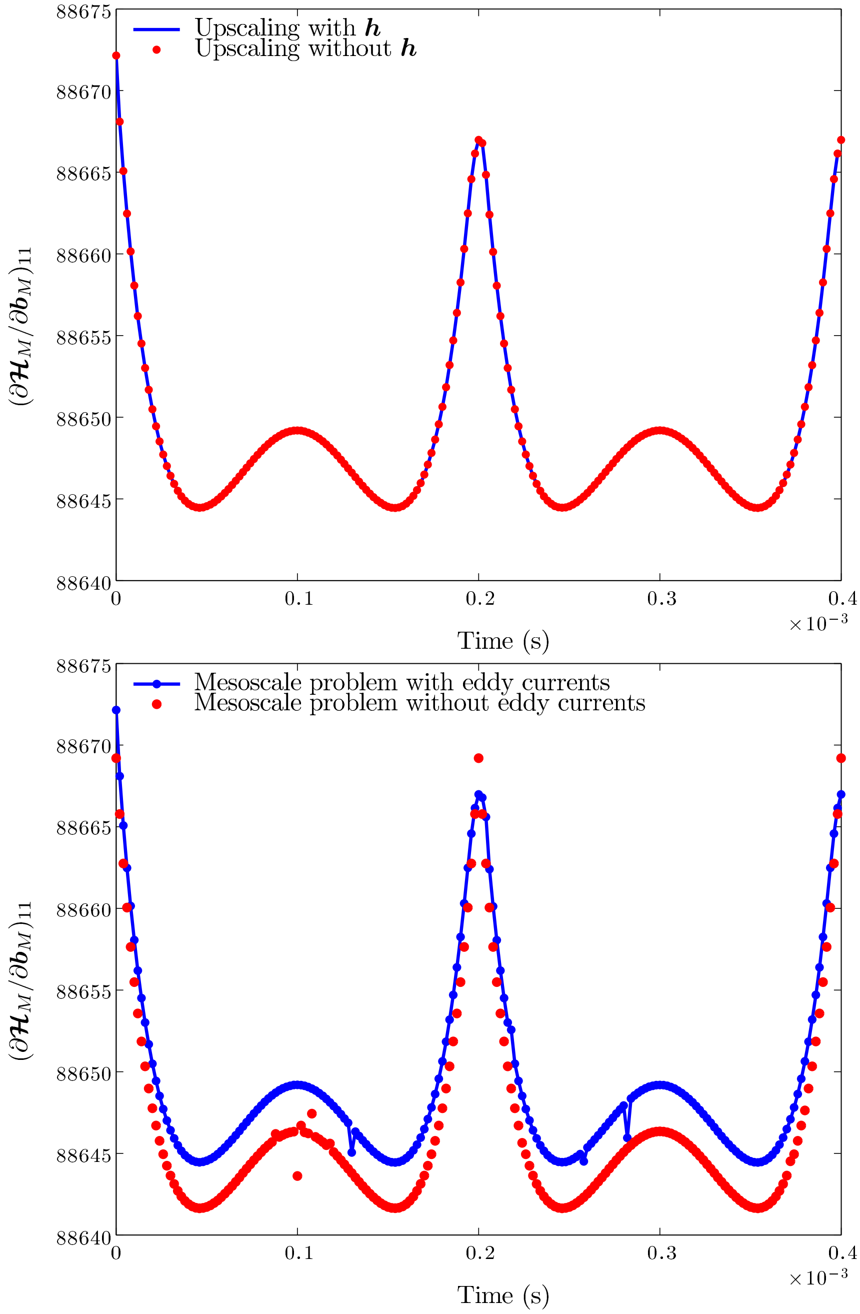

Figure 5.13: SMC problem, $\boldsymbol{b}$-conform formulations, hysteretic case. Evolution of the component $(\partial \boldsymbol{\mathcal{H}}_M/\partial \boldsymbol{b}_M)_{11}$ of the tangent matrix with respect to time. Top: computations done considering the upscaling (or not) of the homogenized magnetic field $\boldsymbol{h}_M$. Bottom: computations done considering (or not) the eddy currents at the mesoscale level.

Figure 5.16 shows the convergence of the residual resulting from the resolution by the Newton–Raphson method as a function of the number of nonlinear iteration. It can be seen that the macroscale problem converges quadratically while the mesoscale

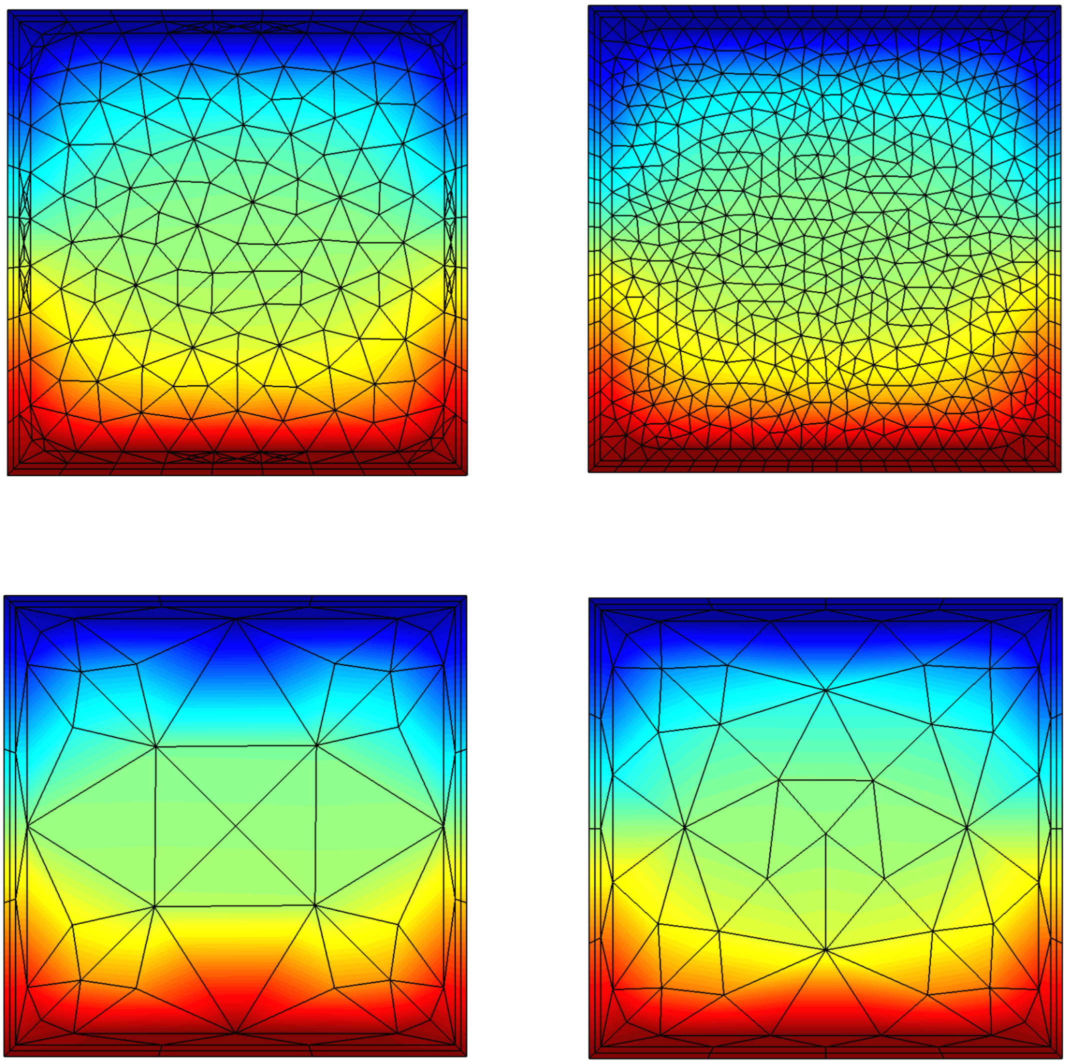

Figure 5.14: SMC problem - $\boldsymbol{b}$-conform formulations, nonlinear case. Influence of the mesoscale mesh. Magnetic field flux lines for a cell centered at $(25, 25, 0)\,\mu$m. Top-right: Mesh 200 with 1424 elements, top-left: Mesh 100 with 612 elements. bottom-right: Mesh 40 with 216 elements and bottom-left: Mesh 25 with 168 elements. $\{f = 50\,\mathrm{KHz}\}$.

problems converge at an average rate of 1.33.

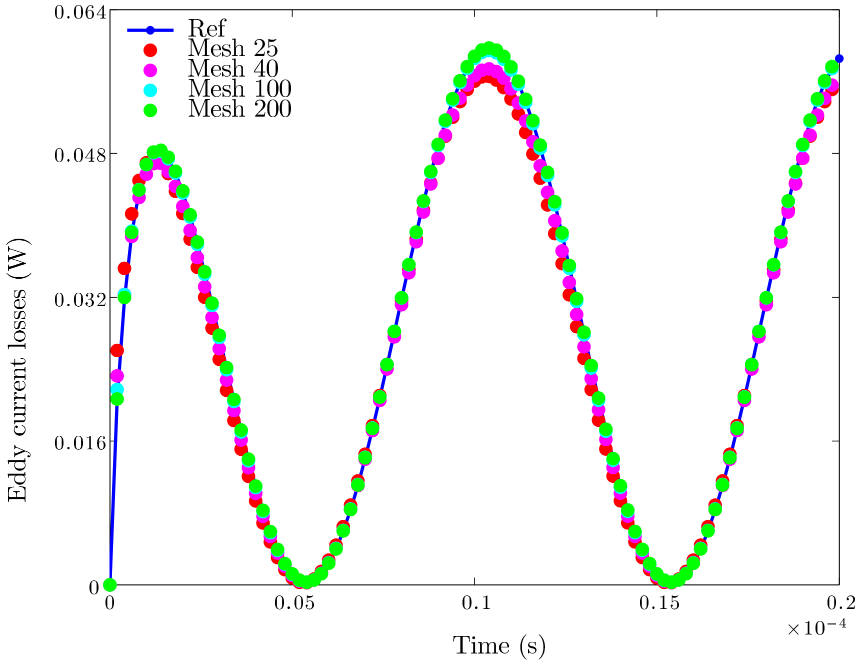

Figure 5.15: SMC problem - $\boldsymbol{b}$-conform formulations, nonlinear case. Influence of the mesoscale mesh on the evolution of the eddy currents losses for a cell centered at $(25, 25, 0)\,\mu$m. $\{f = 50\,\text{KHz}\}$.

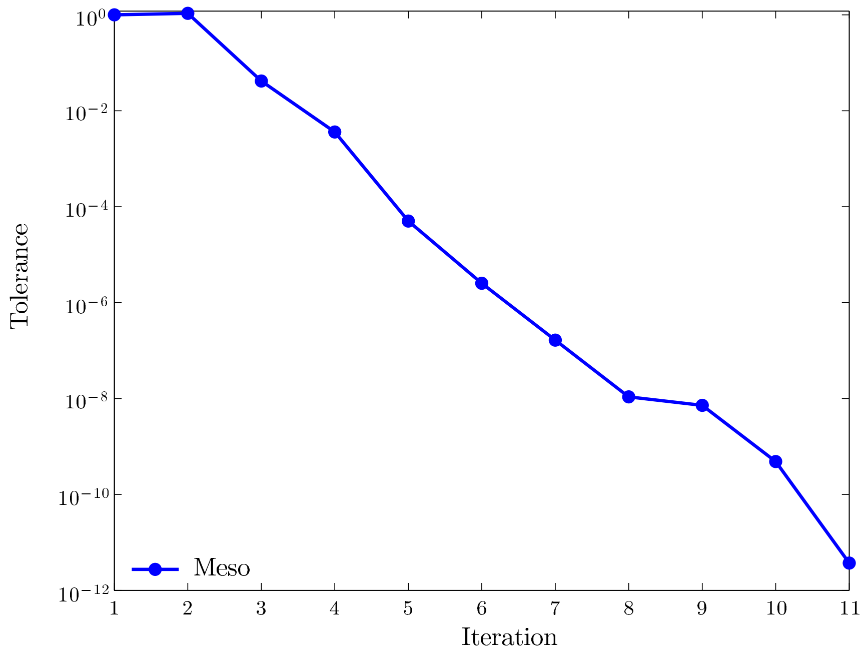

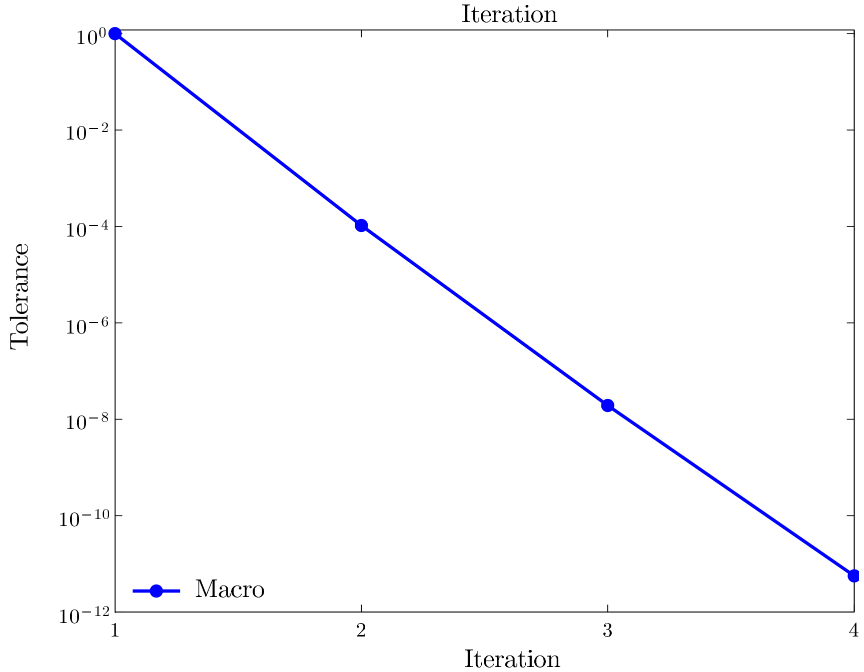

Figure 5.16: SMC problem, $\boldsymbol{b}$-conform formulations, hysteretic case. Convergence of the error as a function of nonlinear iterations. Top: mesoscale problem. Bottom: macroscale problem

5.2.3 Description of the problem for the $\boldsymbol{h}$-conform formulations

To define a two-dimensional problem for $\boldsymbol{h}$-conform formulations which can be solved using nodal elements, the primal unknown must have only the z-component, i.e., $\boldsymbol{h} = (0, 0, h_z)$. The magnetic induction also has only the z-component $\boldsymbol{b} = (0, 0, b_z)$ if the materials considered are isotropic or more generally, orthotropic (which is the case of the materials that we study in this chapter). The two-dimensional geometry is depicted in Figure 5.17. Using Ampère's equation $\mathbf{curl}\, \boldsymbol{h} = \boldsymbol{j}_s + \sigma \boldsymbol{e}$, it can be

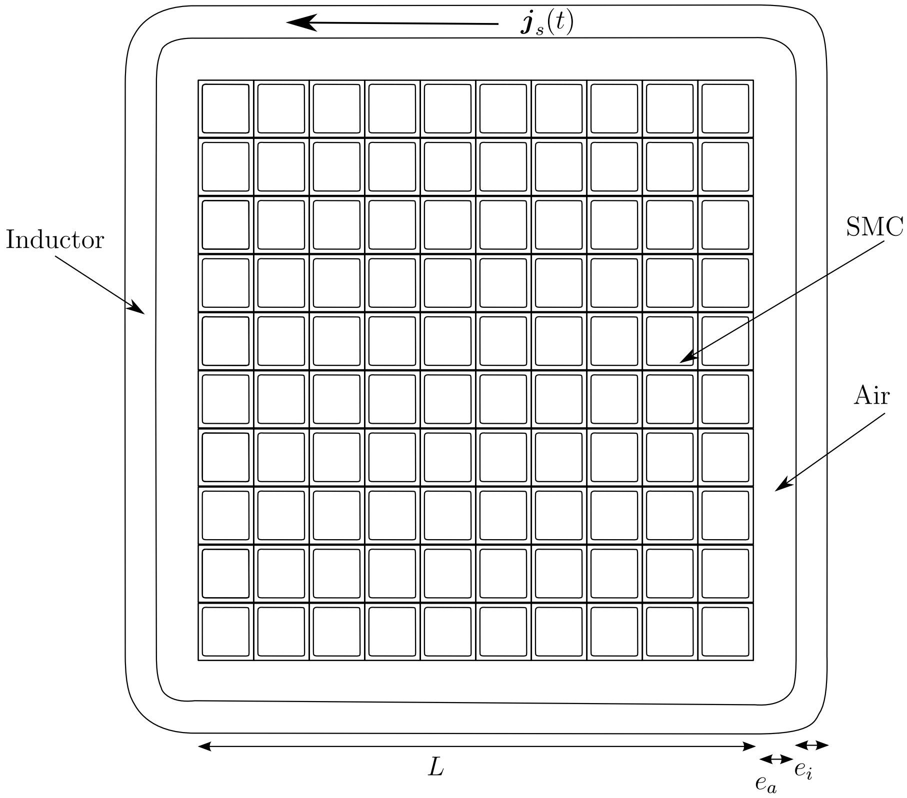

Figure 5.17: SMC two-dimensional geometry used for the $\boldsymbol{h}$ multiscale formulations. A source magnetic field $\boldsymbol{j}_s(t)$ is imposed in the xy-plane. The different dimensions are defined respectively by $L = 1000\,\mu$m, $e_a = 150\sqrt{2}/2\,\mu$m, $e_i = 100\,\mu$m and $e_{gap} = 100\,\mu$m. Only 10×10 SMC grains are shown instead of a 20×20 coarse-grained geometry used for computations.

straightforwardly concluded that eddy currents $\sigma \boldsymbol{e}$ and the source current density $\boldsymbol{j}_s$ must be constrained in the xy plane.

The wavelength corresponding to the highest frequency $f = 25\,$MHz is $\lambda = 12\,$m which is huge in comparison to the size of the structure ($500\,\mu$m) and therefore the magnetoquasistatic assumption can be made.

Applying the integral form of the Ampère's equation:

$$\int_S \mathbf{curl}\, \boldsymbol{h} \cdot \mathrm{d}\boldsymbol{s} = \oint_C \boldsymbol{h} \cdot \mathrm{d}\boldsymbol{l} = \int_S \boldsymbol{j} \cdot \mathrm{d}\boldsymbol{s} = 0, \tag{5.10}$$

on any surface located in the region outside of the inductor allows to conclude the constance of the magnetic field $\boldsymbol{h}$ is the non-conducting region outside the inductor and therefore equal to zero which is the value of the magnetic field at infinity $\boldsymbol{h}|_{\Gamma_{inf}} = \mathbf{0}$. Similarly, applying the integral form of the Ampère's equation on any closed curve surrounding the inductor, a (time-dependent) magnetic source field $\boldsymbol{h}_s(t)$ can be computed in the entire non-conducting region labeled *air* and therefore the problem defined in Figure 5.17 can be replaced by another one where the source field $\boldsymbol{h}_s(t)$ is imposed on the boundary of the conducting region of the SMC Γ (see Figure 5.18).

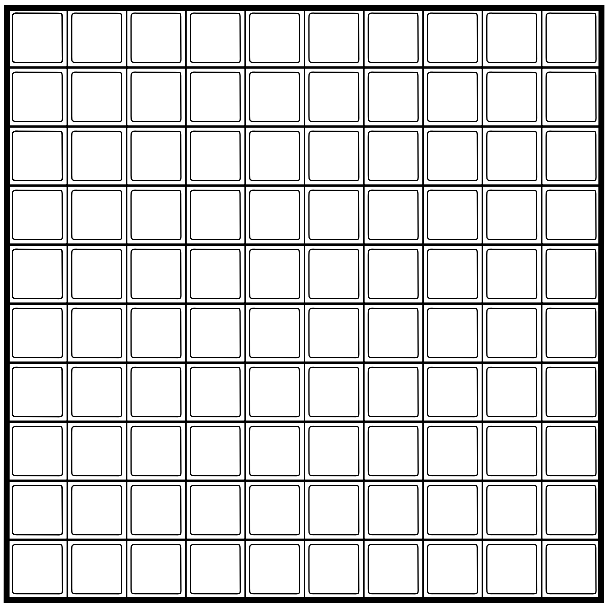

Figure 5.18: Simplified reference geometry used for the $\boldsymbol{h}$ formulations. A source magnetic fields $\boldsymbol{h}_s$ is derived from $\boldsymbol{j}_s$ and imposed on the boundary Γ.

We consider the elementary cell in Figure 5.1-(d) defined on page 79. The conductor has an isotropic conductivity $\sigma_c = 5\,10^6$ S/m and is governed by the following magnetic laws:

1. a (non-magnetic) linear law with $\mu_r = 1$,
2. the Frohlich-Kennelly nonlinear law $\boldsymbol{\mathcal{B}}(\boldsymbol{h}) = \left(\dfrac{1}{\alpha + \beta\,|\boldsymbol{h}|} + \gamma\right)\boldsymbol{h}$ with $\alpha = 1/(\mu_0\,\mu_{rw})$ where $\mu_{rw} \simeq 1000$ is the relative permeability for weak fields, $\beta \simeq 1.8$ is the saturation value of the magnetic induction and $\gamma = \mu_0$ [57].

The dielectric is governed by a linear magnetic law with $\mu_r = 1$ and is slightly conductor with Ratio $= \sigma_c^c/\sigma_c$. We have considered two values of electric conductivity with Ratio $= 10^{-5}$ and Ratio $= 10^{-3}$, respectively. The linear electric conductivity

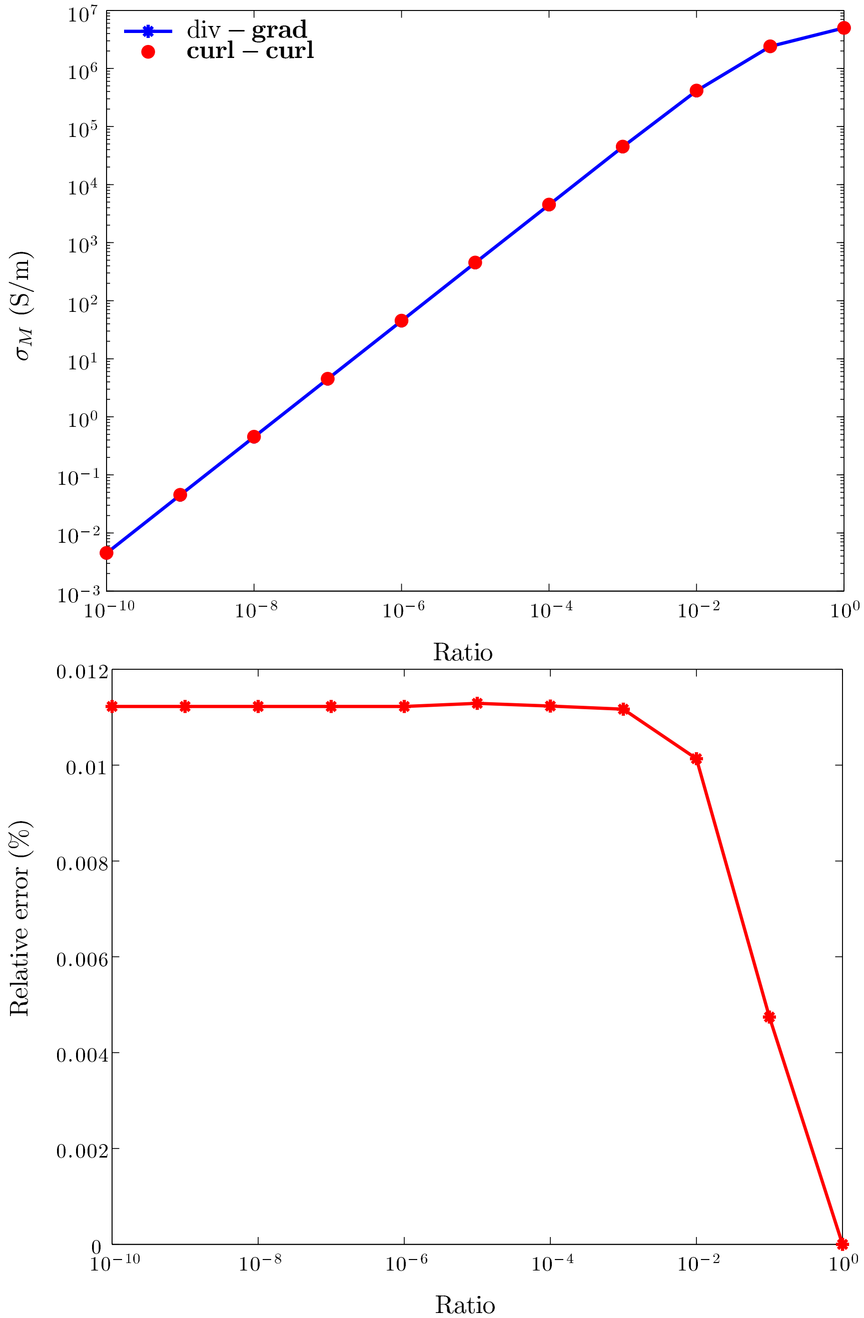

Figure 5.19: Top: the homogenized conductivity σ_M as a function of the ratio of conductivities in Ω_c and Ω_c^C. Two approaches are used: the div $-$ **grad** approach and the **curl** $-$ **curl** approach. Bottom: the relative error between the homogenized conductivities obtained using the div $-$ **grad** and the **curl** $-$ **curl** approaches.

can be homogenized by solving either the div $-$ **grad** problem (3.33),(3.37) or the **curl** $-$ **curl** problem (3.46),(3.48) which provides σ_M^{-1} and then by inversing this.

Figure 5.19–top depicts the values of the homogenized conductivity σ_M as a function of Ratio. The homogenized conductivities obtained using both approaches

are very close. The relative error depicted in Figure 5.19–bottom is defined as:

$$\text{Relative error}(\text{Ratio}) = \frac{|\sigma_{\text{Mcc}}(\text{Ratio}) - \sigma_{\text{Mdg}}(\text{Ratio})|}{|\sigma_{\text{Mcc}}(\text{Ratio})|}, \tag{5.11}$$

where $\sigma_{\text{Mcc}}(\text{Ratio})$ is the homogenized conductivity computed using the **curl** − **curl** problem and $\sigma_{\text{Mdg}}(\text{Ratio})$ is the homogenized conductivity computed using the div − **grad** problem for a given value of Ratio. The relative error reaches a maximum value of 0.012 % for small value of Ratio.

5.2.4 Results for the *h*-conform formulations

To present results for the $\boldsymbol{h}$-conform formulations we proceed in the same way as for the $\boldsymbol{b}$-conform formulations. Figure 5.20 - top shows the reference magnetic field $\boldsymbol{h}_{\text{ref}}$ computed on the entire, finely meshed multiscale structure with 1 526 564 triangular elements. The macroscale results are computed on a coarse mesh similar to the one in Figure 5.20 - bottom. We always use a mesh similar to the one in Figure 5.4 for the mesoscale computations.

The choices of σ_c^c, of the magnetic permeability for the conducting region μ_c and of the frequency f allow to determine whether (or not) there are eddy currents at the mesoscale level and/or at the macroscale level depending on the values of the mesoscale skin depth $\delta_m = 1/\sqrt{\pi f \sigma_c \mu_c}$ and of the macroscale skin depth $\delta_M = 1/\sqrt{\pi f \sigma_M \mu_M}$. The parameters σ_M and μ_M in the expression of δ_M are the homogenized conductivity and the homogenized permeability, respectively. We have used two values of electric conductivities: $\sigma_c^C = 10^5 \sigma_c$ for problems without significant macroscale eddy currents and $\sigma_c^C = 10^3 \sigma_c$ for problems with significant macroscale eddy currents. Studies involve frequencies up to 100 MHz for the linear case and 1 MHz for the nonlinear case.

The contribution of different terms involved in the resolution of the mesoscale problem are depicted in Figure 5.21.

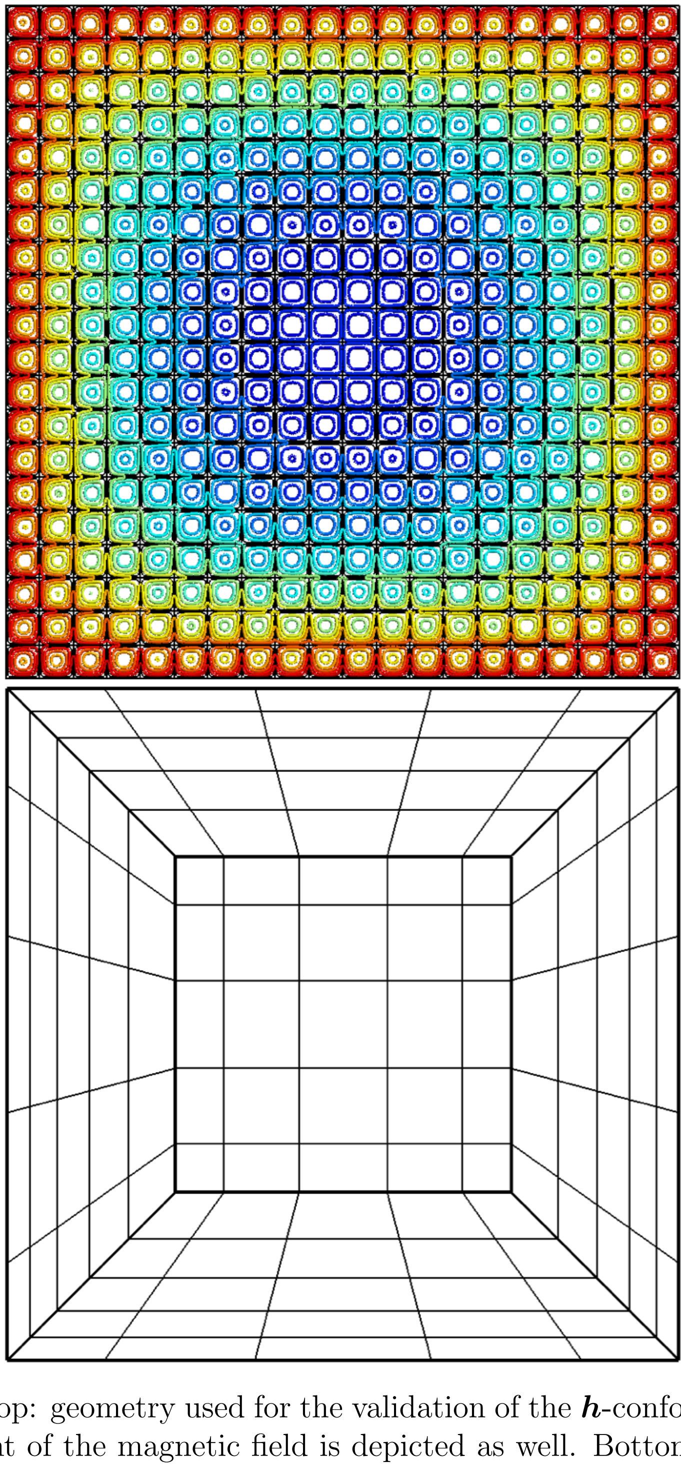

Figure 5.20: Top: geometry used for the validation of the $\boldsymbol{h}$-conform formulations. The z-component of the magnetic field is depicted as well. Bottom: mesh used for the macroscale problem.

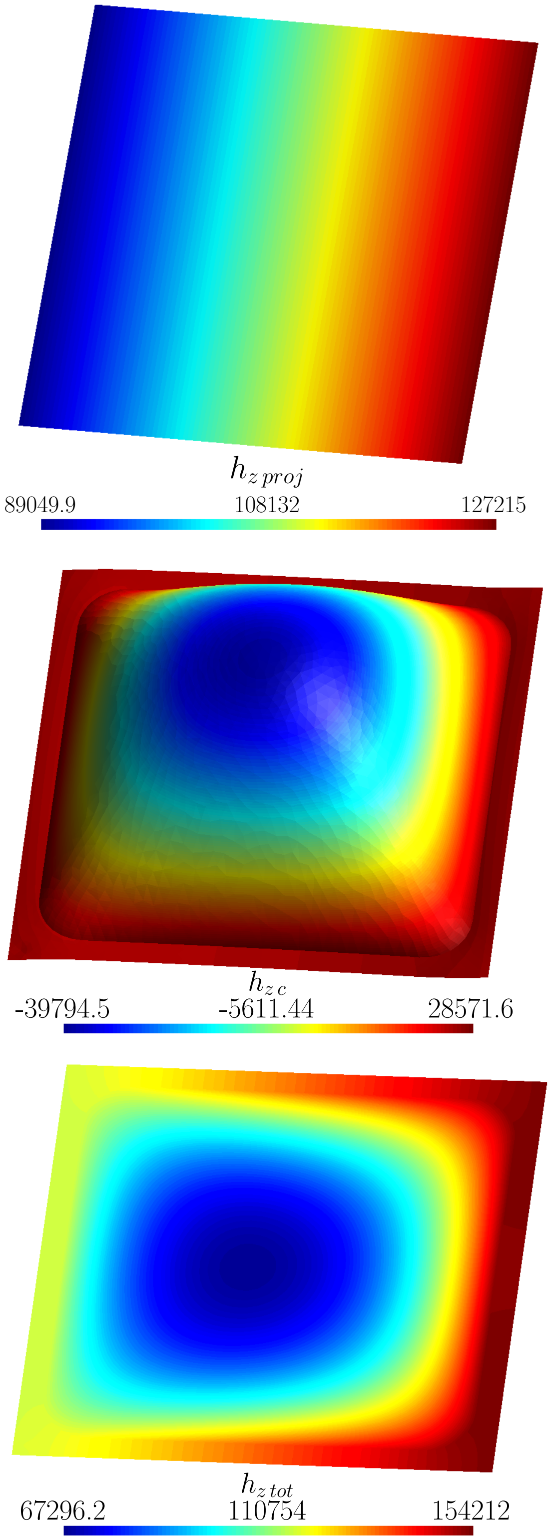

Figure 5.21: Contributing terms to the mesoscale magnetic field for a cell problem centered at $(325, 25, 0)\,\mu$m. Top: the correction term $\boldsymbol{h}_c(\boldsymbol{x}, \boldsymbol{y}, t)$. Middle: the projection term $\boldsymbol{h}_{proj}(\boldsymbol{x}, \boldsymbol{y}, t) = \boldsymbol{h}_M(\boldsymbol{x}, t) + \kappa(\boldsymbol{y} \times \boldsymbol{j}_M(\boldsymbol{x}, t))$. Bottom: the total mesoscale magnetic field $\boldsymbol{h}_{tot}(\boldsymbol{x}, \boldsymbol{y}, t) = \boldsymbol{h}_c(\boldsymbol{x}, \boldsymbol{y}, t) + \boldsymbol{h}_M(\boldsymbol{x}, t) + \kappa(\boldsymbol{y} \times \boldsymbol{h}_M(\boldsymbol{x}, t))$ { linear case with $j_{s0} = 10^6\,\mathrm{A/m^2}$, $f = 25\,\mathrm{MHz}$ and $t = 2\,10^{-9}$}.

The projection term which varies linearly on the cell is computed from the macroscale fields as $\boldsymbol{h}_{proj}(\boldsymbol{x},\boldsymbol{y},t) = \boldsymbol{h}_M(\boldsymbol{x},t) + \kappa(\boldsymbol{y} \times \boldsymbol{j}_M(\boldsymbol{x},t))$. This term is then used as a source term for the computation of the correction term $\boldsymbol{h}_c(\boldsymbol{x},\boldsymbol{y},t)$ which allows to derive the total mesoscale magnetic field $\boldsymbol{h}_{tot}(\boldsymbol{x},\boldsymbol{y},t) = \boldsymbol{h}_c(\boldsymbol{x},\boldsymbol{y},t) + \boldsymbol{h}_M(\boldsymbol{x},t) + \kappa(\boldsymbol{y} \times \boldsymbol{h}_M(\boldsymbol{x},t))$.

For problems with macroscale eddy currents ($\delta_M \approx L_M$ where L_M is the macroscale characteristic length), the imposition of periodic boundary conditions (see section 4.4.3) leads to good results. The comparison of the magnetic induction $\boldsymbol{b}$, of the magnetic field $\boldsymbol{h}$ and of the eddy currents $\boldsymbol{j}$, shows an excellent agreement between the reference solution and the local solution computed on the mesoscale cells centered around points of the computational domain (Figures 5.22-top, 5.23-top and 5.24-top. Small discrepancies are however observed near the boundary of the domain (see Table 5.4).

Table 5.4 displays the values $||\boldsymbol{b}||$ obtained from the reference solution (Reference), the macroscale solution (Macro) and the mesoscale solution (Meso) and the relative pointwise errors $\mathrm{err}_{\mathrm{meso}}$ and $\mathrm{err}_{\mathrm{macro}}$ defined by:

$$\mathrm{err}_{\mathrm{meso}}(\boldsymbol{x},t) = \frac{|\boldsymbol{b}_{\mathrm{ref}}(\boldsymbol{x},t) - \boldsymbol{b}_{\mathrm{meso}}(\boldsymbol{x},t)|}{|\boldsymbol{b}_{\mathrm{ref}}(\boldsymbol{x},t)|}, \tag{5.12}$$

and

$$\mathrm{err}_{\mathrm{Macro}}(\boldsymbol{x},t) = \frac{|\boldsymbol{b}_{\mathrm{ref}}(\boldsymbol{x},t) - \boldsymbol{b}_{\mathrm{macro}}(\boldsymbol{x},t)|}{|\boldsymbol{b}_{\mathrm{ref}}(\boldsymbol{x},t)|}, \tag{5.13}$$

for $t = 4 \times 10^{-9}s$.

For problems without macroscale eddy currents ($\delta_M \ll L_M$), periodic boundary conditions defined in section 4.4.3 lead to erroneous results for the magnetic field and the magnetic flux density. The definition of a new mesoscale problem with zero boundary conditions at boundaries with small values of the electric conductivity (and therefore that are not crossed by important macroscale eddy currents) provides an excellent agreement between the reference solution and the local solution computed on the mesoscale cells centered around points of the computational domain and this for linear and nonlinear problems (Figures 5.22-bottom, 5.23-bottom and 5.24-bottom for the linear case and Figures 5.26 and 5.27 for the nonlinear case). Compared to the previous case with macroscale eddy currents, the accuracy of mesoscale solutions improves even near the boundary of the domain (see Table 5.5 and 5.6). It remains to be fully understood why periodic boundary conditions defined in section 4.4.3 should be changed in order to improve the accuracy.

Table 5.5 displays the values $||\boldsymbol{h}||$ obtained from the reference solution (Reference), the macroscale solution (Macro) and the mesoscale solution (Meso) and the relative pointwise errors $\mathrm{err}_{\mathrm{meso}}$ and $\mathrm{err}_{\mathrm{macro}}$ defined by:

$$\mathrm{err}_{\mathrm{meso}}(\boldsymbol{x},t) = \frac{|\boldsymbol{h}_{\mathrm{ref}}(\boldsymbol{x},t) - \boldsymbol{h}_{\mathrm{meso}}(\boldsymbol{x},t)|}{|\boldsymbol{h}_{\mathrm{ref}}(\boldsymbol{x},t)|}, \tag{5.14}$$

and

$$\mathrm{err}_{\mathrm{Macro}}(\boldsymbol{x},t) = \frac{|\boldsymbol{h}_{\mathrm{ref}}(\boldsymbol{x},t) - \boldsymbol{h}_{\mathrm{macro}}(\boldsymbol{x},t)|}{|\boldsymbol{h}_{\mathrm{ref}}(\boldsymbol{x},t)|}, \tag{5.15}$$

for $t = 4 \times 10^{-9}s$. Tables 5.6 provides relative $L^2(0,T)$ errors between the reference magnetic field $\boldsymbol{h}_{\text{ref}}(\boldsymbol{x},t)$ and the mesoscale magnetic field $\boldsymbol{h}_{\text{meso}}(\boldsymbol{x},t)$ and the macroscale magnetic field $\boldsymbol{h}_{\text{Macro}}(\boldsymbol{x},t)$. For a point $\boldsymbol{x}$ of the computational domain, this L^2 errors are given by the formula:

$$\text{err}_{\text{L}^2\,\text{meso}}(\boldsymbol{x},t) = \frac{||\boldsymbol{h}_{\text{ref}}(\boldsymbol{x},t) - \boldsymbol{h}_{\text{meso}}(\boldsymbol{x},t)||_{L^2(0,T)}}{||\boldsymbol{h}_{\text{ref}}(\boldsymbol{x},t)||_{L^2(0,T)}}, \tag{5.16}$$

and

$$\text{err}_{\text{L}^2\,\text{Macro}}(\boldsymbol{x},t) = \frac{||\boldsymbol{h}_{\text{ref}}(\boldsymbol{x},t) - \boldsymbol{h}_{\text{Macro}}(\boldsymbol{x},t)||_{L^2(0,T)}}{||\boldsymbol{h}_{\text{ref}}(\boldsymbol{x},t)||_{L^2(0,T)}}. \tag{5.17}$$

From results of Table 5.4, it can be seen that the errors on magnetic flux density increase as the point gets close to the boundary of the computational domain.

Table 5.4: SMC problem with global eddy current ($\sigma_c^C = 10^{-3}\,\sigma_c$) - $\boldsymbol{h}$-conform formulations, linear case. Comparison of the reference magnetic flux density and the computational (macroscale and mesoscale) magnetic flux density ($\|\boldsymbol{b}\|$, in T) in different points of the macroscale domain $\{\ t = 4\,10^{-9}s\}$.

Position (μm)	Reference	Meso	Macro	err_{meso}	$\text{err}_{\text{Macro}}$
$(25, 25, 0)$	0.158763	0.160889	0.208962	1.33	31.60
$(25, 475, 0)$	0.525468	0.594662	0.695526	13.16	32.36
$(175, 175, 0)$	0.223458	0.234625	0.252301	4.99	12.90
$(475, 25, 0)$	0.525478	0.594665	0.695526	13.16	32.36
$(475, 475, 0)$	0.569264	0.644839	0.718787	13.27	26.26

The comparison of Joule losses computed from mesoscale densities (Meso) are in good agreement with the reference results (Ref). The developed method allows to effectively represent fields and losses in the transient and in the steady state regimes. Joule losses computed directly from the macroscale fields (Macro) exhibit large deviations with respect to reference results. In all cases, the error increases with frequency (see Figure 5.7). The same conclusions hold for the computation of magnetic power.

Table 5.3 contains the relative $L^\infty(0,T)$ error of the Joule losses as a function of frequency. This $L^\infty(0,T)$ error is defined by the expression (5.9).

The influence of the macroscale mesh is depicted in Figure 5.29 and Figure 5.30. As can be seen in Figure 5.29, the macroscale mesh must be able to capture the variations of the macroscale solution in order to have accurate eddy current losses.

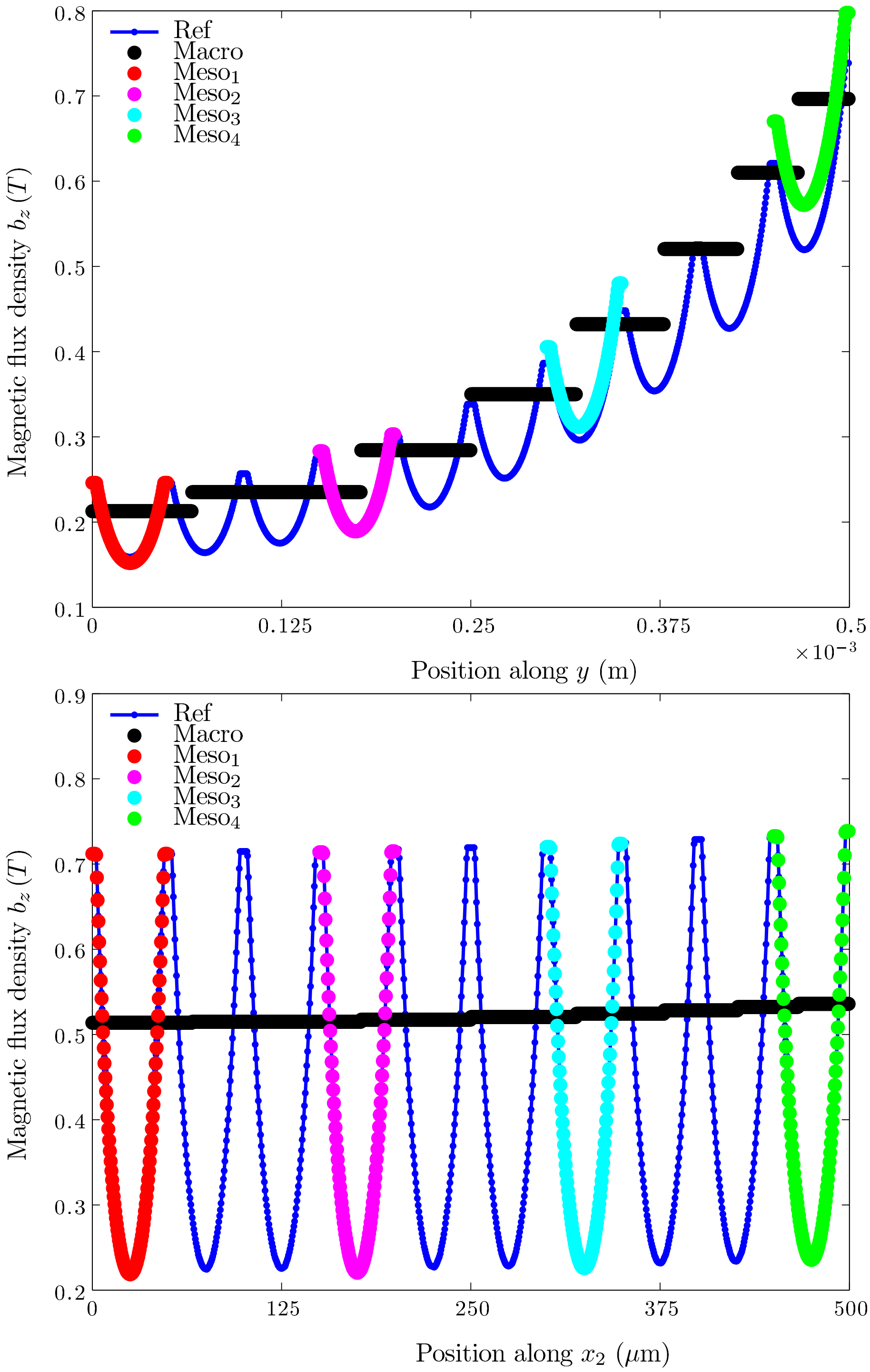

Figure 5.22: SMC problem, $\boldsymbol{h}$-conform formulations, linear case. Spatial cuts of the z-component of the magnetic flux density $\boldsymbol{h}$ along the line $\{\ x = 475, z = 0\}$,μm. Top: case with $\{\sigma_c^C = 10^{-3} \times \sigma_c,\ f = 25\,\mathrm{MHz}$ and $t = 4\,10^{-9}\,\mathrm{s}\}$. Bottom: case with $\{\sigma_c^C = 10^{-5} \times \sigma_c,\ f = 100\,\mathrm{MHz}$ and $t = 10^{-9}\,\mathrm{s}\}$

Table 5.5: SMC problem without global eddy current ($\sigma_c^C = 10^{-5}\,\sigma_c$) - $\boldsymbol{h}$-conform formulations, linear case. Comparison of the reference magnetic field and the computational (macroscale and mesoscale) magnetic field ($\|\boldsymbol{h}\|$, in A/m) in different points of the macroscale domain $\{\ t = 4\,10^{-9}s\}$.

Position (μm)	Reference	Meso	Macro	err_{meso} (%)	$\text{err}_{\text{Macro}}$ (%)
$(25, 25, 0)$	454809	454285	582023	0.1152	27.97
$(25, 475, 0)$	460048	459575	587144	0.1028	27.63
$(175, 175, 0)$	456082	455373	583052	0.1555	27.84
$(475, 25, 0)$	459979	459577	587144	0.0874	27.65
$(475, 475, 0)$	460474	460080	587678	0.0856	27.62

Table 5.6: SMC problem $\boldsymbol{h}$-conform formulations linear case. Relative $L^2(0,T)$ error between the reference and the computational (macroscale-mesoscale) magnetic field.

Position (μm)	Relative error Meso (%)	Relative error Macro (%)
$(25, 25, 0)$	0.0536	14.122
$(25, 475, 0)$	0.0477	14.119
$(175, 175, 0)$	0.0667	14.097
$(475, 25, 0)$	0.0398	14.126
$(475, 475, 0)$	0.0413	14.132

Table 5.7: SMC problem without global eddy current ($\sigma_c^C = 10^{-5}\,\sigma_c$), $\boldsymbol{h}$-conform formulations, linear case. Relative $L^\infty(0,T)$ error on the total Joule losses as a function of the frequency.

Frequency (MHz)	$\text{err}_{L^\infty(0,T)}$ (%)
1	2.60
2.5	1.82
5	2.35
10	2.47
25	2.54
50	3.24
100	3.71

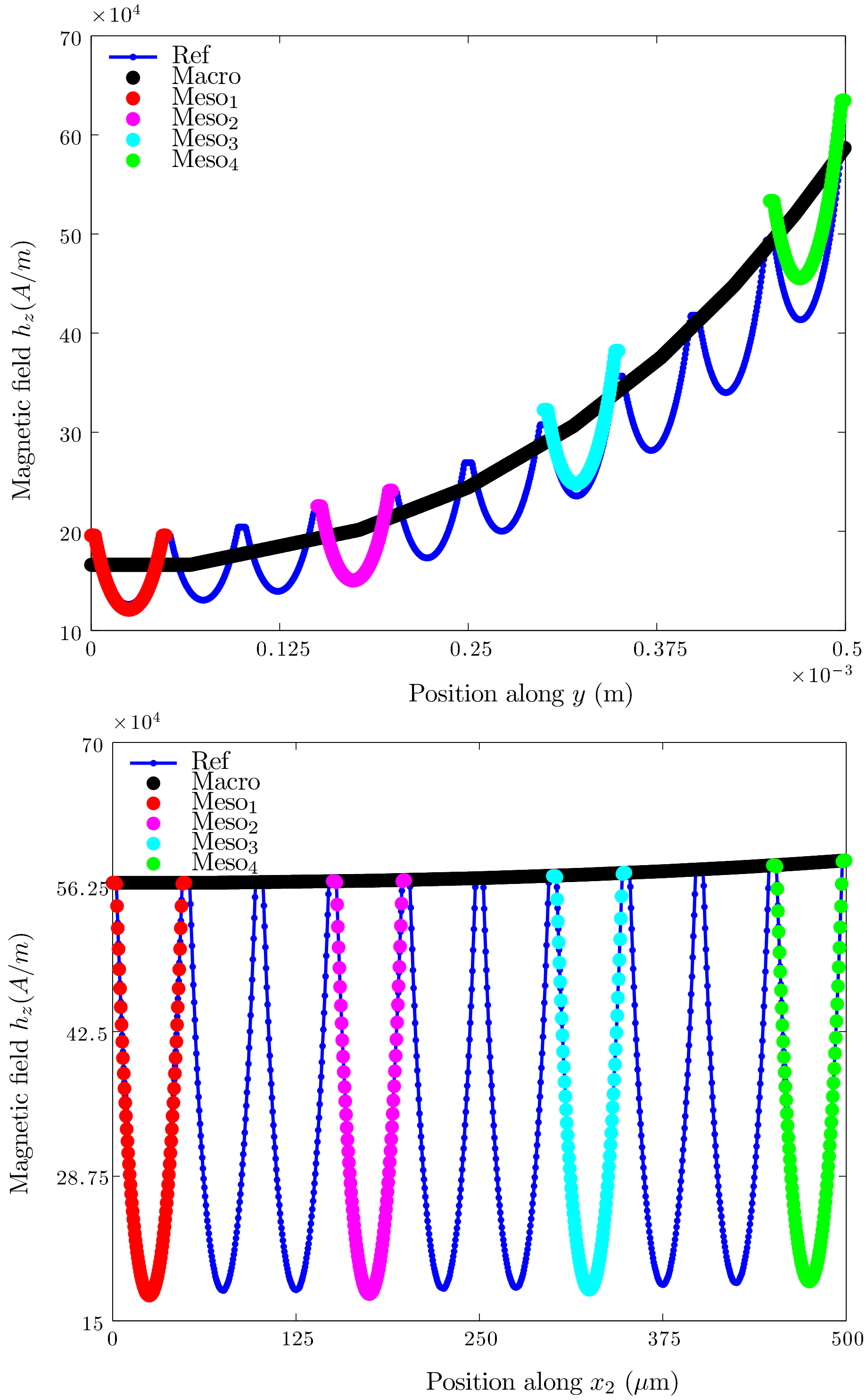

Figure 5.23: SMC problem, $\boldsymbol{h}$-conform formulations, linear case. Spatial cuts of the z-component of the magnetic field $\boldsymbol{h}$ along the line $\{\ x = 475, z = 0\}$,μm. Top: case with $\{\sigma_c^C = 10^{-3} \times \sigma_c,\ f = 25\,\text{MHz and } t = 4\,10^{-9}\ \text{s}\}$. Bottom: case with $\{\sigma_c^C = 10^{-5} \times \sigma_c,\ f = 100\,\text{MHz and } t = 10^{-9}\,\text{s}\}$

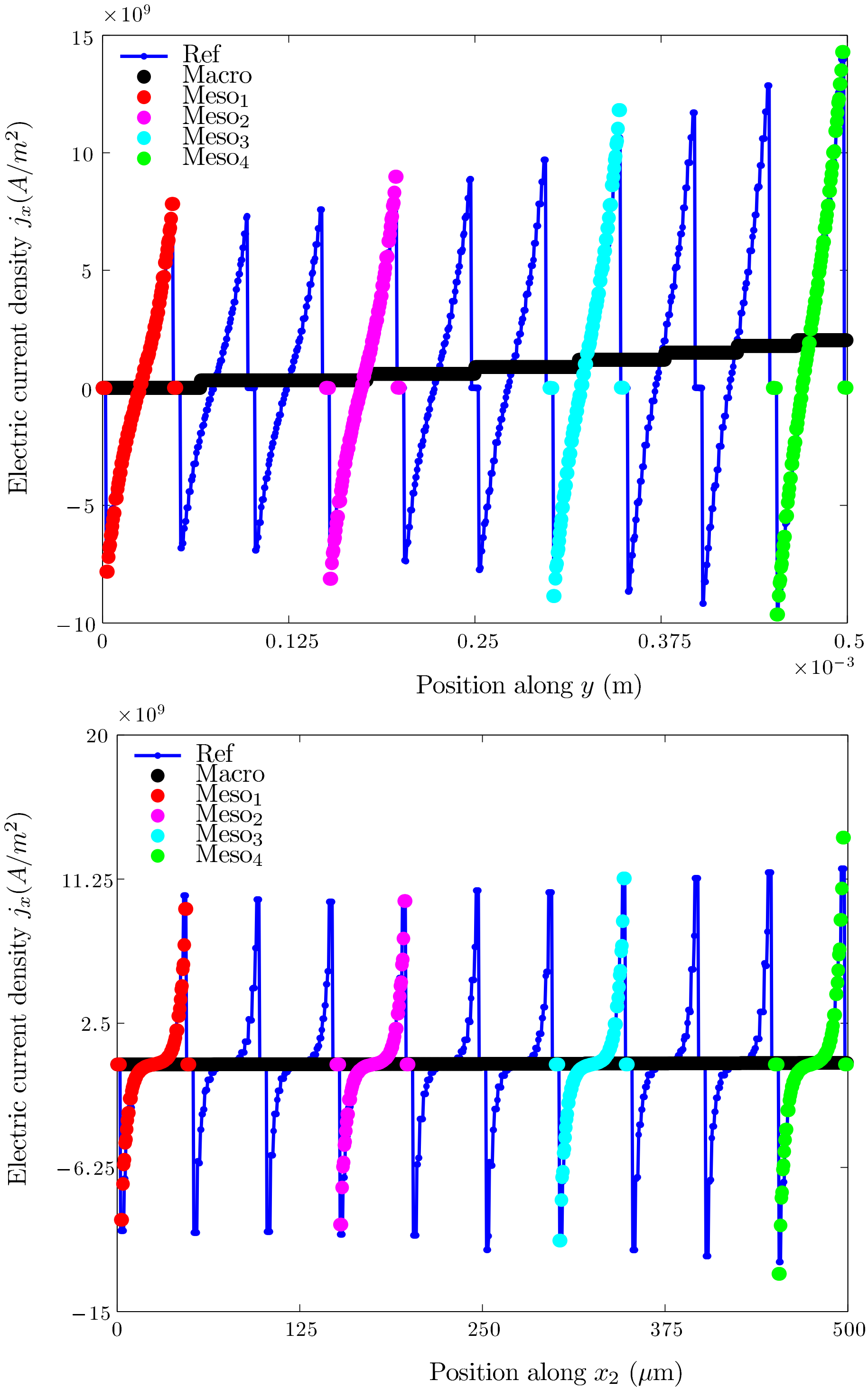

Figure 5.24: SMC problem, $\boldsymbol{h}$-conform formulations, linear case. Spatial cuts of the x-component of the electric current density $\boldsymbol{j}$ along the line $\{\ x = 475, z = 0\}$,μm. Top: case with $\{\sigma_c^C = 10^{-3} \times \sigma_c,\ f = 25\,\text{MHz and } t = 4\,10^{-9}\text{ s}\}$. Bottom: case with $\{\sigma_c^C = 10^{-5} \times \sigma_c,\ f = 100\,\text{MHz and } t = 10^{-10}\,\text{s}\}$

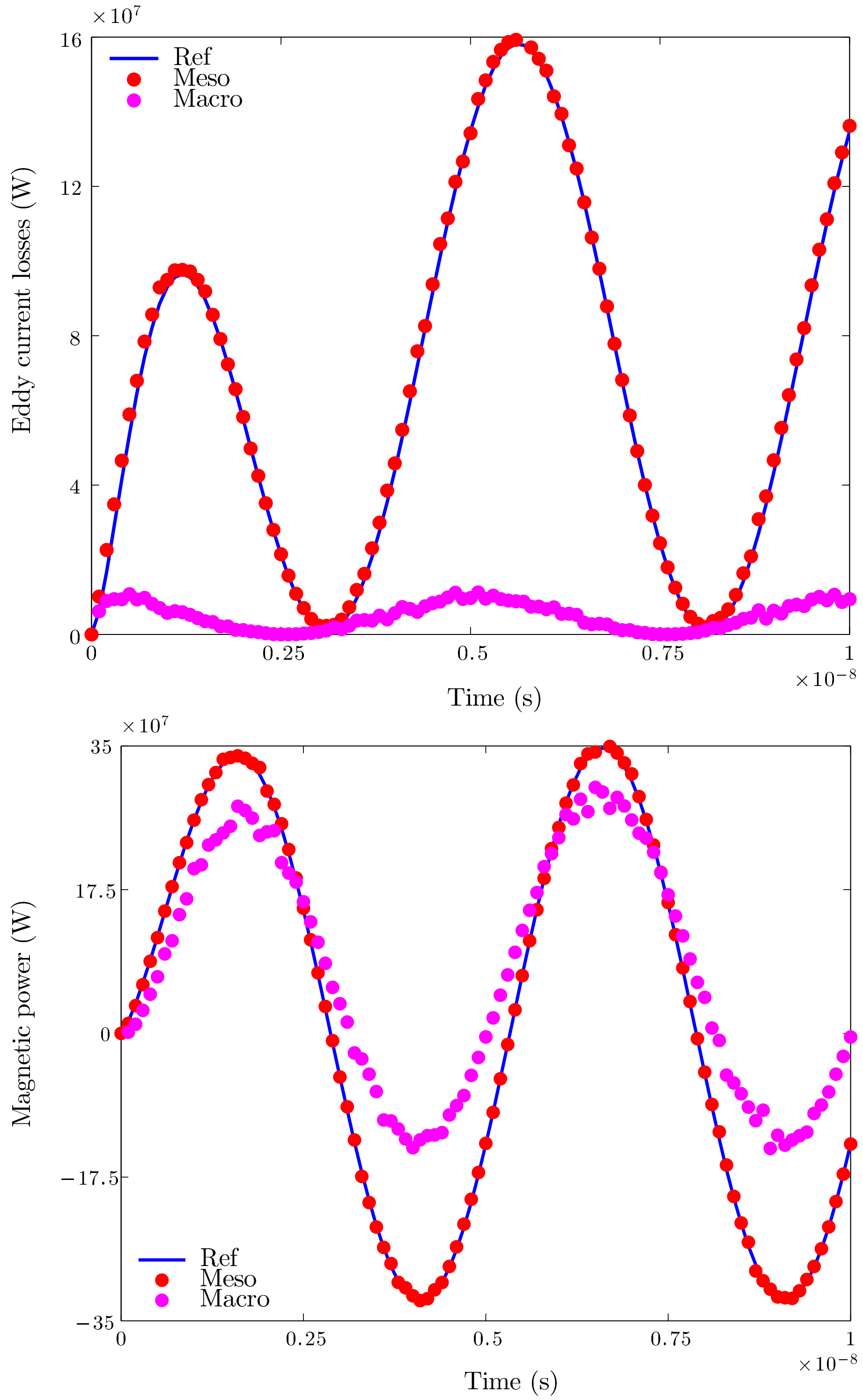

Figure 5.25: SMC problem, $\boldsymbol{h}$-conform formulations, linear case with $\{\sigma_c^C = 10^{-5}\,\sigma_c,\ f = 100\,\mathrm{MHz}\}$. Top: instantaneous Joule losses. Bottom: magnetic power. The curve labeled Ref is obtained from the reference solution, the curve labeled Meso is obtained by upscaling eddy current losses densities from the mesoscale problems and the curve labeled Macro is obtained from the macroscale solution.

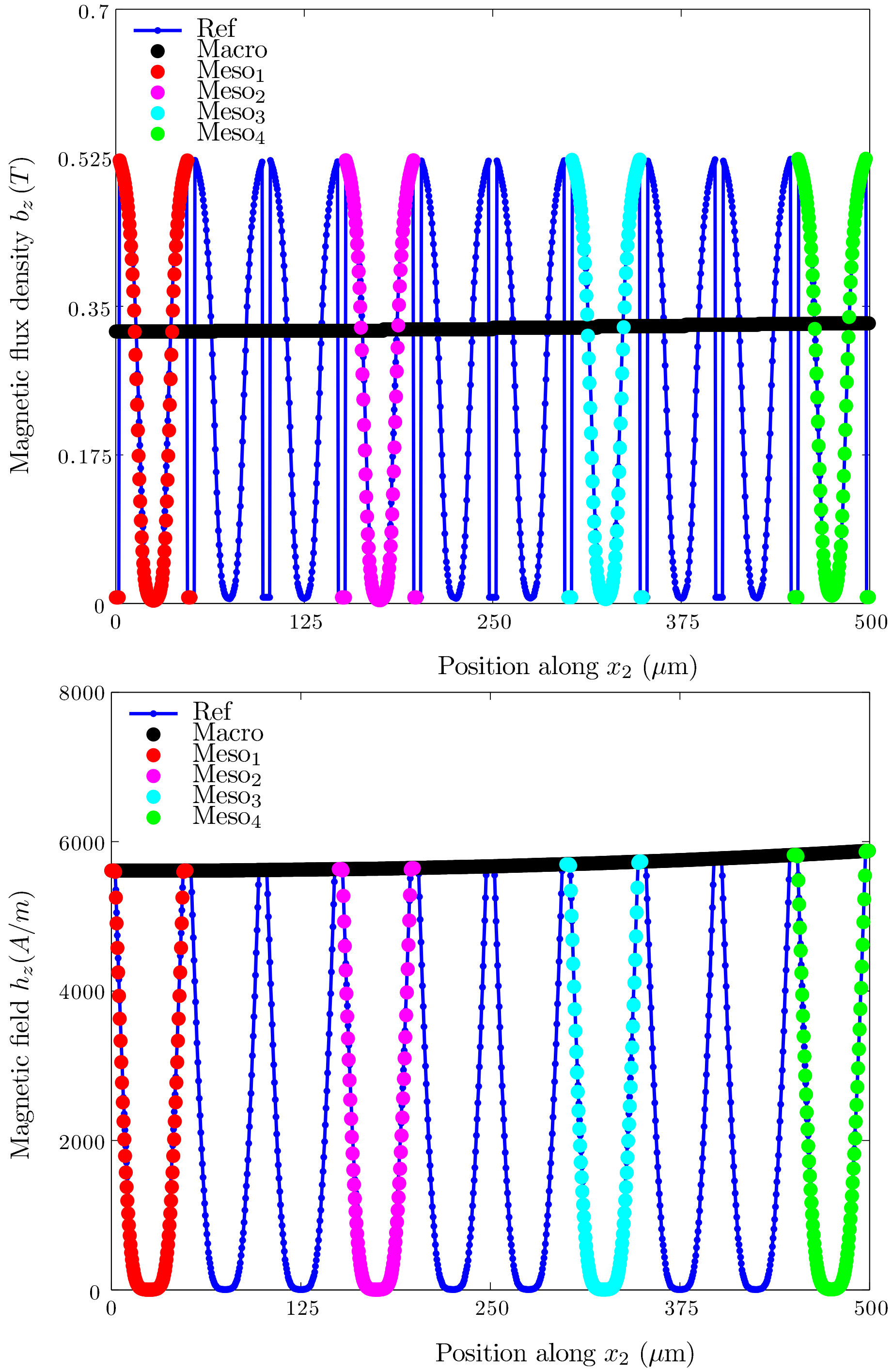

Figure 5.26: SMC problem, $\boldsymbol{h}$-conform formulations, nonlinear case. Spatial cuts of the z-component of the magnetic field $\boldsymbol{h}$ (top) and of the z-component of magnetic flux density $\boldsymbol{b}$ (bottom) along the line $\{\, x = 475, z = 0\}\,\mu$m. $\{f = 1\,$MHz, $\sigma_c^C = 10^{-3}\,\sigma_c$ and $t = 10^{-7}$ s$\}$.

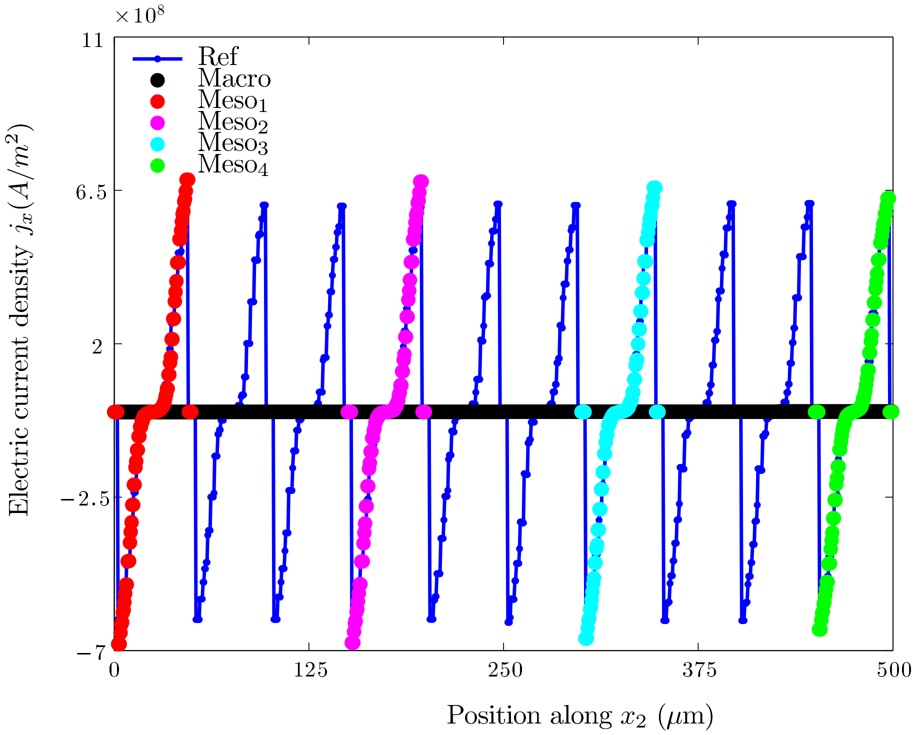

Figure 5.27: SMC problem, $\boldsymbol{h}$-conform formulations, nonlinear case. Spatial cuts of the x-component of the electric current density $\boldsymbol{j}$ along the line $\{\, x = 475, z = 0\}\,\mu$m. $\{f = 1\,$MHz, $\sigma_c^C = 10^{-3}\,\sigma_c$ and $t = 10^{-7}$ s$\}$.

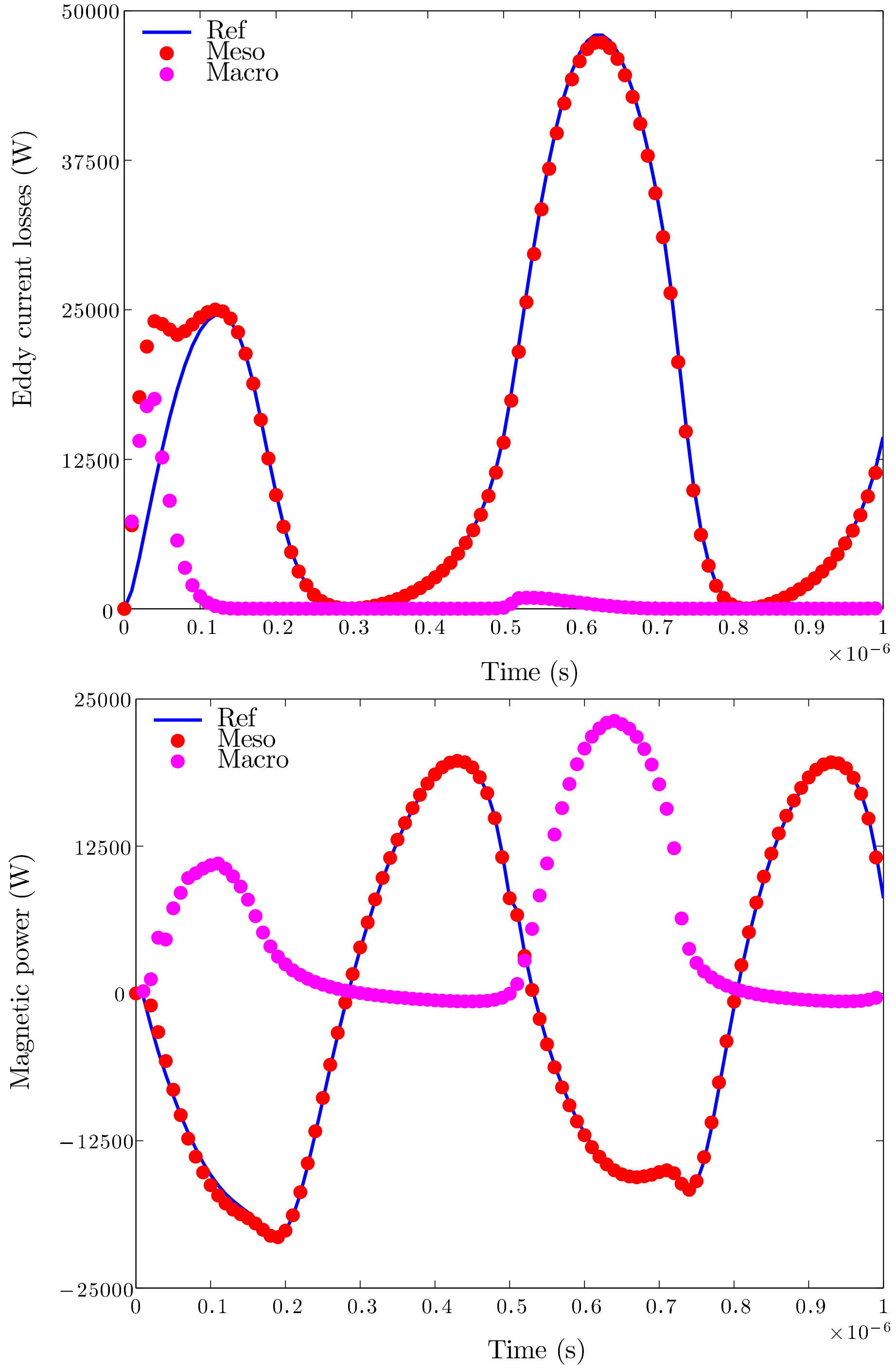

Figure 5.28: SMC problem, $\boldsymbol{h}$-conform formulations, nonlinear case with $\{\sigma_c^C = 10^{-5}\,\sigma_c,\ f = 1\,\text{MHz}\}$. Top: instantaneous Joule losses. Bottom: magnetic power. The curve labeled Ref is obtained from the reference solution, the curve labeled Meso is obtained by upscaling eddy current losses densities from the mesoscale problems and the curve labeled Macro is obtained from the macroscale solution.

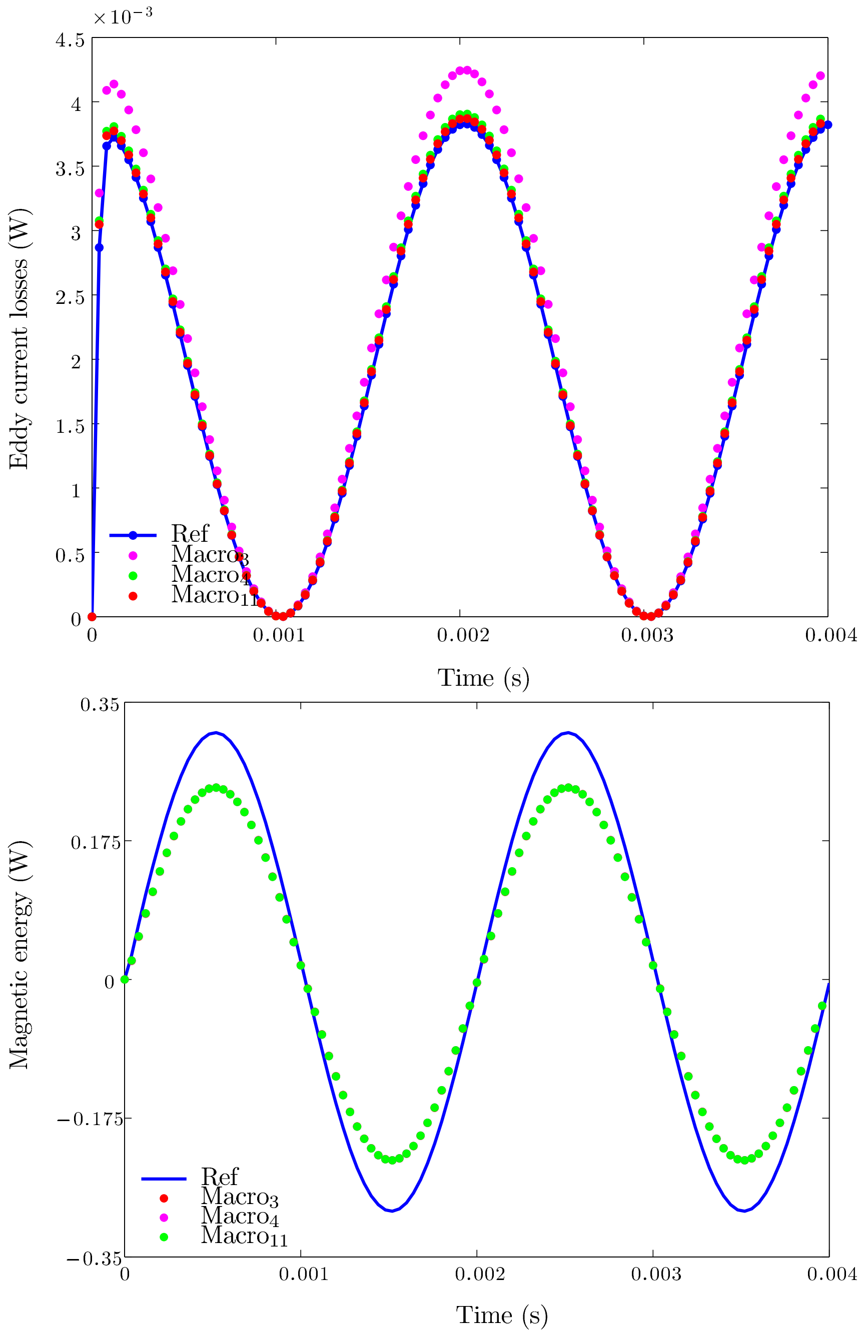

Figure 5.29: SMC problem, $\boldsymbol{h}$-conform formulations, linear case. Influence of the macroscale mesh on the time evolution of the instantaneous Joule losses (top) and the time evolution of the magnetic power (bottom). The curve labeled Macro$_3$ is obtained using the top - left mesh in Figure 5.30, the curve labeled Macro$_4$ is obtained using the top - right mesh in Figure 5.30 and the curve labeled Macro$_1$1 is obtained using the bottom - left mesh in Figure 5.30. $\{ f = 250$ Hz $\}$.

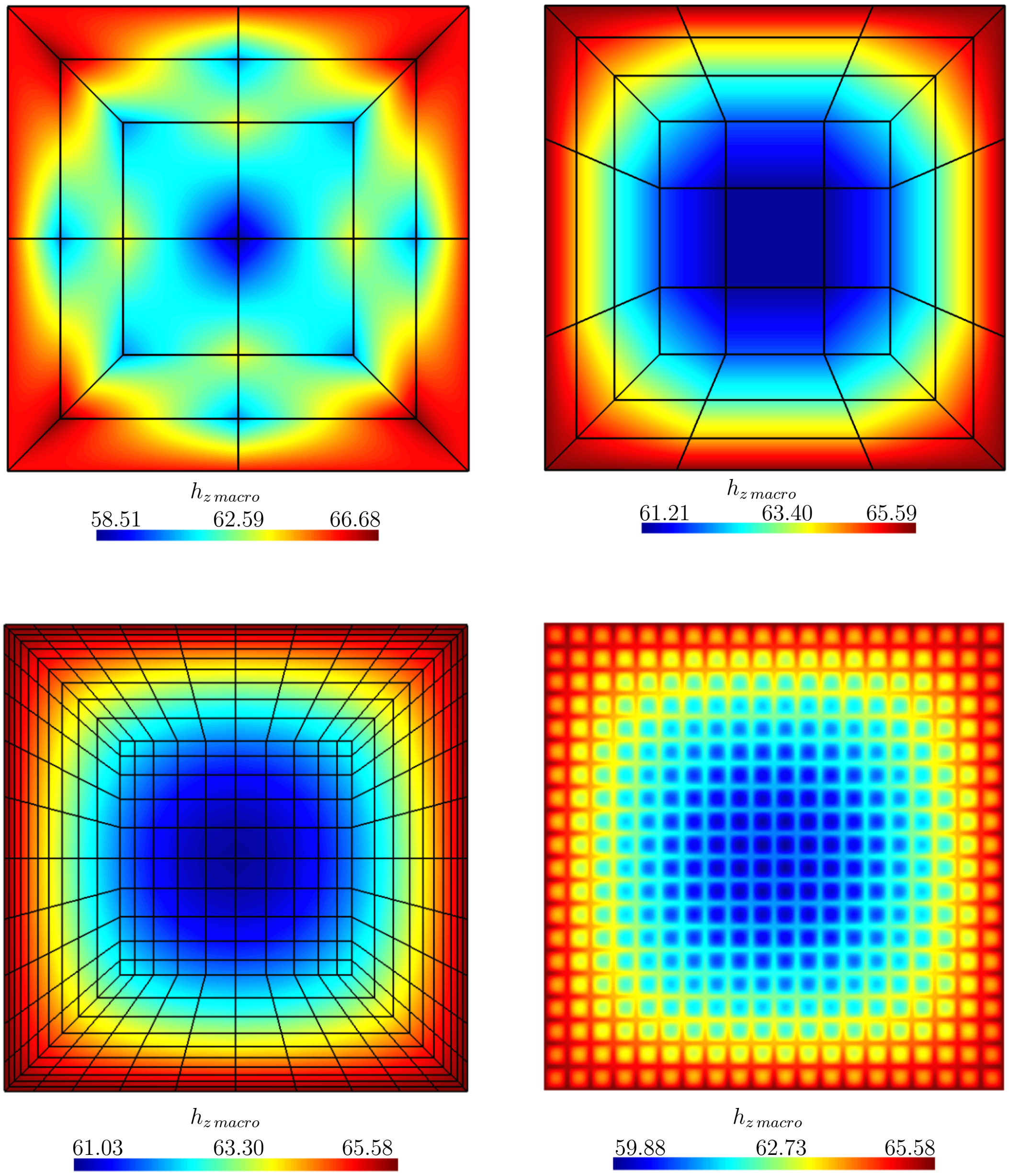

Figure 5.30: SMC problem, $\boldsymbol{h}$-conform formulations, linear case. Influence of the macroscale mesh. Top - left: 20 elements. Top - right: 45 elements. Bottom - left: 500 elements. Bottom - right: reference mesh with 737268 elements.

5.3 Lamination stack

We consider a stack of thin ferromagnetic sheets, as for example can be found in a toroidal transformer surrounded by a wound coil (Figure 5.31 (a)). In this section we will consider such a toroidal laminated structure with two different inductors, amenable to nodal finite element discretization of $\boldsymbol{b}$-conform and $\boldsymbol{h}$-conform multi-scale formulations.

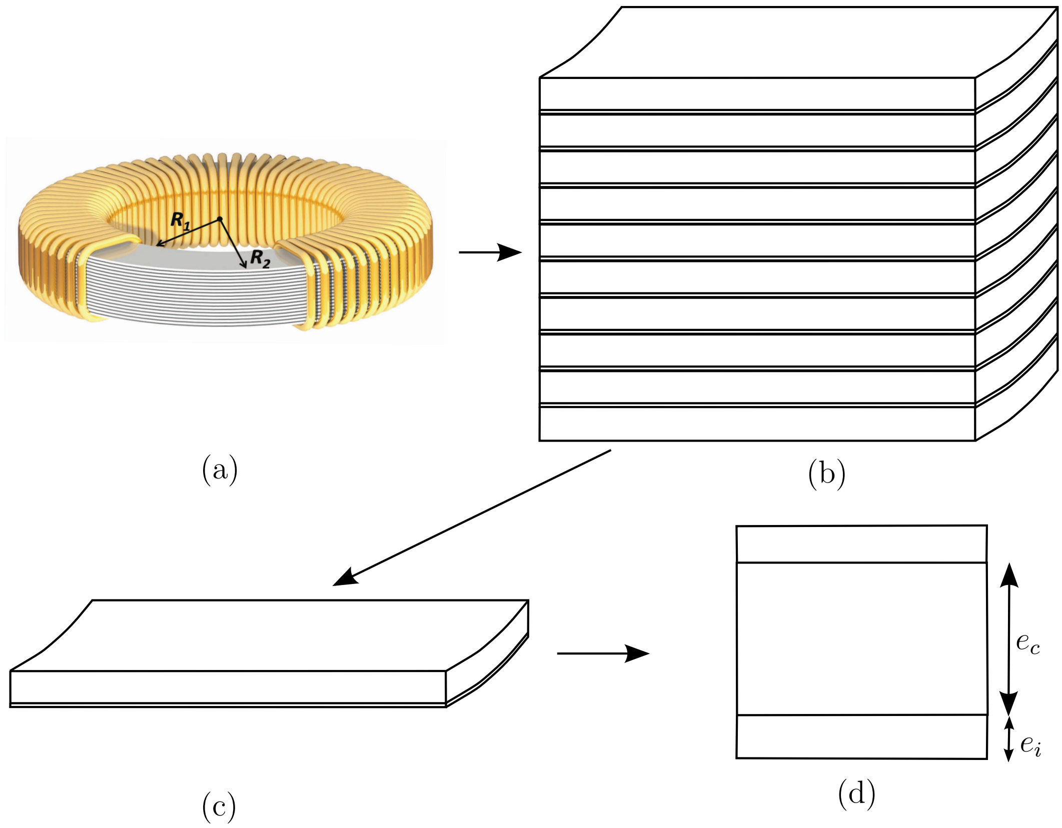

Figure 5.31: Lamination stack two-dimensional geometry used for the multiscale formulations. (a) : A real three-dimensional geometry of the a toroidal transformer [22]. (b) : A piece of lamination stack. (c) : A three-dimensional lamination + insulatio layer. (d) : A square two-dimensional elementary cell used for the homogenization computations ($e_c = 500\mu$m and $e_i = 50\mu$m).

The actual three-dimensional geometry of the lamination stack is depicted in Figure 5.31 (b) and each lamination can be represented by Figure 5.31 (c). Similarly to the SMC case, all cuts that pass through the axis of the toroid are similar and therefore the cell in Figure 5.31 (d) can be used as a reference cell for the multiscale computations. This cell is made of two parts: a metallic part labeled *lamination* which is conducting and magnetic and a dielectric part labeled *dielectric* which is non-magnetic. We consider it non-conducting for the $\boldsymbol{b}$-conform formulations and slightly conducting for the $\boldsymbol{h}$-conform formulations. The latter case allows to have a test case with global eddy currents at the macroscale.

5.3.1 Description of the problem for the $\boldsymbol{b}$-conform formulations

The definition of the problem for the $\boldsymbol{b}$-conform multiscale problem is done like the $\boldsymbol{b}$-conform multiscale problem for SMCs one carried out in section 5.2.1. The goal is to have the unknown field $\boldsymbol{a} = (0, 0, a_z)$ with only the z-component so that we can use the two-dimensional formulations developed in section 4.3.

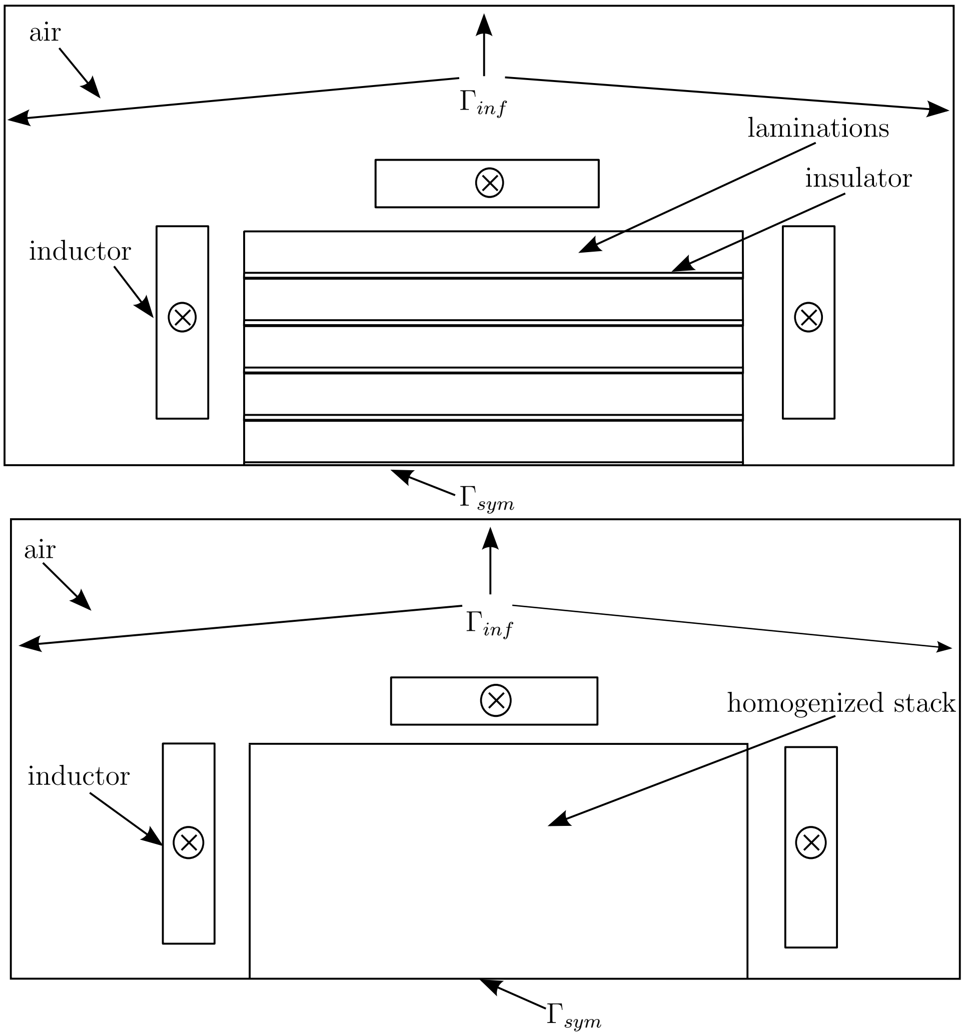

Figure 5.32: Top: reference geometry used for the $\boldsymbol{a} - v$ computations. Only half of the geometry is used thanks to the symmetries. Bottom: geometry used for the computational homogenization method.

To achieve this, we impose a source current density $\boldsymbol{j}_s = (0, 0, j_{sz})$ only the z-component (see Figure 5.32) is imposed in the inductor with $j_s = j_{s0} \sin(2\pi f t)$ where j_{s0} is the constant amplitude.

We consider a model of a laminated core (16.45 mm $\times$ 16.45 mm) consisting of 30 laminations (thickness $d_l = 0.5$ mm) and 29 insulation layers (thickness $d_0 = 0.05$ mm). The filling factor is $\lambda = d_l/(d_l + d_0) = 0.91$. Taking advantage of the symmetry, only half of the model has been studied (See Fig. 5.32). Note that as we consider perfectly isolated laminations, there are no currents flowing from one lamination to the other. Indeed, $(\sigma_M)_{22} = 0$ (where the index $_2$ stands for the direction normal to the laminations) so that no eddy currents are to be accounted for at the macroscale ($\boldsymbol{j}_M = \mathbf{0}$ and $\boldsymbol{e}_M = \mathbf{0}$).

The dielectric which is a perfect insulator is governed by a linear magnetic law with $\mu_r = 1$ and the conductor has an isotropic electric conductivity of $\sigma = 5 \times 10^6$ S/m and is governed by the following magnetic laws:

1. a nonlinear exponential law $\boldsymbol{\mathcal{H}}(\boldsymbol{b}) = \Big(\alpha + \beta \exp(\gamma ||\boldsymbol{b}||^2)\Big)\, \boldsymbol{b}$ with $\alpha = 388, \beta = 0.3774$ and $\gamma = 2.97$ [57].

2. a Jiles - Atherton hysteresis model with parameters $\boldsymbol{\mathcal{M}}_s = 1,145,500$A/m, $a = 59$A/m, $k = 99$A/m, $c = 0.55$ and $\alpha = 1.3\times 10^{-4}$ (see section 4.3.4 [19,94]).

We also impose the following boundary conditions on the boundary of the domain:

$$\boldsymbol{n} \times \boldsymbol{a}|_{\Gamma inf} = \mathbf{0} \longrightarrow \boldsymbol{n} \cdot \boldsymbol{b}|_{\Gamma inf} = 0, \tag{5.18}$$

$$\boldsymbol{n} \cdot \boldsymbol{b}|_{\Gamma_{sym}} = 0. \tag{5.19}$$

Equations (5.18) and(5.19) express the impermeability of the boundary to the magnetic flux (for Γ_{sym}) and the vanishing of the magnetic flux density $\boldsymbol{b}$ at infinity Γ_{inf}.

5.3.2 Results for the $\boldsymbol{b}$-conform formulations

The reference solution is obtained by a brute force approach, i.e. solving a finite element problem on an extremely fine mesh of the whole stack consisting of 30 layers of 81 quadrangles for each lamination and 4 layers of 81 quadrangles for each insulation layer (i.e. 41,148 elements for the conductors and the insulation layers). The mesoscale problems are solved on square domains comprising one lamination and one insulation layer (Figure 5.33 - right).

Each lamination is discretized with 30 layers of 10 quadrangles and each insulation layer with 8 layers of 10 quadrangles. The coarse mesh of the lamination stack contains 225 and 300 quadrangular elements, respectively for the nonlinear and the hysteresis problems with one integration point per element. The computational problem is solved over one period with 20 time steps per period for the nonlinear problem and two periods with 120 time steps per period for the hysteresis problem.

For the nonlinear case, results obtained using the computational homogenization approach are compared to those obtained using a brute force approach. Flux lines obtained with the FE reference model are depicted in Figure 5.33 - left. These lines show the presence of an area in the laminations where the fields weaken before changing direction. Values of the local fields obtained on a cut at $x = 0.275$ mm show a good agreement between the reference and the local mesoscale solutions (see Figure 5.34); small discrepancies are noticeable in regions with small eddy currents.

There are also discrepancies in the extreme layers as they do not have the same environment as the rest of laminations. We have observed the same behavior for $\boldsymbol{j}$ (see Figure 5.35): the macroscale (homogenized) solution is in good agreement with the reference solution.

For the hysteresis case, the analysis is similar to the nonlinear case. The reference and the computational $\boldsymbol{h}-\boldsymbol{b}$ hysteretic curves at point $x_1 = 1.65\,\text{mm}$ (Figure 5.39. Top), as well as the values of the local fields obtained on a cut at $x = 3.7\,\text{mm}$ (Figure 5.39 Middle and Bottom) are in excellent agreement.

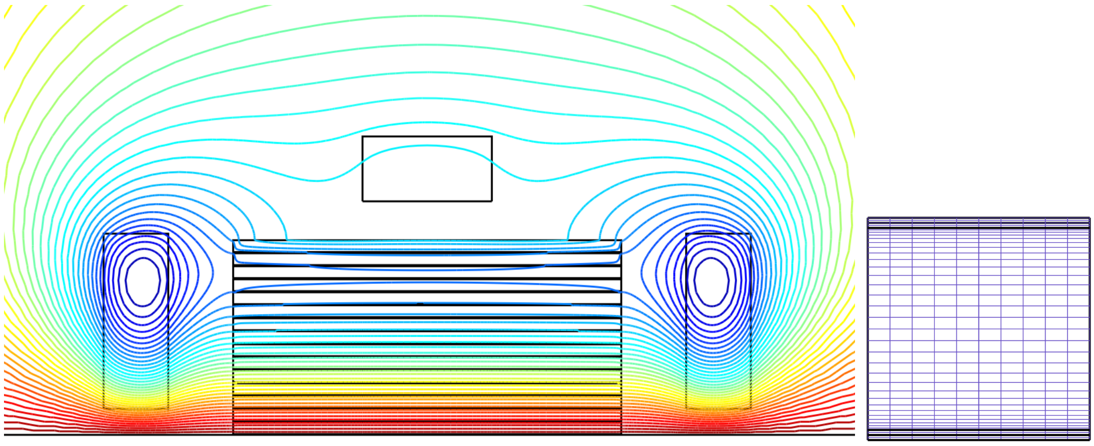

Figure 5.33: Left: geometry used for the validation of the model taking advantage of symmetry. Flux lines are depicted as well. Right: typical mesh used for mesoscale problems on a portion of laminations.

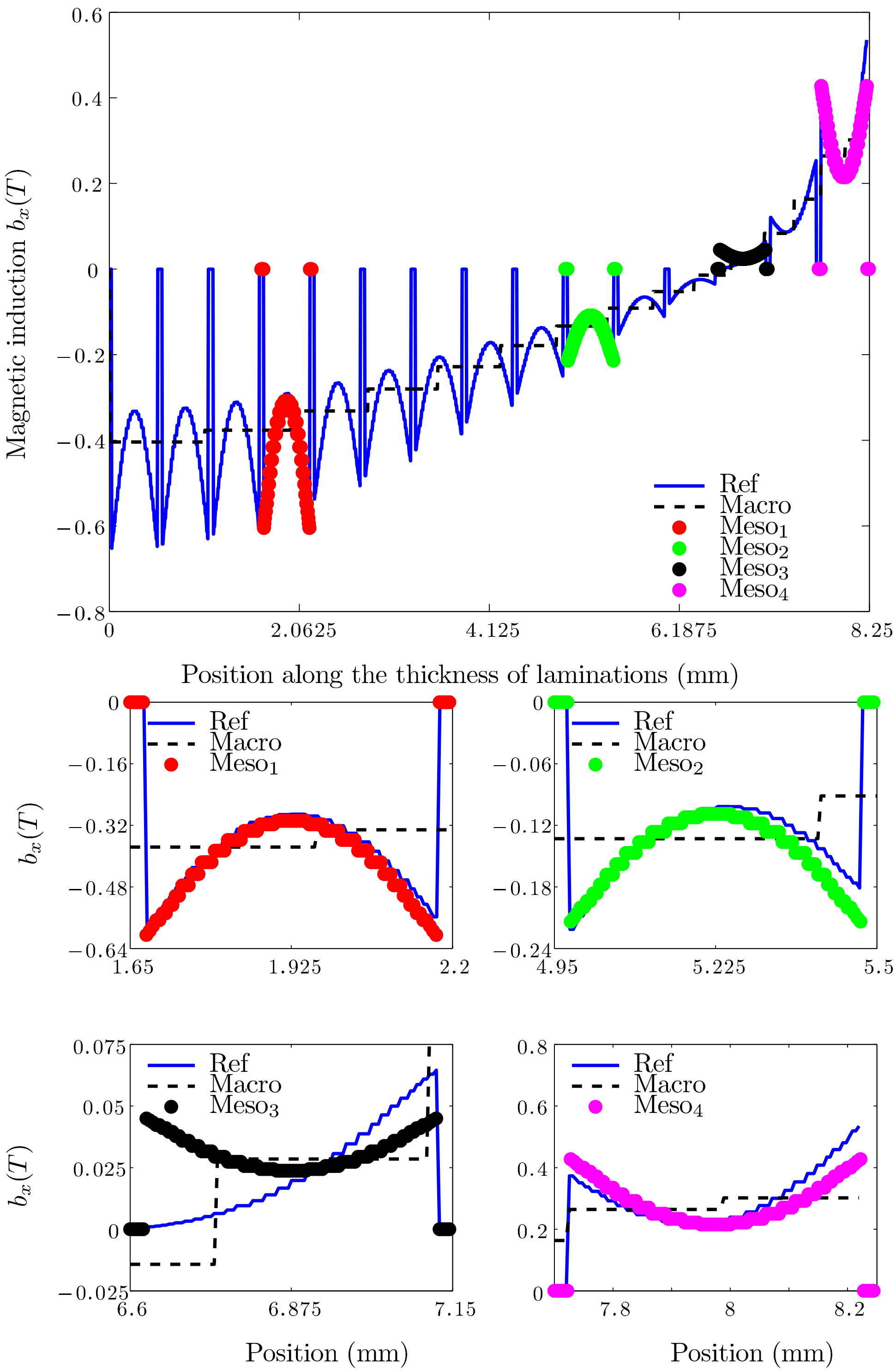

Figure 5.34: Lamination stack problem, $\boldsymbol{b}$-conform formulations, nonlinear case. Top: comparison of spatial cuts of the x-component of the magnetic induction $\boldsymbol{b}$ between the FE reference model (continuous line) and 4 mesoscale solutions defined in the intervals $[1.65, 2.195]$ mm, $[4.95, 5.5]$ mm, $[6.6, 7.15]$ mm, $[7.7, 8.225]$ mm along the y-axis. Bottom: Zoom around the mesoscale fields.

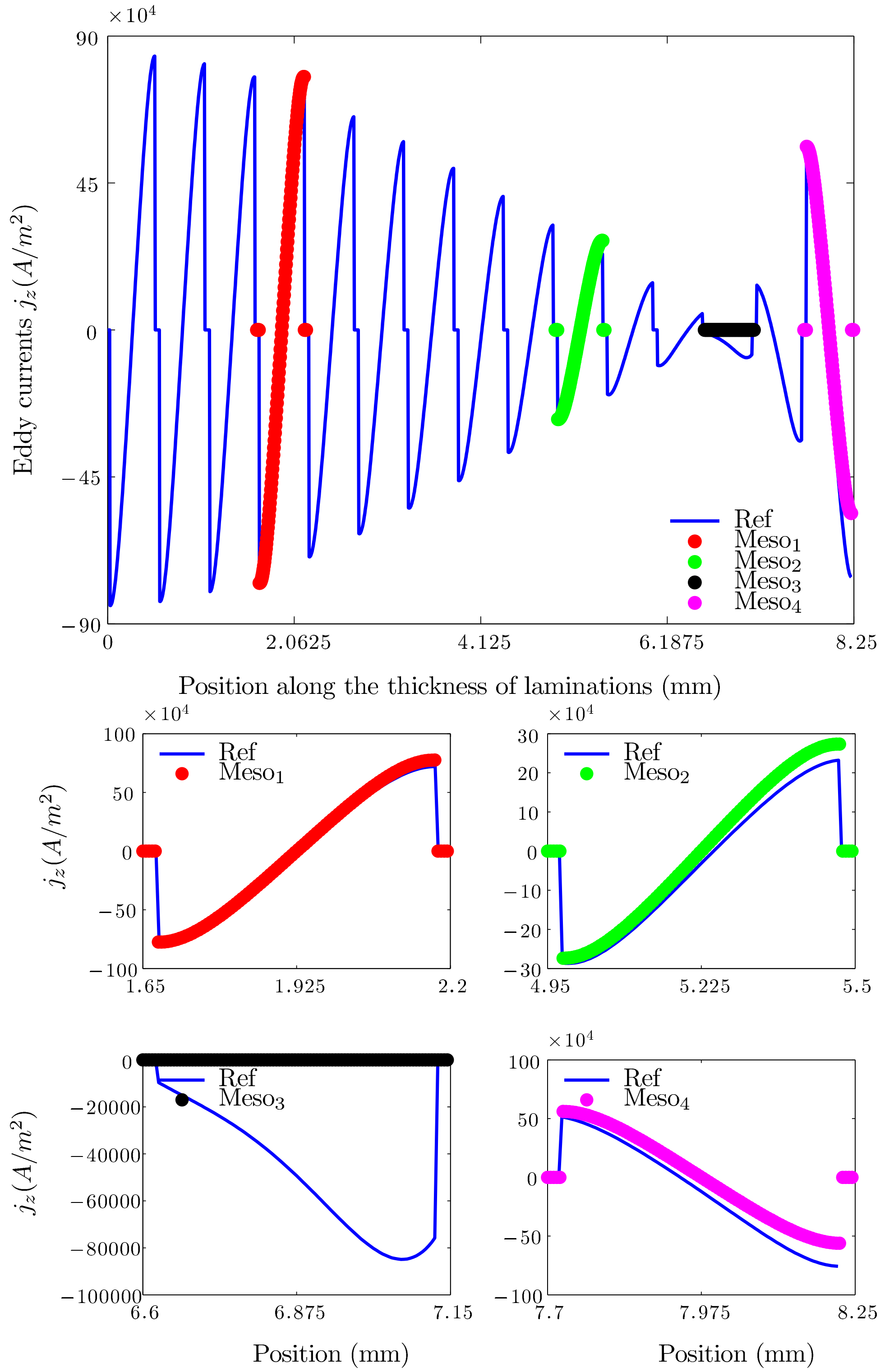

Figure 5.35: Lamination stack problem, $\boldsymbol{b}$-conform formulations, nonlinear case. Top: Comparison of spatial cuts of the x-component of the magnetic induction $\boldsymbol{b}$ between the FE reference model (continuous line) and 4 mesoscale solutions defined in the intervals $[1.65, 2.195]$ mm, $[4.95, 5.5]$ mm, $[6.6, 7.15]$ mm, $[7.7, 8.225]$ mm along the y-axis. Bottom: Zoom around the mesoscale fields.

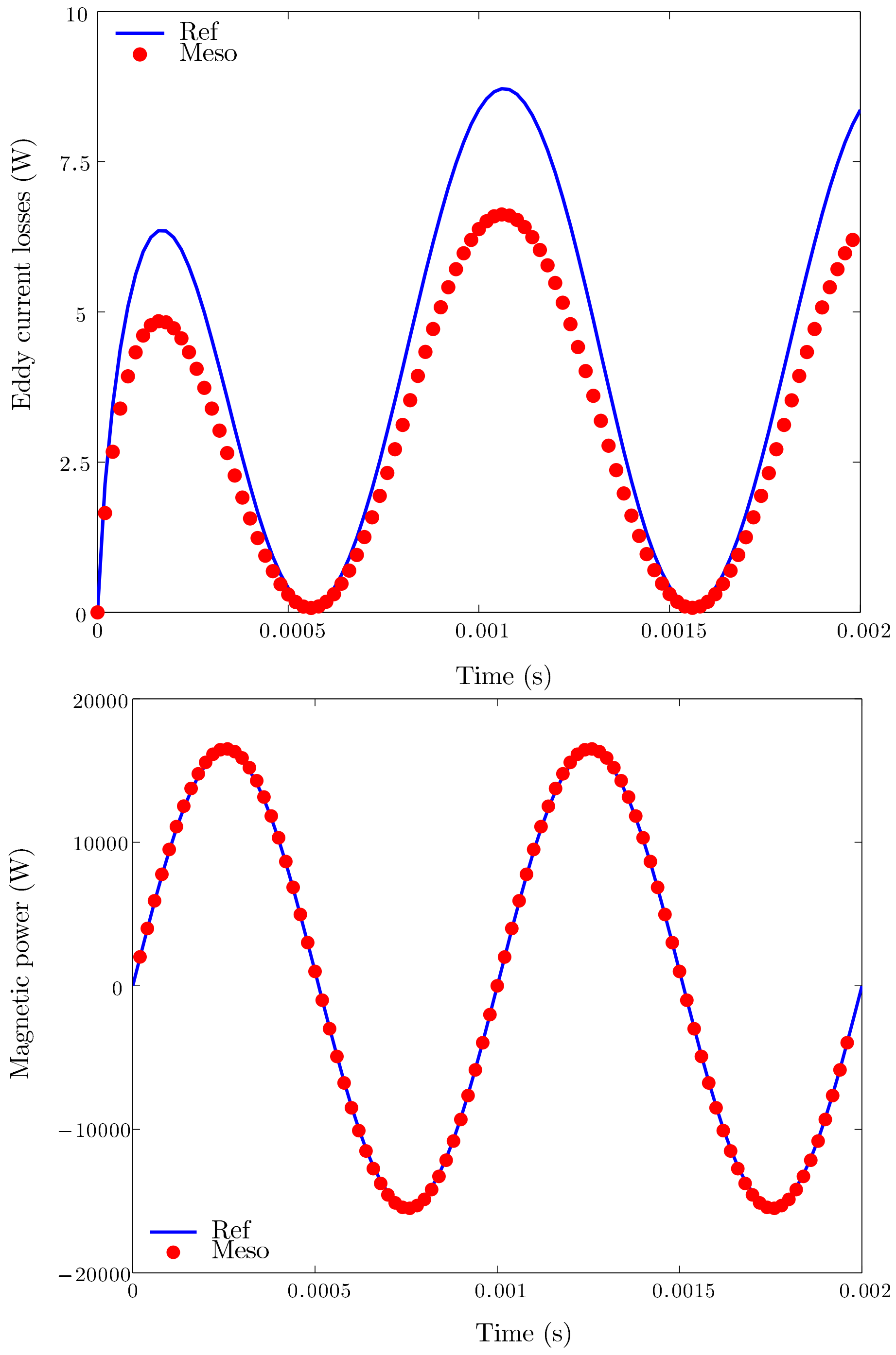

Figure 5.36: Lamination problem, $\boldsymbol{b}$-conform formulations, nonlinear case. Evolution of eddy currents losses and magnetic power as a function of time. Two frequencies are considered $\{ f = 500 \text{ Hz}\}$.

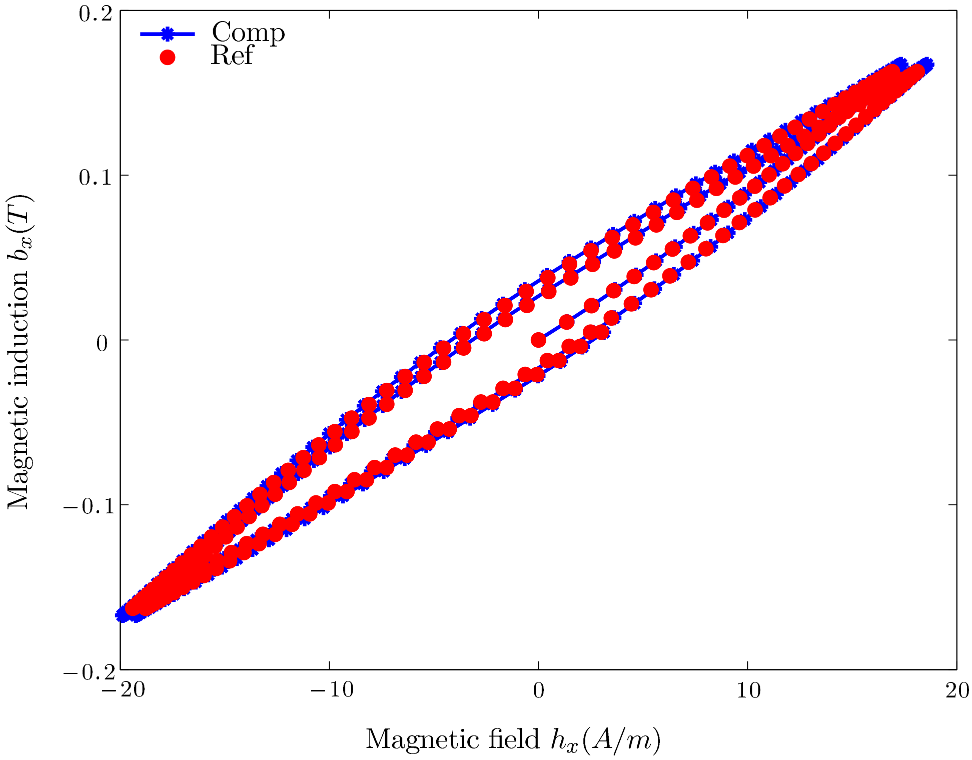

Figure 5.37: Lamination stack problem, $\boldsymbol{b}$-conform formulations, hysteresis case. Reference and computational $\boldsymbol{hb}$ hysteretic curves for a point centered around $(1.65, 3.7, 0)$ mm.

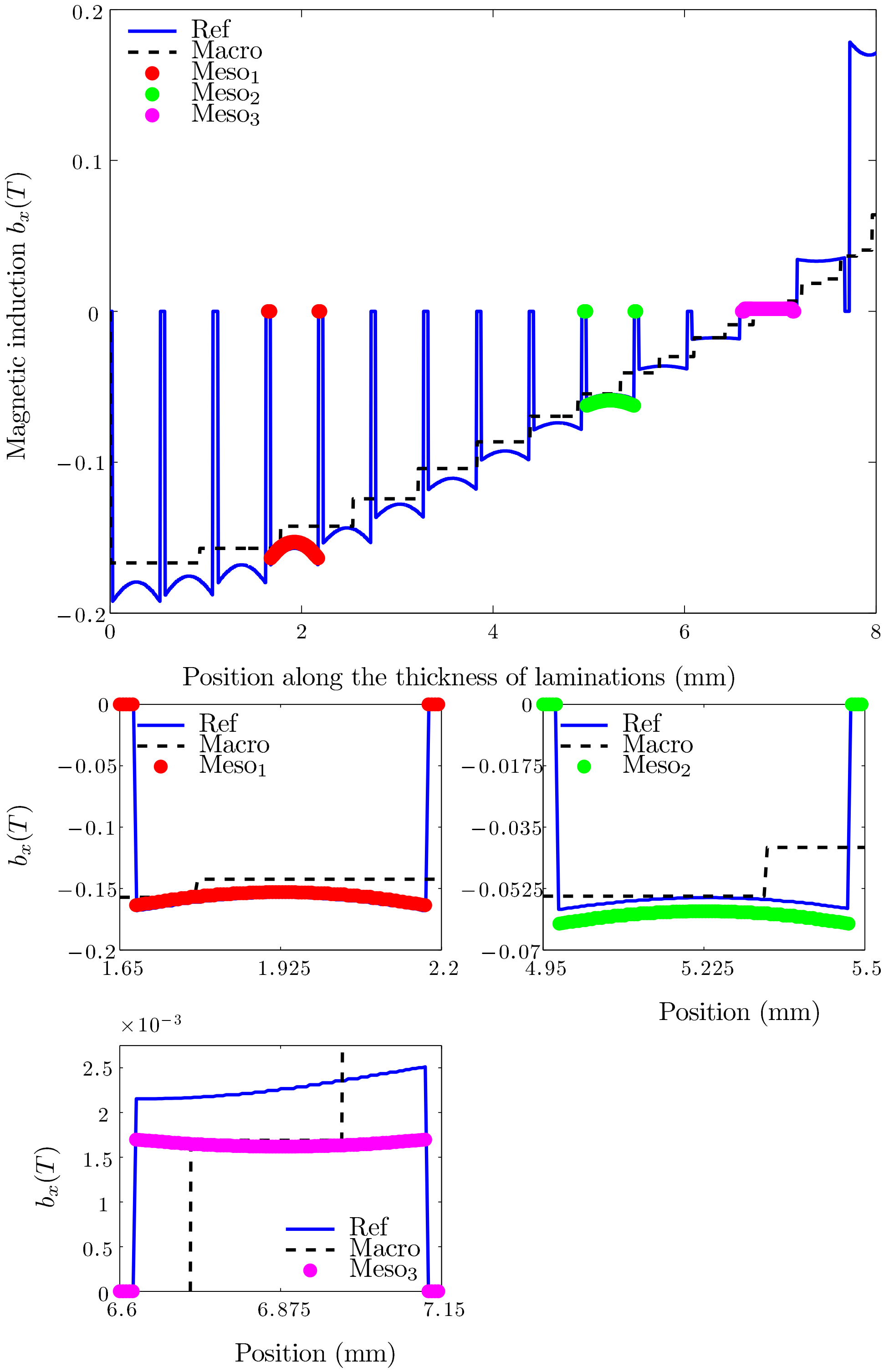

Figure 5.38: Lamination stack problem, $\boldsymbol{b}$-conform formulations, hysteresis case. Top: comparison of spatial cuts of the x-component of the magnetic induction $\boldsymbol{b}$ between the FE reference model (continuous line) and 4 mesoscale solutions defined in the intervals $[1.65, 2.195]$ mm, $[4.95, 5.5]$ mm, $[6.6, 7.15]$ mm, $[7.7, 8.225]$ mm along the line $x = 3.7$ mm. Bottom: zoom of the magnetic induction around the four mesoscale problems.

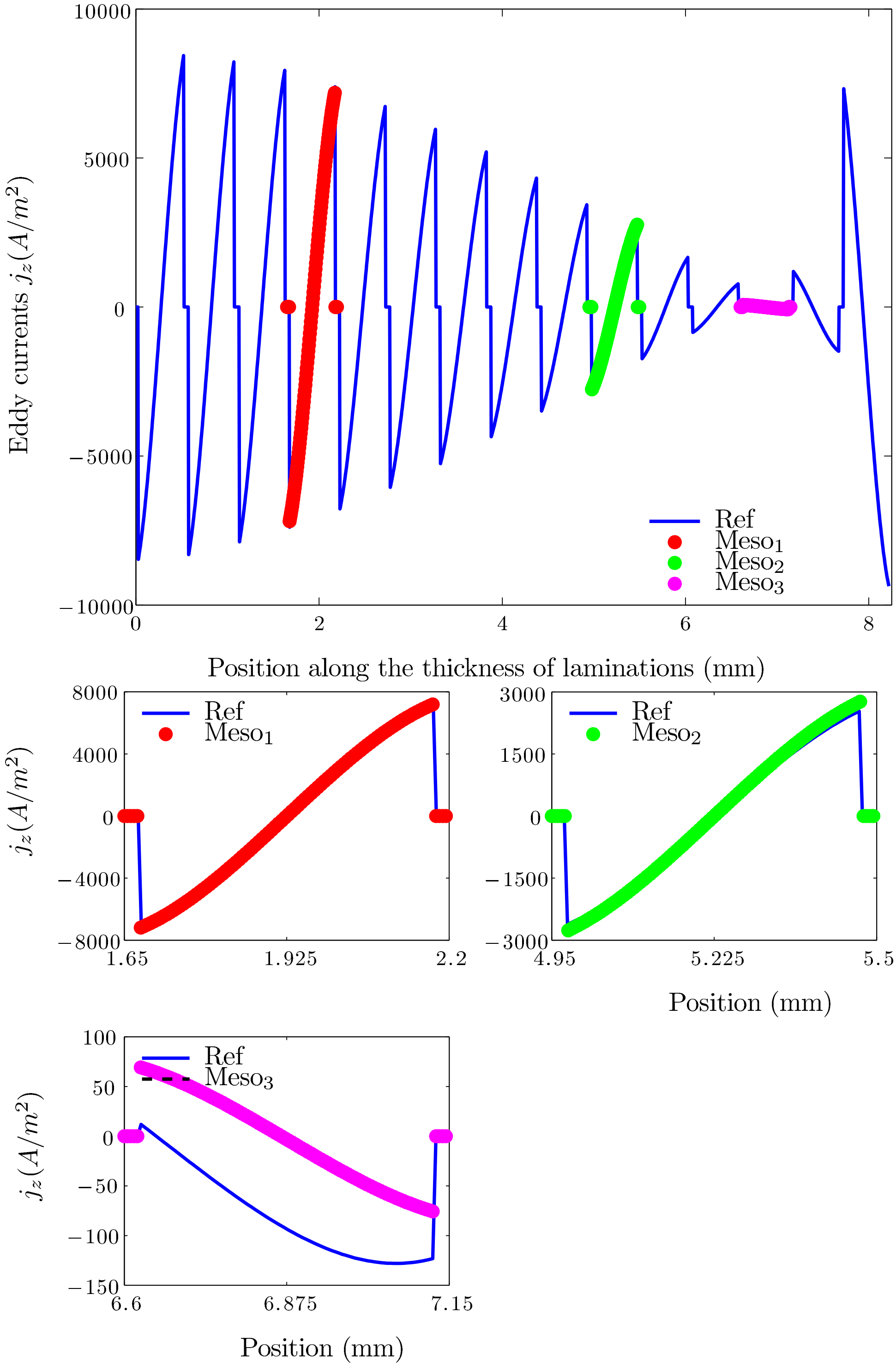

Figure 5.39: Lamination stack problem, $\boldsymbol{b}$-conform formulations, hysteresis case. Top: comparison of spatial cuts of the x-component of the eddy currents $\boldsymbol{j}$ between the FE reference model (continuous line) and 4 mesoscale solutions defined in the intervals $[1.65, 2.195]$ mm, $[4.95, 5.5]$ mm, $[6.6, 7.15]$ mm, $[7.7, 8.225]$ mm along the line $x = 3.7$ mm. Bottom: Zoom of the eddy currents around the two mesoscale problems.

5.3.3 Description of the problem for the $\boldsymbol{h}$-conform (magnetostatic) formulations

The problem used for testing $\boldsymbol{h}$-conform formulations in terms of the scalar potential (see section 4.4.5) is described in this section. The extension to the dynamic case which would allow to compute eddy current losses in laminations has not been implemented. However, it can be considered using formulations of section 4.4.

As an application example, we consider a laminated core (200 mm $\times$ 200 mm) consisting of 101 laminations (thickness $d_l = 1.78\,\text{mm}$) and 100 insulation layers (thickness $d_0 = 0.198\,\text{mm}$, $\mu_r = 1$), so that $\varepsilon \approx 0.01$. The filling factor is $\lambda = d_l/(d_l + d_0) = 0.9$. The material of the laminations is taken as:

– linear with $\mu_r = 10$;

– nonlinear with constitutive law:

$$\boldsymbol{\mathcal{B}}\Big(\boldsymbol{h}^{\varepsilon}(\boldsymbol{x})\Big) = 1000\,\mu_0 \frac{\boldsymbol{h}^{\varepsilon}(\boldsymbol{x})}{\Big(1 + ||\boldsymbol{h}^{\varepsilon}(\boldsymbol{x})||^2\Big)^{0.485}}\,. \tag{5.20}$$

We impose the following value of the magnetic potential 0A and 1A on the boundaries Γ_0 and Γ_1, respectively . This is equivalent to imposing a magnetic flux which comes in the laminated core through the boundary Γ_1 and goes out through the boundary Γ_0. The additional condition $\boldsymbol{n}\cdot\boldsymbol{b} = 0$ is implicitly imposed on $\Gamma\backslash\{\Gamma_0 \cup \Gamma_1\}$.

5.3.4 Results for the $\boldsymbol{h}$-conform formulations

The reference FE solution is obtained on an extremely fine mesh of the whole stack consisting of 15 layers of 10 quadrangles for each lamination and 5 layers of 10 quadrangles for each insulation layer (i.e. 20150 elements in total). The microproblems are solved in a square domain with either two or three laminations and insulation layers, i.e. cells with dimensions $3.96\times3.96\,\text{mm}^2$ or $5.94\times5.94\,\text{mm}^2$. Each lamination is discretized with 13 layers of 5 quadrangles and each insulation layer with 5 layers of 5 quadrangles.

In the linear case, we compare our HMM-based computational homogenization approach with both a classical homogenization technique [95, 96] and a fine reference finite element model. The coarse mesh used for both the macroscale level of the computational homogenization and the classical homogenization comprises 392 triangular elements. We consider 3 Gauss points per element, which leads to 1176 microproblems for each multiscale iteration.

For the classical homogenization, we consider a homogenized domain with an anisotropic constitutive law $\boldsymbol{b} = \mu\,\boldsymbol{h}$ and the permeability symmetric tensor $\mu = (\mu_{||}, \mu_{||}, \mu_{\perp}, 0, 0, 0)$ with diagonal elements that account for the parallel and perpendicular fluxes, i.e., $\mu_{||}$ and $\mu_{\perp}$ can be written as [95]:

$$\mu_{||} = \lambda\mu_l + (1-\lambda)\mu_0\,, \quad \frac{1}{\mu_{\perp}} = \frac{\lambda}{\mu_l} + \frac{1-\lambda}{\mu_0}\,, \tag{5.21}$$

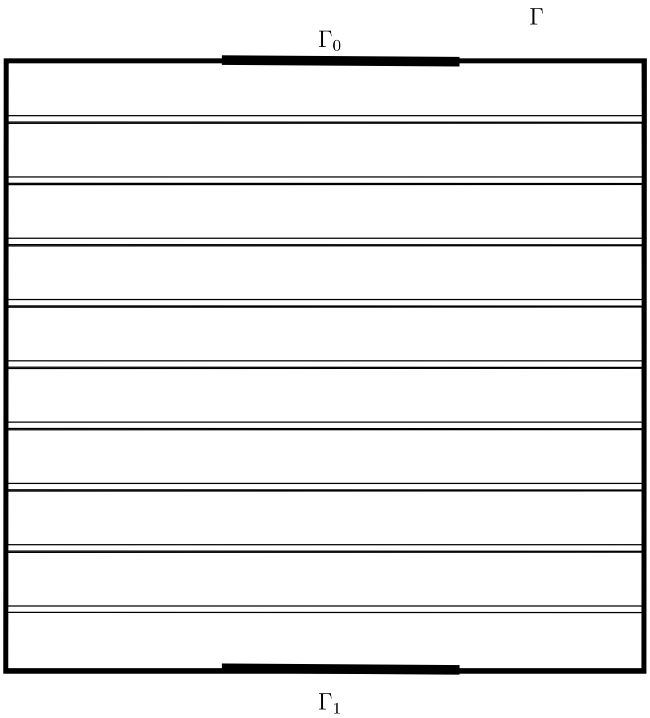

Figure 5.40: Lamination stack two-dimensional geometry used for the magnetostatic problem.

where μ_l is the permeability of the laminations.

Flux lines obtained with the FE reference model and the computational multiscale approach are depicted in Figure 5.41 (top-left and middle). The difference between the computational approach and the reference FE model is shown as well in 5.41 (top-right): it is in interval [1.3%–1.6%], with an average value equal to 0.299%. The magnetic flux density is also represented in 5.41 - (bottom). It is worth mentioning that the error in the vicinity of the surfaces with imposed ϕ is higher. A finer macroscale mesh would help enhancing this solution.

In Figure 5.42, we show the magnetic scalar potential along a cut at $x = 87.5$ mm. In this linear case, the classical homogenization gives an average result that follows the behaviour of the reference solution slightly better. However, the computational homogenization solution captures the variations of the solution of the mesoscale problem.

For the nonlinear case, the coarse mesh used for the macroscale level of the computational homogenization counts 160 triangular elements. We consider 3 Gauss points per element, what amounts to 480 microproblems for each multiscale nonlinear iteration.

In Figure 5.43, one can see the flux lines of the reference and multiscale solution together with the associated error map (top). A detail of the geometry and the coarse mesh is depicted as well. The relative error is in interval [-0.942,0.945]% with an average value of 0.0011%, which is better than in the linear case even though the mesh is coarser. This can be explained when realizing the very small variation of the flux lines with regard to a 1-D problem, i.e. flux lines are nearly horizontal: see Figure 5.44 - (bottom).

The magnetic scalar potential along a cut at $x = 1.666$ mm is represented in Figure 5.44 - (top). The computational homogenization solution fits perfectly well the average of the reference FE model. Besides, an excellent agreement is observed between the mesoscale solution and the reference.

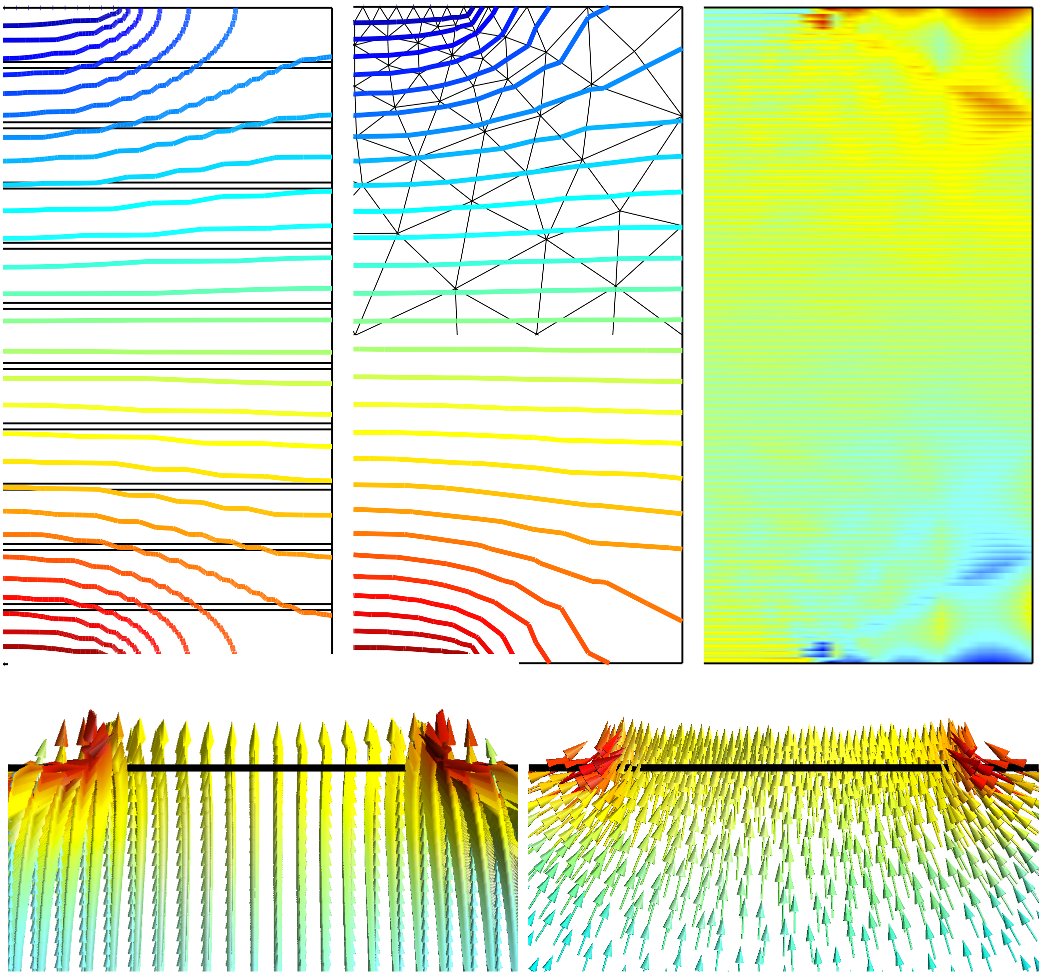

Figure 5.41: Lamination stack problem, $\boldsymbol{h}$-conform formulations, linear case. Top: flux lines for the FE reference model (left) and the computational multiscale method (middle); error map (right). Normalized scale. Representation of the fine scale geometry (11 laminations instead of 101) and coarse mesh. Bottom: zoom of the magnetic flux density near the top with imposed ϕ for the FE reference (left) and the computational multiscale models (right) [148].

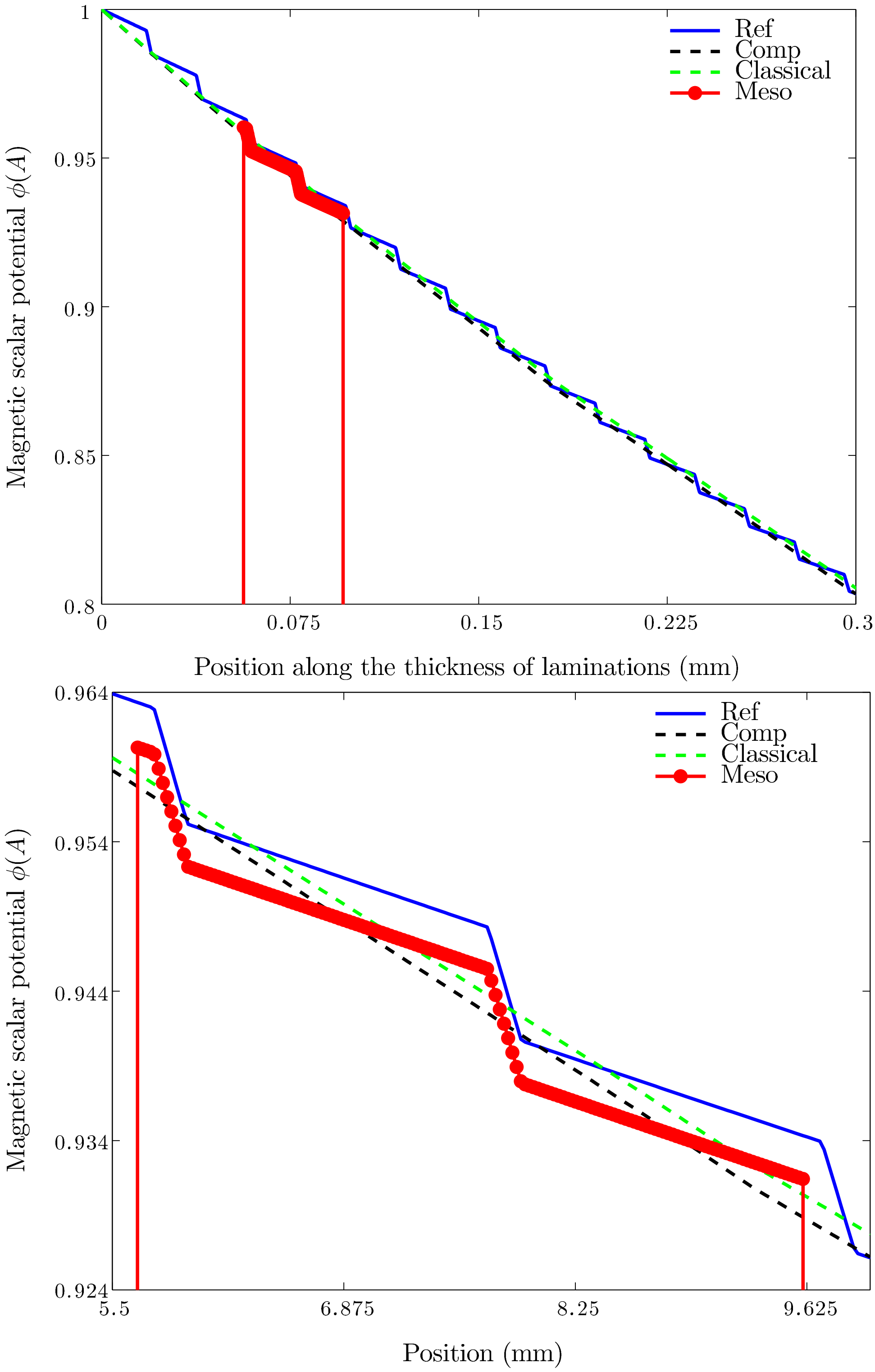

Figure 5.42: Lamination stack problem, $\boldsymbol{h}$-conform formulations, linear case. Top: magnetic scalar potential at $x = 87.5$ mm in the 3.96×3.96 mm^2 cell (2 laminations and 2 insulation layers). Bottom: zoom between 5.5 mm and 10 mm [148].

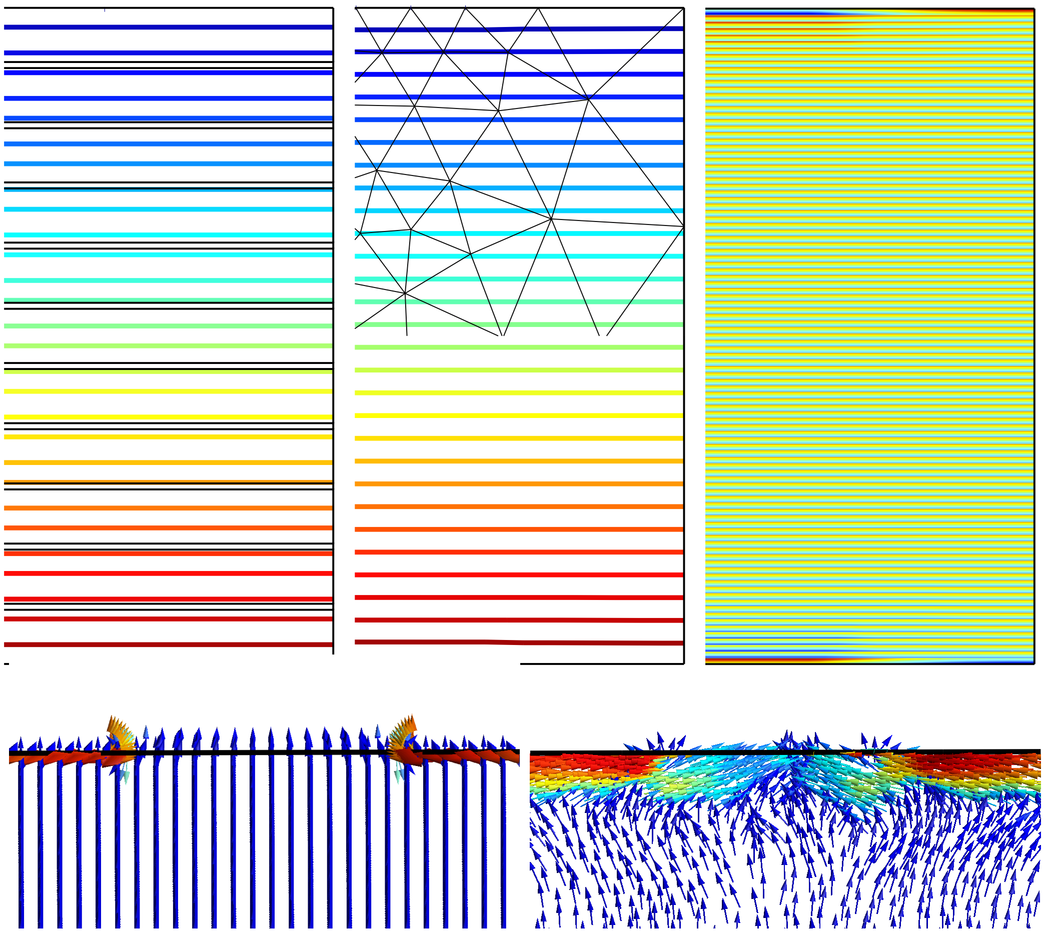

Figure 5.43: Lamination stack problem, $\boldsymbol{h}$-conform formulations, nonlinear case. Top: flux lines for the FE reference model (left) and the computational multiscale method (middle); error map (right). Normalized scale. Representation of the fine scale geometry (11 laminations instead of 101) and coarse mesh. Bottom: zoom of the magnetic flux density near the top with imposed ϕ for the FE reference (left) and the computational multiscale models (right) [148].

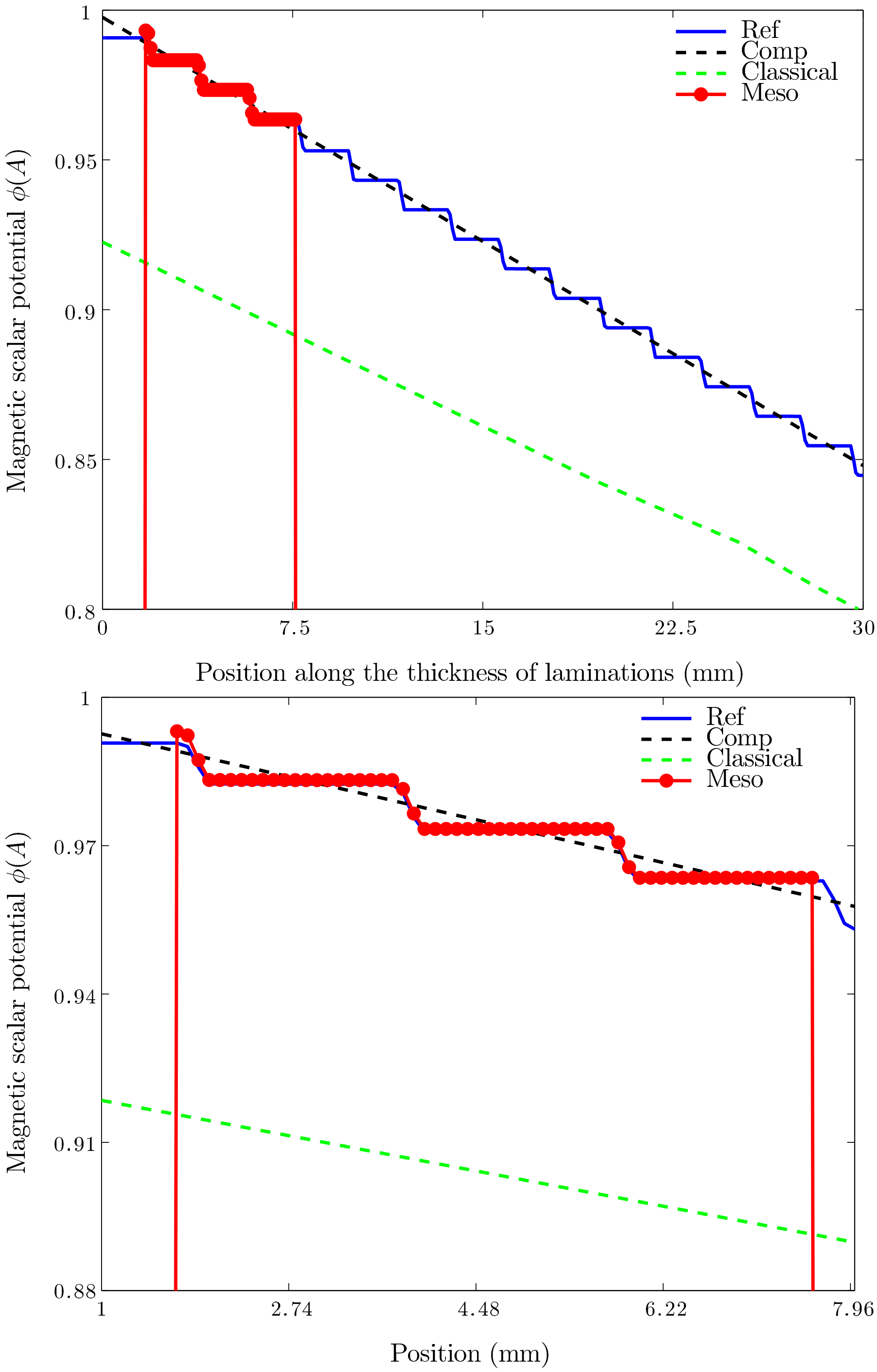

Figure 5.44: Lamination stack problem, $\boldsymbol{h}$-conform formulations, nonlinear case. Top: magnetic scalar potential at $x = 16.66$ mm in the 5.95×5.95 mm^2 mesoscale domain (3 laminations and 3 insulation layers). Bottom: zoom between 1.8 mm and 7.8 mm [148].

Chapter 6

General conclusions

In this thesis we have developed a computational multiscale method to solve nonlinear, possibly hysteretic magnetoquasistatic problems on multiscale domains (e.g. composite materials, lamination stacks, etc.). The resulting method is inspired by the HMM approach [1–4, 6, 7, 43, 67–69, 71–73, 75]. The fine-scale, computationally expensive problem is replaced by a (computationally cheaper) macroscale problem defined on a coarse mesh and many mesoscale problems defined on cells around numerical quadrature points of the macroscale domain and used for recovering the missing information (e.g. the homogenized constitutive laws, the homogenized global quantities such as the eddy currents losses, etc.) at the macroscale level.

In order to construct the computational multiscale model, we combine theoretical results from two-scale convergence theory [11, 120, 141, 143, 196, 201], periodic unfolding [31, 45–47, 130, 197] and asymptotic homogenization [20]. The two-scale convergence and periodic unfolding methods are used for deriving the partial differential equations governing fields at both the macroscale and the mesoscale levels, valid in the nonlinear regime and in the presence of **curl** differential operators. Asymptotic homogenization is used for defining a mesoscale problem in the case of linear constitutive laws (e.g. the linear electric conductivity law).

Although this theoretical foundation is only valid in the case of linear and nonlinear problems governed by a maximal monotone operator, in practice, the resulting numerical multiscale scheme has been successfully applied to general magnetoquasistatic problems also exhibiting memory effects (hysteresis). The numerical tests were performed for magnetostatic and magnetodynamic problems, using both $\boldsymbol{b}$-conform and $\boldsymbol{h}$-conform formulations. For $\boldsymbol{b}$-conform formulations, an excellent agreement has been obtained between the reference solutions (computed using a brute force approach) and the computational (mesoscale) solutions. Small differences are observed near the boundary of the computational domain as the cell problems defined near the boundary are not immersed in a periodic environment. The eddy current losses are also accurately evaluated. The error on these losses increases as a function of the frequency. For $\boldsymbol{h}$-conform formulations, a good agreement was also observed but bigger errors are observed as compared to the $\boldsymbol{b}$-conform formulations. This may result from the type of the imposed source (which is localized in the $\boldsymbol{h}$-conform formulations).

Overall the proposed computational multiscale method fulfills the original goals of the thesis: it allows to solve complex multiscale magnetoquasistatic problems, including the challenging computation of local fields at the mesoscale and the accurate evaluation of electromagnetic losses. Compared to mean-field homogenization [49, 50], the proposed technique naturally handles strongly nonlinear or hysteretic materials and complex periodic mesoscale geometries, in addition to the computation of local electromagnetic fields. These last two advantages also distinguish the newly developed method from ad-hoc homogenization for lamination stacks [95–97], and the last one distinguishes it from approaches where nonlinear constitutive laws are pre-computed representative volume elements [34]. The main disadvantage of our method is its higher computational cost. However, since all the mesoscale problems are independent, it is perfectly suited for modern massively parallel computers, and we thus believe that it has a lot of potential, even compared to brute force approaches, which do not scale well.

Perspectives

This work opens up various perspectives for both short term improvements and for longer term developments. Possible short term improvements include:

- the improvement of results for cells located near the boundary of the computational domain. This requires the modification of the definition of computational mesoscale problems for these cells allowing to account for their non-periodic environment. An alternative solution would be to couple the computational homogenization method with subproblem methods [60] for correcting mesoscale solutions near the boundary;
- the three-dimensional implementation of the multiscale model;
- the hybridization of the developed model with computationally cheaper homogenization techniques, which could be used in non-critical regions (without significant hysteretic losses or fields values);
- the development and the inclusion of the variational model for hysteresis [86] in the mesoscale problem;
- the consideration of non-periodic representative volume elements. This could be done by weakly imposing periodic boundary condition for the mesoscale problem as in [146].

Longer term perspectives include:

- the consideration of representative volume elements with a mesoscale stochastic distribution of phases. This is important in order to accurately model the behaviour of random composites materials. The use of stochastic homogenization [20, 44, 52, 106, 144, 145, 157] or the application of a statistical method to the periodic homogenization [13, 49, 50] would allow to account for this randomness of phase distribution.

- the application of the computational homogenization for multiphysical problems. The coupling may involve problems defined between the macroscale and the mesoscale levels with different physical couplings (electromechanical, electro-thermal, ...) or electromagnetic models involving different scales and physics (e.g. the study of hysteresis by upscaling relevant information from Weiss domains and Bloch walls).
- the extension to high frequency, nonlinear electromagnetic problems.

Appendix A

Convex analysis

Details about most of the mathematical concepts recalled in this appendix can be found in [30, 40, 83, 85, 93, 173].

A.1 Convexity, lower semi-continuity

We denote by $\mathcal{V}$ any vector space and $\mathcal{V}'$ its dual. Let also A be any given set. The *set A is said to be convex* if:

$$tu + (1-t)v \in A \quad \forall u, v \in A \text{ and } t \in [0,1]. \tag{A.1}$$

Vector spaces fulfill this condition (thanks to the linearity property) and are therefore convex sets.

Herein, we introduce the notions of convex and lower semi-continuous functionals. Indeed, these notions can be used to formulate some partial differential equations as a minimization problem of some functionals (the so-called *Euler-Lagrange* equations of a minimization problem).

We define the functional $\varphi : \mathcal{V} \to \mathbb{R} \cup \{+\infty\}$. The *epigraph* of φ (see Figure A.1) is the set:

$$\text{epi } \varphi = \Big\{(x, \lambda) \in \mathcal{V} \times \mathbb{R} : \varphi(x) \leq \lambda\Big\}. \tag{A.2}$$

A functional $\varphi : \mathcal{V} \to \mathbb{R} \cup \{+\infty\}$ is said to be *convex* if:

$$\varphi(tu + (1-t)v) \leq t\varphi(u) + (1-t)\varphi(v) \quad \forall u, v \in \mathcal{V} \text{ and } t \in [0,1]. \tag{A.3}$$

It can then be shown [40] that φ is convex if and only if epi φ is convex in $\mathcal{V} \times \mathbb{R}$ (see Figure A.1).

Let the functional $\varphi : \mathcal{Z} \to \mathbb{R} \cup \{+\infty\}$ be defined from the topological space $\mathcal{Z}$. The functional φ is *lower semi-continuous* if and only if epi φ is closed in $\mathcal{V} \times \mathbb{R}$. For lower semi-continuous functions φ:

$$u_n \rightharpoonup u \quad \text{in } \mathcal{V} \quad \Rightarrow \quad \varphi(u) \leq \liminf_n \varphi(u_n). \tag{A.4}$$

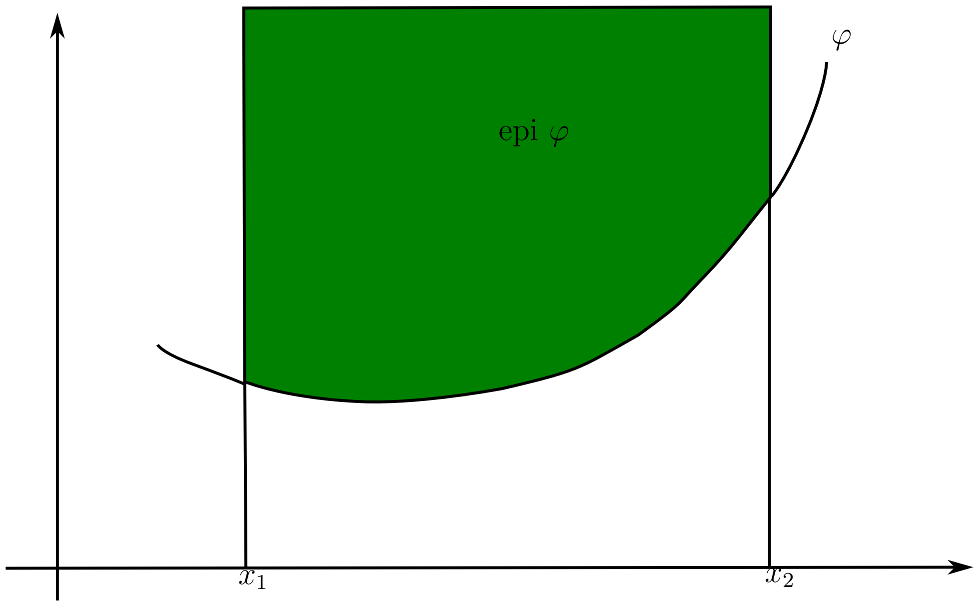

Figure A.1: Epigraph of a function.

A.2 Fenchel transformation, subdifferentiability

For any proper functional φ (proper meaning that domain of the functional φ is non-empty), we define the *convex conjuguate* of φ as:

$$\varphi^* : \quad \mathcal{V}' \to \mathbb{R} \cup \{+\infty\} \tag{A.5}$$

$$f \mapsto \varphi^*(f) = \operatorname*{Sup}_{u \in \mathcal{V}} \Big\{ \Big\langle f, u \Big\rangle_{\mathcal{V} \times \mathcal{V}'} - \varphi(u) \Big\} = - \inf_{u \in \mathcal{V}} \Big\{ \varphi(u) - \Big\langle f, u \Big\rangle_{\mathcal{V} \times \mathcal{V}'} \Big\} \tag{A.6}$$

The notation $\Big\langle \cdot, \cdot \Big\rangle_{\mathcal{V} \times \mathcal{V}'}$ denotes the duality pairing between $\mathcal{V}'$ and $\mathcal{V}$. Later, we replace this notation by the short notation $\Big\langle \cdot, \cdot \Big\rangle$ if there is no ambiguity of notation. From the definition of φ^*, it can easily be shown that the following inequality:

$$\Phi(u, f) = \varphi(u) + \varphi^*(f) - \Big\langle f, u \Big\rangle \geq 0 \tag{A.7}$$

always holds for all $(u, f) \in \mathcal{V} \times \mathcal{V}'$.

For the proper functional $\varphi : \mathcal{V} \to \mathbb{R} \cup \{+\infty\}$, we also define the *subdifferential mapping*:

$$\partial\varphi : \quad \mathcal{V} \to 2^{\mathcal{V}'} \tag{A.8}$$

$$u \mapsto \partial\varphi(u) = \Big\{ v \in \mathcal{V}' : \varphi(w) \geq \varphi(u) + \Big\langle v, w - u \Big\rangle \;\; \forall w \in \mathrm{dom}(\varphi) \Big\} \tag{A.9}$$

where $2^{\mathcal{V}'}$ is the power set of $\mathcal{V}'$ (i.e.: the set of all subsets of $\mathcal{V}'$)

The value of the subdifferential for a differentiable functional (in the Fréchet or the Gateau sense) at a given point is unique and equal to the gradient of the

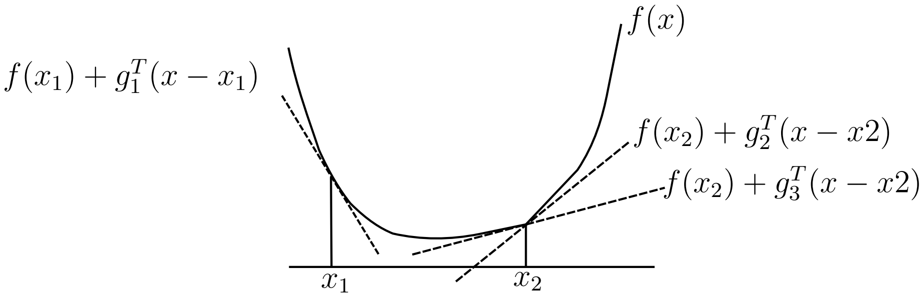

Figure A.2: The subdifferential of a function f. The function is differentiable in x_1 and has only one gradient. In x_2, the function is not differentiable and the subdifferential is multivalued in that point.

functional at the same point. In general, the gradient of the functional may not exist in the classical sense but the subgradient may exist and possibly be multivalued ((e.g. the mapping f in Figure A.2 is non-differentiable in x_2 but it is subdifferentiable and all the values of the subgradient comprised between g_3 and g_2 belong to the subdifferential mapping of f at x_2).

A.3 Monotonicity

We also define the notion of a maximal monotone mapping. Indeed, when combined with adequate coercivity and boundedness conditions this notion can be used for proving the existence and uniqueness of solutions of nonlinear partial differential equations [40, 83, 85].

We denote by $\mathcal{A}$, a (possibly multivalued) mapping:

$$\mathcal{A} : \mathcal{V} \to 2^{\mathcal{V}'} \text{ with } \mathrm{dom}(\mathcal{A}) \in \mathcal{V}. \tag{A.10}$$

$\mathcal{A}$ is said to be a *monotone* mapping if:

$$\left\langle f - g, u - v \right\rangle \;\geq\; 0 \;\; \forall u, v \in \mathcal{V} : f \in \mathcal{A}u, g \in \mathcal{A}v. \tag{A.11}$$

The notation $f \in \mathcal{A}u$ is used to emphasize that f is one of many values that the operator $\mathcal{A}$ can take in u. The operator $\mathcal{A}$ is said to be a *maximal monotone* mapping if in addition there is no other monotone mapping whose graph includes that of $\mathcal{A}$. This means that the application of mapping $\mathcal{A}$ spans the greatest subspace of $2^{\mathcal{V}'}$.

The property of monotonicity is necessary for having the uniqueness of the solution while the property of maximality allows to get the existence of the solutions for partial differential equations governed by (nonlinear) maximal monotone operators [10, 40, 85, 203]. There also exists a connection between maximal monotone mapping and convex lower semi-continuous functional. Indeed, It has been shown that any maximal monotone mapping can be derived as a subdifferential of a convex lower semi-continuous functional [174].

A.4 Example

Assuming the following nonlinear mapping:

$$\boldsymbol{\mathcal{B}}: \quad \mathbb{R}^3 \to \mathbb{R}^3 \tag{A.12}$$

$$\boldsymbol{h} \mapsto \boldsymbol{b} = \boldsymbol{\mathcal{B}}(\boldsymbol{h}), \tag{A.13}$$

used for representing the nonlinear magnetic material law. We can construct the functional

$$\varphi(\boldsymbol{h}) = \int_0^{\boldsymbol{h}} \boldsymbol{\mathcal{B}}(\boldsymbol{h}^0)\mathrm{d}\boldsymbol{h}^0, \tag{A.14}$$

such that $\partial\varphi(\boldsymbol{h}) = \boldsymbol{\mathcal{B}}(\boldsymbol{h})$.

Assuming that φ is strictly convex (i.e. $\partial\boldsymbol{\mathcal{B}}/\partial\boldsymbol{h}$ is definite positive), smooth and bounded below (so that φ is lower semi-continuous [85]), then $\boldsymbol{\mathcal{B}}$ is single-valued. Using the Fenchel transformation (which is a generalization of Legendre transformation), we can define the convex conjuguate:

$$\varphi^*(\boldsymbol{b}) = \underset{\boldsymbol{h}\in\mathbb{R}^3}{\mathrm{Sup}} \Big\{\Big\langle \boldsymbol{b},\boldsymbol{h}\Big\rangle - \varphi(\boldsymbol{h})\Big\} = -\underset{\boldsymbol{h}\in\mathbb{R}^3}{\inf}\Big\{\varphi(\boldsymbol{h}) - \Big\langle \boldsymbol{b},\boldsymbol{h}\Big\rangle\Big\}. \tag{A.15}$$

Assuming that φ is differentiable, the infimum in (A.15) is attained for the value $\boldsymbol{h}_{inf}$ such that

$$\boldsymbol{b} - \partial_{\boldsymbol{h}}\varphi(\boldsymbol{h}_{inf}) = \boldsymbol{0}, \tag{A.16}$$

thus yielding $\boldsymbol{b} - \boldsymbol{\mathcal{B}}(\boldsymbol{h}_{inf}) = \boldsymbol{0}$.

If the mapping $\boldsymbol{\mathcal{B}}$ is inversible (i.e. $\boldsymbol{\mathcal{B}}^{-1} := \boldsymbol{\mathcal{H}}$ exists), then $\boldsymbol{h}_{inf} = \boldsymbol{\mathcal{H}}(\boldsymbol{b})$ and therefore the convex conjugate functional (A.15) becomes:

$$\varphi^*(\boldsymbol{b}) = \Big\langle \boldsymbol{b},\boldsymbol{\mathcal{H}}(\boldsymbol{b})\Big\rangle - \int_{\boldsymbol{0}}^{\boldsymbol{\mathcal{H}}(\boldsymbol{b})} \boldsymbol{\mathcal{B}}(\boldsymbol{h}^0)\mathrm{d}\boldsymbol{h}^0. \tag{A.17}$$

To compute this integral, we define the change of variable $\boldsymbol{h}^0 = \boldsymbol{\mathcal{H}}(\boldsymbol{b}^0)$. The differential are related by $\mathrm{d}\boldsymbol{h}^0 = (\partial\boldsymbol{\mathcal{H}}/\partial\boldsymbol{b}^0)\mathrm{d}\boldsymbol{b}^0$ and (A.17) becomes:

$$\varphi^*(\boldsymbol{b}) = \Big\langle \boldsymbol{b},\boldsymbol{\mathcal{H}}(\boldsymbol{b})\Big\rangle - \int_{\boldsymbol{0}}^{\boldsymbol{b}} \boldsymbol{b}^0\frac{\partial\boldsymbol{\mathcal{H}}}{\partial\boldsymbol{b}^0}\mathrm{d}\boldsymbol{b}^0 = \int_{\boldsymbol{0}}^{\boldsymbol{b}}\Big(\frac{\mathrm{d}}{\mathrm{d}\boldsymbol{b}^0}(\boldsymbol{b}^0\boldsymbol{\mathcal{H}}(\boldsymbol{b}^0)) - \boldsymbol{b}^0\frac{\partial\boldsymbol{\mathcal{H}}}{\partial\boldsymbol{b}^0}\Big)\mathrm{d}\boldsymbol{b}^0 =$$

$$\int_{\boldsymbol{0}}^{\boldsymbol{b}}\Big(\boldsymbol{\mathcal{H}}(\boldsymbol{b}^0)\frac{\partial\boldsymbol{b}^0}{\partial\boldsymbol{b}^0}\Big)\mathrm{d}\boldsymbol{b}^0 = \int_{\boldsymbol{0}}^{\boldsymbol{b}}\boldsymbol{\mathcal{H}}(\boldsymbol{b}^0)\mathrm{d}\boldsymbol{b}^0. \tag{A.18}$$

From the definition of $\varphi^*(\boldsymbol{b})$ the following inequality:

$$\int_{\boldsymbol{0}}^{\boldsymbol{h}} \boldsymbol{\mathcal{B}}(\boldsymbol{h}^0)\mathrm{d}\boldsymbol{h}^0 + \int_{\boldsymbol{0}}^{\boldsymbol{b}}\boldsymbol{\mathcal{H}}(\boldsymbol{b}^0)\mathrm{d}\boldsymbol{b}^0 - \Big\langle \boldsymbol{b},\boldsymbol{h}\Big\rangle \geq 0, \tag{A.19}$$

always holds. Therefore, there exists a representative functional Φ defined as:

$$\Phi(\boldsymbol{h},\boldsymbol{b}) = \int_\Omega\Big(\int_{\boldsymbol{0}}^{\boldsymbol{h}} \boldsymbol{\mathcal{B}}(\boldsymbol{h}^0)\mathrm{d}\boldsymbol{h}^0 + \int_{\boldsymbol{0}}^{\boldsymbol{b}}\boldsymbol{\mathcal{H}}(\boldsymbol{b}^0)\mathrm{d}\boldsymbol{b}^0 - \Big\langle \boldsymbol{b},\boldsymbol{h}\Big\rangle\Big)\mathrm{d}\boldsymbol{x} \tag{A.20}$$

for which the minimization yields the relations $\boldsymbol{b} = \boldsymbol{\mathcal{B}}(\boldsymbol{h})$ and $\boldsymbol{h} = \boldsymbol{\mathcal{H}}(\boldsymbol{b})$ for all $\boldsymbol{x} \in \Omega$. In addition, the functional $\Phi(\boldsymbol{h}, \boldsymbol{b})$ is equal to zero if and only if $\boldsymbol{b}(\boldsymbol{x}) = \boldsymbol{\mathcal{B}}(\boldsymbol{h}(\boldsymbol{x}), \boldsymbol{x}) \in \partial\varphi(\boldsymbol{h}(\boldsymbol{x}), \boldsymbol{x})$ and $\boldsymbol{h}(\boldsymbol{x}) = \boldsymbol{\mathcal{H}}(\boldsymbol{b}(\boldsymbol{x}), \boldsymbol{x}) \in \partial\varphi^*(\boldsymbol{b}(\boldsymbol{x}), \boldsymbol{x})$.

The last term of (A.20) can be written as:

$$\int_\Omega (\boldsymbol{b} \cdot \boldsymbol{h}) \mathrm{d}\boldsymbol{x}. \tag{A.21}$$

With a different choice of function spaces for the fields $\boldsymbol{b}$ and $\boldsymbol{h}$, it can be shown that the minimization of the functional (A.20) leads to the magnetostatic equations. Indeed, the minimization problem:

$$\Phi(\boldsymbol{h}, \boldsymbol{b}) = \inf_{\boldsymbol{h}' \in \boldsymbol{H}(\mathbf{curl}; \Omega), \boldsymbol{b}' \in \boldsymbol{H}(\mathrm{div}; \Omega)} \Phi(\boldsymbol{h}', \boldsymbol{b}'), \tag{A.22}$$

corresponds to the Euler–Lagrange equations of the magnetostatic problem:

$$\mathbf{curl}\, \boldsymbol{h} = \mathbf{0}, \tag{A.23}$$
$$\mathrm{div}\, \boldsymbol{b} = 0, \tag{A.24}$$
$$\boldsymbol{b}(\boldsymbol{x}) \in \partial\varphi(\boldsymbol{h}(\boldsymbol{x}), \boldsymbol{x}), \tag{A.25}$$
$$\boldsymbol{h}(\boldsymbol{x}) \in \partial\varphi^*(\boldsymbol{b}(\boldsymbol{x}), \boldsymbol{x}). \tag{A.26}$$

All the derivatives involved in (A.26) should be understood in the distribution sense

The existence of the solution of the magnetoquasistatic problem (3.3)–(3.7) in $\mathbb{R}^3$ has already been studied by Visintin [196, 201]. Under some assumptions on the mappings $\boldsymbol{\mathcal{B}}$ and $\boldsymbol{\mathcal{J}}$ (e.g. maximal monotone mappings) and the regularity of the data of the problem (e.g. the initial conditions), it has been shown [196, 201] that (3.3)–(3.7) has a unique and bounded solution $\boldsymbol{h}^\varepsilon, \boldsymbol{b}^\varepsilon, \boldsymbol{e}^\varepsilon$ and $\boldsymbol{j}^\varepsilon$ such that:

$$\boldsymbol{h}^\varepsilon \in L^\infty(0, T; \boldsymbol{L}^2(\mathbb{R}^3)) \cap L^2(0, T; \boldsymbol{H}(\mathbf{curl}; \Omega_c)) \cap H^{-1}(0, T; \boldsymbol{H}(\mathbf{curl}; \mathbb{R}^3)), \tag{A.27}$$
$$\boldsymbol{b}^\varepsilon \in L^\infty(0, T; \boldsymbol{L}^2(\mathbb{R}^3)) \cap H^1(0, T; (\boldsymbol{H}(\mathbf{curl}; \mathbb{R}^3))'), \tag{A.28}$$
$$\boldsymbol{e}^\varepsilon \in L^\infty(0, T; \boldsymbol{L}^2(\mathbb{R}^3 \setminus \Omega_c)) \cap \boldsymbol{L}^2(\Omega_c \times]0, T[) \cap H^{-1}(0, T; \boldsymbol{H}(\mathbf{curl}; \mathbb{R}^3)), \tag{A.29}$$
$$\boldsymbol{j}^\varepsilon \in \boldsymbol{L}^2(\Omega_c \times]0, T[), \tag{A.30}$$

where $(\boldsymbol{H}(\mathbf{curl}; \mathbb{R}^3))')$ is the dual of the space $\boldsymbol{H}(\mathbf{curl}; \mathbb{R}^3)$. In section (3.6), we have used these results and derived convergence results for electromagnetic fields. From (A.27)–(A.30) the two-scale weak star convergence is derived for the fields $\boldsymbol{h}^\varepsilon, \boldsymbol{b}^\varepsilon$ and $\boldsymbol{e}^\varepsilon$ as they belong to the space L^∞ and the weak convergence is derived for the field $\boldsymbol{j}^\varepsilon$.

Appendix B

Classical convergence

Details about most of the mathematical concepts recalled in this appendix can be found in [30, 40, 54, 85, 93, 158, 175].

B.1 Convergence in Banach spaces

We denote by $\mathcal{V}$, a real Banach space and $\mathcal{V}'$ its dual. A sequence $\{u_n\} \in \mathcal{V}$ is said to *strongly converge* to $u \in \mathcal{V}$ (what we denote by $u_n \to u$) if:

$$\lim_{n\to\infty} ||u_n - u||_{\mathcal{V}} = 0, \tag{B.1}$$

where $||\cdot||_{\mathcal{V}}$ denotes the norm defined on $\mathcal{V}$. The strong convergence defined on $\mathcal{V}$ enables to define the strong topology on $\mathcal{V}$, the opens of which are defined by the norm on $\mathcal{V}$.

A sequence $\{u_n\} \in \mathcal{V}$ is said to *weakly converge* to $u \in \mathcal{V}$ (what we denote by $u_n \rightharpoonup u$) if:

$$\lim_{n\to\infty} \Big\langle f, u_n \Big\rangle \quad = \quad \Big\langle f, u \Big\rangle \quad , \forall f \in \mathcal{V}'. \tag{B.2}$$

In the case $\mathcal{V}$ is a Hilbert space, the norm is induced by the inner product (u, v) between any two element u and v. The weak convergence can then be expressed as

$$\lim_{n\to\infty} \varphi_f(u_n) = \varphi_f(u), \tag{B.3}$$

with $\varphi_f(u) = \displaystyle\int_\Omega (fu)\,\mathrm{d}x$.

The notion of dual space allows also to define a weak topology on $\mathcal{V}$. This weak topology is the coarsest topology that can be defined on $\mathcal{V}$ and for which all the linear functionals $f \in \mathcal{V}'$ are continuous. We take the space $L^2(\Omega)$ as an example. The inner product is given by $\int_\Omega u\, v\,\mathrm{d}\boldsymbol{x}$. The weak convergence $u_n \rightharpoonup u$ can then be expressed as:

$$\lim_{n\to\infty} \int_\Omega u_n\, v\,\mathrm{d}\boldsymbol{x} = \int_\Omega u\, v\,\mathrm{d}\boldsymbol{x} \Rightarrow \lim_{n\to\infty} \int_\Omega (u_n - u)\, v\,\mathrm{d}\boldsymbol{x} = 0 \quad , \forall v \in \mathcal{V}. \tag{B.4}$$

Using duality, it is also possible to define the weak-$*$ topology on $\mathcal{V}'$. A sequence $\{f_n\} \in \mathcal{V}'$ is said to *converge weakly-$*$* to f in $\mathcal{V}'$ (what we denote by $f_n \overset{*}{\rightharpoonup} f$) if:

$$\lim_{n\to\infty} \left\langle f_n, u \right\rangle \ = \ \left\langle f, u \right\rangle \ , \forall u \in \mathcal{V}. \tag{B.5}$$

It can be shown that [40, 93]:

$$u_n \rightharpoonup u \text{ in } \mathcal{V} \quad \Rightarrow \quad ||u||_{\mathcal{V}} \leq \ \liminf ||u_n||_{\mathcal{V}} \tag{B.6}$$

It can also be shown that [40]:

$$u_n \to u \quad \Rightarrow \quad u_n \rightharpoonup u, \tag{B.7}$$

but the converse is not true.

B.2 Convergence in $L^p(\Omega)$ spaces

In this thesis, we are interested in Banach spaces $\mathcal{V} = L^p(\Omega)$. The norm of these spaces is given by:

$$\Big|\Big|u\Big|\Big|_{L^p(\Omega)} = \begin{cases} \left(\displaystyle\int_\Omega |u|^p \, \mathrm{d}\boldsymbol{x}\right)^{\frac{1}{p}} & \text{if } 1 \leq p < \infty \\ \text{ess sup}_\Omega |u| & \text{if } p = \infty \end{cases} \tag{B.8}$$

where $\text{ess sup}_\Omega |u|$ is defined as the smallest upper bound of $|u|$ on Ω.

Recall that the Banach spaces $L^p(\Omega)$ are reflexive for $p \neq 1$ and $p \neq \infty$ and separable when $p \neq \infty$ [40, 83, 85] . For $p \neq 1$ and $p \neq \infty$ the dual space of $L^p(\Omega)$ is $L^q(\Omega)$ with the conjugate exponent q given by $1/p + 1/q = 1$. In addition, $L^\infty(\Omega)$ is the dual of $L^1(\Omega)$ but the contrary is not true ($L^1(\Omega)$ is contained in the dual of $L^\infty(\Omega)$).

The following compactness theorems generally hold for bounded sequences in appropriat Banach spaces (e.g. reflexive or separable Banach spaces).

Theorem 1 (*Weak compactness theorem* [40, 85, 93])**.** *Let $\mathcal{V}$ be a reflexive Banach space. From any bounded sequence $\{u_n\} \in \mathcal{V}$, one can extract a subsequence denoted $\{u_{nj}\}$ that weakly converges to $u \in \mathcal{V}$.*

This theorem holds for L^p spaces ($p \neq 1$ and $p \neq \infty$). A similar result can be formulated for the separable space $L^1(\Omega)$. The following theorem can be used for the space L^∞:

Theorem 2. *Let $\mathcal{V}$ be a separable Banach space and $\mathcal{V}'$, its dual. From any bounded sequence $\{f_n\} \in \mathcal{V}'$, one can extract a subsequence denoted $\{f_{nj}\}$ that converges weakly-$*$ to $f \in \mathcal{V}'$.*

Choosing $\mathcal{V} = L^1(\Omega)$ and $\mathcal{V}' = L^\infty(\Omega)$, Theorem 2 then holds.

B.3 Examples

The following two examples illustrate the application of these two theorems.

The first example concerns problem (3.19). The weak form of this problem reads:

$$(a^\varepsilon \mathbf{grad}\, u^\varepsilon, \mathbf{grad}\, v) = \Big\langle f, v \Big\rangle \quad , \forall v \in H_0^1(\Omega). \tag{B.9}$$

If a is bounded and satisfies (3.21), the bilinear form $a(u^\varepsilon, v) = (a^\varepsilon \mathbf{grad}\, u^\varepsilon, \mathbf{grad}\, v)$ is coercive and for $v = u^\varepsilon$ we get:

$$c_1 ||\mathbf{grad}\, u^\varepsilon||^2_{L^2(\Omega)} = c_2 ||u^\varepsilon||^2_{H_0^1(\Omega)} \leq a(u^\varepsilon, u^\varepsilon) = \Big\langle f, u^\varepsilon \Big\rangle \leq ||f||_{H^{-1}(\Omega)} ||u^\varepsilon||_{H_0^1(\Omega)} \tag{B.10}$$

where the first equality results from Poincaré inequality. From (B.10), we get:

$$||u^\varepsilon||_{H_0^1(\Omega)} \leq \frac{1}{c} ||f||_{H^{-1}(\Omega)}. \tag{B.11}$$

meaning that the sequence $\{u^\varepsilon\}$ is bounded in $H_0^1(\Omega)$ which is a reflexive Banach space (indeed, $H_0^1(\Omega)$ is a closed subspace of $L^2(\Omega)$ which is reflexive [40]). Therefore, u^ε weakly converges to some $u_0 \in H_0^1(\Omega)$.

The second example concerns conditions (3.21) from which we get the uniform boundedness condition $a^\varepsilon \in \boldsymbol{L}^\infty(\Omega)$. The space $\boldsymbol{L}^\infty(\Omega)$ is neither reflexive nor separable. However it is the dual of $\boldsymbol{L}^1(\Omega)$ which is a separable Banach space [40]. We can therefore deduce from Theorem 2 that:

$$a^\varepsilon \overset{*}{\rightharpoonup} a \quad \text{in } \boldsymbol{L}^\infty(\Omega). \tag{B.12}$$

Appendix C

Two-scale convergence and the periodic unfolding method

Most of the mathematical concepts defined in Appendix C can be found in [11, 31, 45, 46, 120, 130, 141, 143, 197].

C.1 Two-scale convergence of sequence

A sequence $\{u^\varepsilon\}$ of $L^2(\Omega)$ is said to *weakly two-scale converge* to a limit $u_0 \in L^2(\Omega \times Y)$ (which we denote by $u^\varepsilon \underset{2}{\rightharpoonup} u_0$) if the equality:

$$\lim_{\varepsilon \longrightarrow 0} \int_\Omega u^\varepsilon(\boldsymbol{x})\psi(\boldsymbol{x}, \frac{\boldsymbol{x}}{\varepsilon})\mathrm{d}\boldsymbol{x} \longrightarrow \int_\Omega \int_Y u_0(\boldsymbol{x}, \boldsymbol{y})\psi(\boldsymbol{x}, \boldsymbol{y})\mathrm{d}\boldsymbol{x}\mathrm{d}\boldsymbol{y} \tag{C.1}$$

holds for any smooth function $\psi \in \mathcal{B}(\Omega \times Y)$ that is periodic w.r.t the second argument. The definition can be extended to a sequence of vector functions $\{\boldsymbol{u}^\varepsilon\}$ of $\boldsymbol{L}^2(\Omega)$.

The function space $\mathcal{B}(\Omega \times Y)$ of test functions must be a Banach dense subspace of $L^2(\Omega \times Y)$ [11, 120, 141] meaning that the adherence $\overline{\mathcal{B}(\Omega \times Y)}$ formed by all the elements of these spaces and all their limits is $L^2(\Omega \times Y)$ itself. This means that sequence of $\mathcal{B}(\Omega \times Y)$ strongly converge in $L^2(\Omega \times Y)$ up to extraction and that the integral (C.1) has a sense as it involves a product of two sequences, one of which is strongly convergent.

The two-scale convergence results stated in Definition C.1 is similar to the weak compactness Theorem 1 for the classical weak convergence, the only difference is that in the case of the weak two-scale convergence, the sequence $\{u^\varepsilon\}$ of $L^2(\Omega)$ and the limit $u_0 \in L^2(\Omega \times Y)$ do not belong to the same spaces.

C.2 Scale transformation and the periodic unfolding method.

A few variants of periodic unfolding method have been defined [46, 130, 197]. In this thesis, we use ideas from [130] to illustrate the method. To start with, we define the set $\mathcal{Y}$ by identifying opposite sides of $Y = [-\frac{1}{2}, \frac{1}{2}[^n$. This is equivalent to equipping Y with a topological and differential structure of a torus $\mathcal{Y} = \mathbb{R}^n/\mathbb{Z}^n = \mathbb{T}^n$. It is then possible to identify any Y-periodic function defined on $\mathbb{R}^n$ with a function defined on $\mathcal{Y}$. Thus, $L^p(Y)$ can be identified with $L^p(\mathcal{Y})$. However, the identification is not possible for spaces involving derivatives. This is the case for instance for $H^1(Y) \neq H^1(\mathcal{Y}) := H^1_\#(\overline{Y})$ and $C^k(Y) \neq C^k(\mathcal{Y}) := C^k_\#(\overline{Y})$.

Periodic unfolding approach For any $\varepsilon > 0$, the point $\boldsymbol{x} \in \mathbb{R}^n$ has the following unique periodic unfolding [45] (also named two-scale decomposition in [197]):

$$\boldsymbol{x} = \varepsilon\Big[\mathcal{N}\Big(\frac{\boldsymbol{x}}{\varepsilon}\Big) + \mathcal{R}\Big(\frac{\boldsymbol{x}}{\varepsilon}\Big)\Big] \tag{C.2}$$

where

$$\mathcal{N}(\boldsymbol{x}) := (\hat{n}(x_1), ...\hat{n}(x_n)) \in \mathbb{Z}^n \quad \text{with} \quad \hat{n}(x_i) := \max\{n \in \mathbb{Z} : n < x_i\} \tag{C.3a}$$

$$\mathcal{R}(\boldsymbol{x}) := (\hat{r}(x_1), ...\hat{r}(x_n)) \in [0, 1)^n \quad \text{with} \quad \hat{r}(x_i) := x_i - \hat{n}(x_i) \tag{C.3b}$$

The quantities $\varepsilon\mathcal{N}\Big(\frac{\boldsymbol{x}}{\varepsilon}\Big)$ and $\mathcal{R}\Big(\frac{\boldsymbol{x}}{\varepsilon}\Big)$ represent the coarse-scale and the fine-scale variables.

We define the composition mapping $\mathcal{S}^\varepsilon$:

$$\mathcal{S}^\varepsilon : \quad \mathbb{R}^n \times \mathcal{Y} \to \mathbb{R}^n, \tag{C.4}$$

$$(\boldsymbol{x}, \boldsymbol{y}) \mapsto \varepsilon\mathcal{N}\Big(\frac{\boldsymbol{x}}{\varepsilon}\Big) + \varepsilon\boldsymbol{y}, \tag{C.5}$$

which uniformly converges to $\boldsymbol{x}$ in $\mathbb{R}^n$ as $\varepsilon \to 0$. It is then possible to define the periodic unfolding operator $\mathcal{T}^\varepsilon$:

$$\mathcal{T}^\varepsilon : \quad L^p(\Omega) \to L^p(\mathbb{R}^n \times \mathcal{Y}), \tag{C.6}$$

$$u^\varepsilon \mapsto (\mathcal{T}^\varepsilon u^\varepsilon) = u^\varepsilon_{ex} \circ \mathcal{S}^\varepsilon, \tag{C.7}$$

with

$$u^\varepsilon_{ex} \circ \mathcal{S}^\varepsilon(\boldsymbol{x}, \boldsymbol{y}) = \begin{cases} u^\varepsilon(\varepsilon\mathcal{N}\Big(\frac{\boldsymbol{x}}{\varepsilon}\Big) + \varepsilon\boldsymbol{y}) & \text{if } \varepsilon\mathcal{N}\Big(\frac{\boldsymbol{x}}{\varepsilon}\Big) + \varepsilon\boldsymbol{y} \in \Omega, \\ 0 & \text{if } \varepsilon\mathcal{N}\Big(\frac{\boldsymbol{x}}{\varepsilon}\Big) + \varepsilon\boldsymbol{y} \notin \Omega. \end{cases} \tag{C.8}$$

The periodic unfolding operator is a linear isometry [46, 185, 197]. The following equalities:

$$\int_{\mathbb{R}^n} \int_Y (\mathcal{T}^\varepsilon u^\varepsilon)(\boldsymbol{x}, \boldsymbol{y}) \mathrm{d}\boldsymbol{y} \mathrm{d}\boldsymbol{x} = \int_\Omega u^\varepsilon \mathrm{d}\boldsymbol{x} \tag{C.9}$$

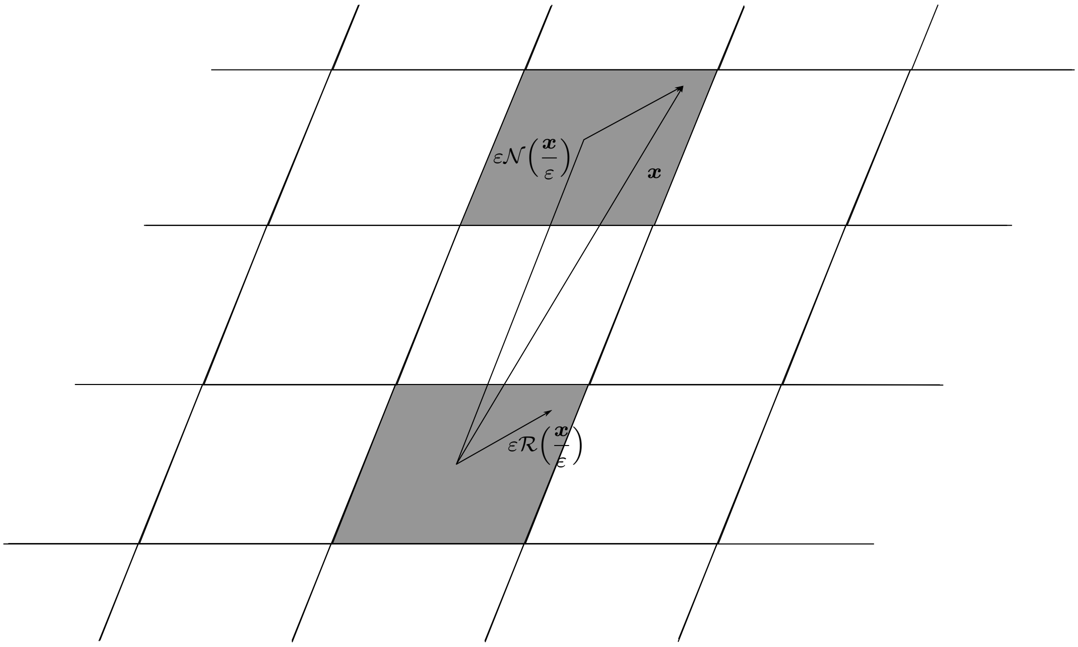

Figure C.1: Decomposition of the point $\boldsymbol{x}$ into the large scale variable $\varepsilon\mathcal{N}\left(\frac{\boldsymbol{x}}{\varepsilon}\right)$ and local scale variable $\mathcal{R}\left(\frac{\boldsymbol{x}}{\varepsilon}\right)$.

and

$$||\mathcal{T}^\varepsilon u^\varepsilon||_{L^2(\mathbb{R}^n\times\mathcal{Y})} = ||u^\varepsilon||_{L^2(\Omega)} \tag{C.10}$$

are valid for all $u^\varepsilon \in L^1(\Omega)$. If the sequence $\{u^\varepsilon\}$ is bounded in $L^2(\Omega)$, the sequence $\{(\mathcal{T}^\varepsilon u^\varepsilon)^\varepsilon\}$ is also bounded in $L^2(\mathbb{R}^n\times\mathcal{Y})$ and applying Theorem 1, it is possible to extract a converging subsequence still denoted $(\mathcal{T}^\varepsilon u^\varepsilon)^\varepsilon$ that weakly converges to some $\overline{u}_0 \in L^2(\mathbb{R}^n\times\mathcal{Y})$ that is *a priori* different from u_0 of (C.1). The major insight of the periodic unfolding method is the proof that the restriction of $\overline{u}_0$ on Ω is equal to u_0.

The periodic unfolding method [31, 45, 46, 130, 197] allows to express the two-scale convergence of a sequence $\{u^\varepsilon\}$ of $L^p(\Omega)$ as the classical convergence (one-scale convergence) in $L^p(\mathbb{R}^n\times\mathcal{Y})$ of the sequence obtained by applying the periodic unfolding operator $\mathcal{T}^\varepsilon$ to sequence original sequence $\{u^\varepsilon\}$. Assuming that $1 \le p \le \infty$ we get the following results for the strong/weak and weak-* two-scale convergence:

$$u^\varepsilon \underset{2}{\rightarrow} u_0 \quad \text{in} \quad L^p(\Omega\times\mathcal{Y}) \qquad \Leftrightarrow \mathcal{T}^\varepsilon u^\varepsilon \rightarrow u_0 \ \text{ in } \ L^p(\mathbb{R}^n\times\mathcal{Y}), \tag{C.11}$$

$$u^\varepsilon \underset{2}{\rightharpoonup} u_0 \quad \text{in} \quad L^p(\Omega\times\mathcal{Y}) \qquad \Leftrightarrow \mathcal{T}^\varepsilon u^\varepsilon \rightharpoonup u_0 \ \text{ in } \ L^p(\mathbb{R}^n\times\mathcal{Y}), \tag{C.12}$$

$$u^\varepsilon \underset{2}{\overset{*}{\rightharpoonup}} u_0 \quad \text{in} \quad L^\infty(\Omega\times\mathcal{Y}) \qquad \Leftrightarrow \mathcal{T}^\varepsilon u^\varepsilon \overset{*}{\rightharpoonup} u_0 \ \text{ in } \ L^\infty(\mathbb{R}^n\times\mathcal{Y}). \tag{C.13}$$

C.3 Convergence of electromagnetic fields and operators of Maxwell's equations.

In this section, we state results of the two-scale convergence for sequences of electromagnetic fields that can appear when solving Maxwell's equations. The results concern time-independent fields but they can easily be extended to time-dependent fields.

Two-scale convergence in $L^p(\mathbb{R}^n)$ [11, 143]

From any bounded sequence $\{u^\varepsilon\}$ of $L^p(\Omega)$, one can extract a subsequence still denoted u^ε that two-scale converges to a limit $u_0 \in L^p(\mathbb{R}^n \times \mathcal{Y})$. The result remains valid for vector valued functions $\boldsymbol{u}^\varepsilon \in \boldsymbol{L}^p(\Omega)$.

Two-scale convergence of the grad of a vector field [11, 198]

Let $\{\phi^\varepsilon\}$ be a bounded sequence in $H^1(\mathbb{R}^n)$ such that $\phi^\varepsilon \to \phi_0$ in $H^1(\mathbb{R}^n)$. Then there exists $\bar{\phi}_1 \in L^2(\mathbb{R}^n; H^1_*(\mathcal{Y}))$ such that

$$\mathbf{grad}\, \phi^\varepsilon \underset{2}{\rightharpoonup} \mathbf{grad}_x\, \phi_0 + \mathbf{grad}_y\, \bar{\phi}_1 \quad \text{in} \quad \boldsymbol{L}^2(\mathbb{R}^n \times \mathcal{Y}). \tag{C.14}$$

Conversely, for any $\phi_M \in H^1(\mathbb{R}^n)$ and $\phi_1 \in L^2(\mathbb{R}^n; H^1_*(\mathcal{Y}))$, there exists a sequence $\{\phi^\varepsilon\}$ of $H^1(\mathbb{R}^n)$ such that

$$\phi^\varepsilon \rightharpoonup \phi_M \quad \text{in} \quad \boldsymbol{L}^2(\mathbb{R}^n), \tag{C.15}$$

$$\mathbf{grad}\, \phi^\varepsilon \underset{2}{\rightharpoonup} \mathbf{grad}_x\, \phi_M + \mathbf{grad}_y\, \phi_1 \quad \text{in} \quad \boldsymbol{L}^2(\mathbb{R}^n \times \mathcal{Y}). \tag{C.16}$$

Results of this proposition can be used for div $-$ **grad** formulations (e.g.: using the scalar potential formulation for the electrokinetic problem).

Two-scale convergence of the curl of a vector field [198]

Let $\{\boldsymbol{h}^\varepsilon\}$ be a bounded sequence in $\boldsymbol{H}(\mathbf{curl}; \mathbb{R}^n)$ such that $\boldsymbol{h}^\varepsilon \underset{2}{\rightharpoonup} \boldsymbol{h}_0$ in $\boldsymbol{L}^2(\mathbb{R}^n \times \mathcal{Y})$. Then $\boldsymbol{h}_0 \in \boldsymbol{L}^2(\mathbb{R}^n; \boldsymbol{H}(\mathbf{curl}; 0, \mathcal{Y}))$, $\hat{\boldsymbol{h}}_0 \in \boldsymbol{H}(\mathbf{curl}; \mathbb{R}^3)$ and there exists $\bar{\boldsymbol{h}}_1 \in \boldsymbol{L}^2(\mathbb{R}^n; \boldsymbol{H}^1_*(\mathcal{Y}))$ such that

$$\mathbf{curl}\, \boldsymbol{h}^\varepsilon \underset{2}{\rightharpoonup} \mathbf{curl}_x\, \hat{\boldsymbol{h}}_0 + \mathbf{curl}_y\, \bar{\boldsymbol{h}}_1 \text{ in } \boldsymbol{L}^2(\mathbb{R}^3 \times \mathcal{Y}). \tag{C.17}$$

Conversely, for any $\boldsymbol{h}_M \in \boldsymbol{H}(\mathbf{curl}; \mathbb{R}^n)$ and $\boldsymbol{h}_1 \in \boldsymbol{L}^2(\mathbb{R}^n; \boldsymbol{H}(\mathbf{curl}; \mathcal{Y}))$, there exists a sequence $\{\boldsymbol{h}^\varepsilon\}$ of $\boldsymbol{H}(\mathbf{curl}; \mathbb{R}^n)$ such that

$$\boldsymbol{h}^\varepsilon \rightharpoonup \boldsymbol{h}_M \quad \text{in} \quad \boldsymbol{L}^2(\mathbb{R}^n), \tag{C.18}$$

$$\mathbf{curl}\, \boldsymbol{h}^\varepsilon \underset{2}{\rightharpoonup} \mathbf{curl}_x\, \boldsymbol{h}_M + \mathbf{curl}_y\, \boldsymbol{h}_1 \quad \text{in} \quad \boldsymbol{L}^2(\mathbb{R}^n \times \mathcal{Y}). \tag{C.19}$$

A gauge condition must be imposed for $\boldsymbol{h}_1$ to be uniquely defined. Coulomb gauge have been proposed in [31, 198].

Two-scale convergence of the div of a vector field [198]

Let $\{\boldsymbol{b}^\varepsilon\}$ be a bounded sequence in $\boldsymbol{H}(\mathrm{div};\mathbb{R}^n)$ such that $\boldsymbol{b}^\varepsilon \underset{2}{\rightharpoonup} \boldsymbol{b}_0$ in $\boldsymbol{L}^2(\mathbb{R}^n \times \mathcal{Y})$. Then $\boldsymbol{b}_0 \in \boldsymbol{L}^2(\mathbb{R}^n; \boldsymbol{H}(\mathrm{div}; 0, \mathcal{Y}))$, $\hat{\boldsymbol{b}}_0 \in \boldsymbol{H}(\mathrm{div};\mathbb{R}^3)$ and there exists $\bar{\boldsymbol{b}}_1 \in \boldsymbol{L}^2(\mathbb{R}^n; \boldsymbol{H}^1_*(\mathcal{Y}))$ such that

$$\mathrm{div}\, \boldsymbol{b}^\varepsilon \underset{2}{\rightharpoonup} \mathrm{div}_x\, \hat{\boldsymbol{b}}_0 + \mathrm{div}_y\, \bar{\boldsymbol{b}}_1 \text{ in } \boldsymbol{L}^2(\mathbb{R}^3 \times \mathcal{Y}). \tag{C.20}$$

Conversely, for any $\boldsymbol{b}_M \in \boldsymbol{H}(\mathrm{div};\mathbb{R}^n)$ and $\boldsymbol{b}_1 \in \boldsymbol{L}^2(\mathbb{R}^n; \boldsymbol{H}(\mathrm{div};\mathcal{Y}))$, there exists a sequence $\{\boldsymbol{b}^\varepsilon\}$ of $\boldsymbol{H}(\mathrm{div};\mathbb{R}^n)$ such that

$$\boldsymbol{b}^\varepsilon \rightharpoonup \boldsymbol{b}_M \quad \text{in} \quad \boldsymbol{L}^2(\mathbb{R}^n), \tag{C.21}$$

$$\mathrm{div}\, \boldsymbol{b}^\varepsilon \underset{2}{\rightharpoonup} \mathrm{div}_x\, \boldsymbol{b}_M + \mathrm{div}_y\, \boldsymbol{b}_1 \quad \text{in} \quad \boldsymbol{L}^2(\mathbb{R}^n \times \mathcal{Y}). \tag{C.22}$$

A gauge condition must be imposed for $\boldsymbol{b}_1$ to be uniquely defined. The gauge $\mathbf{curl}_y\, \boldsymbol{b}_1 = \mathbf{0}$ has been used in [198].

C.4 The div – curl lemma

Hereafter we recall the two-scale version of the div – **curl** lemma [199–201].

The two-scale div – curl lemma for time-independent problems

Assume that $\{\boldsymbol{u}^\varepsilon\}$ is a bounded sequence in $\boldsymbol{H}(\mathbf{curl};\mathbb{R}^3)$ and that $\{\boldsymbol{w}^\varepsilon\}$ is a bounded sequence in $\boldsymbol{H}(\mathrm{div};\mathbb{R}^3)$. Assume in addition that:

$$\boldsymbol{u}^\varepsilon \underset{2}{\rightharpoonup} \boldsymbol{u}_0 \quad \text{in } \boldsymbol{L}^2(\mathbb{R}^3 \times \mathcal{Y}) \tag{C.23a}$$

$$\boldsymbol{w}^\varepsilon \underset{2}{\rightharpoonup} \boldsymbol{w}_0 \quad \text{in } \boldsymbol{L}^2(\mathbb{R}^3 \times \mathcal{Y}) \tag{C.23b}$$

Then the sequence $\{\boldsymbol{w}^\varepsilon \cdot \boldsymbol{u}^\varepsilon\}$ converges to $\hat{\boldsymbol{w}}_0 \cdot \hat{\boldsymbol{u}}_0$ in the sense:

$$\int_\Omega \Big(\boldsymbol{w}^\varepsilon(\boldsymbol{x}) \cdot \boldsymbol{u}^\varepsilon(\boldsymbol{x})\Big)\theta(\boldsymbol{x})\mathrm{d}\boldsymbol{x} \to \int_\Omega \Big(\hat{\boldsymbol{w}}_0(\boldsymbol{x}) \cdot \hat{\boldsymbol{u}}_0(\boldsymbol{x})\Big)\theta(\boldsymbol{x})\mathrm{d}\boldsymbol{x}$$
$$= \iint_{\Omega\times\mathcal{Y}} \Big(\boldsymbol{w}_0(\boldsymbol{x},\boldsymbol{y}) \cdot \boldsymbol{u}_0(\boldsymbol{x},\boldsymbol{y})\Big)\theta(\boldsymbol{x})\mathrm{d}\boldsymbol{x}\mathrm{d}\boldsymbol{y}, \forall\theta \in \mathcal{D}(\mathbb{R}^3). \tag{C.24}$$

The two-scale lemma developed above can be used for proving the convergence of magnetic energy for magnetostatic problems (e.g.: governed by a maximal monotone mapping):

$$\mathbf{curl}\, \boldsymbol{h}^\varepsilon = \boldsymbol{j}_s, \tag{C.25a}$$

$$\mathrm{div}\, \boldsymbol{b}^\varepsilon = \mathbf{0}, \tag{C.25b}$$

$$\boldsymbol{b}^\varepsilon(\boldsymbol{x}) \in \partial\varphi(\boldsymbol{h}^\varepsilon(\boldsymbol{x}), \boldsymbol{x}). \tag{C.25c}$$

In this case, with $\boldsymbol{u}^\varepsilon = \boldsymbol{h}^\varepsilon \in \boldsymbol{H}(\mathbf{curl}; \mathbb{R}^3)$ and $\boldsymbol{w}^\varepsilon = \boldsymbol{b}^\varepsilon \in \boldsymbol{H}(\mathrm{div}; \mathbb{R}^3)$, we have the following two-scale results:

$$\boldsymbol{h}^\varepsilon \underset{2}{\rightharpoonup} \boldsymbol{h}_0, \tag{C.26a}$$
$$\boldsymbol{b}^\varepsilon \underset{2}{\rightharpoonup} \boldsymbol{b}_0, \tag{C.26b}$$

and

$$\boldsymbol{h}^\varepsilon \rightharpoonup \hat{\boldsymbol{h}}_0, \tag{C.27a}$$
$$\boldsymbol{b}^\varepsilon \rightharpoonup \hat{\boldsymbol{b}}_0, \tag{C.27b}$$

and therefore the convergence of magnetic energy:

$$\int_\Omega \Big(\boldsymbol{b}^\varepsilon(\boldsymbol{x}) \cdot \boldsymbol{h}^\varepsilon(\boldsymbol{x})\Big)\theta(\boldsymbol{x})\mathrm{d}\boldsymbol{x} \to \int_\Omega \Big(\hat{\boldsymbol{b}}_0(\boldsymbol{x}) \cdot \hat{\boldsymbol{h}}_0(\boldsymbol{x})\Big)\theta(\boldsymbol{x})\mathrm{d}\boldsymbol{x}$$
$$= \iint_{\Omega\times\mathcal{Y}} \Big(\boldsymbol{b}_0(\boldsymbol{x}, \boldsymbol{y}) \cdot \boldsymbol{h}_0(\boldsymbol{x}, \boldsymbol{y})\Big)\theta(\boldsymbol{x})\mathrm{d}\boldsymbol{x}\mathrm{d}\boldsymbol{y} \quad \forall\, \theta \in \mathcal{D}(\mathbb{R}^3) \tag{C.28}$$

The two-scale div – curl lemma for time-dependent problems

The following assumptions must be made for the div – **curl** lemma to hold for time-dependent fields. If $\{\boldsymbol{u}^\varepsilon\}$ is a sequence of $L^2(0, T; \boldsymbol{H}(\mathbf{curl}; \mathbb{R}^3))$ and $\{\boldsymbol{w}^\varepsilon\}$ is a sequence of $L^2(0, T; \boldsymbol{H}(\mathrm{div}; \mathbb{R}^3))$. If in addition $\exists\, r > 0, s \in \mathbb{R}$ such that either $\{\boldsymbol{u}^\varepsilon\}$ or $\{\boldsymbol{w}^\varepsilon\}$ is bounded in $H^1(0, T; \boldsymbol{H}^s(\mathbb{R}^3))$ and that:

$$\boldsymbol{u}^\varepsilon \underset{2}{\rightharpoonup} \boldsymbol{u}_0 \qquad \text{in } \boldsymbol{L}^2(\mathbb{R}^3_T \times \mathcal{Y}) \tag{C.29a}$$
$$\boldsymbol{w}^\varepsilon \underset{2}{\rightharpoonup} \boldsymbol{w}_0 \qquad \text{in } \boldsymbol{L}^2(\mathbb{R}^3_T \times \mathcal{Y}) \tag{C.29b}$$

Then the sequence $\{\boldsymbol{w}^\varepsilon \cdot \boldsymbol{u}^\varepsilon\}$ converges to $\hat{\boldsymbol{w}}_0 \cdot \hat{\boldsymbol{u}}_0$ in the following sense:

$$\iint_{\mathbb{R}^3_T} \Big(\boldsymbol{w}^\varepsilon(\boldsymbol{x}, t) \cdot \boldsymbol{u}^\varepsilon(\boldsymbol{x}, t)\Big)\theta(\boldsymbol{x}, t)\mathrm{d}\boldsymbol{x}\mathrm{d}t \to \iint_{\mathbb{R}^3_T} \Big(\hat{\boldsymbol{w}}_0(\boldsymbol{x}, t) \cdot \hat{\boldsymbol{u}}_0(\boldsymbol{x}, t)\Big)\theta(\boldsymbol{x}, t)\mathrm{d}\boldsymbol{x}\mathrm{d}t$$
$$= \iiint_{\mathbb{R}^3_T\times\mathcal{Y}} \Big(\boldsymbol{w}_0(\boldsymbol{x}, \boldsymbol{y}, t) \cdot \boldsymbol{u}_0(\boldsymbol{x}, \boldsymbol{y}, t)\Big)\theta(\boldsymbol{x}, t)\mathrm{d}\boldsymbol{x}\mathrm{d}\boldsymbol{y}\mathrm{d}t, \forall\theta \in \mathcal{D}(\mathbb{R}^3_T). \tag{C.30}$$

The two-scale lemma for time-dependent problems can be used for the magnetodynamic problem (3.3)–(3.7). In that case, only $\boldsymbol{h}^\varepsilon$ and $\boldsymbol{e}^\varepsilon$ fulfill the role played by the field $\boldsymbol{u}^\varepsilon$ and only $\boldsymbol{b}^\varepsilon$ fulfills the role played by the field $\boldsymbol{w}^\varepsilon$ (see [196,201]). Therefore, the only results of converging products of sequences for the magnetodynamic problem are:

$$\iint_{\mathbb{R}^3_T} \Big(\boldsymbol{b}^\varepsilon(\boldsymbol{x}, t) \cdot \boldsymbol{h}^\varepsilon(\boldsymbol{x}, t)\Big)\theta(\boldsymbol{x}, t)\mathrm{d}\boldsymbol{x}\mathrm{d}t \to \int_{\mathbb{R}^3_T} \Big(\hat{\boldsymbol{b}}_0(\boldsymbol{x}, t) \cdot \hat{\boldsymbol{h}}_0(\boldsymbol{x}, t)\Big)\theta(\boldsymbol{x}, t)\mathrm{d}\boldsymbol{x}\mathrm{d}t$$

$$= \iint_{\mathbb{R}^3_T \times \mathcal{Y}} \Big(\boldsymbol{b}_0(\boldsymbol{x}, \boldsymbol{y}, t) \cdot \boldsymbol{h}_0(\boldsymbol{x}, \boldsymbol{y}, t) \Big) \theta(\boldsymbol{x}, t) \mathrm{d}\boldsymbol{x} \mathrm{d}\boldsymbol{y} \mathrm{d}t \quad , \forall\ \theta \in \mathcal{D}(\mathbb{R}^3_T) \tag{C.31}$$

and

$$\iint_{\mathbb{R}^3_T} \Big(\boldsymbol{b}^\varepsilon(\boldsymbol{x}, t) \cdot \boldsymbol{e}^\varepsilon(\boldsymbol{x}, t) \Big) \theta(\boldsymbol{x}, t) \mathrm{d}\boldsymbol{x} \mathrm{d}t \to \int_{\mathbb{R}^3_T} \Big(\hat{\boldsymbol{b}}_0(\boldsymbol{x}, t) \cdot \hat{\boldsymbol{e}}_0(\boldsymbol{x}, t) \Big) \theta(\boldsymbol{x}, t) \mathrm{d}\boldsymbol{x} \mathrm{d}t$$

$$= \iint_{\mathbb{R}^3_T \times \mathcal{Y}} \Big(\boldsymbol{b}_0(\boldsymbol{x}, \boldsymbol{y}, t) \cdot \boldsymbol{e}_0(\boldsymbol{x}, \boldsymbol{y}, t) \Big) \theta(\boldsymbol{x}, t) \mathrm{d}\boldsymbol{x} \mathrm{d}\boldsymbol{y} \mathrm{d}t \quad , \forall\ \theta \in \mathcal{D}(\mathbb{R}^3_T) \tag{C.32}$$

Equation (3.116) expresses the consistency of magnetic energy between the macroscale and the mesoscale.

Bibliography

[1] A. Abdulle, *Analysis of a heterogeneous multiscale FEM for problems in elasticity*, Math Mod Meth Appl S **16** (2006), no. 4, 615–635 (English).

[2] ______, *Heterogeneous multiscale methods with quadrilateral finite elements*, Numerical Mathematics and Advanced Applications **20** (2006), 743–751.

[3] ______, *The finite element heterogeneous multiscale method: a computational strategy for multiscale PDEs*, GAKUTO International Series Math. Sci. Appl., Multiple scales problems in Biomathematics, Mechanics, Physics and Numerics **31** (2009), 133–181.

[4] A. Abdulle and W. E, *Finite difference heterogeneous multi-scale method for homogenization problems*, Journal of Computational Physics **191** (2003), 18–39 (English).

[5] A. Abdulle, W. E, B. Engquist, and E. Vanden-Eijnden, *The heterogeneous multiscale method*, Acta Numerica (2012), 1–87.

[6] A. Abdulle and B. Engquist, *Finite element heterogeneous multiscale methods with near optimal computational complexity*, Multiscale Model. Simul. **6** (2007), no. 4, 1059–1084 (English).

[7] A. Abdulle and C. Schwab, *Heterogeneous multiscale FEM for diffusion problems on rough surfaces*, Multiscale Model. Simul. **3** (2005), no. 1, 195–220 (English).

[8] F. F. Abraham, J. Q. Broughton, N. Bernstein, and E. Karixas, *Concurrent coupling of length scales: Methodology and application*, Phys. Rev. B **60** (1999), no. 4, 2391–2402.

[9] M. Ainsworth and J. T. Oden, *A posteriori error estimation in finite element analysis*, Wiley-Interscience, 2000.

[10] G. Akagi, *A study on evolution equations governed by sub-differential operators in reflexive Banach spaces and its applications to nonlinear partial differential equations*, Ph.D. thesis, Waseda University, Japan, 1996.

[11] G. Allaire, *Homogenization and the two-scale convergence*, SIAM J. Math. Anal. **23** (1992), 1482–1518.

[12] N. Antonic, C. J. van Duijn, W. Jager, and A. Mikelic, *Multiscale problems in science and technology*, Springer, 2000.

[13] C. Appino, O. Bottauscio, O. de la Barriere, F. Fiorillo, A. Manzin, and C. Ragusa, *Computation of eddy current losses in soft magnetic composites*, IEEE Transactions on Magnetics **48** (2012), no. 11, 3470–3473.

[14] T. Arbogast, G. Pencheva, M.F. Wheeler, and I. Yotov, *A multiscale mortar mixed finite element method*, SIAM Journal of Multiscale Modeling and Simulation **6** (2007), 319–346.

[15] S. Attinger and P. Koumoutsakos, *Multiscale modeling and simulation*, Springer, 2004.

[16] I. Babuska, G. Caloz, and E. Osborn, *Special finite element methods for a class of second-order elliptic problems with rough coefficients*, SIAM J. Math. Anal. **31** (1994), 945–981.

[17] I. Babuska and E. Osborn, *Generalized finite element methods: their performance and their relation to mixed methods*, SIAM J. Math. Anal. **20** (1983), 510–536.

[18] M Belkadi, B. Ramdane, D. Trichet, and J. Fouladgar, *Non linear homogenization for calculation of electromagnetic properties of soft magnetic composite materials*, IEEE: Transaction on Magnetics **45** (2009), no. 10, 4317–4320.

[19] A. Benabou, S. Clénet, and F. Piriou, *Comparison of Preisach and Jiles-Atherton models to take into account hysteresis phenomenon for finite element analysis*, Journal of Magnetism and Magnetic Materials **261** (2003), 305–310.

[20] A. Bensoussan, J.-L. Lions, and G. Papanicolaou, *Asymptotic analysis for periodic structures*, American Mathematical Society, 2011.

[21] Y. Benveniste, *A new approach to the application of Mori-Tanaka's theory in composite materials*, Mechanics of Materials **6** (1973), no. 2, 147–157.

[22] A. Bermúdes, D. Gómez, R. Rodriguez, and P. Venegas, *Axisymmetric eddy-current problems in conductive non linear magnetic media: numerical approximation and error estimates*, 2013, Presented at the 9^{th} International Symposium on Electric and Magnetic Fields in April 2013 in Bruges, Belgium.

[23] L. Bernarz, B. Engquist, A. Saib, I. Huynen, C. Bailly, J.-M. Thomassin, C. Detrembleur, and R. Jerome, *Matériaux composites à base de nanotubes de carbone pour le blindage d'interférences électromagnétiques*, Revue E tijdschrift **1** (2007), no. april/avril, 14–19.

[24] A. Bossavit, *Whitney forms: a class of finite elements for three-dimensional computations in electromagnetism*, IEE Proceedings **135, Pt. A** (1988), no. 8, 493–499.

[25] ———, *Un nouveau point de vue sur les éléments mixtes*, Bulletin de la Société de Mathématiques Appliquées et Industrielles **20** (1989), 23–35.

[26] ———, *Électromagnétisme, en vue de la modélisation*, Springer-Verlag, 1993.

[27] ———, *Effective penetration depth in spatially periodic grids: a novel approach to homogenization*, 1994, pp. 859–864.

[28] ———, *Homogenizing spatially periodic materials with respect to maxwell equations: Chiral materials by mixing simple ones*, 1996, pp. 564–567.

[29] ———, *Computational electromagnetism. Variational formulations, edge elements, complementarity*, Academic Press, 1998.

[30] ———, *A course in convex analysis*, University Lecture, 2003.

[31] A. Bossavit, G. Griso, and B. Miara, *Modelling of periodic electromagnetic structures bianisotropic materials with memory*, J. Math. Pures Appl. **84** (2005), 819–850.

[32] A. Bossavit and J.-C. Vérité, *A mixed FEM-BIEM method to solve 3D eddy current problems*, IEEE Transactions on Magnetics **18** (1982), no. 2, 431–435.

[33] ———, *The "TRIFOU" code: Solving the 3-D eddy-currents problem by using H as state variable*, IEEE Transactions on Magnetics **19** (1983), no. 6, 2465–2471.

[34] O. Bottauscio, V. Chiado Piat, M. Chiampi, M. Codegone, and A. Manzin, *Nonlinear homogenization technique for saturable soft magnetic composites*, IEEE Transactions on Magnetics **44** (2008), no. 11, 2955–2958.

[35] O. Bottauscio, M. Chiampi, and A. Manzin, *Multiscale modeling of heterogeneous magnetic materials*, Proceedings of the EMF2013 Conference (Brugges, Belgium), April 2013.

[36] ———, *Multiscale modeling of heterogeneous magnetic materials*, International Journal of numerical modeling: electronic networks, devices and fields **27** (2014), 373–384.

[37] O. Bottauscio and A. Manzin, *Comparison of multiscale models for eddy current computation in granular magnetic materials*, Journal of Computational Physics **253** (2013), 1–17.

[38] A. Brandt, *Multi-level adaptive solutions to boundary value problems*, Math. Comput. **31** (1977), no. 138, 137–180.

[39] L. Brassart, I. Doghri, and Delannay L., *Homogenization of elasto-plastic composites coupled with a nonlinear finite element analysis of the equivalent inclusion problem*, International Journal of Solids and Structures **47** (2010), 716–729.

[40] H. Brézis, *Analyse fonctionnelle : Théorie et applications*, Éditions Masson, 2005.

[41] F. Brezzi, L. P. Franca, T. J. R. Hughes, and A. Russo, $b = \int g$, Computer Methods in Applied Mechanics and Engineering **145** (1997), 329–339.

[42] Caltech, http://www.wag.caltech.edu/multiscale/multsicale_computations.htm.

[43] M. P. Calvo and Sanz-Serna J. M., *Heterogeneous multiscale methods for mechanical systems with vibrations*, SIAM J. Sci. Comput. **to appear** (2010), 1–17.

[44] J. Casado-Diaz and I. Gayte, *A general compactness result and its application to the two-scale convergence of almost periodic functions*, C. R. Math. Acad. Sci. Paris, Ser. 1 **323** (1996), 329–334.

[45] D. Cioranescu, A. Damlamian, and G. Griso, *Periodic unfolding and homogenization*, C.R. Acad. Sci. Paris, Ser. I **335** (2002), no. 1, 99–104.

[46] D. Cioranescu, P. Donato, and R. Zaki, *The periodic unfolding method in perforated domains*, Portugaliae Mathematica **63** (2006), no. 4, 467–496.

[47] ———, *The periodic unfolding method in homogenization*, S.I.A.M. J. Math. Anal. **40** (2008), no. 4, 1585–1620.

[48] R. Clausius, *Abhandlungen uber die mechanische warmetheorie*, Friedrich Vieweg und Sohn, Braunschweig **2** (1867), 143.

[49] R. Corcolle, *Détermination de lois de comportment couplé par des techniques d'homogénéisation: application aux matériaux du génie electrique*, Ph.D. thesis, Universite Paris-Sud XI, 2009.

[50] R. Corcolle, V. Préault, and L. Daniel, *Second order moments in linear smart material composites*, IEEE Transactions on Magnetics **48** (2012), no. 2, 663–666.

[51] G. Dal Maso, *Introduction to Γ-convergence*, Birkhauser, 1993.

[52] G. Dal Maso and L. Modica, *Nonlinear stochastic homogenization*, Annali di Matematica Pura ed Applicata **144** (1986), no. 1, 347–389.

[53] I. Daubechies, *Ten lectures on wavelets, CBMS-NSF regional conference series in applied mathematics, SIAM publications*, 1992.

[54] R. Dautray and J.-L. Lions, *Analyse mathématique et calcul numérique pour les sciences et les techniques*, vol. 3, Transformations, Sobolev, Opérateurs, Masson, 1987.

[55] ______, *Analyse mathématique et calcul numérique pour les sciences et les techniques*, vol. 4, Méthodes variationnelles, Masson, 1988.

[56] E. De Giorgi, *G-operators and Γ-convergence*, In Proc. Int. Congr. Math. (1984), 1175–1191.

[57] F. Delincé, *Modélisation des régimes transitoires dans les systèmes comportant des matériaux magnétiques non-linéaires et hystérétiques*, Ph.D. thesis, Université de Liège, 1994.

[58] H. Douanala, *Two-scale convergence and homogenization of some partial differential equations*, Ph.D. thesis, Chalmers University of Technology and University of Gothenburg, 2013.

[59] P. Dular, *Modélisation du champ magnétique et des courants induits dans des systèmes tridimensionnels non-linéaires*, Ph.D. thesis, Université de Liège, Belgium, 1996.

[60] P. Dular, Mauricio V. Ferreira da Luz, P. Kuo-Peng, and K. Krï¿½henbï¿½hl, *Correction of homogenized foil windings and lamination stacks in transformers via a subproblem finite element method*, Proceedings of the 16th Biennial IEEE Conference on Electromagnetic Field Computation (Annecy, France), May 2014.

[61] P. Dular and C. Geuzaine, *Getdp: a general environment for the treatment of discrete problems*, http://www.geuz.org/getdp/.

[62] P. Dular, C. Geuzaine, F. Henrotte, and W. Legros, *A general environment for the treatment of discrete problems and its application to the finite element method*, IEEE Transactions on Magnetics **34** (1998), no. 5, 3395–3398.

[63] P. Dular, C. Geuzaine, and W. Legros, *A natural method for coupling magnetodynamic h-formulations and circuit equations*, IEEE Transactions on Magnetics **35** (1999), no. 3, 1626–1629.

[64] P. Dular, P. Kuo-Peng, C. Geuzaine, N. Sadowski, and J. P. A. Bastos, *Dual magnetodynamic formulations and their source fields associated with massive and stranded inductors*, IEEE Transactions on Magnetics **36** (2000), no. 4, 1293–1299.

[65] E. Durand, *Magnétostatique*, Masson, 1968.

[66] L. J. Durlofsky, *Numerical calculation of equivalent grid block permeability tensors for heterogeneous porous media*, Water Resources Research **27** (1991), 699–708.

[67] W. E, *Analysis of the heterogeneous multiscale method for ordinary differential equations*, Comm. Math. Sci. **1** (2003), no. 3, 423–436.

[68] ______, *Principles of multiscale modeling*, Cambridge, 2011.

[69] W. E and B. Engquist, *The heterogeneous multiscale methods*, Comm. Math. Sci. **1** (2003), no. 1, 87–132.

[70] ______, *Multiscale modeling and computation*, Notices Amer. Math. Soc. **50** (2003), no. 9, 1062–1070.

[71] ______, *The heterogeneous muti-scale method for homogenization problems*, Multiscale Methods in Sci. and Eng., Lect. Notes in Comput. Sci. Eng., Springer, Berlin **44** (2005), 89–110.

[72] W. E, B. Engquist, and Z. Huang, *Heterogeneous multiscale method: A general methodology for multiscale modeling*, Physical Review B **67** (2003), no. 9, 092101.

[73] W. E, B. Engquist, X. Li, W. Ren, and E. Vanden-Eijnden, *Heterogeneous multiscale methods: A review*, Communications in Computational Physics **3** (2007), 367–450.

[74] ______, *Heterogeneous multiscale methods: A review*, Commun Comput Phys **2** (2007), no. 3, 367–450.

[75] W. E, D Liu, and E. Vanden-Eijden, *Analysis of multiscale methods for stochastic differential equations*, Commun. Pure Appl. Math. **LVIII** (2005), 1544–1585.

[76] Y. Efendiev and T. Hou, *Multiscale finite element methods*, Springer, 2009.

[77] Y. Efendiev, T. Hou, and V. Ginting, *Multiscale finite element methods for nonlinear partial differential equations*, Communications in Mathematical Sciences **2** (2004), no. 4, 553–589.

[78] Y. R. Efendiev, *The multiscale finite element method MsFEM and its applications*, Ph.D. thesis, California Institute of Technology Pasadena, California, USA, 1999.

[79] Y. R. Efendiev and T. Y. Hou, *Multiscale finite element methods for porous media flows and their applications*, Applied Numerical Mathematics **57** (2007), 577–596.

[80] Y. R. Efendiev, T. Y. Hou, and X.-H. Wu, *Convergence of a nonconforming multiscale finite element method*, SIAM J. Numer. Anal. **37** (2000), 888.

[81] Y. R. Efendiev and A. Pankov, *Numerical homogenization of nonlinear random parabolic operators*, Multiscale Model. Simul. **2** (2004), 237.

[82] Y. R. Efendiev and X.-H. Wu, *Multiscale finite element for problems with highly oscillatory coefficients*, Numer. Math. **90** (2002), 459–486.

[83] I. Ekeland and R. Temam, *Analyse convexe et problèmes variationnelles*, Dunod, Paris, 1974.

[84] M. El Feddi, Z. Ren, A. Razek, and A. Bossavit, *Homogenization technique for Maxwell equations in periodic structure*, IEEE Transactions on Magnetics **33** (1997), no. 2, 1382–1385.

[85] L. C. Evans, *Partial differential equations*, American Mathematical Society, Providence, Rhode Island, 2010.

[86] V. Francois-Lavet, F. Henrotte, L. Stainier, L. Noels, and C. Geuzaine, *An energy-based variational model of ferromagnetic hysteresis for finite element computations*, Journal of Computational and Applied Mathematics **246** (2013), 243–250.

[87] F. Gardiol, *Electromagnétisme*, Traité d'électricité de l'Ecole Polytechnique Féderale de Lausanne, Volume III, Editions Georgis, Suisse, 1979.

[88] C. Garing, *Milieux magnétiques*, Ellipses, 1995.

[89] M. G. D. Geers, V. G. Kouznetsova, and Brekelmans, *Gradient-enhanced computational homogenization for the micro-macro scale transition*, Journal de Physique IV **11** (2001), no. 5, 5145–5152.

[90] C. Geuzaine, *High order hybrid finite element schemes for Maxwell's equations taking thin structures and global quantities into account*, Ph.D. thesis, Université de Liège, Belgium, 2002.

[91] C. Geuzaine and J. F. Remacle, *Gmsh: a finite element mesh generator with built-in pre- and post-processing facilities*, http://www.geuz.org/gmsh/.

[92] ———, *Gmsh: a three-dimensional finite element mesh generator with built-in pre- and post-processing facilities*, International Journal for Numerical Methods in Engineering **79** (2009), no. 11, 1309–1331.

[93] C. Geuzaine and P. Tossing, *Functional analysis and the finite element method*, GraSMech Lecture Notes, 2012.

[94] J. Gyselinck, *Incorporation of a Jiles-Atherton vector hysteresis model in 2-D FE magnetic computations*, COMPEL: The International Journal for Computation and Mathematics in Electrical and Electronic Engineering **23** (2004), no. 3, 685–693.

[95] J. Gyselinck and P. Dular, *A time-domain homogenization technique for laminated iron cores in 3-D finite element models*, IEEE: Transaction on Magnetics **40** (2004), no. 2, 856–859.

[96] J. Gyselinck, R. V. Sabariego, and P. Dular, *A nonlinear time-domain homogenization technique for laminated iron cores in three-dimensional finite element models*, IEEE: Transaction on Magnetics **42** (2006), no. 4, 763–766.

[97] ______, *Time-domain homogenization of windings in 2-D finite element mode*, IEEE: Transaction on Magnetics **43** (2007), no. 4, 1297–1300.

[98] R. F. Harrington, *Time-harmonic electromagnetic fields*, McGraw-Hill, 1961.

[99] R. Hill, *A self-consistent mechanics of composite materials*, Journal of the Mechanics and Physics of Solids **13** (1965), no. 4, 213–222.

[100] T. Y. Hou and X. H. Wu, *A multiscale finite element method for elliptic problems in composite materials and porous media*, Journal of Computational Physics **134** (1997), 169–189.

[101] T. Y. Hou, X. H. Wu, and Z. Cai, *Convergence of a multiscale finite element method for elliptic problems with rapidly oscillating coefficients*, Mathematics of computation **68** (1990), no. 227, 913–943.

[102] T. J. R. Hughes, *Multiscale phenomena: Green's functions, the Dirichlet-to-Neumann formulation, subgrid scale models, bubbles and the origins of stabilized methods*, Computer Methods in Applied Mechanics and Engineering **127** (1995), 387–401.

[103] T. J. R. Hughes, G. R. Feijoo, L. Mazzei, and J. B. Quincy, *The variational multiscale method - A paradigm for computational mechanics*, Computer Methods in Applied Mechanics and Engineering **166** (1998), 3–24.

[104] I Huynen, P. P. Barbier, J.-M. Thomassin, C. Pagnoulle, R. Jerome, and C. Detrembleur, *Microwave absorbers based on foamed nanocomposites with graded concentration of carbon nanotubes*, 2008 38th European Microwave Conference (2008), 5–8.

[105] J. D. Jackson, *Classical electrodynamics*, third ed., John Wiley & Sons, 1998.

[106] O. Jeanette Silfver, *On general two-scale convergence and its application to the characterization of G-limits*, Applications of Mathematics **52** (2007), no. 4, 285–302.

[107] D. C. Jiles, *Introduction to magnetism and magnetic materials*, Chapman and Hall, 1991.

[108] D. C. Jiles and D. L. Atherton, *Theory of ferromagnetic hysteresis*, Journal of Magnetism and Magnetic Materials **61** (1986), no. 1–2, 48–60.

[109] R. Juanes and T. W. Patzek, *A variational multiscale finite element method for multiphase flow in porous media*, Finite Elements in Analysis and Design **41** (2005), no. 7–8, 763–777.

[110] I. G. Kevrekidis, *Equation-free, coarse-grained multiscale computation: enabling microscopic simulators to perform system-level analysis*, Commun. Math. Sci. **1** (2003), no. 4, 715–762.

[111] KIT, http://www.hiu.kit.edu/104.php.

[112] W. E. Kohler and G. C. Papanicolaou, *Some applications of the coherent potential approximation*, Multiple Scattering and Waves in Random Media (P. L. Chow, W. E. Kohler, and G. C. Papanicolaou, eds.), 1981, pp. 199–223.

[113] V. Kouznetsova, C.-W. Qiu, S. Zouhdi, Li L.-W., and A. Razek, *Homogenization of 3-D periodic bianisotropic metamaterials*, IEEE Trans. Microwave Theory Tech. **54** (2006), no. 11, 3893–3898.

[114] V. G. Kouznetsova, W. A. M. Brekelmans, and F. P. T. Baaijens, *An approach to micro-macro modeling of heterogeneous materials*, Computational Mechanics **27** (2001), 37–48.

[115] G. Lacroux, *Les aimants permanents*, Lavoisier, 1989.

[116] C. S. Liang and A. K. Jin, *Applied electromagnetism*, PWS, 1995.

[117] W. Ling, L. Noels, L. Adam, and I. Doghri, *A multiscale mean-field homogenization method for fiber-reinforced composites with gradient-enhanced damage models*, Computer Methods in Applied Mechanics and Engineering **233-236** (2012), 164–179.

[118] ———, *A combined incremental-secant mean-field homogenization scheme with per-phase residual strains for elasto-plastic composites*, International Journal of Plasticity **51** (2013), 80–102.

[119] ———, *An implicit-gradient-enhanced incremental-secant mean- field homogenization scheme for elasto-plastic composites with damage*, International Journal of Solids and Structures **50** (2013), no. 24, 3843–3860.

[120] D. Lukkassen, G. Nguetseng, and P. Wall, *Two-scale convergence*, International Journal of Pure and Applied Mathematics **2** (2002), no. 1, 33–81.

[121] P. Marcellini, *Periodic solutions and homogenization of non-linear variational problems*, Ann. Mat. Pura Appl. **IV** (1978), no. Ser. 117, 139–152.

[122] J. C. Maxwell Garnett, *Colors in metal glasses and metal films*, Phil. Trans. R. Soc. Lond. A **203** (1904), no. 359-371, 385–420.

[123] GKN Sinter Metal, http://www.gkn.com/sintermetals/.

[124] G. Meunier, *Homogenization for periodical electromagnetic structure: Which formulation?*, IEEE Transactions on Magnetics **42** (2010), no. 4, 763–766.

[125] G. Meunier, Y. Le Floch, and C. Guerin, *A nonlinear circuit coupled* $\boldsymbol{t}-\boldsymbol{t}_0-\omega$ *formulation for solid conductors*, IEEE Transactions on Magnetics **39** (2003), no. 3, 1729–1732.

[126] G. Meunier, H. T. Luong, and Y. Maréchal, *Computation of coupled problem of 3D eddy current and electrical circuit by using $\boldsymbol{t}_0 - \boldsymbol{t} - \omega$ formulation*, IEEE Transactions on Magnetics **34** (1998), 3074–3077.

[127] J. C. Michel, H. Moulinec, and P Suquet, *Effective properties of composites materials with periodic microstructure: a computational approach*, Comput. methods Appl. Mech. Engrg **172** (1999), 109–143.

[128] ———, *A computational scheme for linear and non-linear composites with arbitrary phase contarst*, International journal for numerical methods in engineering **52** (2001), 139–160.

[129] C. Miehe, *Numerical computational of algorithmic (consistent) tangent moduli in large-strain computational inelasticity*, Computer Methods in Applied Mechanics and Engineering **134** (1996), 223–240.

[130] A. Mielke and A. Timofte, *Two-scale homogenization for evolutionaly variational inequalities via the energetic formulation*, S.I.A.M. Journal of Mathematical Analysis **39** (2008), no. 2, 642–668.

[131] G. W. Milton, *The theory of composites*, Cambridge, 2002.

[132] I. Molenberg, I. Huynen, A.-M. Baudouin, C. Bailly, J.-M. Thomassin, and C. Detrembleur, *Foamed nanocomposites for emi shielding applications*, Advanced Microwave and Millimeter Wave Technologies Semiconductor Devices Circuits and Systems **23** (2010), 1–18.

[133] T. Mori and K. Tanaka, *Average stress in the matrix and average elastic energy of materials with misfitting inclusions*, Acta Metallurgica **21** (1973), no. 5, 571–574.

[134] O.F. Mossotti, *Discussione analitica sull'influenza che l'azione di un mezzo dielettrico ha sulla distribuzione dell'elettricità alla superficie di più corpi elettrici disseminati in esso*, 1846.

[135] H. Moulinec and P Suquet, *A numerical method for computing the overall response of nonlinear composites with complex microstructures*, Comput. methods Appl. Mech. Engrg **157** (1998), 69–94.

[136] S. Muller, *Homogenization of nonconvex integral functionals and cellular elastic materials*, Arch. Rational Mech. Anal. **99** (1987), no. 3, 189–212.

[137] F. Murat, *Compacité par compensation*, Ann. Scuola Norm. Sup. Pisa Cl. Sci. **4** (1978), no. 5, 489–507.

[138] ———, *Compacité par compensation: condition nécessaire et suffisante de continuité faible sous une hypothèse de rang constant*, Ann. Scuola Norm. Sup. Pisa Cl. Sci. **8** (1981), no. 1, 69–102.

[139] F. Murat and L. Tartar, *H-convergence*, Séminaire d'analyse fonctionnelle et numérique de l'université d'Alger, 1977.

[140] ______, *Calcul des variations et homogénéisation*, Progress in Nonlinear Differential Equations and their Applications, Birkhauser, 1995.

[141] A. K. Nandakumaran and S. Sivaji Ganesh, *Lectures on two-scale convergence and homogenization*, Report, Indian Institute of Science, Bangalore, 2010.

[142] M. H. Nayfeh and M. K. Brussel, *Electricity and magnetism*, John Wiley & Sons Inc. New York, 1985.

[143] G. Nguetseng, *A general convergence result for a functional related to the theory of homogenization*, S.I.A.M. Journal of Mathematical Analysis **20** (1989), 608–623.

[144] ______, *Homogenization structures and applications*, I. Zeit. Anal. Anwend. **22** (2003), 73–107.

[145] G. Nguetseng and J. L. Woukeng, *σ-convergence of nonlinear parabolic operators*, Nonlinear Anal. **66** (2007), no. 4, 968–1004.

[146] V. D. Nguyen, E. Béchet, C. Geuzaine, and L. Noels, *Imposing periodic boundary condition on arbitrary meshes by polynomial interpolation*, Computational Materials Science **55** (2012), 390–406.

[147] I. Niyonzima, R. V. Sabariego, P. Dular, and C. Geuzaine, *Finite element computational homogenization for heterogeneous materials in magnetodynamics*, Proceedings of the Fifth International Conference on Advanced COmputational Methods in ENgineering (ACOMEN 2011) (Liége, Belgium), November 2011.

[148] ______, *Finite element computational homogenization of nonlinear multiscale materials in magnetostatics*, IEEE Transactions on Magnetics **48** (2012), no. 2, 587–590.

[149] ______, *A computational homogenization method for the evaluation of eddy current in nonlinear soft magnetic composites*, Proceeding of the 9$^{\text{th}}$ International Symposium on Electric and Magnetic Fields, (EMF2013) (Bruges, Belgium), April 2013.

[150] ______, *Nonlinear computational homogenization method for the evaluation of eddy currents in soft magnetic composites*, IEEE Transactions on Magnetics **50** (2014), no. 2.

[151] I. Niyonzima, R. V. Sabariego, P. Dular, F. Henrotte, and C. Geuzaine, *Multiscale quasistatic homogenization for laminated ferromagnetic cores*, Proceedings of the 7$^{\text{th}}$ European Conference on Numerical Methods in Electromagnetism (NUMELEC 2012) (Marseille, France), July 2012.

[152] ———, *Computational homogenization for laminated ferromagnetic cores in magnetodynamics*, IEEE Transactions on Magnetics **49** (2013), no. 5, 2049–2052.

[153] J. Nolen, G. Papanicolaou, and O. Pironneau, *A framework for adaptive multiscale method for elliptic problems*, SIAM Journal of Multiscale Modeling and Simulations **7** (2008), 171–196.

[154] M. Olsson, *G-convergence and homogenization of some monotone operators*, Ph.D. thesis, Mid Sweden University, Sweden, 2008.

[155] O. Ouchetto, *Modélisation large bande de métamatériaux bianisotropes et de surfaces structurées*, Ph.D. thesis, Université Paris-Sud XI, 2006.

[156] O. Ouchetto, S. Zouhdi, A. Bossavit, G. Griso, and A. Razek, *Homogenization of structured electromagnetic materials and metamaterials*, Journal of Materials Processing Technology **181** (2007), 225–229.

[157] A. Pankov, *G-convergence and homogenization of nonlinear partial differential operators*, Kluwer academic publishers, 1997.

[158] G. A. Pavliotis and A. M. Stuart, *Multiscale methods: averaging and homogenization*, Springer, 2007.

[159] J. B. Pendry, *Negative refraction makes a perfect lens*, Physical Review Letters **85** (2000), no. 18, 3966–3969.

[160] M. Peszynska, *Mortar adaptivity in mixed methods for flow in porous media*, International Journal of Numerical Analysis and Modeling **2** (2005), no. 3, 241–282.

[161] M. Peszynska, M. F. Wheeler, and I. Yotov, *Mortar upscaling for multi-phase flow in porous media*, Computers and Geosciences **6** (2002), no. 1, 73–100.

[162] N. C. Pop and O. F. Caltun, *Jiles-Atherton magnetic hysteresis parameter identification*, Acta physica polonica A **120** (2011), 491–496.

[163] V. Préault, R. Corcolle, L. Daniel, and L. Pichon, *Effective permittivity of shielding composite materials for microwave frequencies*, IEEE Transactions on Electromagnetic compatibility **55** (2013), no. 6.

[164] ———, *Influence of skin effect on homogenization of composite materials : Application to shielding effectiveness*, Proceedings of the Conference on the Computation of Electromagnetic Fields, (COMPUMAG2013) (Budapest, Hungary), 2013.

[165] ———, *Shielding effectiveness of composite materials: Effect of inclusion shape*, IEEE Transactions on Magnetics **49** (2013), no. 5, 1941–1944.

[166] ______, *Influence of skin effect on the effective shielding effectiveness of composite materials*, Journal of Applied Physics **115** (2014), no. 15.

[167] A. Quarteroni and A. Valli, *Domain decomposition methods for partial differential equations*, Oxford Science Publications,, 1999.

[168] L. Rayleigh, *On the influence of obstacles arranged in rectangular order upon the properties of the medium*, Philisophical magazine **34** (1982), 481–502.

[169] Z. Ren, F. Bouillault, A. Razek, A. Bossavit, and J.-C. Vérité, *A new hybrid model using electric field formulation for 3D eddy current problems*, IEEE Transactions on Magnetics **26** (1990), no. 2, 470–473.

[170] Z. Ren, C. Li, and A. Razek, *Hybrid FEM-BIM formulation using electric and magnetic variables*, IEEE Transactions on Magnetics **28** (1992), no. 2, 1647–1650.

[171] Z. Ren and A. Razek, *Coupling of boundary integral methods with dual finite element methods for electromagnetic field computation*, Boundary Element Technology X, Computational Mechanics Publications, Elsevier Applied Science, September 1995, pp. 89–98.

[172] A. J. Roberts and I. G. Kevrekidis, *General tooth boundary conditions for equation free modeling*, SIAM Journal on Scientific Computing **29** (2007), no. 4, 1495–1510.

[173] R. T. Rockafellar, *Convex analysis*, Princeton Univ. Press, Princeton, NJ, 1969.

[174] ______, *On the maximal monotonicity of subdifferential mappings*, Pacific Journal of Mathematics **33** (1970), no. 1, 209–216.

[175] W. Rudin, *Functional analysis*, McGraw-Hill, Inc, 1991.

[176] R. V. Sabariego, *The fast multipole method for electromagnetic field computation in numerical and physical hybrid systems*, Ph.D. thesis, Université de Liège, Belgium, 2004.

[177] ______, *Course on homogenization techniques within the finite element modelling of electrical machines*, Fields and material models within the finite element simulation of electrical machines pages: 15–135, Helskinki University of Engineering, Multiprint, 2009.

[178] ______, *Homogenization techniques in electromagnetism*, 2011, Presented at the Institute of Analysis and Scientific Computing (IACS) at EPFL in Lausanne, Switzerland.

[179] A. Saib, L. Bednarz, R. Daussin, C. Bailly, X. Lou, J.-M. Thomassin, C. Pagnoulle, C. Detrembleur, R. Jérome, and I. Huynen, *Carbon nanotube composites for broadband microwave absorbing materials*, IEEE Transactions on Microwave Theory and Techniques **54** (2006), no. 6, 2745–2754.

[180] G. Samaey, D. Roose, and I. G. Kevrekidis, *The gap-tooth scheme for homogenization problems*, SIAM MMS **4** (2005), no. 1, 278–306.

[181] A. Sihvola, *Electromagnetic mixing formulas and applications*, IEEE Electromagnetic Waves Series, 47), 1999.

[182] D. R. Smith and J. B. Pendry, *Homogenization of metamaterials by field averaging (invited paper)*, Journal of the Optical Society of America B **23** (2006), no. 3, 391–403.

[183] S. Spagnolo, *Sulla convergenza delle soluzioni di equazioni paraboliche ed ellittiche*, Ann. Scuola Norm. Sup. Pisa Cl. Sci. **22** (1968), 571–597.

[184] ———, *Convergence in energy for elliptic operators, numerical solution of partial differential equations iii*, Proc. Third Sympos. (1975), 469–498.

[185] P. E. Stelzig, *On problems in homogenization and two-scale convergence*, Ph.D. thesis, Università Degli Studi di Trento, Italy, 2012.

[186] J. A. Stratton, *Electromagnetic theory*, McGraw-Hill, 1941.

[187] E. B. Tadmor, M. Ortiz, and R. Phillips, *Quasicontinuum analysis of defects in crystals*, Philosophical magazine A **73** (1996), 1529–1563.

[188] L. Tartar, *Course peccot*, Collège de France, Paris, 1977.

[189] L. Tartar, *Compensated compactness and applications to partial differential equations*, Nonlinear analysis and mechanics: Heriott-Watt Symposium **IV** (1979), 136–212.

[190] L. Tartar, *The general theory of homogenization a personalized introduction*, Springer Berlin Heidelberg, 2009.

[191] J.-M. Thomassin, X. Lou, C. Pagnoulle, A. Saib, L. Bednarz, I. Huynen, R. Jérome, and C. Detrembleur, *Multiwalled carbon nanotube/poly(ε-caprolactone) nanocomposites with exceptional electromagnetic interference shielding properties*, Journal of Physical Chemistry C **111** (2007), 11186–11192.

[192] J.-M. Thomassin, C. Pagnoulle, P. P. Barbier, I. Huynen, R. Jerome, and C. Detrembleur, *Foams of polycaprolactone/mwnt nanocomposites for efficient emi reduction*, Journal of Materials Chemistry **18** (2008), 792–796.

[193] TWI, http://www.twi-global.com/EasysiteWeb/getresource.axd?AssetID=12384&type=full&servicetype=Inline.

[194] E. Vanden-Eijden, *Numerical techniques for multi-scale dynamical systems with stochastic effects*, Comm. Math. Sci. **1** (2003), no. 2, 385–391.

[195] A. Visintin, *Some properties of two-scale convergence*, Atti Acad. Naz. Lincei Cl. Sci. Fis. Mat. Natur. Rend. Lincei (9) Mat. Appl. **15** (2004), 93–107.

[196] ———, *Homogenization of doubly-nonlinear equations*, Rend. Lincei Mat. Appl. **17** (2006), 211–222.

[197] ———, *Towards a two-scale calculus*, E.S.A.I.M. Control, Optimization and Calculus of Variations **12** (2006), 371–397.

[198] ———, *Two-scale convergence of first-order operators*, Journal of Analysis and its Applications **26** (2007), 133–164.

[199] ———, *Two-scale convergence of some integral functionals*, Calc. Var. **29** (2007), 239–265.

[200] ———, *Two-scale div-curl lemma*, Calc. Var. **29** (2007), 239–265.

[201] ———, *Electromagnetic processes in doubly-nonlinear composites*, Communications in Partial Differential Equations **33** (2008), 804–841.

[202] ———, *A short introduction to the two-scale modelling*, Presented at the Workshop on Multiscale analysis and homogenization, Bangalore, India, 2010.

[203] ———, *Homogenization of a parabolic model of ferromagnetism*, Journal of Differential Equations **250** (2011), 1521–1552.

[204] N. Wellander, *Homogenization of some linear and nonlinear partial differential equations*, Ph.D. thesis, Lulea University of Technology, 1998.

[205] ———, *Homogenization of the Maxwell equations: Case I. linear theory.*, Applications of Mathematics **46** (2001), no. 1, 29–51.

[206] L. Wu, L. Noels, L. Adam, and I. Doghri, *A combined incremental-secant mean-field homogenization scheme with per-phase residual strains for elasto-plastic composites*, International Journal of Plasticity **51** (2013), 80–102.

[207] Xiang Zhang and Zhaowei Liu, *Superlenses to overcome the diffraction limit*, Nature Materials **7** (2008), 435–441.

[208] V. V. Zhikov, S. M. Kozlov, and O. A. Oleinik, *Homogenization of differential operators and integral functionals*, Springer-Verlag, 1991.

Author Index

Version history

September 09, 2014 : original revision

Generated on September 10, 2014